Structures Research
Report 2014/104971

University of Florida
Civil and Coastal Engineering

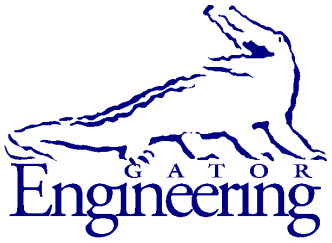

University of Florida
Civil and Coastal Engineering

Final Report July 2014

Determination of barge flotilla impact loads on pile founded concrete guide walls & Development of a unified impact load prediction model for navigational structures

Principal investigator:
Gary R. Consolazio, Ph.D.

Graduate research assistants:
John R. Wilkes, P.E.
Charles R. Rodrigues

Department of Civil and Coastal Engineering
University of Florida
P.O. Box 116580
Gainesville, Florida 32611

Sponsor:
Digital Engineering and Imaging, Inc.
U.S. Department of the Army
Point of Contact:
Robert C. Patev, Senior Risk Advisor, Risk Management Center, US Army Corps of Engineers

Contract:
UF Project No. 104971
Digital Engineering and Imaging, Inc. No. 674-02-HPA1-41
U.S. Dept. of the Army No. W912P8-08-D-0002

DISCLAIMER

The opinions, findings, and conclusions expressed in this publication are those of the authors and not necessarily those of the U.S. Department of the Army or Digital Engineering and Imaging, Inc.

ACKNOWLEDGEMENTS

The authors would like to thank the U.S. Department of the Army and Digital Engineering and Imaging, Inc. for providing the funding that made this research possible.

TABLE OF CONTENTS

LIST OF FIGURES

LIST OF TABLES

Table Page

CHAPTER 1
INTRODUCTION AND BACKGROUND

1.1 Introduction

The United States Army Corps of Engineers (USACE) maintains more than 10,000 miles of inland waterways throughout the United States. Barge flotillas (also called 'barge tows') are used to transport bulk materials such as coal, grains, sand, and gravel along these waterways. Navigational structures along these inland waterways maintain the most feasible means of transport without altering the natural flow of the water body. Navigational walls are installed to guide the barge flotillas into river locks, provide mooring facilities, and mitigate damage to dams and locks from potential barge impacts. It is relatively common for guide walls to be impacted by barge flotillas as they align to enter a river lock. As such, design and construction of guide walls must account for impact forces (loads) caused by oblique flotilla impact events.

The USACE is presently in the process of developing improved guidelines for the design of waterway structures. A range of different barge impact studies, some experimental and some numerical in nature, have been previously carried out, or sponsored, by the USACE. For example, full-scale experimental barge impact tests were performed by the USACE against a 'rigid' concrete lock wall at Robert C. Byrd Lock and Dam, near Gallipolis Ferry, West Virginia. Similar tests were conducted on a 'semi-flexible' concrete lock approach wall at Winfield Lock and Dam near Winfield, West Virginia. Subsequently, the USACE sponsored analytical studies—conducted by the Department of Civil and Coastal Engineering at the University of Florida—in which nonlinear dynamic finite element analysis techniques were used to simulate barge impacts on a variety of different structural types, including: hurricane protective structures (flood walls and dolphins), rigid walls, semi-flexible concrete walls, flexible timber guide walls, and bullnose structures.

In addition to the waterway structural types investigated in these previous experimental and analytical studies, the USACE is also responsible for, and maintains a substantial inventory of, pile-founded concrete guide walls. Such structures consist of relatively massive, tall, and structurally stiff concrete monoliths that are supported on much more flexible timber piles. Two variants of this structural type are common. In the first, the bottom surface elevations of the monoliths coincide with the top of soil elevation, such that the timber piles are completely supported (encased) in soil. In the second, a timber crib structure is constructed between the bottom of monolith elevation and the top of soil elevation. With a 'box-like' geometry, the timber cribbing completely surrounds the timber piles and is filled with large rocks that bear against both the cribbing and piling. Since both of these wall variants are significantly different than previously investigated structures, the study presented in this report is carried out to quantify—using finite element impact simulation—barge impact loads on such walls, and specifically for shallow angle oblique impact conditions.

Results from the pile-founded guide wall impact simulations are then combined with results from previous oblique impact studies to develop a unified impact load prediction model for oblique flotilla impacts against inland waterway navigational structures. Previous studies from which data are drawn to develop the unified load prediction model include: barge flotillas impacting rigid concrete guide walls (Consolazio et al, 2012), barge flotillas impacting semi-flexible concrete guide walls (Consolazio and Walters, 2012), and flexible timber guide walls (Consolazio and Wilkes, 2013). By merging the results from these prior studies together with the pile-founded guide wall simulation results obtained in the present study, a comprehensive

database of impact force data are produced for walls spanning a wide range of structural stiffnesses (and flexibilities). Such data are then used to develop a unified model for predicting peak forces on walls subjected to oblique barge impacts (Consolazio and Wilkes, 2013). In addition, results from the preceding bullnose study are used to develop a unified load prediction model for head-on flotilla impacts against bullnose waterway structures.

1.2 Objective

The objective of this study is to use nonlinear dynamic finite element impact simulations to quantify time-varying (transient) barge flotilla impact forces on pile-founded guide wall structures over a range of different impact conditions (flotilla size, impact speed, impact angle, without rock-filled timber cribbing, with rock-filled timber cribbing, wall impact location, soil strength, etc.). The second objective is to develop a method for efficiently computing (i.e., predicting) impact loads corresponding to barge flotilla impacts against a variety of inland waterway structures.

1.3 Scope of work

The first portion of the study presented in this report quantifies oblique barge flotilla impact loads on pile-founded guide walls using high-resolution dynamic nonlinear finite element simulation techniques. Specifically, the study focuses on oblique flotilla impacts against two navigation structures: Mississippi River Lock and Dam 2 (MRLD2) and Mississippi River Lock and Dam 3 (MRLD3). Simulations involve glancing impact conditions (angles $\leq 25°$) with approach speeds between 1 and 6 feet-per-second (FPS). The second portion of this study entails the development of unified load prediction models as described below.

1.3.1 Determination of impact loads for pile-founded guide wall MRLD2 (without cribbing)

The upper pool interior monoliths (UPIM) at Mississippi River Lock and Dam 2 (MRLD2) consist of a concrete guide wall resting on a series of battered and plumb timber piles whose full depth is embedded in soil. Development of the MRLD2 finite element guide wall model, and determination of barge impact loads on this guide wall, is accomplished by completing the following tasks:

- Develop a finite element model of UPIM at MRLD2 with timber pile foundation.
- Develop soil resistance curves and integrate them into MRLD2 model as nonlinear spring elements.
- Merge wall model and barge flotilla models of varying sizes, and conduct necessary initialization simulations
- Conduct dynamic finite element simulations, using LS-DYNA (LSTC 2013), of barge flotilla impacts against the wall model to quantify impact forces over a range of typical impact angles and impact speeds.

1.3.2 Determination of impact loads for pile-founded guide wall MRLD3 (with cribbing)

The lower pool interior monoliths (LPIM) at Mississippi River Lock and Dam 3 (MRLD3) consist of a guide wall resting on a series of battered and plumb piles whose partial depth is surrounded by rocks confined by timber cribbing and with the remnant surrounded by soil. Development of the MRLD3 finite element guide wall model, and determination of barge impact loads on this guide wall, is accomplished by completing the following tasks:

- Develop a finite element model of LPIM at MRLD3 with pile foundation.
- Develop a discrete rock-filled crib finite element model for determining rock-pile interaction (force-deformation) curves. Subsequently, integrate these curves into the MRLD3 finite element wall model.
- Develop soil resistance curves and integrate them into MRLD3 model as nonlinear spring elements. Merge wall model and barge flotilla models of varying sizes, and conduct necessary initialization simulations
- Conduct dynamic finite element simulations, using LS-DYNA (LSTC 2013), of barge flotilla impacts against the wall model to quantify impact forces over a range of typical impact angles and impact speeds.

1.3.3 Development of a unified impact load prediction models

A series of finite element studies simulating barge flotilla impacts against an array of inland waterway structures are performed to develop unified load prediction models. Specifically, peak force data from simulated flotilla impacts are collected from previous studies and are generated in the current study. The scope of these studies include flotilla sizes ranging from a single fully-loaded jumbo barge model (1x1) to three strings by five rows of fully-loaded jumbo hopper barges (3x5). The following USACE wall structures are considered: a Hurricane Protection Office (HPO) wall located near St. Bernard Parish; a Protection and Restoration Office (PRO) wall located near Algiers Canal; a PRO wall fronting protection system (dolphin) located near Hero pumping station; a typical rigid concrete wall; single-span semi-flexible concrete wall at Winfield Lock and Dam near Red House, WV; upper pool interior monolith walls at MRLD2 near Hastings, Minnesota; lower pool interior monolith walls at MRLD3 near Welch, Minnesota; and a flexible timber guide wall at Catfish Point Control Structure 2 near Grand Chenier, LA. The following bullnose structures are also included: a 2:1 sloped-V bullnose at Mississippi River Lock and Dam No. 7 (MRLD7) near Onalaska, WI; a typical 35 ft diameter semi-circular bullnose; and a typical 10 ft diameter semi-circular bullnose.

Unified load prediction models are presented for two types of flotilla impact events: oblique impacts on walls, and head-on impacts on bullnose structures. For oblique flotilla impacts on walls, unified load prediction models are developed using a database of force results collected from a rigid wall study (Consolazio et al, 2012), a semi-flexible guide wall study (Consolazio and Walters, 2012), flexible-timber guide wall study (Consolazio and Wilkes, 2013), and the current pile founded guide wall study. Two basic approaches are employed to develop oblique wall impact load prediction models: empirical bilinear curve-fitting, and a two-dimensional low-order (low degree-of-freedom; low-DOF) dynamic model. For head-on flotilla impacts on bullnose structures, load prediction models are developed using empirical bilinear curve-fitting.

CHAPTER 2
BARGE FLOTILLA FINITE ELEMENT MODEL

2.1 Introduction

A significant component of the present study involves quantifying loads that are imparted to large-mass pile-founded guide walls during oblique flotilla impacts. A barge flotilla (Figure 2.1) is an assembly of individual barges of similar size and configuration that are connected together by steel wire ropes known as lashings. The flotilla models used in this study are comprised of fully loaded jumbo hopper barges. All finite element simulations performed for this study utilize a highly discretized, high resolution, impacting barge model. This high-resolution barge model is attached to lower resolution non-impacting barge models to form a given flotilla configuration. The maximum size flotilla of interest in this study is a 3x5, which includes fifteen (15) barges comprised of three (3) strings with five (5) barges per string. Additional flotilla configurations that are also modeled include a 1x3, 2x3, and 3x3.

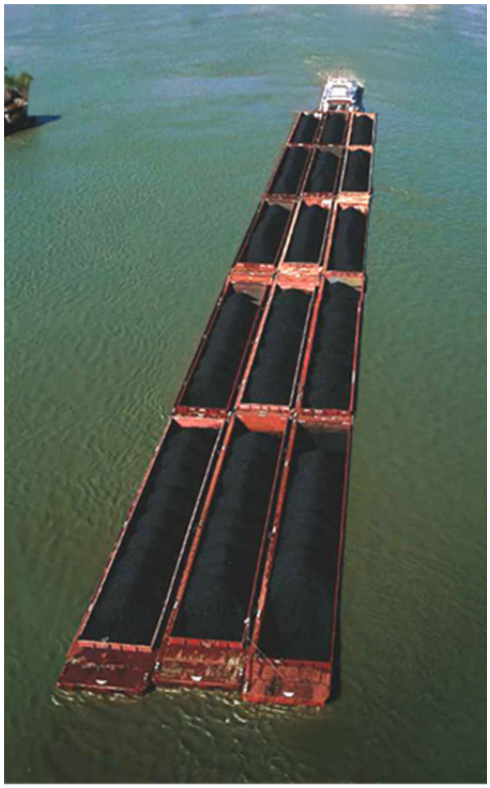

Figure 2.1. Typical 3x5 barge flotilla in transit (after USACE 2007)

Barge models used in this study are created using the methodology described in Consolazio et al. (2012), Consolazio and Walters (2012), and Consolazio and Wilkes (2013) which provide additional information of the methods used in the development of the barge flotilla models.

All flotilla models are comprised of jumbo hopper river barges measuring 195 ft long by 35 ft wide and weighing 2000 tons each (where 1 ton = 2000 lbf). Overall dimensions and weights of all flotilla configurations used in this study are listed in Table 2.1.

Table 2.1. Jumbo hopper barge flotilla dimensions and weights

Flotilla Size	Flotilla Length (ft)	Flotilla Width (ft)	Flotilla Weight (tons)
1 x 3	585	35	6,000
2 x 3	585	70	12,000
3 x 3	585	105	18,000
3 x 5	975	105	30,000

The two versions of the jumbo hopper river barge included in all flotilla models used in this study are the single-raked and double-raked barge. Single-raked barges are raked (tapered through the depth) at either the bow (Figure 2.2.a) or stern end only, whereas double-raked barges are raked at both the bow and stern (Figure 2.2.b). In configuring a flotilla, single-raked barges are positioned in exterior rows while double-raked barges are positioned in interior rows.

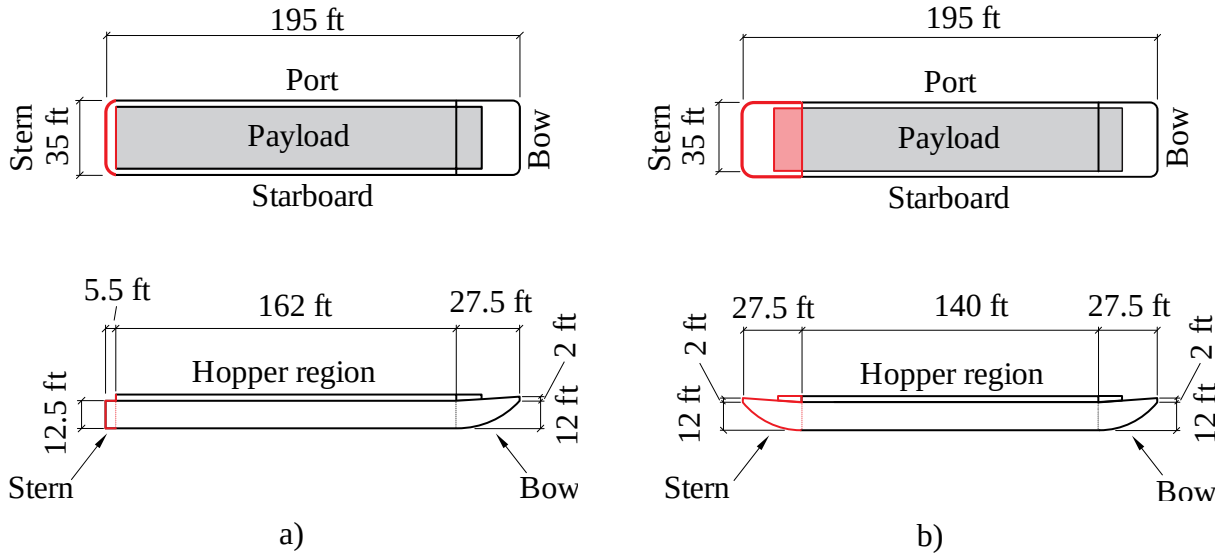

Figure 2.2. Jumbo hopper barge schematics:
a) Single-raked barge; b) Double-raked barge

Two (2) of the four (4) flotilla configurations used in this study are illustrated in Figure 2.3. Single-raked barges are oriented such that the raked-end is on the exterior of the flotilla; i.e. the raked-end is in the stern position for trailing row barges and in the bow position for leading row barges (Figure 2.3).

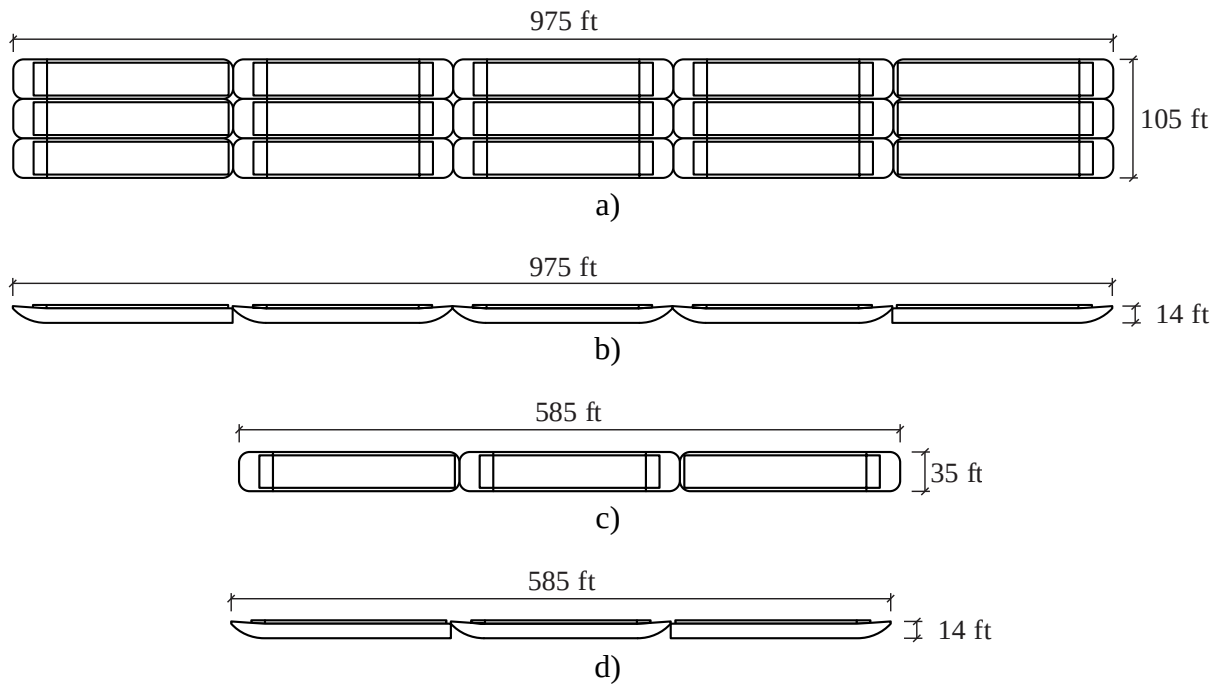

Figure 2.3. Jumbo hopper barge flotilla schematics:
a) 3x5 plan view; b) 3x5 elevation view; c) 1x3 plan view; d) 1x3 elevation view

2.2 Modeling of barges

Two types of barge models are used for each unique flotilla configuration (Figure 2.4). A single high-resolution barge, referred to as the *impacting* barge, is the only barge to make physical contact with the target structure (pile-founded guide wall). The high level of discretization associated with the impacting barge is necessary to enable accurate representation of the contact between the target structure and impacting barge as well as internal contact, or crushing, within the impacting barge itself. The remaining low-resolution barges within a flotilla are referred to as *non-impacting* barges. The primary role of these non-impacting barges is to facilitate modeling the dynamic inter-barge behavior (resulting from barge-to-barge contact and lashing interactions of adjacent barges) during impact. This inter-barge behavior forms the basis for the stiffness of a given flotilla during an impact event. Thus, accurately modeling the inter-barge dynamics within a flotilla captures the influence of each individual barge, including mass contribution and stiffness contribution. Note the non-impacting barges do not make contact with the target structure at any point in time during the impact event.

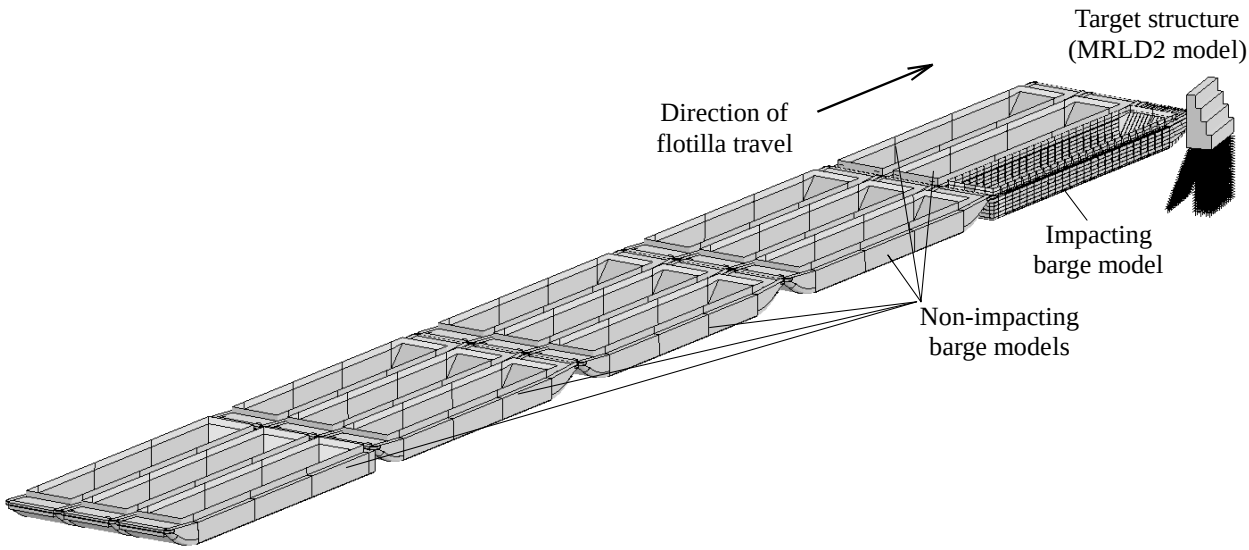

Figure 2.4. Flotilla impact simulation model consisting of a single 'impacting barge' model, multiple non-impacting barge models, and target structure (Note: only key geometric edge lines are shown; element mesh not shown for clarity)

2.2.1 Impacting barge

The high resolution impacting FE barge model is composed of more than 900,000 nonlinear shell elements. The barge structural model is consistent with available detailed structural plans and is made up of three barge zones: the bow zone, the stern zone, and the hopper zone. Each zone is discretely modeled with internal structural members and external plate surfaces. Internal structural members consist of angle, channel, or gusset plate sections. Internal member thicknesses and external plate thicknesses vary between 5/16 in. and 5/8 in., as determined from structural plans. Figure 2.5 shows a rendering of the impacting barge. Illustration of the mesh discretization in the bow zone is shown (Figure 2.6).

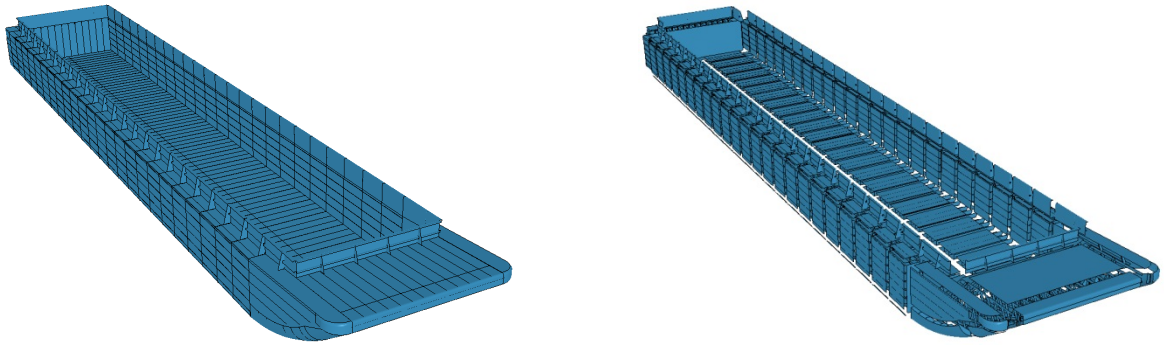

a) b)

Figure 2.5. Jumbo hopper barge FE model (mesh not shown for clarity):
a) Perspective view; b) Exploded view

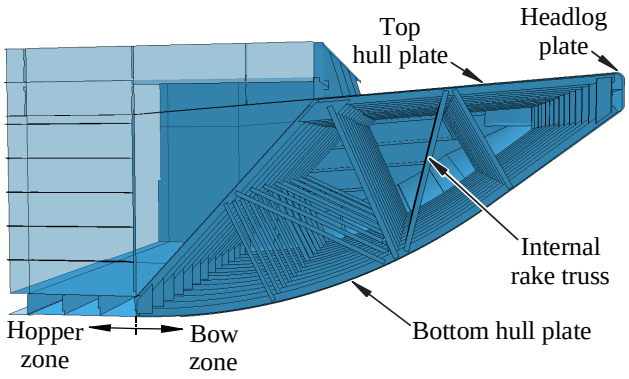

a)

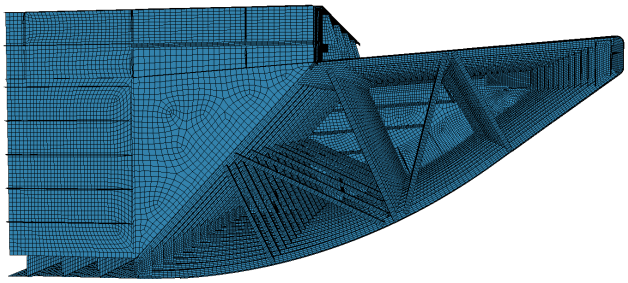

b)

Figure 2.6. Barge bow zone: a) Structural configuration; b) FE mesh

The material definition for this high resolution impacting barge model has a nonlinear constitutive relationship (effective true stress vs. effective plastic strain) representing A36 structural steel with Cowper-Symonds strain rate parameters as provided in Consolazio and Walters (2012). All components are defined by 4-node, fully integrated shell elements with sufficient mesh density to allow for local buckling and local material failure. Material failure is represented by element deletion at an effective plastic strain of 0.2 in./in. Additional information regarding the steel material model is available in the semi-flexible wall (Winfield) report (Consolazio and Walters, 2012).

A majority of the impacting barge is rigidized (Figure 2.7) for computational efficiency and barge-to-barge contact compatibility. Rigidization is a process in which the material definition for selected components (solid elements, shell elements, beam elements, etc.) within an LS-DYNA model are switched to a rigid definition. Thus, mass-related inertial properties are maintained but no internal strains or deformations can occur. Rigidization is constrained to regions sufficiently distant from the impacting starboard-bow corner such that the remaining deformable portion extends well beyond areas involved in force-crush interactions, thereby not affecting force-deformation behavior of barge-wall contact.

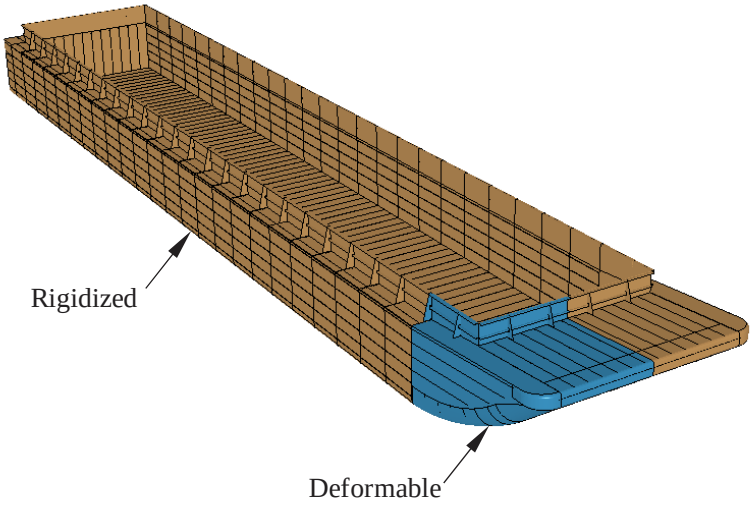

Figure 2.7. Partial rigidization of high resolution impacting barge FE model
(Note: mesh not shown for clarity)

2.2.2 Impacting barge – internal contact

An LS-DYNA self-contact algorithm is used to account for the structural stiffness of the deformable region of the high-resolution barge model (Figure 2.7). In accord with literature and previous USACE-funded barge-impact studies, (Consolazio et al. 2010), (Consolazio et al. 2012), (Consolazio and Walters 2012), and (Consolazio and Wilkes 2013), static and dynamic coefficients of friction (μ) for intra-barge steel-to-steel (self) contact have constant values of 0.55 and 0.45, respectively. Again, the rigidized portion of the high-resolution barge model cannot experience strains or deformations, and thus self-contact is necessarily omitted.

2.2.3 Non-impacting (decimated) barges

The primary role of non-impacting FE barge models is to accurately represent mass-related inertial properties and inter-barge contact-stiffness in an efficient manner. Thus, performing an analysis with multiple high resolution barges is neither computationally feasible nor an effective or judicious use of computational resources. Due to the computational expense of performing an analysis with a nearly one-million element high resolution barge model, it is impractical and unnecessarily inefficient to utilize a fully discretized high resolution deformable barge model in a non-impacting position within a flotilla. Therefore, each non-impacting barge is modeled in a way that retains the external geometry of a high resolution barge, as well as the inertial and mass properties, but has a lower mesh resolution (a 'decimated resolution') than the high resolution barge finite element model. Dynamic inter-barge behavior is accounted for with contact and lashings.

Each low resolution ('decimated') non-impacting barge model (Figure 2.8) consists of approximately 4,000 shell elements, as compared to the 900,000 shell elements included in the high resolution impacting barge model. Shell elements defining external geometry of each non-impacting barge are modeled with rigid material definitions, thus no internal structural elements are included. Inertial and mass properties, quantified from the high resolution barge model, are assigned to each non-impacting barge to ensure appropriate dynamic behavior during impact.

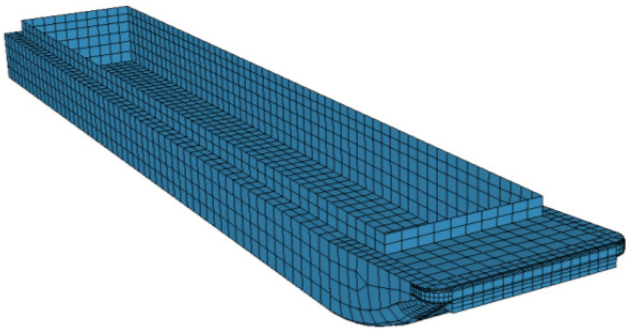

Figure 2.8. Non-impacting barge finite element model
(Note: actual mesh resolution shown)

2.3 Modeling barge interactions

Barges are connected to each other with steel wire rope, or lashings, to form a cohesive unit (for navigation) known as a barge flotilla (or barge tow). Lashings, anchored to steel cleats and wrapped around bitts (cylindrical steel posts), both of which are integral to the barge deck, are tensioned with turnbuckles, shackles, or similar (Figure 2.9) to improve maneuverability during navigation. Adjacent barges are connected by encircling the barge bits in a specified pattern, referred to as a lashing configuration. Lashings are layered on top of each other when more than one configuration is required at the same location. Different configurations are used to lash different barge pairs (end-to-end, side-to-side, or diagonal) and to resist different loads imposed by common flotilla maneuvers.

Figure 2.9. Typical lashing configuration on barge flotilla

Seven different lashing configurations, in either a port or starboard location, are used in this study. For finite element models of flotillas with 3 strings (called ‘3x’ flotillas), the lashing configurations used in this study are consistent with those used in the full-scale barge impact tests conducted by the USACE at Gallipolis Locks (Patev et al. 2003) and in a previous analytical barge impact study of rigid walls (Consolazio et al., 2012). For flotillas with one string

(1x) and two strings (2x), analogous lashing configurations were developed in previous analytical studies (Consolazio and Walters 2012, Consolazio and Wilkes 2013). For a detailed discussion of all lashing configurations used in this study, see Appendix A.

Each wire rope within the flotilla model is assigned an appropriate geometric configuration; a set of material properties that represent the nonlinear stiffness of the lashing; and a failure criterion based on ultimate capacity. Depending upon the location of the wire rope within the overall flotilla, an appropriate ultimate tensile of either 90 kips (for 1 in. diameter wire rope) or 120 kips (for 1.25 in. diameter wire rope) is assigned. By including a failure criterion, all flotillas have the ability to experience either full or partial break-up, wherein the individual barges are free to separate from one another and move independently. For a detailed description of the mathematical finite element procedures used to model of the lashing elements, see Consolazio et al. (2012).

Inter-barge behavior is modeled with a combination of both lashings and contact, where contact definitions counter-balance lashings forces between adjacent barge models. Non-impacting barge models and or rigidized portions of the deformable barge are mathematically rigid and hence inter-barge contact stiffness cannot be calculated from deformations. Instead, inter-barge contact forces are accounted for with rigid-to-rigid contact definitions, which reference force-deformation curves developed from crushing two adjacent high-resolution deformable barge models together. Development of the nonlinear force-deformation curves extracted from quasi-static crushing simulations for each of the various barge-to-barge contact stiffnesses (side-to-side, bow-to-bow, and bow-to-stern) is detailed in Consolazio et al. (2012).

2.4 External loading (gravity and buoyancy)

In each impact simulation conducted in this study, the effects of both gravitational forces and buoyancy forces acting on the barge flotilla are included. Buoyant uplift forces underneath each barge are modeled by introducing individual buoyancy springs over the bottom surface of the barge model. For the high-resolution impacting barge model, approximately 26,400 discrete springs are attached to the barge bottom nodes; whereas each non-impacting barge employs approximately 900 buoyancy springs.

The stiffness of each buoyancy spring is computed by determining the tributary area of the barge bottom surface supported by the spring, and then multiplying this value by the density of water (62.4 lb/ft^3). By using a large number of springs with relatively small tributary areas, the resulting stiffness values are small, thereby precluding the development of unrealistically concentrated buoyant forces during barge motions.

Each buoyancy spring is 200 inches in length and connects to a support node (above the barge) that is freely able to translate in the horizontal plane (Figure 2.10) but restrained against vertical motion. As such, the barge model “hangs” from the collection of buoyancy springs and is able to translate arbitrarily large distances in the horizontal plane (plan view) without resistance. Vertical motions of the barge, however, cause appropriate changes in the distribution of vertical uplift forces, which are based on changes in the submerged depth of the barge. Because the buoyancy springs are always in tension, the vertical support node of each spring “tracks” (in plan view) with the corresponding node at the bottom surface of the barge. Consequently, the buoyancy springs remain vertical at all points in time during the simulation, regardless of the horizontal motions that the flotilla may undergo. This is particularly beneficial should a partial or full flotilla breakup occur during a simulation. Additional aspects of buoyancy

modeling, such as calibration of the buoyancy springs and gapping of buoyant springs at the raked barge bow, are described in Consolazio et al. (2012).

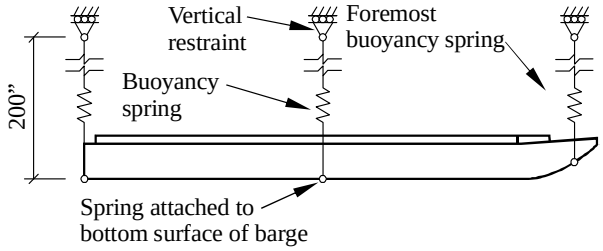

Figure 2.10. Barge buoyancy spring schematic

CHAPTER 3
FINITE ELEMENT MODELING OF PILE-FOUNDED GUIDE WALLS

3.1 Introduction

The USACE maintains a significant inventory of large-mass concrete walls supported by timber piling foundations, herein referred to as pile-founded guide walls. This study quantifies forces generated during oblique barge flotilla impacts against two types of pile founded guide wall structures using FE analysis. The first pile founded guide wall FE model is developed from the upper pool interior monoliths (UPIM) at Mississippi River Lock and Dam No. 2 (MRLD2) near Hastings, Minnesota (Figure 3.1), herein referred to as the MRLD2 finite element model. The second wall, referred to as the MRLD3 finite element model, is developed from the lower pool interior monoliths (LPIM) at Mississippi River Lock and Dam No. 3 (MRLD3) near Welch, Minnesota (Figure 3.2).

Figure 3.1. Mississippi River Lock and Dam No. 2 (MRLD2)
(Source: United States Army Corps of Engineers)

Figure 3.2. Mississippi River Lock and Dam No. 3 (MRLD3)
(Source: United States Army Corps of Engineers)

The USACE provided as-built plan sheets for guide walls at MRLD2 (Figure 3.3), MRLD3 (Figure 3.4), Mississippi River Lock and Dam No. 24 (MRLD24), and Mississippi

River Lock and Dam No. 25 (MRLD25). Interior guide walls at these four lock structures are representative of typical pile founded guide wall structures for purposes of performing finite element impact simulations. The as built plans used for developing the finite element models are the upper pool interior monoliths at MRLD2 (Figure 3.3) and lower pool interior monoliths at MRLD3 (Figure 3.4). The MRLD2 finite element model, with a 'typical' timber foundation, is developed from the upper pool interior monoliths at MRLD2 (Figure 3.3). This model is representative of the USACE inventory of pile founded guide walls supported on plumb and battered timber piling with typical grid spacing. The MRLD3 finite element model, which includes a rock-filled timber cribbing substructure, is developed from as built plans of the lower pool interior monoliths at MRLD3 (Figure 3.4). The MRLD3 finite element model is representative of the USACE inventory of pile founded guide walls with rock-filled timber-cribbing substructures. The finite element wall models developed in this study (Figures 3.5 and 3.6) represent the most vulnerable portions of the USACE pile founded guide wall inventory. It is anticipated the predicted impact forces for the specific guide walls considered here will also be representative of similarly constructed pile founded guide walls.

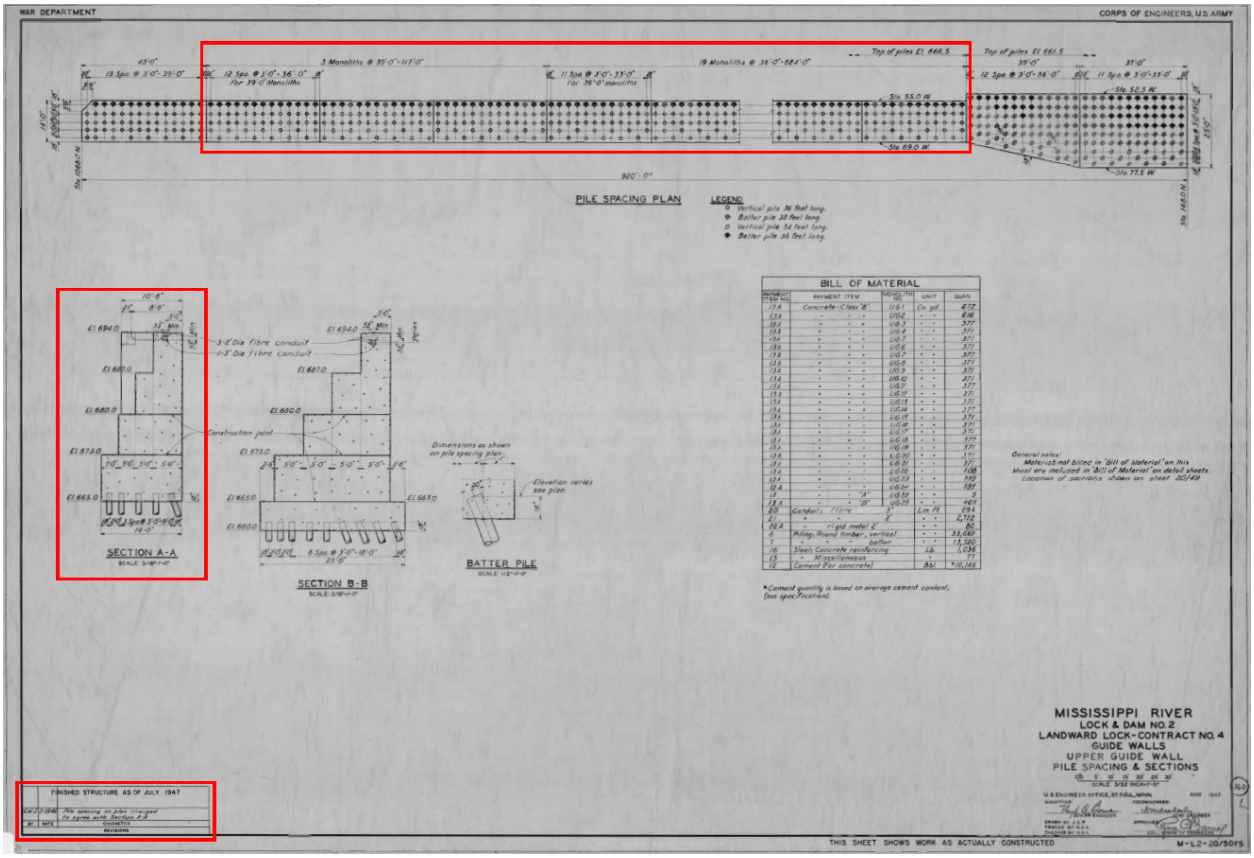

Figure 3.3. As built plans of upper pool interior monoliths at MRLD2
(Source: U.S. Army Corps of Engineers)

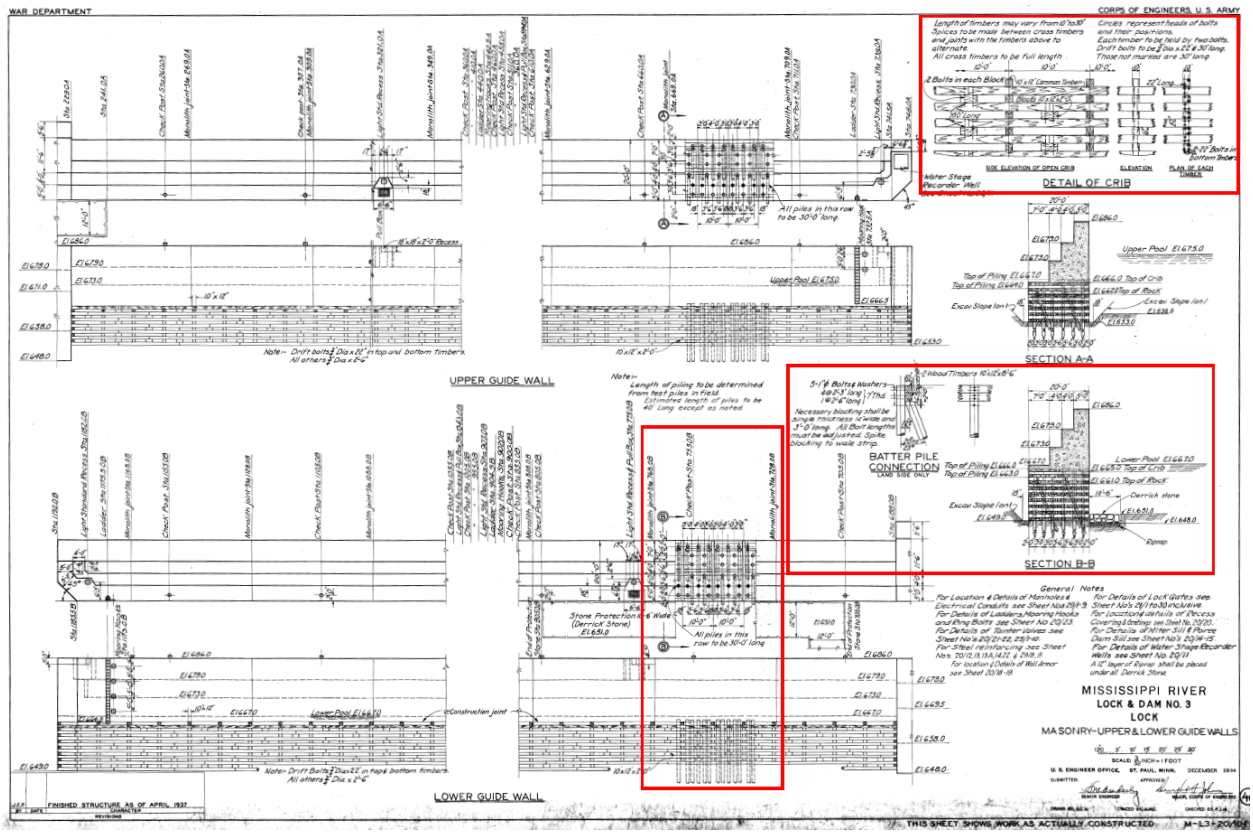

Figure 3.4. As built plans of lower pool interior monoliths at MRLD3
(Source: U.S. Army Corps of Engineers)

Both the MRLD2 and MRLD3 structures include plain concrete walls structure supported on timber piles. In the corresponding finite element models, the concrete walls are modeled with three-dimensional solid brick elements and the timber piles are modeled with beam elements. Linear elastic material properties are used for both the concrete wall and the timber piles since this study intended to quantify conservative impact loads that are representative of forces generated on structures of similar construction and configuration. The use of linear elastic behavior ensures that individual structural components do not limit the impact forces in a manner specific to the finite element wall models presented herein.

In the MRLD2 (Figure 3.5) model, nonlinear single degree-of-freedom spring elements are used to represent the stiffness contribution from soil surrounding the piles. In the MRLD3 model (Figure 3.6), spring elements are used to represent the stiffness contributions of both the soil surrounding the piles (below the crib), as well as the rock fill inside the timber crib. (Details are provided later in this chapter as to how the soil and rock fill springs are developed.). Although MRLD2 and MRLD3 wall models differ in cross-sectional geometry and timber piling layout, the primary objective in modeling the MRLD3 guide walls is to quantify the effect of a rock-filled timber-cribbing substructure on flotilla impact forces.

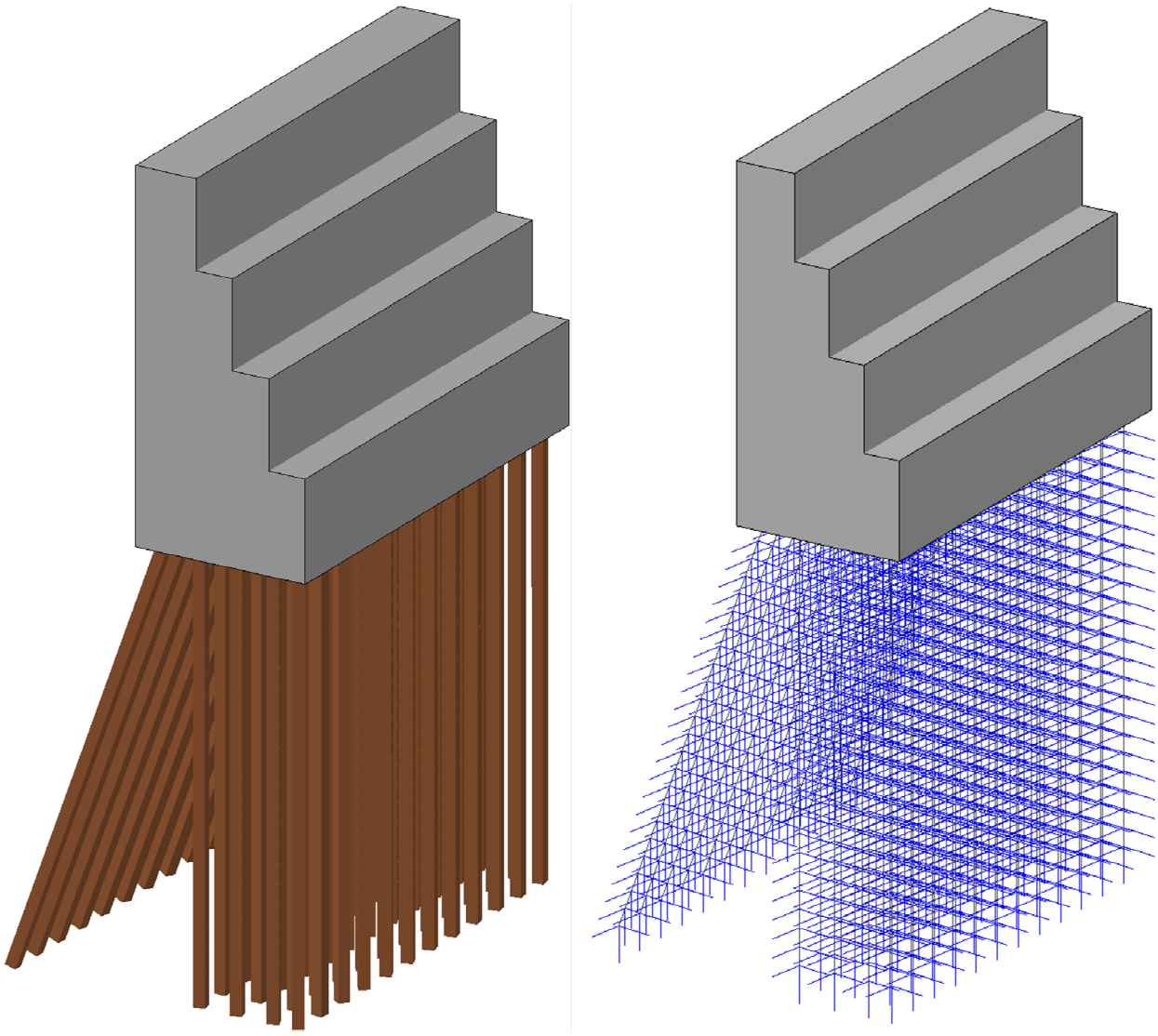

a) b)

Figure 3.5. Finite element model of MRLD2 wall monolith:
a) Pile elements ‘prism’ rendered at 12” thickness and soil spring elements not shown for clarity;
b) Pile elements (black) and soil spring elements (blue) rendered as lines

3.2 Structural components of pile-founded guide wall models

The interior monoliths at MRLD2 consist of plain concrete walls supported by timber piling (Figure 3.7a), both of which are defined with linear elastic material models. The interior monoliths at MRLD3 consist of plain concrete walls supported by a combination of rock-filled timber cribbing and timber piling (Figure 3.7b). Modeling techniques used to represent these structural components and the connections between them are discussed in detail in the following sections.

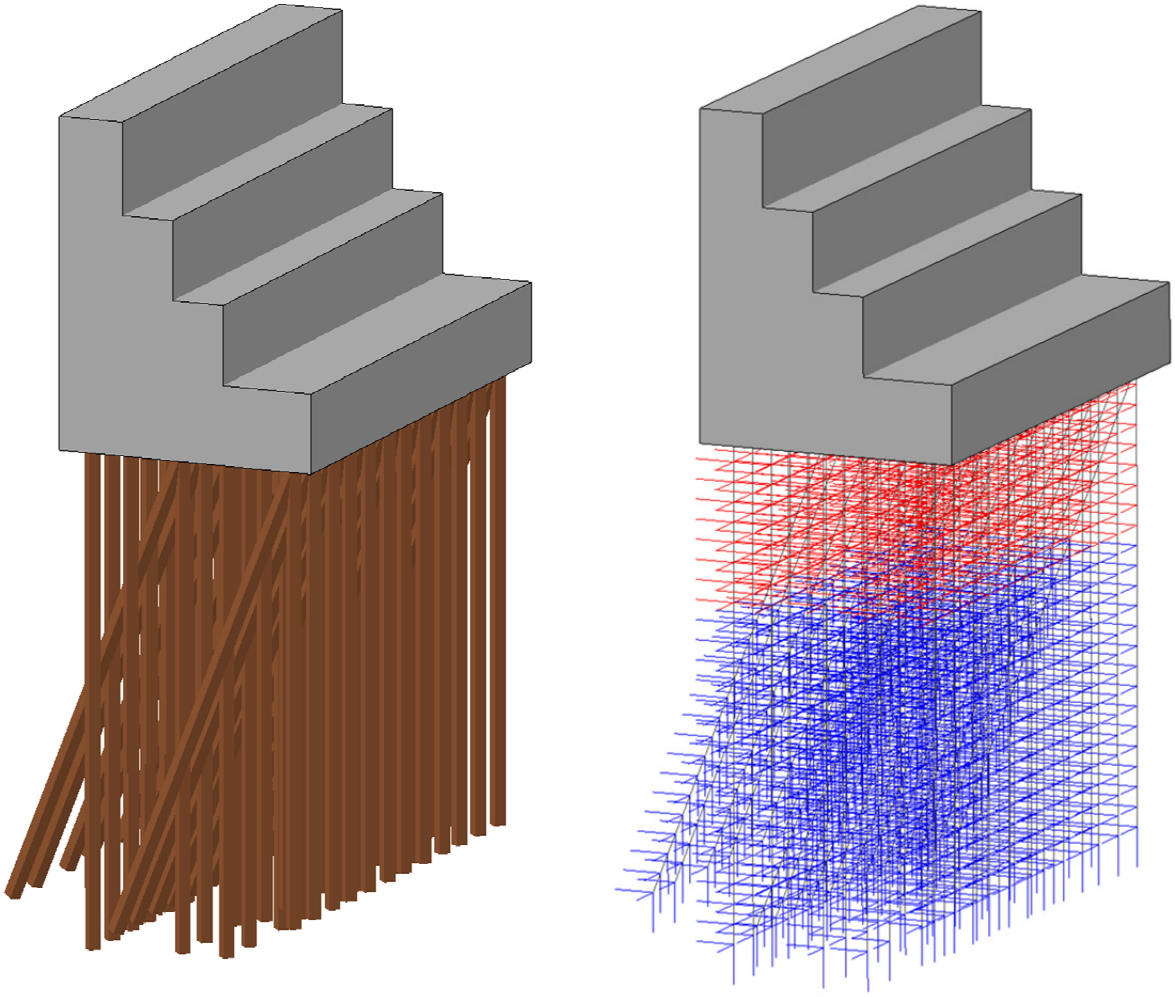

a) b)

Figure 3.6. Finite element model of MRLD3 wall monolith:
a) Pile elements ‘prism’ rendered at 12” thickness and soil spring elements not shown for clarity;
b) Pile beam elements (black), rock spring (red), and soil spring elements (blue) rendered as lines

3.2.1 Plain concrete guide wall

Each plain concrete guide walls is modeled with 8-node solid brick elements with cubic dimensions of 6” x 6” x 6”. Elements are sized as 6” cubes, in part, in order to be no larger than approximately twice the size of the smallest impacting shell elements on the surface of the deformable barge bow. Maintaining a size ratio no greater than 2:1 for elements in contact is desirable for impact simulations (e.g. the accuracy of detecting penetration is compromised with an increase in mesh resolution disparity between the contacting surfaces). The concrete walls are represented with these 6” cubic solid elements as shown in the following cross-sectional (Figure 3.8) and isometric views (Figure 3.9) of the LS-DYNA models.

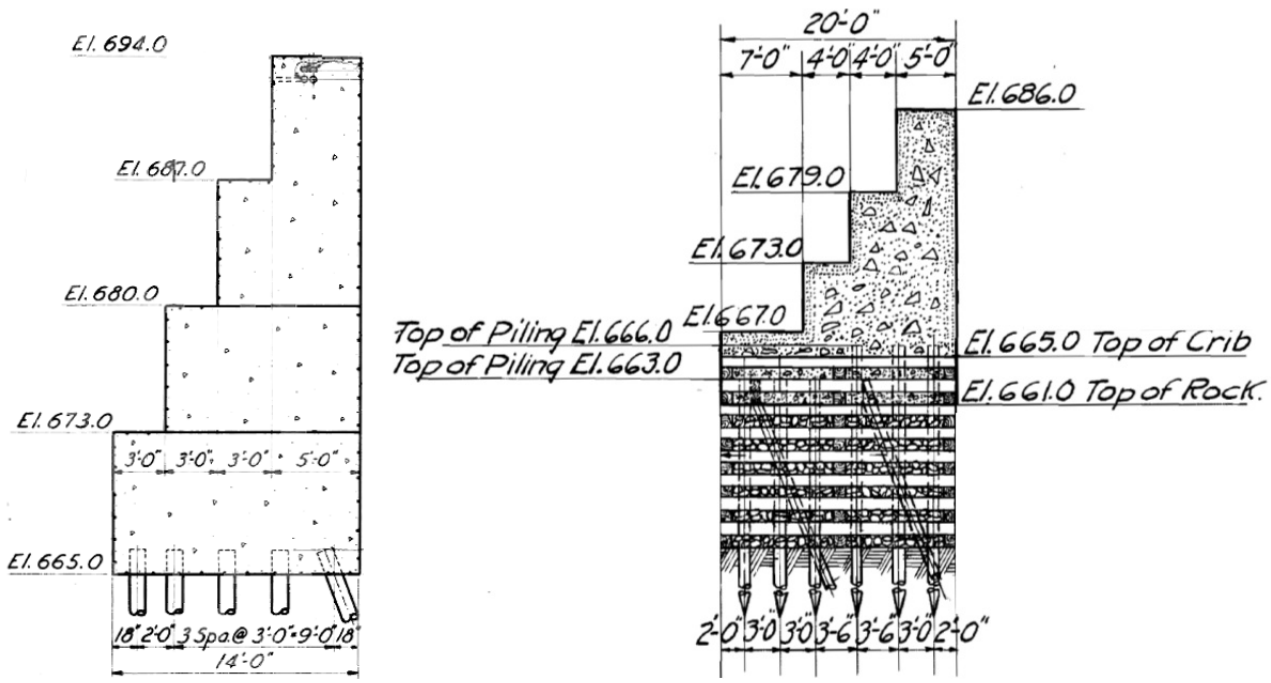

a) b)

Figure 3.7. Pile founded guide wall cross-sections:
a) MRLD2 upper pool interior monolith; b) MRLD3 lower pool interior monolith
(Source: U.S. Army Corps of Engineers)

The upper pool interior monolith at MRLD2 has clearly defined top and bottom elevations at El. 694 ft and El. 665 ft respectively (Figure 3.7.a), thus the corresponding finite element model unambiguously matches height of the MRLD2 guide wall cross-section (Figure 3.8.a). While the top elevation of the lower pool interior monolith at MRLD3 is clearly defined (at El. 686 ft, Figure 3.7.a), the elevation and geometry of the bottom surface are less exact due to the transition from plain concrete wall to cribbing and rock fill. For purposes of developing a representative finite element model, the base of the MRLD3 guide wall is defined at 'Top of Rock', El. 661 ft (Figure 3.7b). Consequently, the concrete portion of the MRLD3 model is 25'-0" in height with a 6'-0" thick base (Figure 3.8.b). Thus, the 4 ft. thick mixture of concrete, cribbing, and rock fill from 'Top of Rock' at El. 661.0 ft. to 'Top of Crib' at 665.0 ft. is modeled simply as plain concrete material.

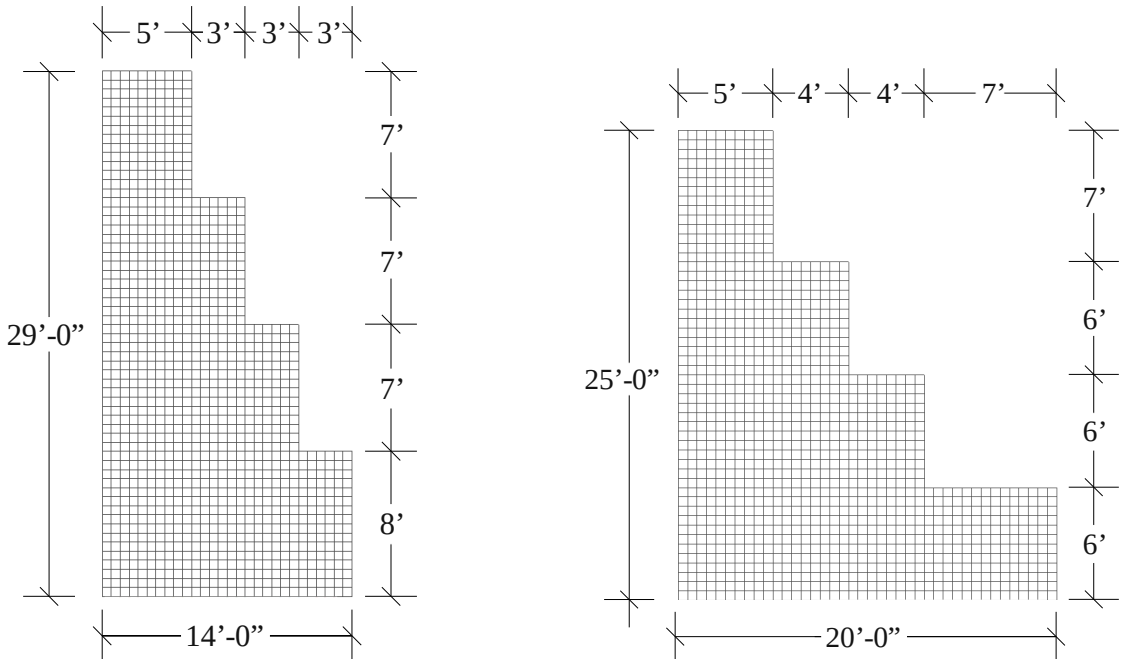

Figure 3.8. Cross-sections of concrete portions of finite element models:
a) MRLD2; b) MRLD3

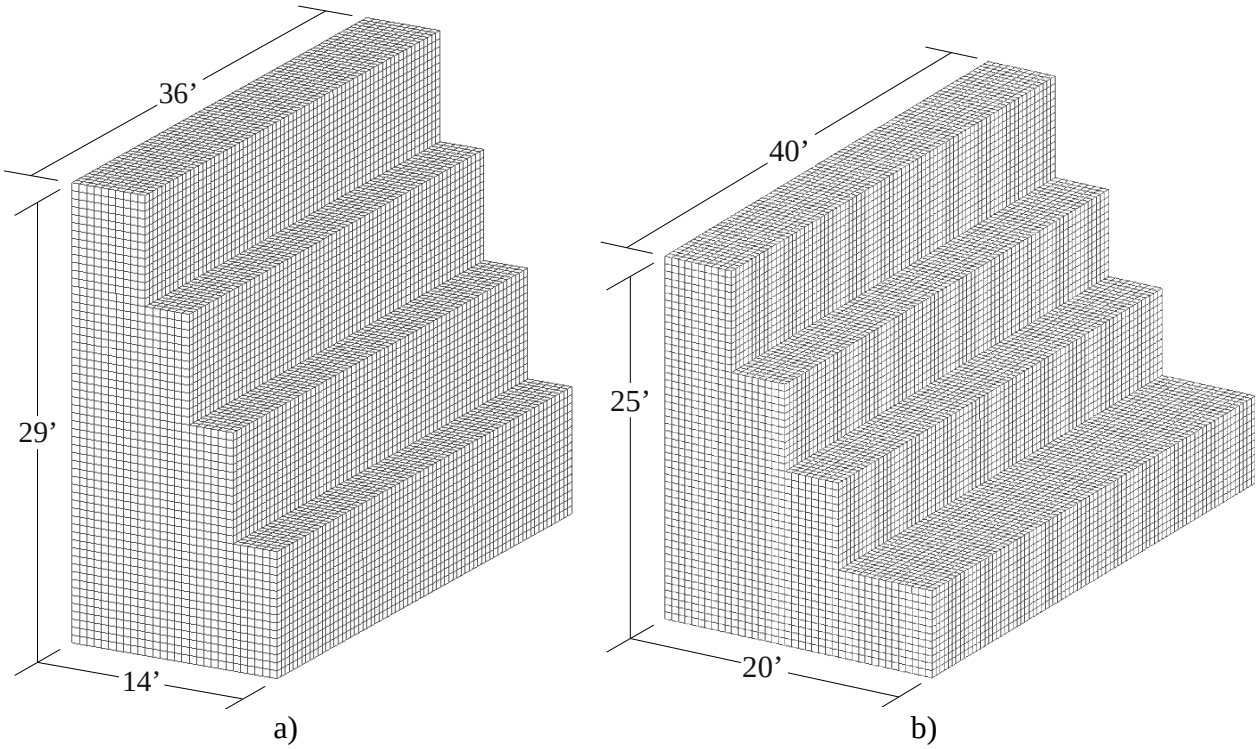

Figure 3.9. Isometric views of concrete portions of finite element models:
a) MRLD2; b) MRLD3

Based on the as built plans provided by the USACE, (Figure 3.3), construction of the guide walls at MRLD2 was completed in July 1947 with class "B" concrete. Although the USACE provided plans for MRLD2, MRLD3, MRLD24, and MRLD25, no additional information was obtained regarding concrete material specifications (e.g., minimum strength, aggregate size, sieve testing, etc.) As such, reasonably conservative materials properties are selected. For example, increasing the density of any pile founded guide wall component will increase the mass, thereby potentially increasing peak impact force. Thus, a higher material density is understood to be conservative for impact load prediction. Consequently, normal weight concrete, with a density 145 pounds-per-cubic foot (pcf), is selected. Given the class "B" designation, practices at the time of construction, and age of the structure, a compressive strength (f'_c) of approximately 2000 psi is selected. The modulus of elasticity (E), i.e. Young's Modulus, is determined to be approximately 2500 ksi based on present-day specifications (ACI 318 §8.5, 2011) and the selected compressive strength of 2000 psi. A Poisson's ratio of 0.16 is selected following a review of relevant literature (McCormac and Nelson, 2005). In summary, the plain concrete portions of the MRLD2 and MRLD3 guide wall finite element models use a linear elastic material model with ρ = 145 pcf, E = 2500 ksi, and ν = 0.16.

3.2.2 Timber piles

All timber piles in this study are modeled using 'resultant' beam elements to which gross cross-sectional properties are assigned. As such, the beam elements (and nodes) are positioned along the pile centerlines. Pile element nodes are evenly spaced at 18'-0" vertical intervals throughout the length of each pile. Thus, beam elements representing plumb piles are 18" in length and those representing piles battered at 20° are approximately 19.2" in length. For the MRLD2 model, there is a single pile 'group' consisting of five piles, of which four are plumb and one is battered. This pile group is replicated every 3'-0" longitudinally along the wall with all piles extending 34'-6" vertically below the base of the guide wall (Figure 3.10). All pile spacings presented in this report are center of pile to center of pile.

For the MRLD3 model, two alternating sets of pile groups support the guide wall. Piles are either 30'-0" or 40-0" in length and have embedment depths of either 2'-0" or 5'-0", depending on their location within the footprint of the wall. This matrix (or grid) of pile lengths and embedment depths yields a collection of piles with six (6) different pile tip elevations below the base of the MRLD3 guide wall (Figure 3.11 and 3.12). The pile layout for a single MRLD3 monolith consists of four repeating 'sets' of pile groups, spaced at 3'-0". Each pile group set includes five pile groups, three sets of pile group A (Figure 3.11) and two sets of pile group B (Figure 3.12). Within these sets, pile groups are arranged in an alternating fashion, with the two (interior) sets of pile group B being bordered by the three sets of pile group A; i.e. each set contains an A-B-A-B-A arrangement. The spacing between an exterior pile group and the first interior group is 1'-6". The spacing between interior pile groups is 2'-0". This pile layout was developed directly from the provided as-built plans (Figure 3.4).

Section stiffnesses for all timber pile beam elements is specified by defining a cross-sectional area and moments of inertia. Based on the 12" diameter circular cross-section, section properties include an area of 133.1 in^2, flexural moments of inertia of 1017.9 in^4 (about both local axes), and polar moment of inertia of 2035.8 in^4. Although the timber piling is tapered, with the given diameter representing the cross-section at 3'-0" from butt end, all piling in this study is modeled with a constant cross-sectional diameter of 12" throughout its entire length.

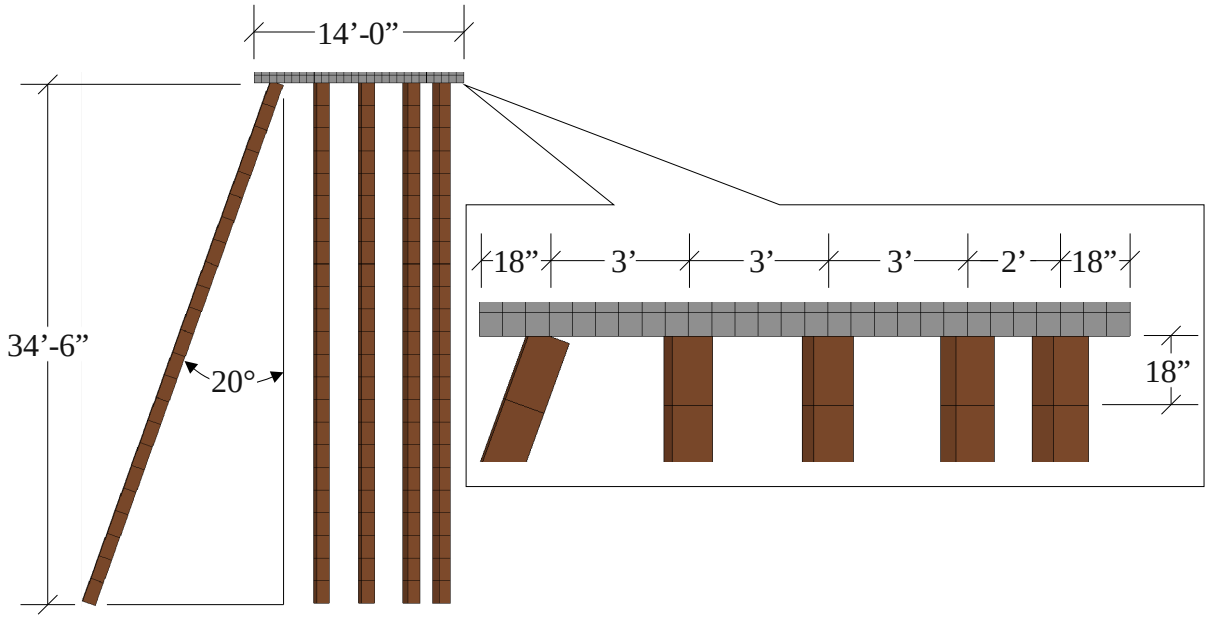

Figure 3.10. Elevation view of pile group at MRLD2:
(Note: beam elements rendered as ‘prisms’ for illustration)

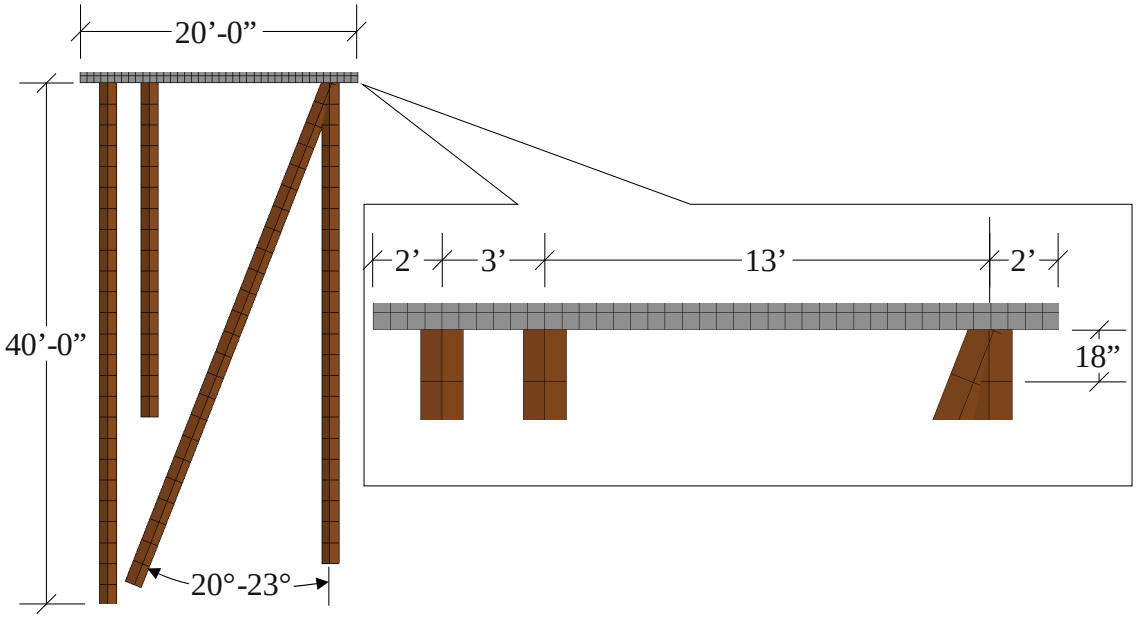

Figure 3.11. Elevation view of pile group A at MRLD3:
(Note: beam elements rendered as ‘prisms’ for illustration)

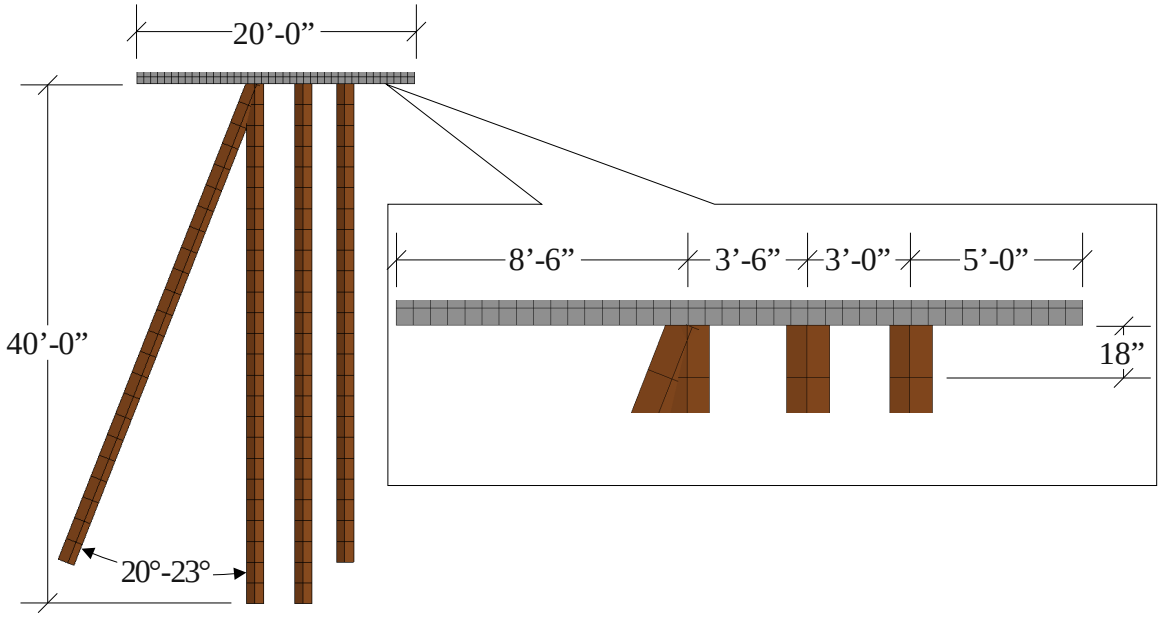

Figure 3.12. Elevation view of pile group B at MRLD3:
(Note: beam elements rendered as ‘prisms’ for illustration)

Multiple specifications were reviewed to select the most appropriate material properties for the timber piling. Specifically, density, elastic modulus, and Poisson’s ratio were selected from a review of literature from FHWA, USDOT, USDA, FDOT, AWPA, NDS, ASTM, and USACE. As previously stated, increasing the density of any pile founded guide wall component will increase mass and inertial properties, thereby increasing peak impact forces. Thus, as with modeling of the plain concrete wall, using a reasonably high material density for timber piling is conservative for impact force prediction. As such, an upper-end density of 50.0 pcf is selected. Timber piling at Mississippi River Lock and Dam 6 (MRLD6) in Trempealeau, WI includes “elm, maple, hickory, ash, oak, yellow birch, and pine” species (USACE, 2012). As no additional information regarding the timber used in the construction of pile founded guide walls in either the Upper Mississippi or other regions throughout the United States, the substantial amount of timber needed for construction of a pile founded guide wall (e.g. over 47,000 lineal feet of 12’ diameter timber piling at MRLD2 (Figure 3.3)), it is assumed that a wide range of wood species, as documented for MRLD6, is typical. Given this variability, a representative elastic modulus of 1000 ksi is selected. Based on a review of the literature referenced above, a Poisson’s ratio of 0.10 is typical for wood. In summary, all beam elements representing timber piles are defined as a linear elastic material with ρ = 50 pcf, E = 1000 ksi, and ν of 0.10.

3.2.3 Guide wall-to-timber pile connection

Timber piles are embedded in the concrete guide walls a minimum of 18” at MRLD2 and either 2’-0” or 5’-0” at MRLD3. Given a 12” diameter cross-section with these embedment depths, the guide wall-pile interface is assumed to behave as a fixed connection. As noted above, timber piles are modeled with beam elements and the guide walls are modeled with solid brick elements. To connect these two element types together, nodes along the bottom surface of the guide wall solid elements are merged with nodes at the tops of the timber pile beam elements;

i.e. the timber piles are connected to the concrete wall through nodal merging. However, because solid brick element nodes do not have rotational degrees of freedom, nodally merging the beam elements (timber piles) to the solid elements (concrete guide wall) would represent a pinned connection as opposed to a fixed connection.

In order to model a fixed pile head connection, a connection capable to transferring moments is needed between the guide wall and timber pile. The selected connection mechanism used in this study is the constrained nodal rigid body. The coincident, or merged, pile-to-wall interface node is defined as the master node. The additional (slave) nodes included in the nodal rigid body are the four adjacent coplanar guide wall nodes spaced at 6" from the master node (Figure 3.13). Constraining these additional four guide wall nodes to the merged wall-pile node corresponds to a 12" diameter embedment area, not only providing additional justification for using 6" cubic solid brick elements for the guide walls, but also more accurately representing the behavior of the guide wall-to-pile connection. Nodal rigid bodies are installed at all guide wall-to-pile connections for both finite element models: all sixty (60) piles present in the MRLD2 model (Figure 3.14.a), and all eighty (80) piles in the MRLD3 model (Figure 3.14.b). In addition, a supplementary study, comparing fixed-head to pinned-head pile modeling, is performed to evaluate the sensitivity of impact forces to the pile head fixity condition (see Section D.1). Results from the sensitivity study confirm that the fixed-head condition modeled using nodal rigid bodies produces conservative impact forces.

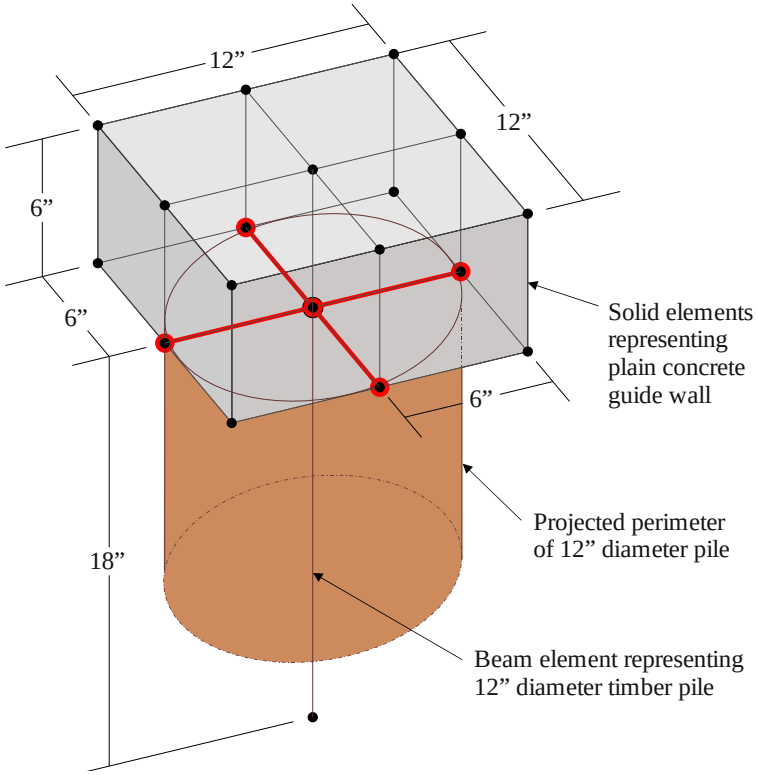

Figure 3.13. Constrained nodal rigid body at guide wall-to-pile connection

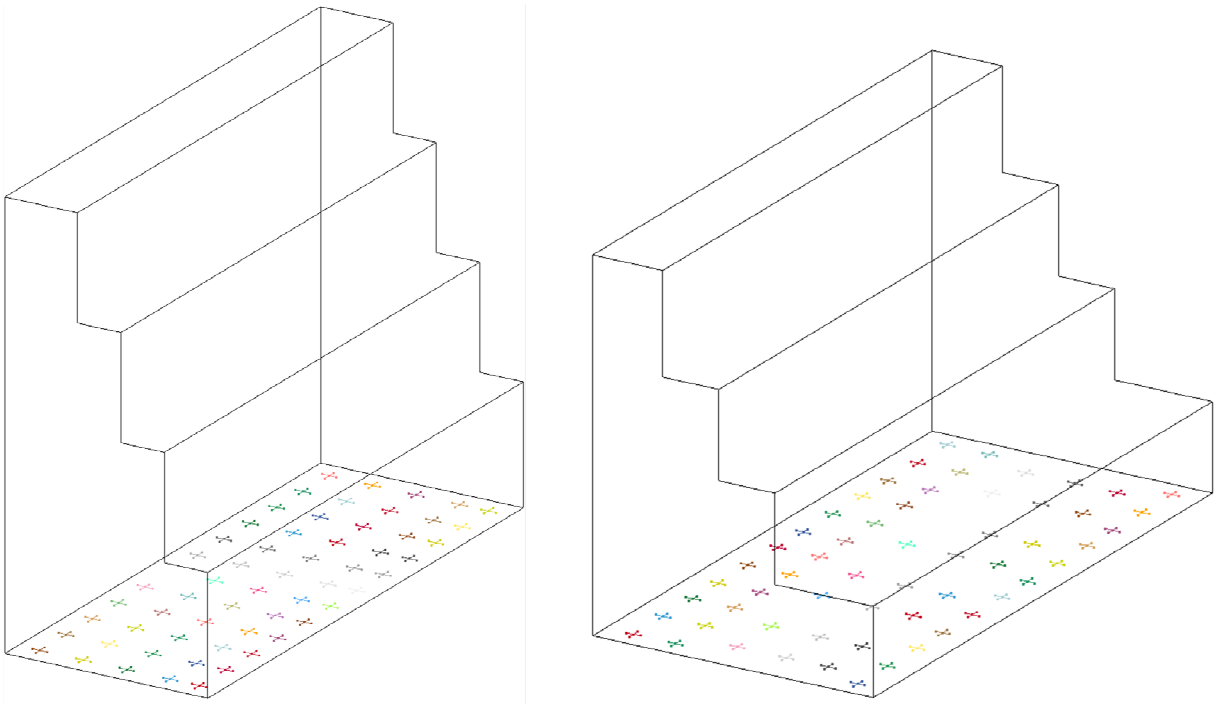

a) b)

Figure 3.14. Constrained nodal rigid bodies at interfaces between guide walls and piles: a) MRLD2 pile founded guide wall model; b) MRLD3 pile founded guide wall model

3.3 Soil components of pile-founded guide wall models

Soil representations in the MRLD2 and MRLD3 models are based on geotechnical data provided by the USACE, the use of FB-MultiPier (FB-MultiPier 2013), and empirical relationships. Nonlinear soils curves, extracted from FB-MultiPier, are integrated into the MRLD2 and MRLD3 models as lateral and vertical nonlinear spring elements.

3.3.1 Foundation soils

The soil profile selected for use in this study (Figure 3.15) is based on from data provided by the USACE for the MRLD3 site (USACE, 2013). Soil properties corresponding to the layers included in the profile are summarized in Table 3.1. Based on discussions with the USACE, this soil profile (Figure 3.15) and the associated soil parameters are deemed representative of typical pile founded guide walls in the USACE inventory. As such, the selected soil profile is used as the basis for soil characterization in *both* the MRLD2 and MRLD3 finite element models. In the MRLD3 structure, this profile (Figure 3.15) starts at the base of the timber cribbing. For purposes of using the same profile for MRLD2, the soil profile is shifted vertically to coincide with the base of the concrete wall. In Table 3.2, soil descriptions provided by the USACE are correlated to corresponding soil types as defined in FB-MultiPier.

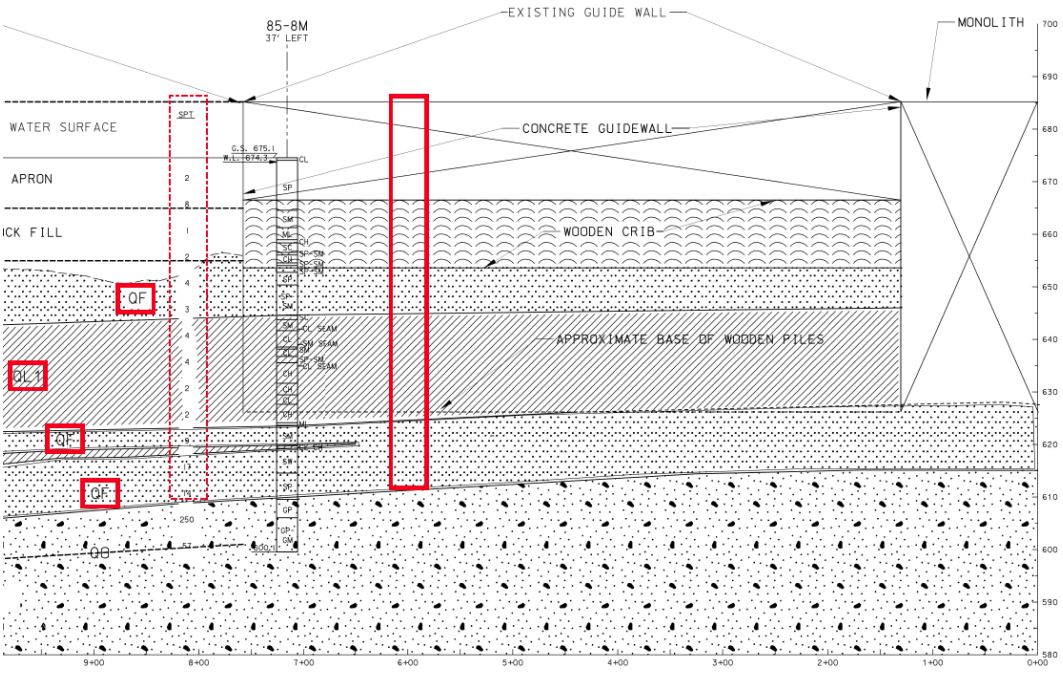

Figure 3.15. Soil profile from MRLD3
(Source: USACE)

Table 3.1. Soil properties at MRLD3
(Source: USACE)

			Q (UU)		S (CD)		
Unit	γ_m (pcf)	γ_{sat} (pcf)	c (tsf)	ϕ (deg)	c' (tsf)	ϕ' (deg)	Description
Q_L	115.5	115.2	0.21	0	0	33	Lacustrine Sediment
Q_{L1}	112.0	113.0	0.31	0	0	32	Glacio-Lacustrine Sediments
Q_{L2}	112.0	113.0	0.31	0	0	32	Lacustrine Sediment (Deep) Mostly CL
E_f	104.0	123.0	0	30	0	30	Fill (Fine to Medium Sand, Loose…)
$Q_{f(upper)}$	121.6	121.6	0	29	0	29	Fluvial sands
$Q_{f(middle)}$	121.5	121.5	0	29	0	29	Fluvial sands
$Q_{f(lower)}$	122.6	122.6	0	32	0	32	Fluvial sands
Q_o	136.5	136.5	0	52	0	45	Glacial Outwash

Table 3.2. Soil profile near STA 7+00 at USACE MRLD3
(Source: USACE)

Unit	Layer	Layer Depth	Soil Description (as per USACE definitions)	Soil Type (FB-MultiPier)
$Q_{f(upper)}$	1	9' – 0"	Fluvial Sands	Cohesionless
Q_{L1}	2	20' – 0"	Glacio-Lacustrine Sediments	Cohesive
$Q_{f(middle)}$ & $Q_{f(lower)}$	3	13' – 0"	Fluvial Sands	Cohesionless

For each layer, SPT blow counts (Figure 3.15) and soil parameters (Table 3.1) are taken directly from the provided geotechnical report (USACE 2013). SPT blow counts are averaged, per layer, using the SPT boring profile at 37' left of STA 7+00 centerline (Figure 3.15). Soil parameters such as subgrade modulus, shear modulus, Poisson's ratio, and major principal strains at 50% and 100% are unavailable and thus calculated using well established empirical

relationships (e.g. Tomlinson, Kulhawy and Mayne (1990), Skempton (1986), etc.) Calculated soil strength parameters for the representative profile are listed in Table 3.3.

Table 3.3. Soil parameters used in present study (FB-MultiPier input data)

Unit	Layer	Depth	γ (pcf)	ϕ	c_u (psf)	K	q_c (ksi)	R_t (kip)	E_{50}	E_{100}	G (ksi)	ν	f_s (psf)	E_s (pci)
$Q_{f(upper)}$	1	9’	121.6	29 °	–	0.515	–	–	–	–	0.542	0.25	0 126.0	34.09
Q_{L1}	2	20’	113.0	–	310	–	–	–	0.02	0.06	9.581	0.42	168.0 487.0	–
$Q_{f(middle)}$ $Q_{f(lower)}$	3	13’	122.6	29 ° 32 °	– –	0.470	– 1.011	– 114.3	–	–	0.978	0.25	373.2 562.3	131.9

γ: unit weight
ϕ: internal angle of friction
c_u: undrained shear strength
K: coefficient of lateral earth pressure

q_c: ultimate unit end bearing
R_t: axial bearing failure
E_{50}: major principal strain at 50
E_{100}: major principal strain at 100

G: shear modulus
ν : Poisson’s ratio
f_s : ultimate unit skin friction
E_s : subgrade modulus

An FB-MultiPier model (Figure 3.16) is developed using this profile (Table 3.2) of soil parameters (Table 3.3). The finite element model (Figure 3.16) includes a 12” diameter timber pile, with an 18” embedment in the wall, and extending 34’-6” down into the soil profile. The timber pile is modeled with 18” long resultant beam elements, similar to the beam elements in the LS-DYNA MRLD2 and MRLD3 models. The resulting nonlinear force-displacement soil curves (Figure 3.17) from the FB-MultiPier model are extracted at each pile node, re-sampled, mirrored if needed, and integrated into LS-DYNA MRLD2 and MRLD3 models (Figure 3.18).

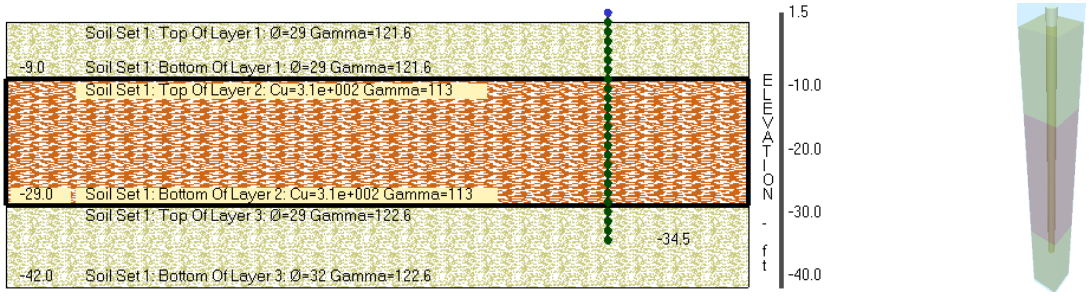

a) b)

Figure 3.16. FB-MultiPier timber pile model and soil information:
a) Soil profile with soil strength parameters; b) 3-D rendering of model

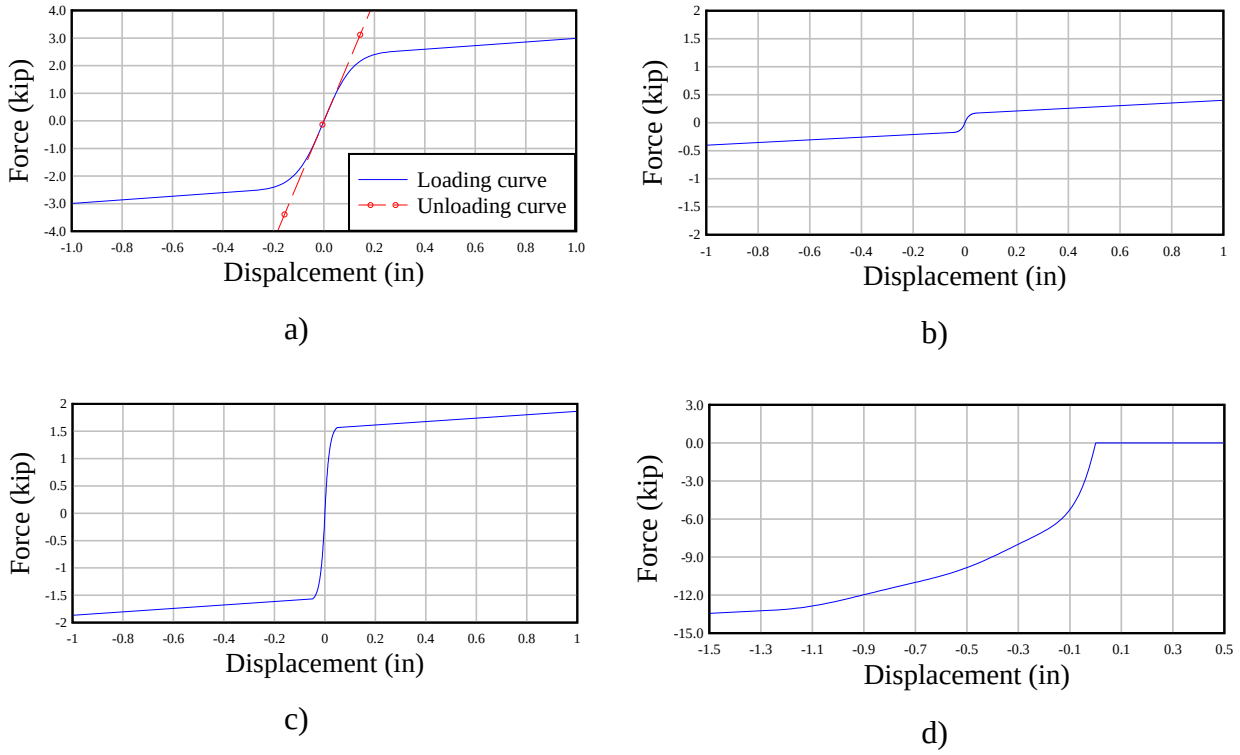

Figure 3.17. Typical soil force-displacement curves used in finite element models: a) P-x and p-y curves at 3' below soil surface; b) T-z curve at 3' below soil surface; c) T-z curve at 30' below soil surface; d) Q-z curve at pile tip (-34.5' below soil surface)

Horizontal and vertical soil resistance is represented in the LS-DYNA models using nonlinear soil spring elements attached to pile nodes (Figure 3.18) at 18" vertical spacings (corresponding to the FB-MultiPier model (Figure 3.16)). Soil elements include p-x and p-y springs in the horizontal direction for lateral resistance, and t-z and q-z springs in the vertical direction for skin friction and pile tip bearing resistance, respectively. The lateral (p-x and p-y) springs are modeled to undergo loading and unloading, where the loading curve is nonlinear and the unloading curve is linear and parallel to the initial portion of the loading curve (Figure 3.17a). As only a single spring represents lateral stiffness in either the x- or y-directions, the p-x and p-y springs include both a tensile and compressive component (to the compressive soil resistance in both the positive and negative directions). Vertical skin friction (t-z) springs are modeled to undergo nonlinear elastic force-deformation and vertical pile tip (q-z) springs are modeled as compression-only nonlinear elastic elements.

In order to achieve these desired behaviors, the force-deformation curves calculated by FB-MultiPier (Figure 3.17) are re-sampled (and mirrored) prior to integration into the LS-DYNA models. In the case of the lateral springs (p-x and p-y) and the skin friction (t-z) springs, the force-deformation curves from FB-MultiPier are mirrored in addition to being re-sampled. The pile tip, q-z, springs are resampled without mirroring as compression-only (no tension) resistance is modeled.

All force-deformation curves are implemented in the LS-DYNA MRLD2 and MRLD3 models with curve definition references in the soils spring material models. As with the soil

spring elements employed in previous research studies (e.g., Consolazio et al., 2012), translational restraints at the soil spring anchor nodes require that the soil spring element axes be oriented parallel to global axes.

In addition to the use of a representative soil profile for MRLD2 and MRLD3, a supplementary study of flotilla-wall impacts is also performed to assess the sensitivity of impact forces to soil resistance (see Appendix D).

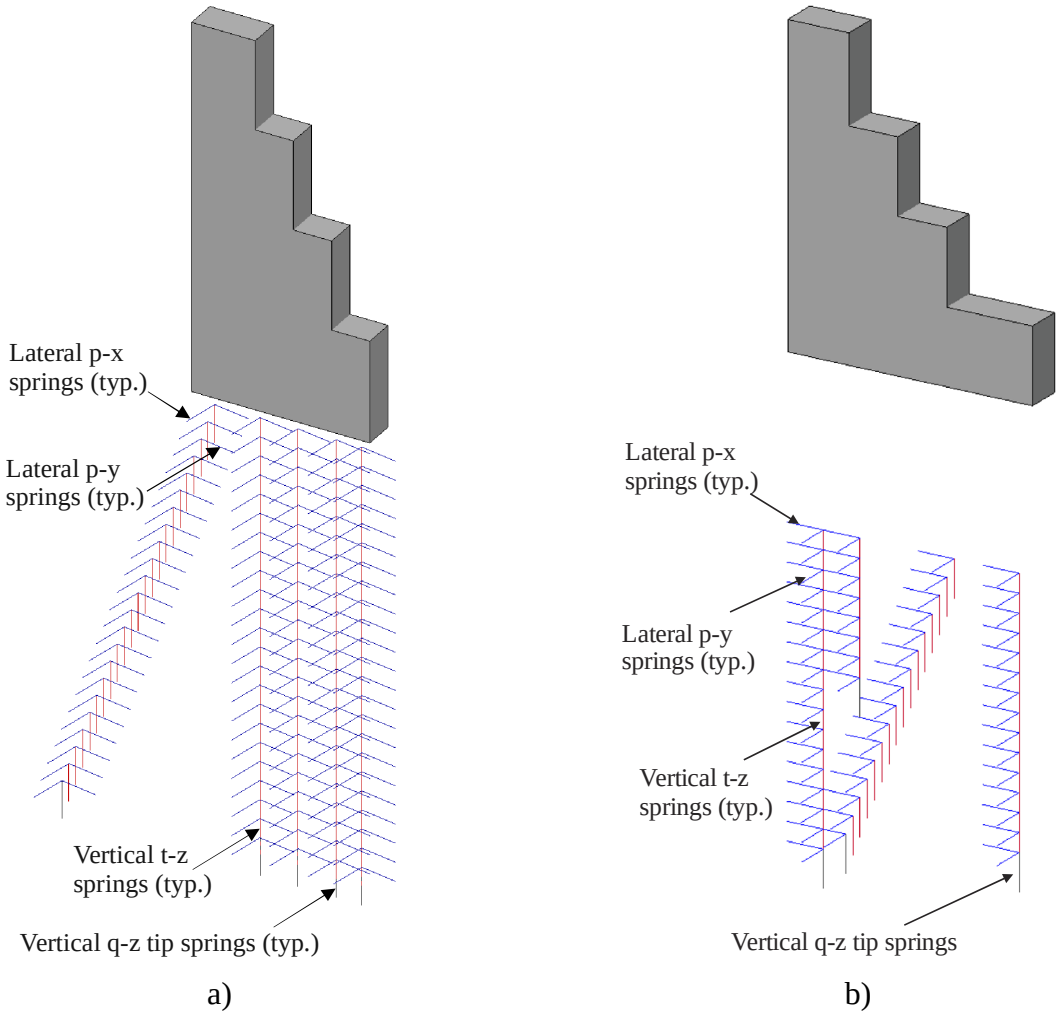

Figure 3.18. Longitudinal slices of pile founded guide wall models with soils springs included: a) MRLD2 finite element model; b) MRLD3 finite element model (rock crib extending between bottom of wall and soil surface not shown)

In the inventory of pile founded guide walls maintained by the USACE, some walls possess soil backfill, whereas others do not. In the MRLD2 and MRLD3 models used in this study—to conduct parametric impact studies (described in Chapter 5)—backfill soil is not explicitly included. However, the stiffening effect of overburden pressure from a full-depth backfill condition is included in the computation of the soil springs that attach to the pile nodes. An increase in the stiffness of any pile founded guide wall component will increase the peak forces generated during barge impact. Thus, using reasonably stiff soil curves that account for

the effects of overburden stiffening is conservative with respect to quantifying impact forces. The stiffening effect is therefore included in the interest of conservatism. (It is also noted that *supplementary* sensitivity studies, described in Appendix D, are also conducted to quantify impact force sensitivities to the presence of absence of backfill soils. Backfill soil modeling, however, is only explicitly included in the wall models that are described in Appendix D).

3.4 Rock filled timber cribbing substructure of MRLD3

The substructure of MRLD3 is split in two zones: an upper zone consisting of timber piles surrounded by rock fill that is encased in timber cribbing, and a lower zone consisting of timber piles that are completely embedded in soil. In this study, the rock filled timber cribbing is unique to the MRLD3 structure. A site-specific (structure-specific) modeling simplification is developed to efficiently model the influence that the MRLD3 rock filled crib has on impact forces. Specifically, a separate, high resolution, and discretely meshed finite element model of the rock filled crib is created. This model is analyzed—under the effects of lateral deformation—to develop an approximate characterization of the lateral stiffness of the rock filled crib substructure. Lateral stiffness thus computed for the overall crib structure is subsequently distributed into a network (a grid) of spring elements (force-deformation curves) that are attached to pile nodes in the upper pile zone of the MRLD3 model (recall Figure 3.6). Thus, the detailed rock fill crib model is *only* used as an intermediate step to obtaining a more efficient, simplified, and site-specific representation of the rock filled crib at MRLD3. Modeling of the components of the detailed rock filled crib model are presented below.

3.4.1 Timber cribbing

Timber cribbing in the MRLD3 substructure is made of 10’-0” long 10” x 12” timber elements that are stacked orthogonal to each other. The timber cribbing (Figure 3.19) only serves the purpose of holding the rocks in place; i.e., the cribbing is not attached to the timber piles supporting the guide wall. For the development of a corresponding finite element model, the timber cribbing is idealized using 10” thick 4 node fully integrated rigid shell elements that are 10” x 12” in size. The thickness of shell elements is consistent with the thickness of the timber elements shown in the as-built plans (Figure 3.4) provided by the USACE. The timber cribbing (Figure 3.19) is split in multiple blocks of 10’-0” x 10’-0” area in plan, which encase piles and rock fill. Since the timber cribbing is modeled only to surround discrete ‘rock’ elements, , the internal subdivision of physical timber cribbing—into multiple 10’-0” x 10’-0” blocks—is ignored and only the external geometry is modeled.

The timber cribbing is modeled as a series of casings (rings) of shell elements (Figure 3.20) that are separated by 6” vertical gaps. Each crib casing (ring) is modeled to rest on horizontal rollers, to avoid any lateral resistance introduced by the timber cribbing (as opposed to the rock fill). To further contain the discrete ‘rock’ elements that will fill the crib, the base of the timber cribbing is modeled using 12” thick rigid shell elements that are 10” x 10” in size. The base of the timber cribbing (also referred as base confinement) is modeled to represent the bottom of the timber cribbing and the top of the soil strata.

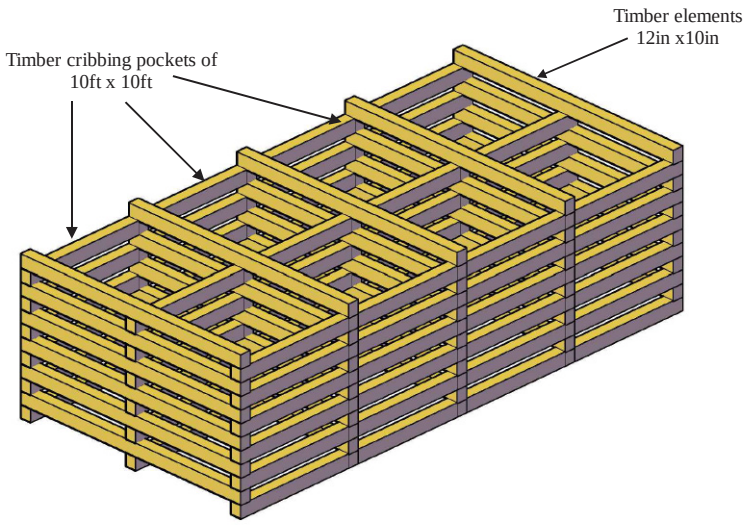

Figure 3.19. Configuration of timber crib at MRLD3

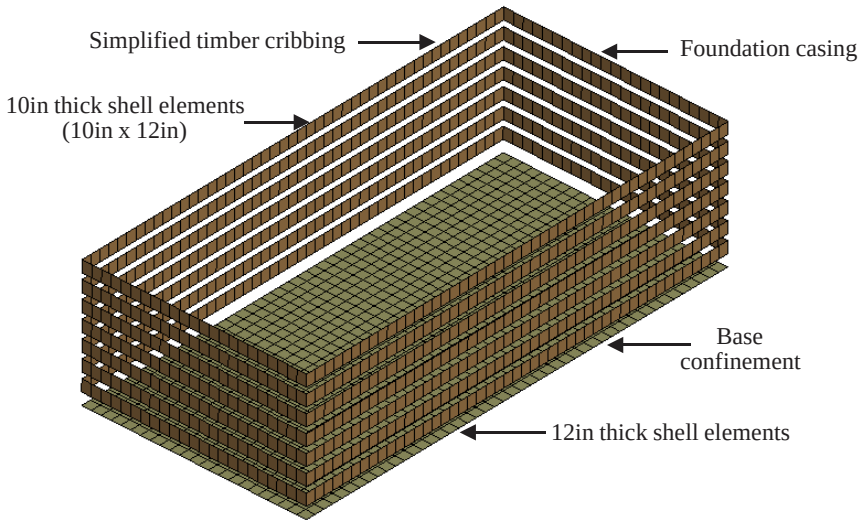

Figure 3.20. Timber crib modeled as a series of casings (rings) and base confinement

3.4.2 Corner 'overlap' elements

At each corner of the timber cribbing, the timber elements overlap and are connected together by 3 bolts of either 22" or 30" length, which introduces a later stiffness contribution. To approximate this effect, the corner overlap regions are modeled as 12" diameter circular beam elements—with timber material properties—running from the base of the guide wall to the first soil spring The connection between the corner overlap elements and the base of the concrete guide wall is the same as the guide wall to timber pile connection as described in Section 3.2.3.

Corner overlap elements are present along the outer periphery of the guide-wall and are position every 10 ft along the length of the guide wall (Figure 3.21).

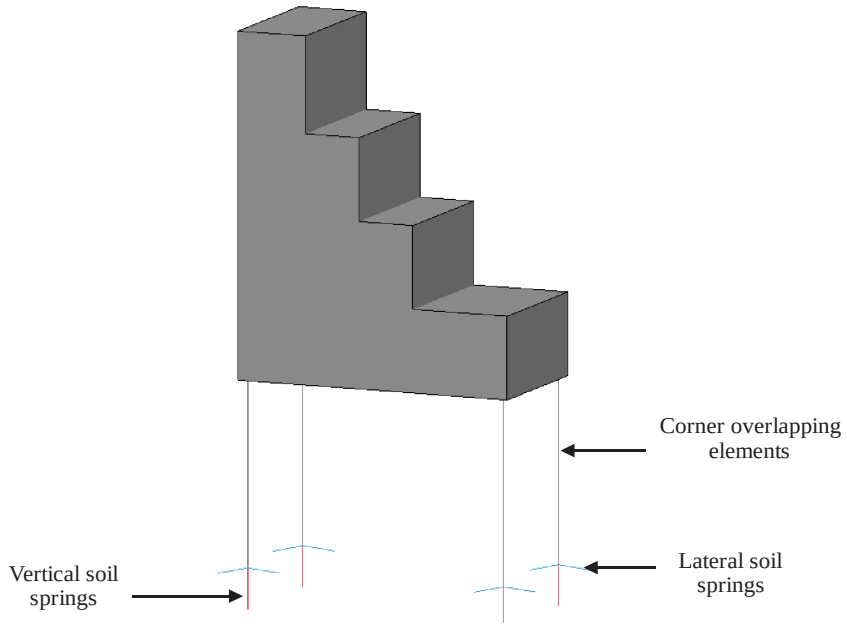

Figure 3.21. Corner overlapping elements modeled as beams every 10 ft.

3.4.3 Pile casing

As previously noted, all timber piles in the MRLD3 model are represented using beam elements. To capture the effect of rock fill interacting with the pile beam elements, four sided hollow ‘contact’ prisms (casings) made up of 1” thick shell elements are modeled to surround each pile node that lies inside the timber cribbing. The size of the prisms is 7.778” x 7.778”, to model a diagonal length of 11”, which when combined with 1” of shell thickness yields an effective diagonal dimension of 12” (the diameter of the timber piles). The ends of the contact prisms are connected to the pile nodes using rigid links (constrained nodal rigid bodies; CNRBs) as shown in Figure 3.22. Each plumb pile contact prism is 16” in length with 2” clear spacing between adjacent prisms and every battered pile contact prism is approximately 18” in length with a clear vertical spacing of 2” between adjacent prisms. Clear spacing between adjacent prisms avoids flexural locking and allows the pile beam elements to bend freely (Figure 3.23). The ability to define contact between shell elements and discrete ‘rock’ elements then makes it possible to simulate rocks interacting with timber piles in the MRLD3 LS-DYNA crib model.

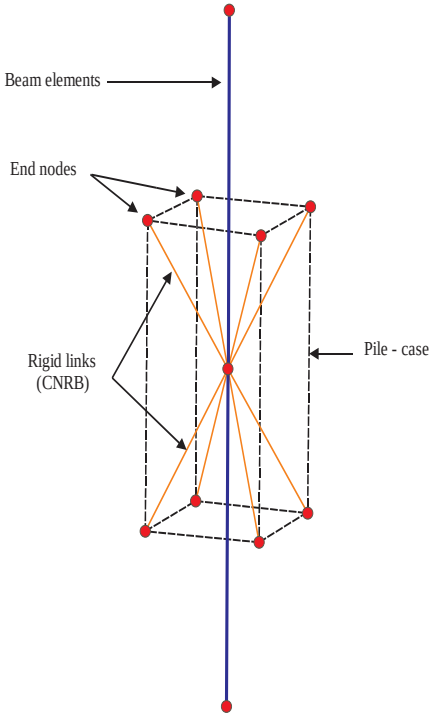

Figure 3.22. Rigid links connecting contact a prism to a pile node

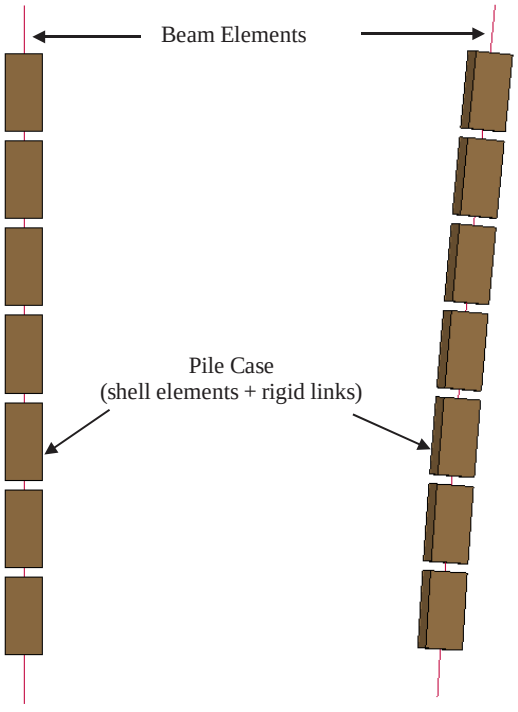

a) b)

Figure 3.23. Pile contact prisms (casing) permit bending of piles:
a) Un-deflected shape; b) Deflected shape

3.4.4 Rock fill

In the finite element model of MRLD3, rock fill inside the cribbing provides lateral stability to the timber piles (by interacting with them through contact) and by shear transfer due to mutual interaction of different layers of rocks. Due to the uncertain state of compaction of the rock fill, the transfer of vertical (gravity) load from the wall to the soil is assumed to take place through axil forces in the piles, and not through the rock fill itself.

As properties of the rock fill are not specified in the as-built MRLD3 wall plans provided by the USACE, basalt fill rock is assumed. Properties of the basalt rock are assumed to be: density = 165 pcf, modulus of elasticity = 7251 ksi, and Poisson's ratio = 0.38. The rocks are modeled in the LS-DYNA MRLD3 model using fully integrated quadratic 8 node solid discrete elements with nodal rotations and a discrete rigid material formulation. Discrete elements (DE) are a mesh-free modeling method, where the physical presence of the elements is represented as spherical elements in LS-DYNA. The spherical presence of discrete elements makes them capable of physically interacting (rolling, sliding, etc.) with each other and surrounding elements (e.g., the timber crib casing elements described earlier).

A sliding coefficient of friction = 0.30 and rolling coefficient of friction = 0.01 are used, along with a damping coefficient of 0.20, to define contact between the discrete elements and the shell elements that represent the timber crib casing and pile casing (i.e., contact prisms). Contact interaction between discrete elements is established by defining control properties for discrete elements.

The maximum opening (gap) between horizontal timbers in the physical cribbing at MRLD3 is 12", hence the discrete elements used to model the rocks must be greater than 12" in diameter. As will be demonstrated in the following section, for reasonable variations in the sizes (diameters) of the discrete elements, there is only moderate effect on the shear resistance of the rock fill. Hence, for computational efficiency, 18" diameter discrete elements are used to model the rocks in the finite element model. The finite element crib model, with discrete elements, timber pile elements, and crib casing elements, is shown in Figure 3.24.

3.4.5 Effects of discrete element size and overburden pressure

To quantify the effects of changes in size of discrete elements, and changes of overburden pressure on the transfer of lateral shear force (and therefore resistance) between layers of discrete rock elements, a sensitivity study is performed. The maximum gap size between horizontal timbers in the timber cribbing at MRLD3 is 12", hence the discrete elements used to model rocks need to be at least 12" or greater size. The sensitivity study thus involves discrete elements of 12" diameter, and 18" diameter, and overburden depths of 9' and 12'. The simulation model (Figure 3.25) used in the sensitivity analyses consists of two containment boxes made of shell elements: a lower box (30' x 25' x 10') and an upper box (20' x 20'). Discrete rock elements of either 12" diameter or 18" diameter are placed into the containment boxes. The depth of the upper box is either 9' or 12' depending upon the overburden depth under investigation. In all simulations, the lower box remains fixed in position, the upper box is subjected to imposed lateral displacement at a rate of 1 in./sec for a total distance of 12", and vertical gravity load is applied to all discrete elements.

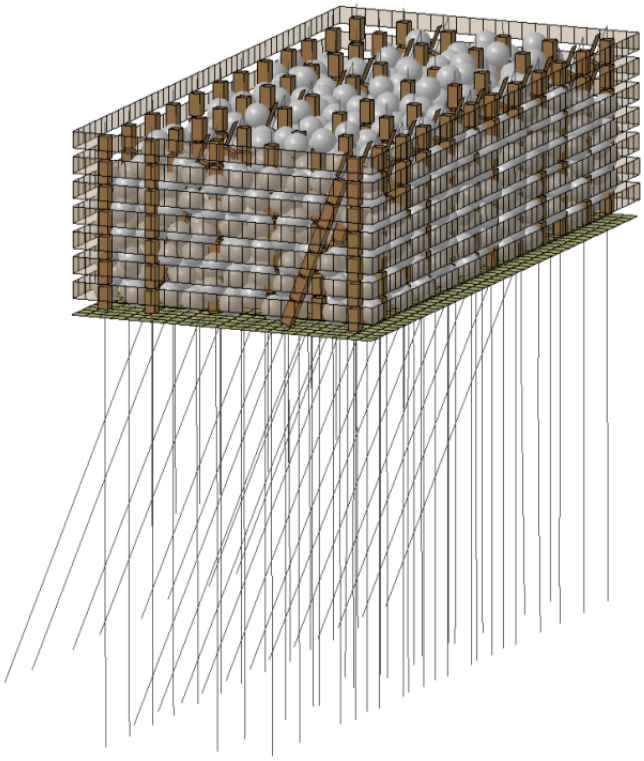

Figure 3.24. Finite element model of MRLD3 crib substructure
(Note: soil springs attached to piles below cribbing are included, but not shown for clarity)

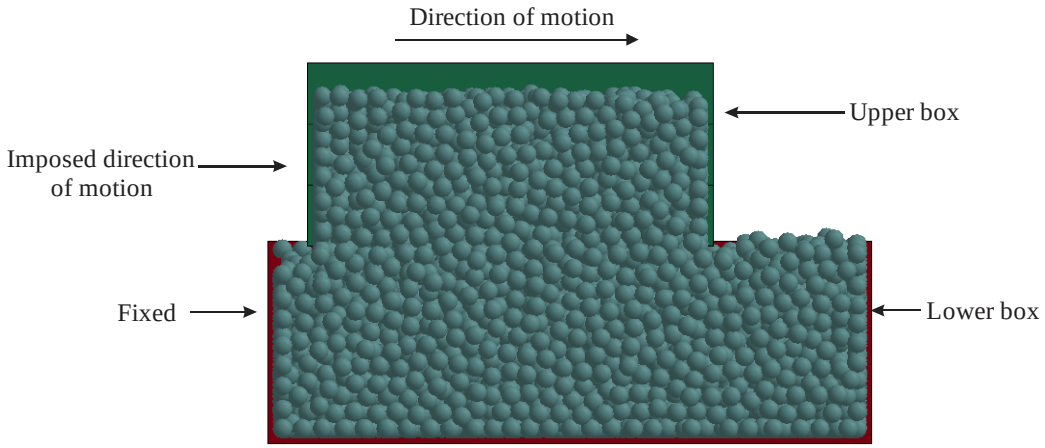

Figure 3.25. Cross-sectional view of shear-box simulation model

As the upper containment box is displaced laterally, the force exerted by discrete elements against the upper box is equal to the shear force exerted between the upper and lower layers of discrete elements. Hence, a lateral force-deformation (resistance) relationship for the discrete elements is determined by pairing lateral force data with corresponding lateral displacement data. By performing this operation for different discrete element sizes and

overburden depths, the sensitivity of the lateral force-deformation relationship to such changes is evaluated for the following conditions:

- Simulation 1: 12 in. diameter discrete elements, 12 ft overburden.
- Simulation 2: 12 in. diameter discrete elements, 9 ft overburden.
- Simulation 3: 18 in. diameter discrete elements, 12 ft overburden.
- Simulation 4: 18 in. diameter discrete elements, 9 ft overburden.

Comparing the total shear force of Simulation 1 against Simulation 3, and Simulation 2 against Simulation 4 reveals that for a given overburden depth, the change in shear force due to change in the size of discrete elements is approximately 10-15%. Hence, it can be assumed that discrete elements of reasonable (for timber cribbing) but somewhat different sizes (with same material properties) will produce similar shear resistances. As illustrated in Figure 3.26 and Figure 3.27, the differences in shear resistances exhibited by 12” and 18” diameter discrete elements is not significant, especially for small displacement levels. Hence, for computational efficiency, 18” diameter discrete elements are used to quantify lateral rock filled crib resistance.

Comparing the total shear force of Simulation 1 against Simulation 2 (Figure 3.28), and Simulation 3 against Simulation 4 (Figure 3.29) indicates that for a given size of discrete elements, an increase in overburden pressure produces a significant increase in total shear force (and therefore the lateral resistance).Thus, in establishing equivalent lateral resistance (force-deformation) curves to represent the effect of rock fill in the overall MRLD3 model, separate curves are computed for each representative depth (and overburden pressure).

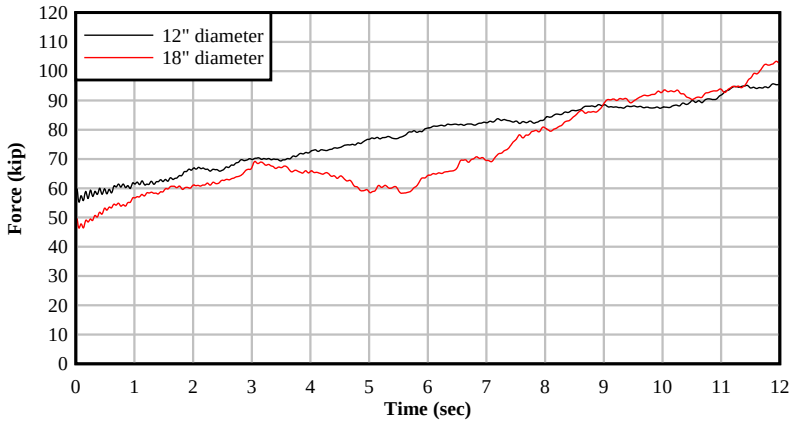

Figure 3.26. Effect of change in discrete element diameter on total shear force for 12’ over-burden pressure

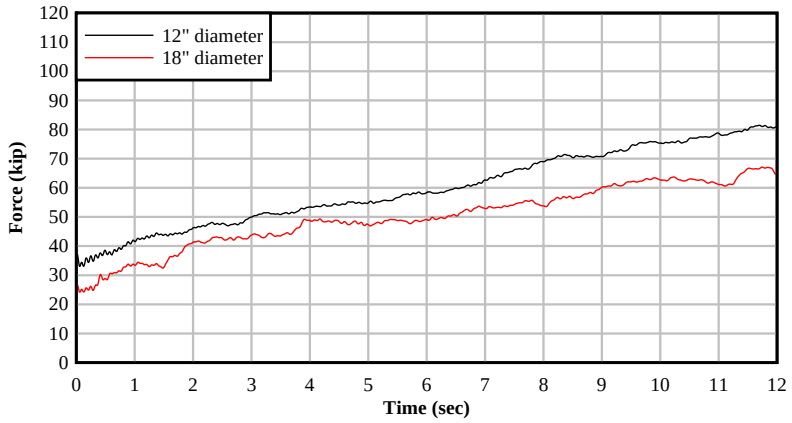

Figure 3.27. Effect of change in discrete element diameter on total shear force for 9’ over-burden pressure

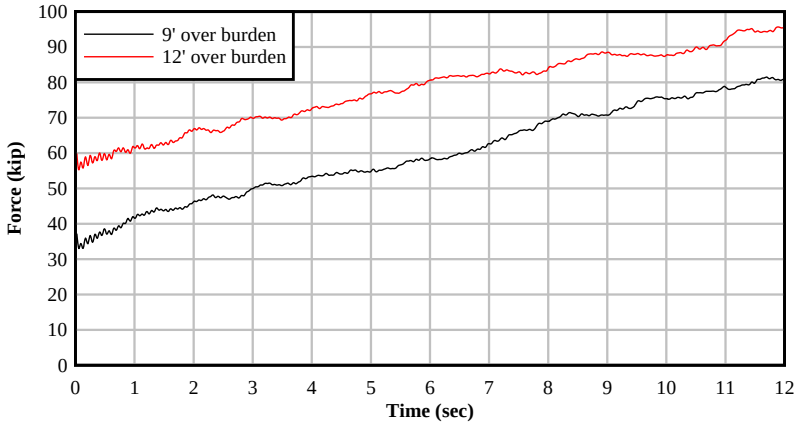

Figure 3.28. Effect of change in overburden depth for 12” diameter discrete elements

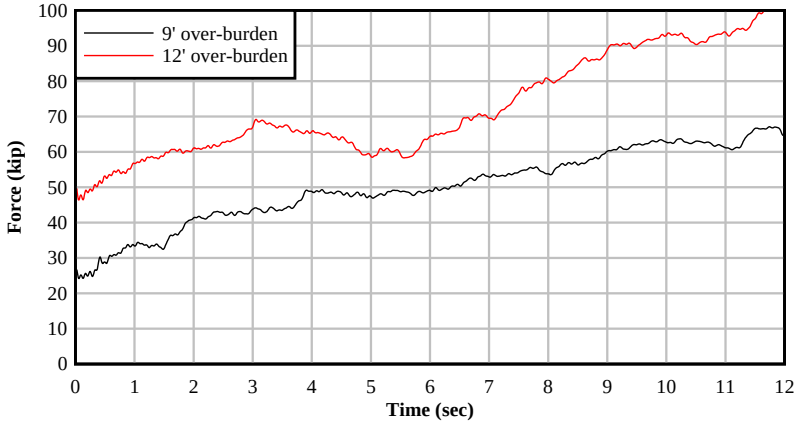

Figure 3.29. Effect of change in overburden depth for 18” diameter discrete elements

3.4.6 Discrete element compaction algorithm

Compaction of discrete elements into the volume enclosed by the timber cribbing at MRLD3 is achieved using the following multiple simulations and data integration steps:

- Generate a model with only the timber crib casing, base confinement, and discrete elements. Discrete elements are placed into a rectangular grid pattern and temporarily given contact parameters representative of water (wet condition), rather than rock, to achieve rapid and maximum compaction.
- Subject the entire crib model to an oscillatory (sine wave) displacement-based 'shaking motion' to encourage the compaction process under simultaneous application of gravity load. Upon completion of the oscillatory compaction simulation, record the final positions of all discrete elements in the model.
- Create a new model with timber crib casing, base confinement, timber piles, pile casing, and discrete elements. Initial positions of discrete elements are taken from the previously noted final positions and the discrete element contact parameters are modified to represent rock properties.
- Initiate a subsequent gravity load analysis on the model and note all discrete elements identified by LS-DYNA as having initial penetrations with the pile casings.
- Create a new model, based on the one noted above, but which excludes discrete elements that were identified as having initial penetration conflicts. Subject the new model to oscillatory (sine wave) displacement-based shaking motions to further compact the discrete elements. On completion of this additional compaction simulation, record the final positions of all discrete elements in the model.

The final model contains discrete elements positioned such that they represent the closest approximation of fully compacted rock fill.

3.4.7 Representing the influence of rock-filled timber cribbing in the MRLD3 model

As noted previously in Section 3.4, the detailed model described above (of the rock filled timber cribbing substructure) is used only as an intermediate step to developing a simplified, more computationally efficient approach to incorporating timber cribbing effects into the overall MRLD3 model (which is used for barge flotilla impact simulations). In the overall model, the effect of the rock filled timber cribbing is represented using a collection of lateral 'rock springs' of equivalent lateral stiffness. The rock springs are in pairs (one spring oriented perpendicular to the guide wall and the other oriented along the guide wall) at every 18" of depth along the piles (within the cribbing region). To develop the rock fill resistance curves that define the rock springs, the process described in the following section is used.

3.4.7.1 Static lateral resistance (stiffness) of rock fill

To generate stiffness (resistance) curves for the rock springs, two distinct pseudo-static lateral displacement simulations are performed on the finite element model shown previously in Figure 3.24, which includes cribbing elements, rock elements, pile elements, and soil spring elements (below the cribbing). Each simulation involves 'shearing' (laterally displacing) the pile head nodes in one particular direction (either perpendicular or parallel to the wall). All pile head

nodes are fixed rotationally to match the fixed connection between timber piles and the concrete guide wall. To simulate lateral movement of the concrete wall perpendicular to its longitudinal axis, all pile head nodes are subjected to an identical imposed linearly increasing perpendicular lateral displacement. As the pile head nodes laterally displace, the pile beam elements deflect laterally inside the volume (and mesh) of the rock filled timber cribbing model. As this process occurs, contact forces are generated between the discrete (rock) elements and the pile (contact) elements; between the discrete elements and the crib mesh; and between adjacent discrete elements. At each pile node elevation, the lateral deflection (displacement) of the piles can be quantified (from the simulation results), as can the force exerted on the pile by the surrounding discrete rock elements. This process is repeated for each level of lateral displacement that is imposed at the tops of the piles (on the pile head nodes). Using the force and lateral deflection data thus collected at each pile node elevation, force-deformation (static resistance) curves for simplified, equivalent rock springs are formed. This process is performed twice—once for lateral pile node displacements perpendicular to the wall, and again for lateral pile node displacements parallel to the wall (along the wall)—such that static resistance rock spring are formed for two orthogonal directions. Example rock fill resistance curves produced in this manner are shown in Figure 3.30 (perpendicular to wall) and Figure 3.31 (parallel to wall).

Using the stiffness curves generated in this manner, non-linear elastic 1-DOF discrete beam elements (i.e., nonlinear spring elements) are installed at each pile node within the cribbing area of the overall MRLD3 model to model the rock fill effect. A typical slice (transverse section) of the MRLD3 model highlighting only the installed rock-springs is shown in Figure 3.32.

To verify that the process of simplifying the rock filled timber cribbing model into an equivalent set of rock springs produces the same lateral resistance, additional pseudo-static simulations are performed. A model consisting of pile (beam) elements, attached rock springs, and attached soil springs (below the bottom elevation of the cribbing) is subjected to lateral shearing deformation (displacement) at the pile head nodes once in the direction perpendicular to the wall and once parallel to the wall. Reviewing results from such simulations reveals that the total shear resistance of the simplified model at any given depth is in close agreement with the total shear resistance of the discrete element rock filled timber cribbing model (at the same depth).

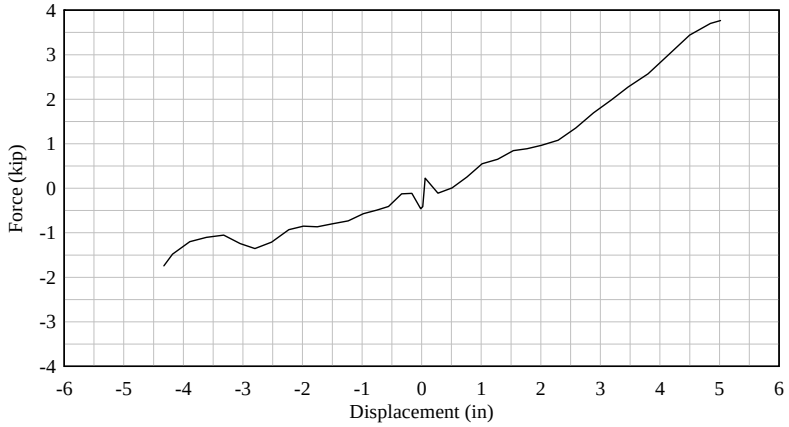

Figure 3.30. Rock fill static resistance curve
(Direction = perpendicular to wall; Overburden depth = 126 in.)

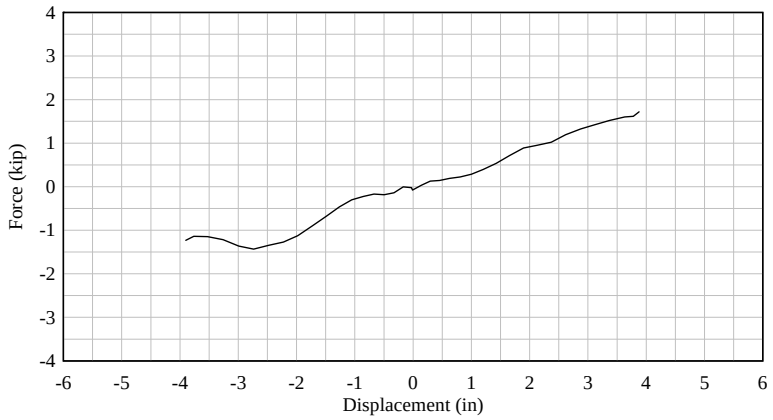

Figure 3.31. Rock fill static resistance curve
(Direction = parallel to wall; Overburden depth = 126 in.)

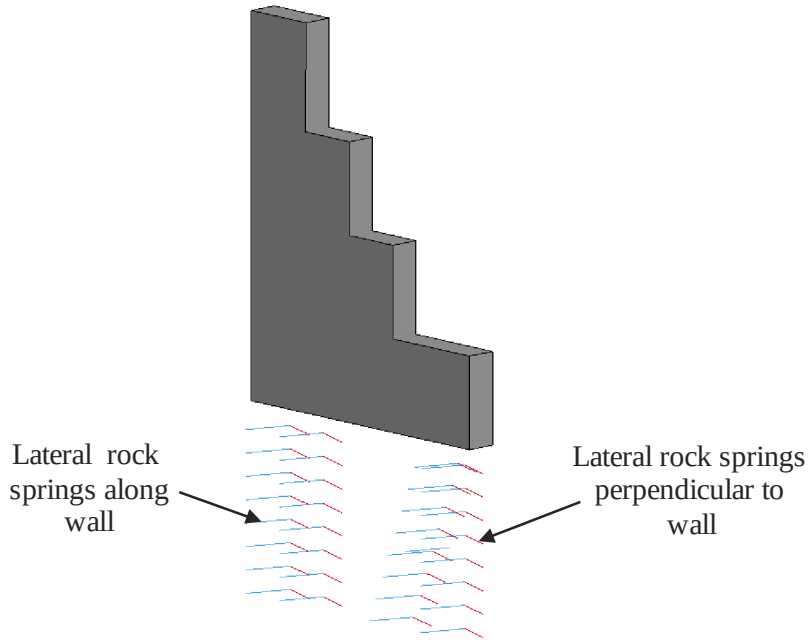

Figure 3.32. Rock springs installed at each pile node in a slice of the overall MRLD3 model

3.4.7.2 Mass of rock fill

To approximately represent the influence rock fill *mass* has on the response of the overall MRLD3 model (in which the discrete rock elements are not included), the total mass of the rock fill is distributed to all pile nodes that lie within the volume associated with the timber crib. At each such node, a concentrated mass is added based on the tributary volume of rock (and volume averaged rock density) that is associated with that particular pile node. Note that concentrated rock masses added in this manner are in addition to the mass contributed by the timber pile elements themselves.

3.5 External loading of pile-founded guide wall models

In all MRLD2 and MRLD3 impact simulations performed in this study, the effects of both gravitational and buoyancy forces are included. Prior to initiating an impact simulation, in which the barge flotilla is prescribed an initial velocity, the integrated flotilla-guide wall model undergoes a gravity calibration simulation. This 'initialization simulation' is performed to achieve static equilibrium under self-weight (gravity) load and buoyant uplift pressure. Details regarding the application of gravity and buoyancy during the initialization simulation are discussed below.

3.5.1 Gravity loading

Gravity loading is applied to each model in such a way that equilibrium is achieved prior to initiating the impact simulation. Specifically, gravitational (self-weight) loading is applied to all structural elements in the model in an instantaneous and constant manner. The gravity initialization simulation takes place over a time span of one second of simulation time, which is sufficient for the integrated (merged) barge and pile founded guide wall models to reliably reach static equilibrium under gravity and buoyancy loads. With the aid of global critical damping, the computational cost of reaching static equilibrium is minimized, i.e. the merged barge pile founded guide wall models reach static equilibrium under gravity loading in an efficient manner. Gravity loads, buoyant uplift loads, and critical damping (for the first 0.99 seconds) are applied as constant values before the point of barge impact (t = 0.0 sec.). Critical damping is applied to the flotilla model and pile founded guide wall model separately, and is removed from both prior to completion of the initialization simulation at 0.99 seconds. From 0.99 to 1.00 seconds, the flotilla model and pile founded guide wall model remain in their equilibrium positions, without the presence of critical damping.

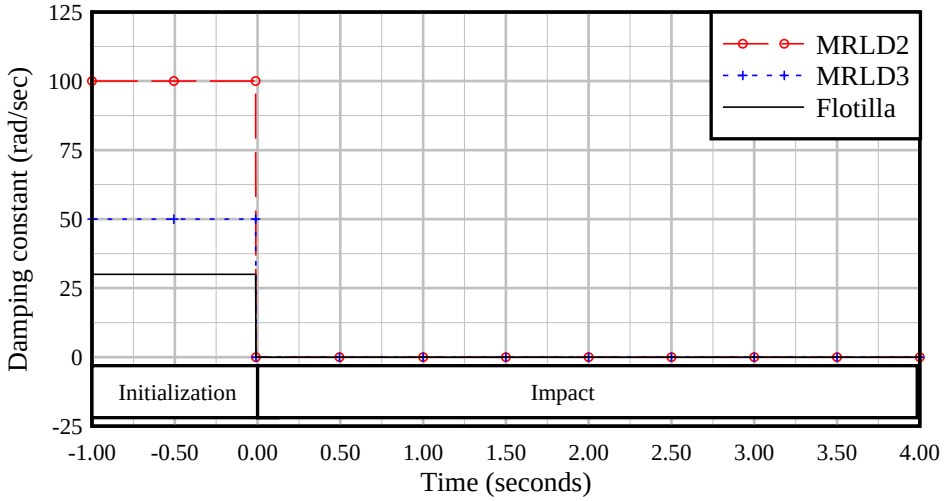

Figure 3.33. Application of damping during initialization simulation of finite element models

3.6 Barge flotilla and pile founded guide wall contact-impact loading

Integrating (merging) barge flotilla and pile founded guide wall models requires defining contact between the impacting barge and the pile founded guide wall. From this contact definition, force-time histories of barge impact load can be quantified. Because interaction between the flotilla and the pile founded guide wall models is limited to the starboard bow corner of the deformable barge ('contacting barge') and to a portion of the vertical face of the concrete wall (Figure 3.34), computational efficiency is gained by limiting contact definition references to the portions of the deformable barge and guide wall that can potentially come into contact. Specifically, contact between the barge and pile founded guide wall is defined with a set of nodes in the deformable region of the starboard bow corner of the impacting barge and a set of segments along the lower portion of the vertical face of the pile founded guide wall model. In accord with literature and previous barge-impact studies (Consolazio et al. (2010), Consolazio et al. (2012), Consolazio and Walters (2012), and Consolazio and Wilkes (2013)) static and dynamic coefficients of friction (μ) between the steel barge and concrete wall are assigned values of 0.50 and 0.45, respectively.

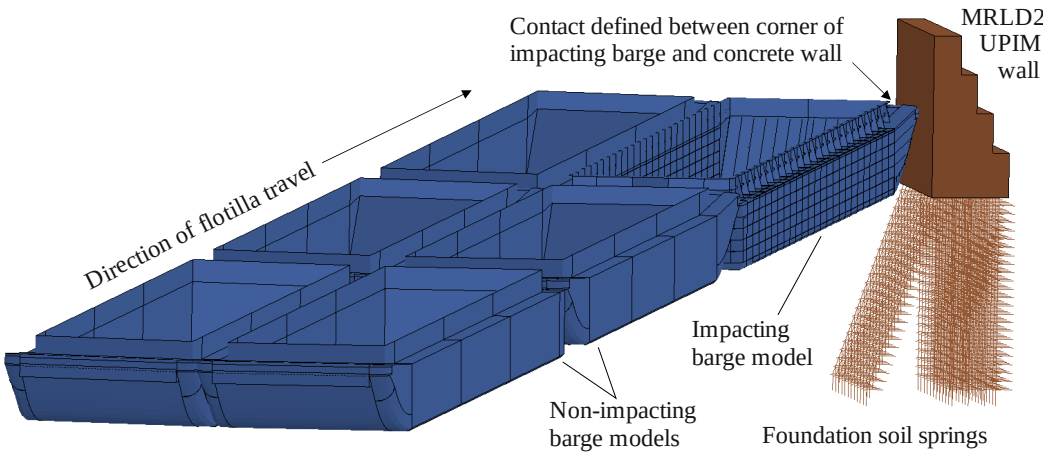

Figure 3.34. Contact between a 2x3 barge flotilla and the MRLD2 upper pool interior monolith (UPIM) finite element model

Since pile founded guide wall monoliths (MRLD2 and MRLD3) are laterally stiffest when impacted near mid-span, the barge flotilla model in each impact simulation near the mid span location. A review of multiple impact simulations conducted on pile founded guide wall monoliths—at varying speeds and angles— revealed that maximum impact forces (normal to the wall) occurred approximately 2'-0" downstream (in the longitudinal direction) from the initial point of barge contact on the wall. Hence, in each simulation, the barge flotilla model is positioned to make initial contact with the wall at approximately 2'-0" *upstream* from the mid-span of the impacted monolith, such that maximum force will be applied to the wall at approximately the mid-span location.

CHAPTER 4
DETERMINATION OF IMPACT FORCES ON PILE-FOUNDED GUIDE WALLS

4.1 Introduction

To quantify barge impact loads on pile-founded guide walls, the MRLD2 and MRLD3 guide wall models discussed in Chapter 3 are merged together with four different barge flotilla configurations to form integrated barge-guide wall impact models. In total, 57 dynamic barge impact simulations are conducted on MRLD2 (Table 4.1) and 14 dynamic barge impact simulations are conducted on MRLD3 (Table 4.2). The selected impact conditions are based on typical operational velocities near lock structures and practical approach angles, as noted by the USACE. Impact conditions considered in the MRLD2 and MRLD3 parametric studies cover angles of obliquity (Figure 4.1) (θ) ranging from 5° to 25° and impact velocities (V_0) ranging from 1 FPS to 6 FPS.

Based on previous studies of oblique barge impacts on wall structures (Consolazio and Walters 2012, Consolazio and Wilkes 2013), it is expected that the momentum of the lead row of the impacting barge flotilla will have the greatest effect on the peak impact forces generated. Four (4) distinct barge flotilla configurations are thus used in the present study to determine if the same trends hold true for pile founded guide walls:

- 1x3 : Single (1) string, three (3) barges long
- 2x3 : Two (2) strings, each three (3) barges long
- 3x3 : Three (3) strings, each three (3) barges long
- 3x5 : Three (3) strings, each five (5) barges long

For the configurations with three (3) strings, the total barge flotilla width is 105'. However, navigable width of the locks at MRLD2 and MRLD3 is restricted to 110'. Due to this physical restriction, it is highly unlikely for a barge flotilla with three (3) strings to impact the guide walls at 20° or 25°. Hence, impact studies for larger angles of obliquity are restricted only to one string and two string barge flotilla models.

4.1.1 Selection of additional impact conditions for parametric studies

In addition to impact speed, impact angle, and flotilla configuration, several additional factors have the potential to influence computed barge impact forces. Among these are: the guide wall-to-pile connection (fixed or pinned); the presence of backfill soil behind the wall; the barge impact elevation on the wall; and the presence of adjacent monoliths. Since it is impractical to conduct parametric studies that include all possible combinations of these factors as well as the previously noted impact condition parameters (impact speed, angle, flotilla size), a separate series of limited-scope sensitivity studies are performed to identify parameter selections that lead to reasonably conservative predictions of impact force. These sensitivity studies are documented in Appendix D, and are conducted primarily using the MRLD2 wall model.

Table 4.1 MRLD2 impact conditions and results

Flotilla Size	Impact Speed (V_0)	Impact Angle On Wall (θ)	Impact Force (kip)
1 x 3	1 FPS	5°	29
1 x 3	2 FPS	5°	70
1 x 3	4 FPS	5°	130
1 x 3	1 FPS	10°	84
1 x 3	2 FPS	10°	145
1 x 3	6 FPS	10°	343
1 x 3	1 FPS	15°	114
1 x 3	2 FPS	15°	225
1 x 3	4 FPS	15°	357
1 x 3	1 FPS	20°	163
1 x 3	2 FPS	20°	290
1 x 3	4 FPS	20°	424
1 x 3	1 FPS	25°	169
1 x 3	2 FPS	25°	300
1 x 3	4 FPS	25°	439
1 x 3	6 FPS	25°	523
2 x 3	1 FPS	5°	39
2 x 3	2 FPS	5°	73
2 x 3	4 FPS	5°	149
2 x 3	1 FPS	10°	105
2 x 3	2 FPS	10°	190
2 x 3	6 FPS	10°	388
2 x 3	1 FPS	15°	154
2 x 3	2 FPS	15°	281
2 x 3	4 FPS	15°	417
2 x 3	1 FPS	20°	212
2 x 3	2 FPS	20°	360
2 x 3	4 FPS	20°	496
2 x 3	1 FPS	25°	155
2 x 3	2 FPS	25°	216
2 x 3	4 FPS	25°	314
3 x 3	1 FPS	5°	61
3 x 3	2 FPS	5°	126
3 x 3	4 FPS	5°	222
3 x 3	1 FPS	10°	146
3 x 3	2 FPS	10°	256
3 x 3	4 FPS	10°	379
3 x 3	6 FPS	10°	443
3 x 3	1 FPS	15°	228
3 x 3	4 FPS	15°	494
3 x 3	6 FPS	15°	596
3 x 3	4 FPS	20°	621
3 x 3	6 FPS	20°	786
3 x 3	8 FPS	20°	814
3 x 3	4 FPS	25°	751
3 x 3	6 FPS	25°	886
3 x 3	8 FPS	25°	902
3 x 5	1 FPS	5°	62
3 x 5	2 FPS	5°	128
3 x 5	4 FPS	5°	227
3 x 5	1 FPS	10°	147
3 x 5	2 FPS	10°	259
3 x 5	4 FPS	10°	382
3 x 5	6 FPS	10°	446
3 x 5	1 FPS	15°	229
3 x 5	4 FPS	15°	496
3 x 5	6 FPS	15°	596

Table 4.2 MRLD3 impact conditions and results

Flotilla Size	Impact Speed (V_0)	Impact Angle On Wall (θ)	Impact Force (kip)
1 x 3	2 FPS	5°	93
1 x 3	4 FPS	20°	421
1 x 3	6 FPS	25°	608
2 x 3	6 FPS	10°	358
2 x 3	4 FPS	15°	381
2 x 3	4 FPS	20°	468
2 x 3	4 FPS	25°	530
3 x 3	6 FPS	10°	364
3 x 3	4 FPS	15°	399
3 x 3	6 FPS	15°	478
3 x 5	2 FPS	5°	177
3 x 5	4 FPS	5°	164
3 x 5	6 FPS	10°	423
3 x 5	6 FPS	15°	478

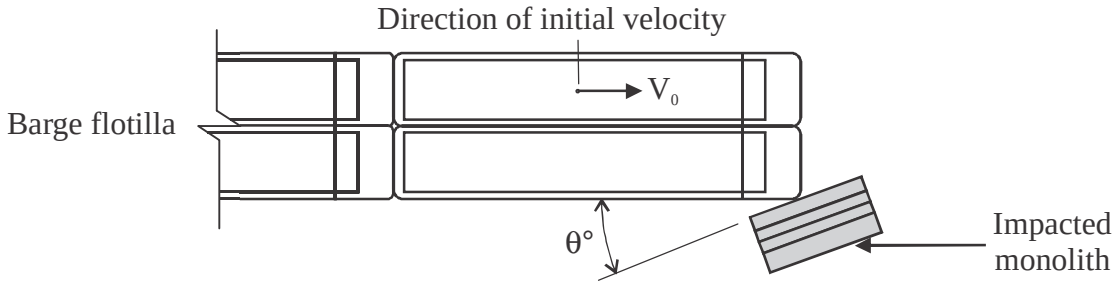

a)

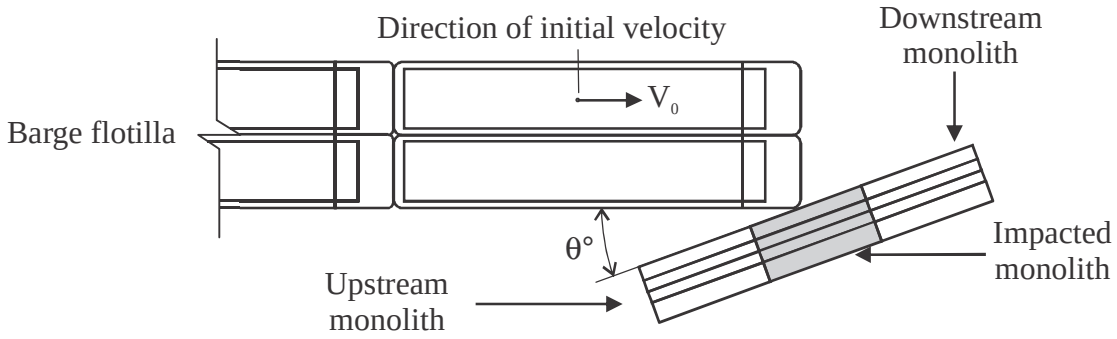

b)

Figure 4.1. Impact conditions:
a) MRLD2; b) MRLD3

Based on results obtained from the limited-scope sensitivity studies, the primary parametric studies (Table 4.1 and Table 4.2) for MRLD2 and MRLD3 are conducted with the following constant parameter selections:

- 'Fixed-head' pile-to-wall connections (see Appendix D.1)
- No backfill soil present (see Appendix D.2)
- Impact elevation based on lowest water pool elevation (see Appendix D.3)
- Single (1) monolith included in the MRLD2 model (see Appendix D.4)
- Three (3) monoliths included in the MRLD3 model (see Appendix D.5)
- Initial impact point ~2' upstream from mid-span of impacted monolith

Sensitivity studies carried out for MRLD2 (Appendix D.4) indicate that the presence of adjacent monoliths has negligible influence on peak impact forces and hence all primary impact simulations for MRLD2 (Table 4.1) are carried out using single monolith models. In contrast, sensitivity studies conducted on MRLD3 using one (1) and three (3) monolith models indicate that the presence adjacent monoliths has a *non-negligible* influence on computed impact forces. Due to the flexibility of the rock-filled timber cribbing present in the MRLD3 model, the lateral restraint provided to the impacted monolith by adjacent monoliths (through frictional forces) has a significant influence on wall response and therefore on the impact force generated. As a result, maximum (conservative) impact forces are computed when adjacent monoliths are present in the MRLD3 model. Consequently, all primary impact simulations on MRLD3 (Table 4.2) are conducted with three (3) monolith models—an impacted monolith, and adjacent upstream and downstream monoliths.

4.2 Impact force results

All time-varying impact forces presented in this report are dynamic contact forces between the high-resolution deformable barge model and the concrete guide wall model. Horizontal forces are resolved into the direction *normal to* (perpendicular to) the guide wall structure. Furthermore, all results are low-pass filtered at approximately 10 Hz so the force-time histories presented are not unduly influenced by higher frequency oscillations that may be present in the finite element analysis results. The focus of this study is to quantify peak (maximum) barge impact forces (Table 4.1 and Table 4.2) for varying impact conditions. For the MRLD2 wall, peak impact forces occur within the first several load pulses, therefore the impact simulations for all MRLD2 parametric studies are terminated after three to four pulses; or after complete loss of contact with the wall; or after a total impact duration of 3.5 seconds. For the MRLD3 wall, peak impact forces nearly always occur during the first load pulse, therefore most MRLD3 impact simulations are terminated after two load pulses (the second pulse being included to confirm a reduction in force relative to the first pulse).

4.2.1 Typical MRLD2 results

In Figure 4.2, a typical force-time history for a barge flotilla impact on the MRLD2 guide wall is presented. The specific impact condition—i.e., flotilla size, impact speed, and angle, and structure—presented in the figure is: 2x3 – 4 FPS – 20° – MRLD2. Several important characteristics of the time-varying impact force, flotilla motion, flotilla deformation, and wall response are worth describing. Most obvious, the force-time history consists of several (four in

this case) distinct ‘pulses’ of impact force, which are separated by periods of zero impact force, and which decay in magnitude through time. The first pulse is of particular importance because it: 1) is where the overall maximum (peak) impact force occurs; 2) has separate, identifiable characteristics associated with mass-related and stiffness-related sources of wall resistance; and 3) possesses a characteristic that will be shown (later) to be missing from the MRLD3 impact data.

During a flotilla impact on a *non-rigid* wall, several distinct sources of stiffnesses affect the impact forces generated: 1) lateral wall stiffness; 2) bending (flexural) stiffness of the barge flotilla; and 3) crushing stiffness of the impacting barge bow corner. Similarly, several masses also influence impact forces: 1) mass of the wall; 2) mass (and therefore momentum) of the lead row of barges in the flotilla; and 3) mass (and rotary inertia) of trailing barge rows in the flotilla. Examining Figure 4.2, two ‘local’ force maxima are evident in the first force pulse: an initial maximum at approximately t = 0.2 sec., and a second slightly larger maximum at approximately t = 0.4 sec. Note that the second maximum is also the *overall* maximum force (peak force) for the entire impact event, and corresponds to the 496 kip impact force reported in Table 4.1 for condition 2x3 – 4 FPS – 20°.

Importantly, the *initial* local maximum in Figure 4.2 relates strongly to the *mass-related inertial resistance* of the wall. Due to the large volume of concrete contained within each MRLD2 monolith, the structure possesses substantial weight and mass. Initially, this mass is stationary (i.e., at rest). Laterally accelerating and displacing the wall monolith thus requires substantial impact force. In Figure 4.2, the initial force spike (at t = 0.2 sec) is primarily related to the process of accelerating the wall mass and overcoming its *inertial* (mass-related) resistance. Note that the lateral *displacement* of the wall (Figure 4.3) at this same point in time is only half of the maximum level that will eventually be reached, therefore resistance force associated with wall *stiffness* (lateral pile and soil stiffness) is *secondary* in comparison to the *primary* mass-related inertial resistance.

After the local force maximum at t = 0.2 sec, lateral acceleration and displacement of the wall, together with the initiation of flexing of the barge flotilla, momentarily reduce the magnitude of impact force (Figure 4.2). However, with continued longitudinal travel of the barge flotilla toward the wall, the impact force rises again, reaching the second maximum level at t = 0.4 sec. Just prior to this point in time, lateral displacement of the wall maximizes (Figure 4.3), thus also maximizing stiffness related resistance force. Therefore, for MRLD2, the overall maximum force generated by barge flotilla impact is related primarily to wall stiffness, and secondarily to wall mass. Additionally, as Figure 4.2 indicates, the *overall maximum* impact force occurs during the *first impact pulse*; all subsequent pulses are all of smaller magnitude.

In Figure 4.4, the deformed shape of the barge flotilla at various stages of impact is illustrated (with displacements magnified by ten (10) to aid in visual interpretation). It is noteworthy that during the first impact pulse, when the maximum impact force is generated, flexural deformation of the flotilla *only* involves rotation of the *lead row of barges*. Due to the rotary inertia (mass-related rotational inertia) of the trailing rows and the flexibility of the wire rope lashings, barges in the trailing rows remain un-rotated during the first load pulse. This phenomenon is consistent with previous studies of oblique flotilla impacts on wall structures (Consolazio and Walters 2012, Consolazio and Wilkes 2013) and suggests that the mass (and momentum) of the *lead row* of barges—rather than the mass (and momentum) of the entire flotilla—is most important in terms of predicting maximum impact forces. (This assertion will be confirmed quantitatively later in this chapter).

As a result of impact force generated on the barge bow during pulse 1, and flexing of the barge flotilla, the flotilla and wall temporarily separate for a short period of time during which the impact force is zero (Figure 4.2). However, with continued longitudinal travel, the lead barge once again makes contact with the wall and a second pulse of impact force is generated. This second pulse, however, is smaller in magnitude than the first pulse due to both energy dissipation and a slight reduction in impact angle that occurs due to barge flotilla rotation. During the second load pulse, both the lead row of barges and the second row of barges rotate (Figure 4.4) relative to the trailing row.

As Figure 4.2 and Figure 4.4 illustrate, multiple impacts of decaying magnitude continue to repeat until the entire flotilla has been redirected and the impact event is complete.

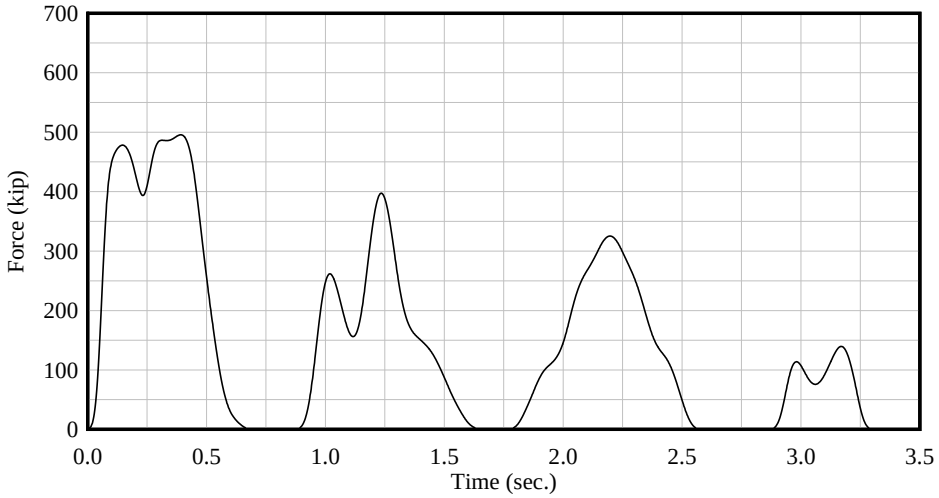

Figure 4.2. Force-time history for 2x3 – 4 FPS – 20° – MRLD2

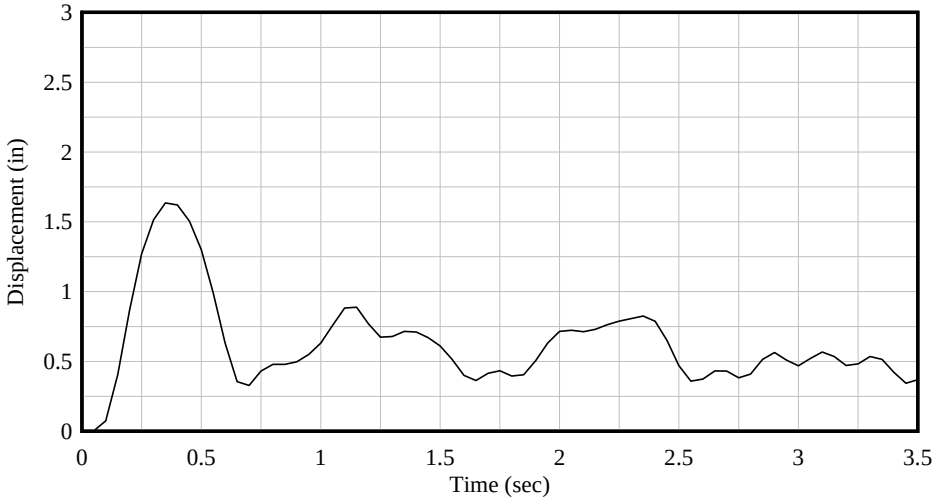

Figure 4.3. Displacement-time history for 2x3 – 4 FPS – 20° – MRLD2

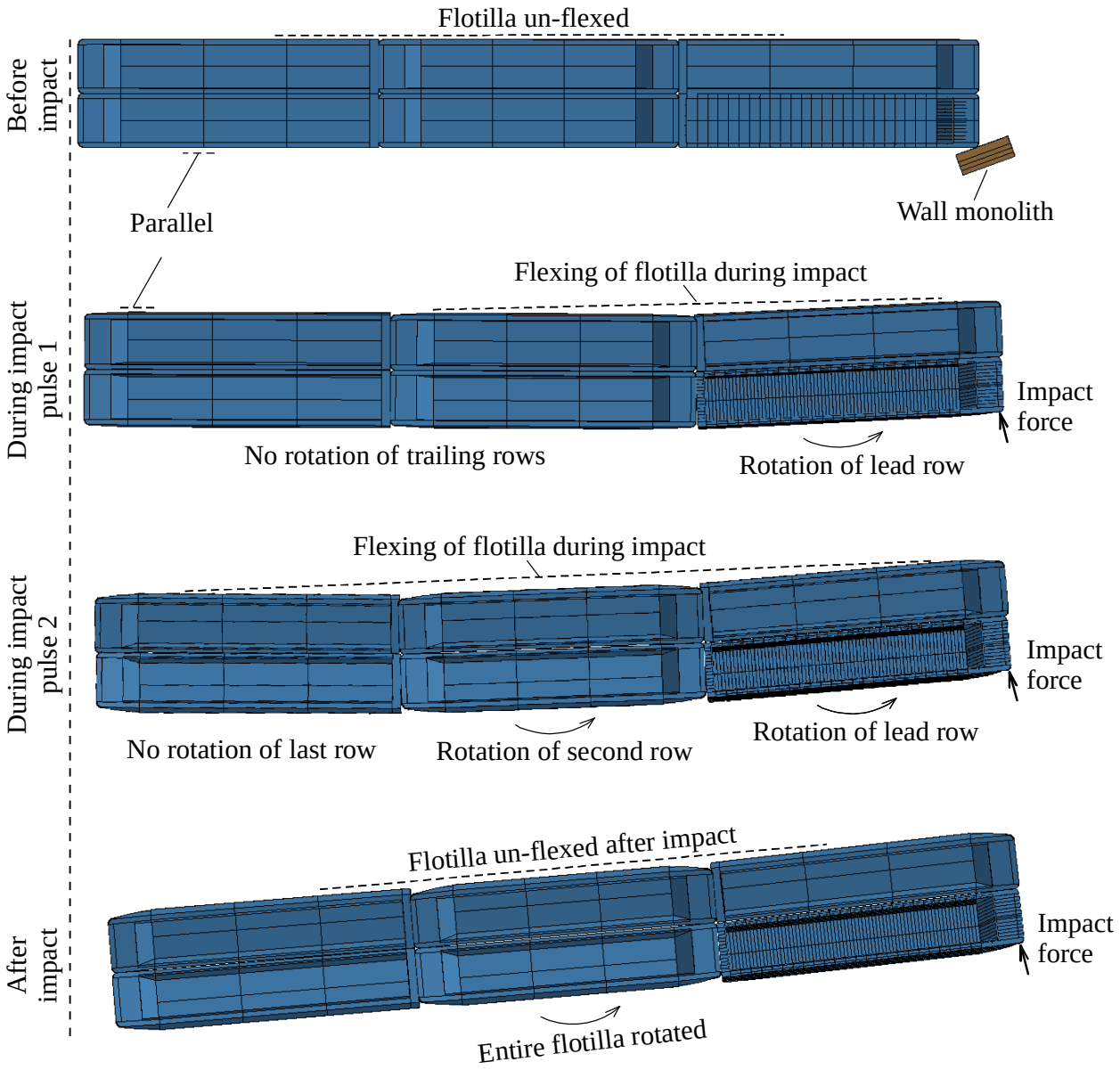

Figure 4.4. Flexing of barge flotilla during impact on MRLD2 wall
(Note: displacements magnified by 10 to aid in visualization
of flotilla deformation and rotation)

4.2.2 Typical MRLD3 results and influence of rock-filled timber cribbing

As discussed in Chapter 3, the MRLD3 structure differs primarily from MRLD2 in that the MRLD3 wall sits atop a 12 ft height of rock-filled timber cribbing which significantly decreases its lateral stiffness (or increases its flexibility) relative to MRLD2. However, what the structures have in common is that both make use of large-volume concrete walls that are very substantial in mass (and weight). To illustrate how these differences and similarities affect forces generated during barge flotilla impacts, the MRLD3 model is subjected to the same impact condition (2x3 – 4 FPS – 20°) as that discussed above for the MRLD2 structure.

In Figure 4.5, the impact force-time history for case 2x3 – 4 FPS – 20° – MRLD3 is presented. In comparison to the corresponding force-time history for MRLD2 (Figure 4.2), several similarities are evident: the maximum impact force occurs during the first impact pulse; the impact force pulses generally decay in magnitude; and the impact pulses are separated by short periods of non-contact (zero force) between barge and wall. To directly compare the MRLD3 and MRLD2 impact force data, both cases are presented together in Figure 4.6.

It very noteworthy that despite the fact that MRLD3 is far less stiff (more flexible) than MRLD2, the maximum impact force for MRLD3 is nearly identical to the initial 'local' maximum force for MRLD2. Based on the discussion provided in the previous section (for MRLD2), this outcome is to be expected. Since the initial maximum impact force is related to *mass-related inertial resistance* of the walls (rather than stiffness based resistance), and since both walls make use of very large-mass concrete monoliths, the magnitudes of the initial maximum impact forces are virtually the same.

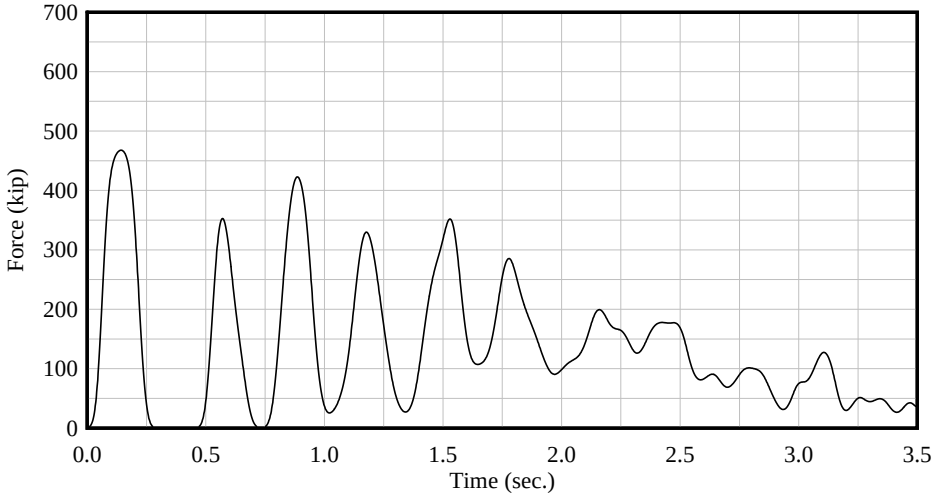

Figure 4.5 Force-time histories for 2x3 – 4 FPS – 20° – MRLD3

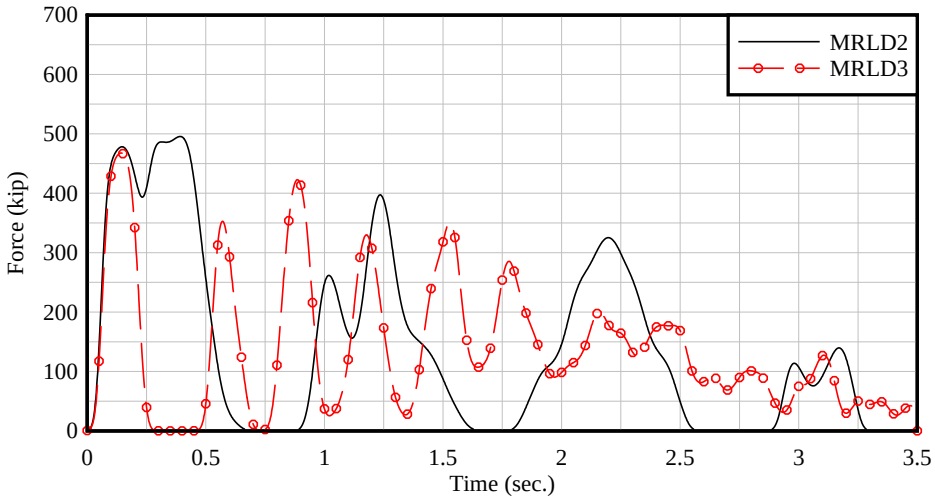

Figure 4.6. Force-time histories for 2x3 – 4 FPS – 20° – MRLD2 and 2x3 – 4 FPS – 20° – MRLD3 compared

However, also evident in Figure 4.6 is the fact that the different wall stiffnesses lead to different impact forces *after* the initial peak. As described in the previous section, wall stiffness—not mass—is primarily responsible for the continued increase in force—to the second (and overall) maximum—that is observed in MRLD2 case. In contrast, no such subsequent rise of impact force is observed in the MRLD3 case. Instead, due to the reduced stiffness of the rock-filled timber cribbing, the MRLD3 wall displaces laterally away from the barge until contact is lost, and the impact force reduces to zero. Given a sufficient period of time and continued flotilla travel, the barge flotilla once again impacts the wall, causing a second force pulse, the magnitude of which is *again* primarily related to the mass—not the stiffness—of the wall. This process repeats itself with moderate energy dissipation during each impact, and consequently gradually decaying pulse magnitudes.

In Table 4.3, maximum MRLD2 and MRLD3 impact forces are compared for a variety of different impact conditions. Consistent with Figure 4.6, in most cases, the MRLD2 impact forces are larger than the corresponding MRLD3 forces. In general, for moderate to high-energy impact conditions, maximum MRLD2 impact forces are 10 - 20% larger than corresponding MRLD3 forces. It must be noted, however, that for select low-energy impacts (small angle of obliquity and low impact velocity), maximum MRLD3 forces are instead larger than the MRLD2 forces. For such conditions, lateral wall displacements are minimal which leads to reduced stiffness-based resistance and a greater contribution from mass-based inertial resistance. Since the mass of the three (3) monolith MRLD3 wall model is greater than that of the single (1) monolith MRLD2 model, the MRLD3 model yields impact forces that are somewhat larger for these low energy cases.

Table 4.3 Comparison of maximum MRLD2 and MRLD3 impact forces

Impact condition	Peak normal impact force on MRLD2 (kip)	Peak normal impact force on MRLD3 (kip)	% by which MRLD2 force is greater than MRLD3 force
1x3 - 5° - 2 FPS	70	93	-32.9
1x3 - 20° - 4 FPS	424	421	0.7
1x3 - 25° - 6 FPS	523	608	-16.3
2x3 - 10° - 6 FPS	388	358	7.7
2x3 - 15° - 4 FPS	417	381	8.6
2x3 - 20° - 4 FPS	496	468	5.7
2x3 - 25° - 4 FPS	314	530	-68.8
3x3 - 10° - 6 FPS	443	364	17.8
3x3 - 15° - 4 FPS	494	399	19.2
3x3 - 15° - 6 FPS	596	478	19.8
3x5 - 5° - 2 FPS	128	177	-38.3
3x5 - 5° - 4 FPS	227	164	27.8
3x5 - 10° - 6 FPS	446	423	5.2
3x5 - 15° - 6 FPS	596	478	19.8

4.3 Impact force sensitivity to number of barge strings and number of barge rows

As noted earlier, previous studies of oblique flotilla impacts on other types of wall structures (Consolazio and Walters 2012, Consolazio and Wilkes 2013) have revealed that the mass (and momentum) of the *lead row* of barges—rather than the mass (and momentum) of the entire flotilla—is most important in terms of predicting maximum impact forces. In the present

study, results such as those shown above in Figure 4.2 and Figure 4.4 suggest the lead row momentum phenomenon likely applies to pile founded guide wall structures as well. To quantitatively establish whether this is the case, the sensitivities of maximum impact forces to flotilla size (number of strings and number of rows) are investigated for several cases using the MRLD2 wall model.

The sensitivity of impact forces to the number of barge rows—either 3 or 5—present in the impacting flotilla is illustrated in Figures 4.7 and Figure 4.8. Each plot compares force levels (normal to the wall) produced by impact conditions that are identical in every way except in the number of barge rows. It is important to note that 3x3 and 3x5 flotillas differ *significantly* in total mass (and total momentum), but not at all in lead row mass (and lead row momentum). Figures 4.7 and Figure 4.8 reveal that flotillas of differing total mass, but equal lead row mass, produce maximum impact forces that are nearly identical.

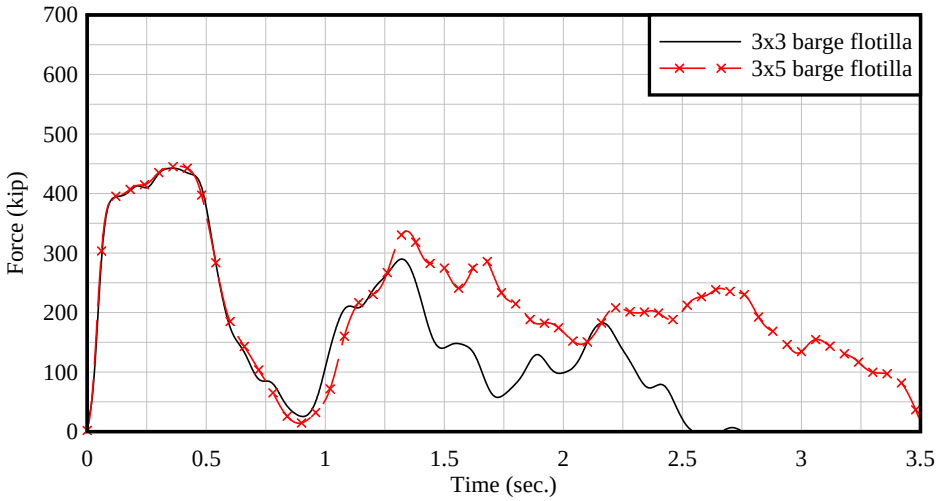

Figure 4.7. Sensitivity to number of rows: 3 strings x [3, 5] rows – 6 FPS – 10° – MRLD2

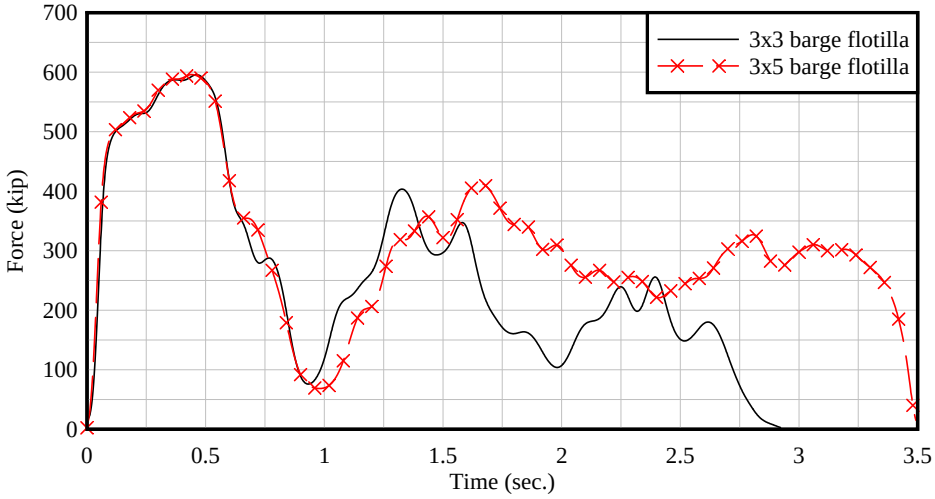

Figure 4.8. Sensitivity to number of rows: 3 strings x [3, 5] rows – 6 FPS – 15° – MRLD2

To confirm that changing the mass of the lead row, by changing the number of strings in the flotilla, changes the maximum impact forces, the sensitivity of impact forces to the number of barge strings—either 1, 2, or 3—is illustrated in Figures 4.9 and Figure 4.10. Each plot compares force levels produced by impact conditions that are identical in every way except in the number of barge strings (and therefore lead row mass). Evident from these figures is the fact that changing the lead row mass produces significant changes of maximum impact force. Therefore, taken collectively, the results presented in Figure 4.7 – Figure 4.10 quantitatively confirm that lead row mass and momentum—rather than total flotilla mass and momentum—are the strongest predictors of maximum impact force for pile founded guide walls similar to MRLD2.

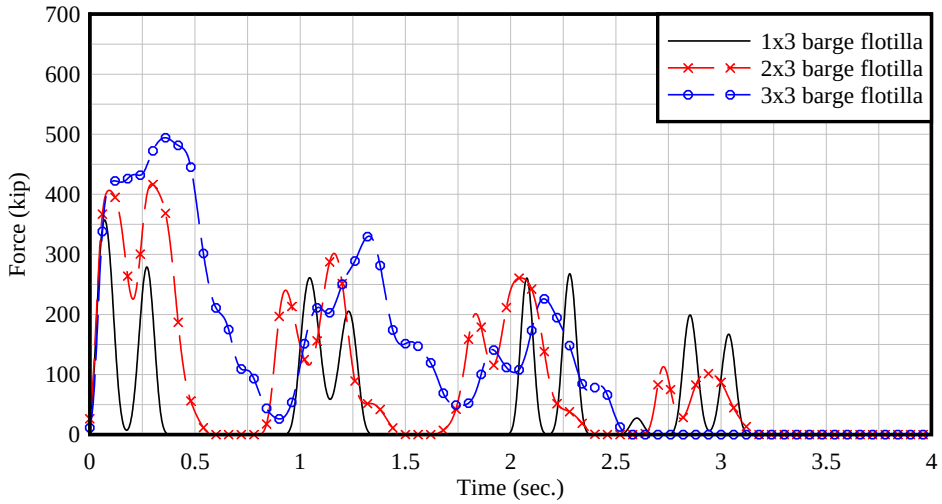

Figure 4.9. Sensitivity to number of strings: [1, 2, 3] strings x 3 rows – 4 FPS – 15° – MRLD2

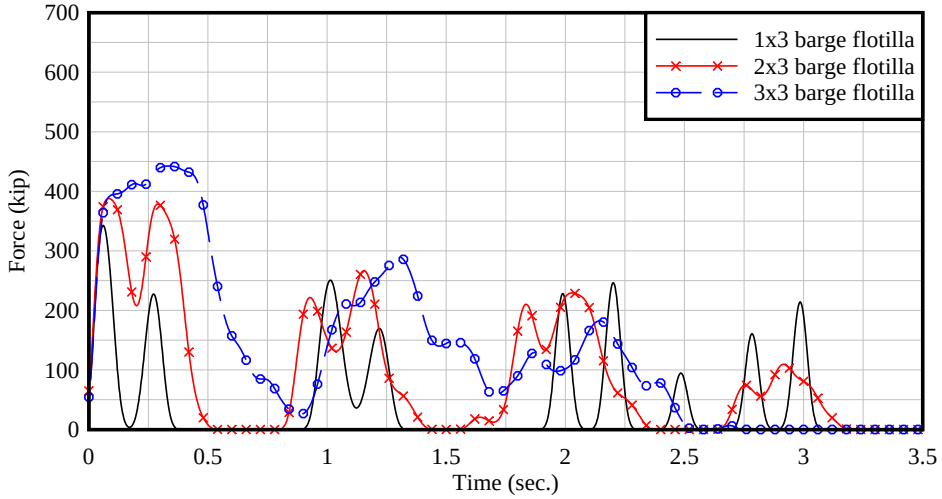

Figure 4.10. Sensitivity to number of strings: [1, 2, 3] strings x 3 rows – 6 FPS – 10° – MRLD2

4.4 Relationship between impact force and momentum

Based on the established importance of lead row momentum as a predictor of maximum impact force, all force data from the parametric studies conducted on MRLD2 (recall Table 4.1) and MRLD3 (recall Table 4.2) are plotted as a function of lead row momentum (normal to the wall) in Figure 4.11. In Figure 4.12, a subset of the data is shown for ranges of momentum and force that are typical of design conditions for the MRLD2 and MRLD3 walls. Particularly evident in these figures, the data exhibit a linear relationship at low momentum levels, followed by an *approximately-linear* relationship—but with reduced slope—at moderate to high momentum levels. Such observations suggest that a load prediction model for these walls might be developed by fitting a bilinear curve to the data. However, rather than fitting such a relationship specifically to the MRLD2 and MRLD3 data, a *unified* (generalized) relationship for computing oblique barge impact forces for wall structures will be developed in the following chapter.

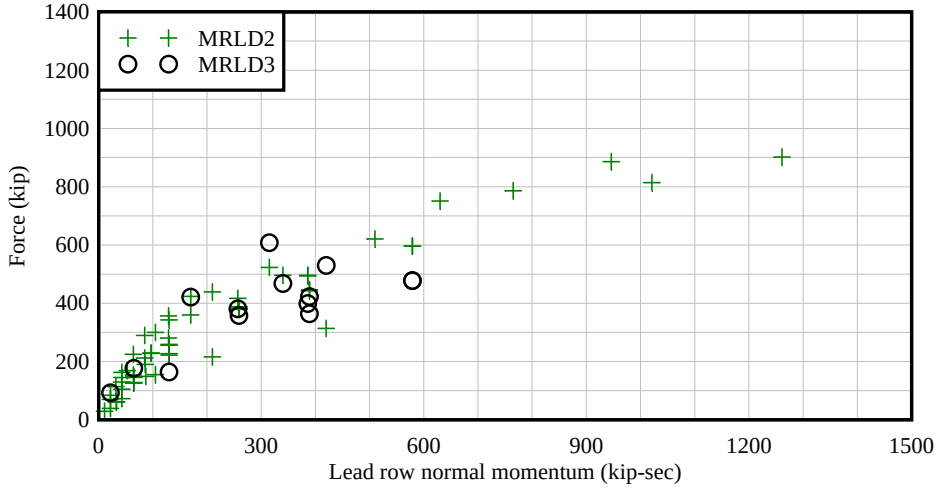

Figure 4.11. Maximum impact forces for MRLD2 and MRLD3

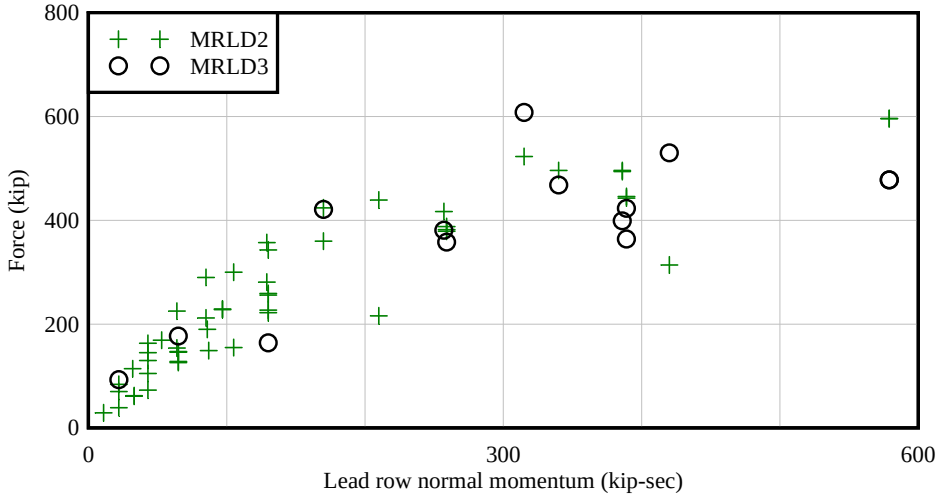

Figure 4.12. Maximum impact forces for MRLD2 and MRLD3 over reduced-ranges of momentum and force

In developing the unified relationship (impact load prediction model), only the MRLD2 data will be used. As discussed earlier in this chapter, impact forces for MRLD2 are generally larger than those for MRLD3 due to the contributions of *both* mass and stiffness based resistance in MRLD2. Consequently, inclusion of the MRLD3 force data in the development of a unified load prediction model would tend to bias the force prediction model 'downward'. Therefore, with the goal of maintaining a reasonable level of conservatism in the unified load prediction model, only the MRLD2 data will be utilized.

CHAPTER 5
UNIFIED LOAD PREDICTION MODELS

5.1 Background and overview

Several impact simulation studies have been performed to develop an improved understanding of barge flotilla impact loads for an array of different types of waterway structures. These studies have included aberrant single barges impacting floodwalls in a hurricane wind environment, and multi-barge flotillas impacting rigid concrete guide walls, semi-flexible concrete guide walls, pile founded guide walls, flexible timber guide walls, and bullnose structures. Impact simulations with finite element models of target structures representing the following USACE inland waterway structures have been performed during the course of the aforementioned analytical studies: Hurricane Protection Office (HPO) wall located near St. Bernard Parish; Protection and Restoration Office (PRO) wall located near Algiers Canal; PRO fronting protection (dolphin) system located near Hero pumping station; rigid concrete wall; single-span semi-flexible concrete wall at Winfield Lock and Dam near Red House, WV; Mississippi River Lock and Dam 2 (MRLD2) upper pool interior monolith wall near Hastings, Minnesota; Mississippi River Lock and Dam 3 (MRLD3) lower pool interior monolith wall near Welch, Minnesota; flexible timber guide wall replacement of Catfish Point Control Structure 2 near Grand Chenier, LA; 2:1 sloped-V bullnose at Mississippi River Lock and Dam No. 7 (MRLD7) near Onalaska, Wisconsin; 35 ft diameter semi-circular bullnose, and 10 ft diameter semi-circular bullnose. More than 300 impacts with these USACE waterway structures have been simulated, of which an approximate 100 sensitivity simulations are excluded from the data presented herein.

Results from each study are categorized into one of the following: oblique flotilla impacts, head-on flotilla impacts, and aberrant single barge impacts in a hurricane wind environment. The USACE waterway structures included in the oblique flotilla impact category includes the rigid wall, semi-flexible concrete wall (Winfield), pile-founded guide walls (MRLD2 and MRLD3), and flexible timber guide wall (Catfish Point). The results from these four studies constitute the database of impact forces for development of a unified approach to oblique impact load prediction for waterway structures of interest to the USACE. The USACE waterway structures included in the head-on flotilla impact category includes the 2:1 sloped-V (MRLD7), 35 ft, and 10 ft bullnose structures. The merged data from impact simulations with these three bullnose structures forms the database of impact forces for development of a unified approach to head-on load prediction for bullnose structures of interest to the USACE. The USACE waterway structures included in the aberrant single barge impacts in a hurricane wind environment category include the HPO wall (St. Bernard Parish), PRO wall (Algiers canal), and PRO dolphin (Hero pumping station).

Peak forces, and the associated impact condition parameters, from these analytical studies form data populations used for development two types of unified load prediction models (oblique and head-on multi-barge flotilla impacts) presented herein. Resultant data from the hurricane study are excluded from the combined oblique and head-on impact databases due to the differing nature of these impact simulations. The primarily difference is the consequence of these simulations being limited to single barge impacts for a single, or over a small range of, impacting energy level(s). Simulations for the hurricane study are limited to a single barge, which consequently results in impact energy levels limited to values well below the range simulated for all other studies. Moreover, the matrices of impact conditions included in the hurricane study

involve varying barge orientation while making no, or minimal changes in velocity, thereby resulting in different portions of the barge contacting the impacted structure at the same, or similar, energy level(s). For example, all simulations with the PRO wall and PRO dolphin structures included one and two impact energy levels, respectively. As a result, data from these hurricane-environment-based simulations do not allow for meaningful correlations with energy-related impact parameters. Thus, simulations from the hurricane study are of minimal value if impacts involving flotillas, as opposed to a single barge, over a range of impact event conditions are under consideration; i.e. results are not applicable if a range of flotilla impact angles, speeds, and configurations are to be considered. In addition, the defined impact angle for the hurricane study refers to the orientation of the barge centerline, not the direction of travel. Specifically, the impact angle refers to the orientation of the barge centerline relative to the impacted structure for the hurricane study, whereas the impact angle for all other studies refers to the direction of travel of the impacting barge (flotilla) relative to the longitudinal axis of the impacted structure.

All studies subsequent to the 'aberrant single barge impacts in a hurricane wind environment' study include impact condition matrices with varied impact energy levels that are achieved by changing flotilla size and configuration, speed, and angle of impact, while keeping the portion of the deformable barge contacting the impacted structure consistent. Following completion of the hurricane study, flotilla models were developed using decimated barges as described earlier in this report (recall Section 2.2.3) that used force-deformation curves to model contact stiffness between adjacent barges. During development of these inter-barge force-deformation curves, it was determined that the raked-end of a jumbo-hopper barge is the stiffest portion of the barge due to the raked geometry and internal framing structure (Consolazio et al. 2012). Thus, the most conservative, i.e. highest peak, impact forces occur during a bow impact event. Consequently, most analytical studies performed after the hurricane studies are performed primarily with bow impacts. For these reasons, results from the hurricane study are not used in developing the load prediction models presented herein. Thus, the two types of unified load prediction models presented here are for oblique and head-on barge flotilla impacts.

5.2 Oblique impacts on walls

A majority of the finite element simulations conducted in previous studies and in the current study have focused on oblique flotilla impacts against inland waterway structures. Impacts using a variety of flotillas, ranging from a 1x1, or single barge, to a 3x5, have been simulated impacting finite element models of a range of different USACE waterway structures. Results from the oblique impact simulation studies are concatenated to form a merged database, which is used to develop a unified approach to load prediction for oblique flotilla impacts with USACE waterway structures.

5.2.1 Summary of data used in developing unified load prediction models

Five distinct finite element models representing a range of USACE waterway wall structures have been used for simulating oblique flotilla impact events over the course of four consecutive USACE-funded analytical research projects. Preceding studies include models of the following three structures: rigid concrete wall, semi-flexible concrete wall (Winfield), and a flexible timber guide wall (Catfish Point). The combined results obtained from these three previous studies, and results obtained from the current pile-founded large-mass guide wall study, which includes two distinct representative USACE waterway walls (MRLD2 and MRLD3),

forms a database of impact force data for waterway structures subjected to oblique flotilla impact loading. This database of peak force results, and the associated impact condition parameters, allows for development of a unified approach to predict peak loads from oblique flotilla impacts. Note that, as discussed in Chapter 4, in the interest of conservatism, results from impact simulations with the MRLD3 finite element model are not included in the development of unified load prediction models.

Tabulated force data presented below are limited to peak force normal to the surface of the impacted wall structure, herein referred to as peak force or peak normal force. The normal force component is reported exclusively as loading in the normal (lateral) direction is typically of principal interest in structural design. If needed, frictional forces along the longitudinal axis of the impacted wall can be approximated using the constant dynamic friction coefficient of 0.45 used throughout all five of these analytical studies. Vertical forces are not reported, as their magnitudes are generally insignificant relative to normal forces.

In addition to the tabulated force results in the following sections, peak forces are also plotted with respect to lead-row momentum. More specifically, the component of the momentum of the lead-row barge(s) normal to the surface of the impacted wall structure is plotted versus the analogous normal component of peak impact force.

5.2.1.1 Rigid wall

Results from twenty (20) impact simulations against a rigid wall model (Table 5.1) for use in developing a unified load prediction model for oblique flotilla impacts are presented. Results from multiple sensitivity studies, e.g. lead-row barges with no payload, as well as simulations with 10% pre-tensioning force applied to the lashing elements are not included in the interest of conservatism. Further discussion regarding the effects of lashing pre-tensioning forces on impact forces can be found in Consolazio et al. (2012).

Table 5.1. Peak force results from rigid wall study

Flotilla	Speed (FPS)	Angle (deg)	Normal Lead-Row Momentum (kip-in)	Peak Normal Force (kip)	Flotilla	Speed (FPS)	Angle (deg)	Normal Lead-Row Momentum (kip-in)	Peak Normal Force (kip)
3 x 3	1.0	10	65	143	3 x 5	4.0	20	510	603
3 x 3	3.0	20	383	352	3 x 5	5.0	20	638	639
3 x 5	1.0	10	65	164	3 x 5	3.0	25	473	622
3 x 5	2.0	10	130	240	3 x 5	0.5	30	93	266
3 x 5	3.0	10	194	279	3 x 5	1.0	30	186	349
3 x 5	4.0	10	259	315	3 x 5	2.0	30	373	546
3 x 5	5.0	10	324	351	3 x 5	3.0	30	559	768
3 x 5	1.0	20	128	295	3 x 5	4.0	30	746	818
3 x 5	2.0	20	255	383	3 x 5	5.0	30	932	833
3 x 5	3.0	20	383	475	3 x 5	8.0	30	1492	1198

Note: all results include a 50% pre-tensioning force applied to lashing elements during initialization

Analysis of results from the rigid wall study revealed the highest correlation with peak impact force is momentum of the lead-row barges normal to the surface of the impacted waterway wall. Thus, the tabulated results (Table 5.1) are plotted against lead-row momentum normal to the rigid wall (Figure 5.1).

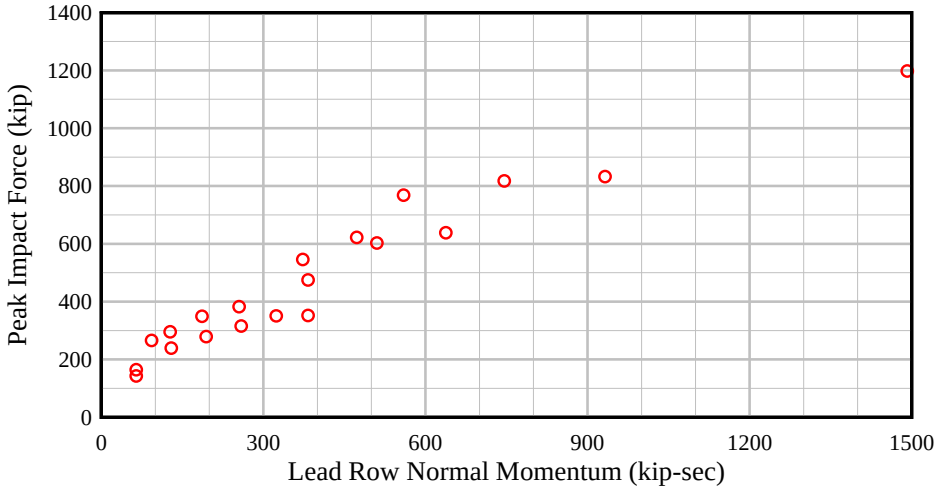

Figure 5.1. Peak force results from rigid wall study (20 cases)

5.2.1.2 Semi-flexible wall (Winfield)

Results from thirty-four (34) impact simulations against a (semi-)flexible wall (Winfield) model (Table 5.2) for use in developing a unified load prediction model for oblique impacts are presented. Sensitivity simulations, e.g. various combinations of lead-row barges without payload, are excluded in the interest of conservatism.

Table 5.2. Peak force results from semi-flexible wall (Winfield) study

Flotilla	Speed (FPS)	Angle (deg)	Normal Lead-Row Momentum (kip-in)	Peak Normal Force (kip)
1 x 3	0.5	20	21	82
1 x 3	1.0	20	43	142
1 x 3	1.5	20	64	202
1 x 3	2.0	20	85	230
1 x 3	2.5	20	106	287
1 x 3	3.0	20	128	308
2 x 3	3.0	20	255	405
3 x 1	3.0	20	383	432
3 x 2	3.0	20	383	461
3 x 3	2.0	10	130	224
3 x 3	3.0	10	194	267
3 x 3	4.0	10	259	306
3 x 3	2.7	14	237	348
3 x 3	2.9	17	316	418
3 x 3	3.0	20	383	471
3 x 3	4.0	20	510	579
3 x 3	5.0	20	638	639
3 x 3	8.0	20	1021	670
3 x 3	1.0	30	186	338
3 x 3	3.0	30	559	757
3 x 3	5.0	30	932	883
3 x 3	5.0	30	932	853
3 x 3	6.0	30	1119	960
3 x 3	7.0	30	1305	998
3 x 3	8.0	30	1492	1028
3 x 5	2.0	10	130	222
3 x 5	3.0	10	194	267
3 x 5	2.0	20	255	365
3 x 5	3.0	20	383	467
3 x 5	4.0	20	510	579
3 x 5	4.0	30	746	815
3 x 5	5.0	30	932	859
3 x 5	6.0	30	1119	959
3 x 5	7.0	30	1305	1038

Analysis of results from the semi-flexible wall study revealed the highest correlation with peak impact force is momentum of the lead-row barges normal to the impacted surface. Further discussion regarding this relationship can be found in Consolazio and Walters (2012). Thus, the tabulated results (Table 5.2) are plotted against lead-row momentum normal to the semi-flexible (Winfield) wall (Figure 5.2).

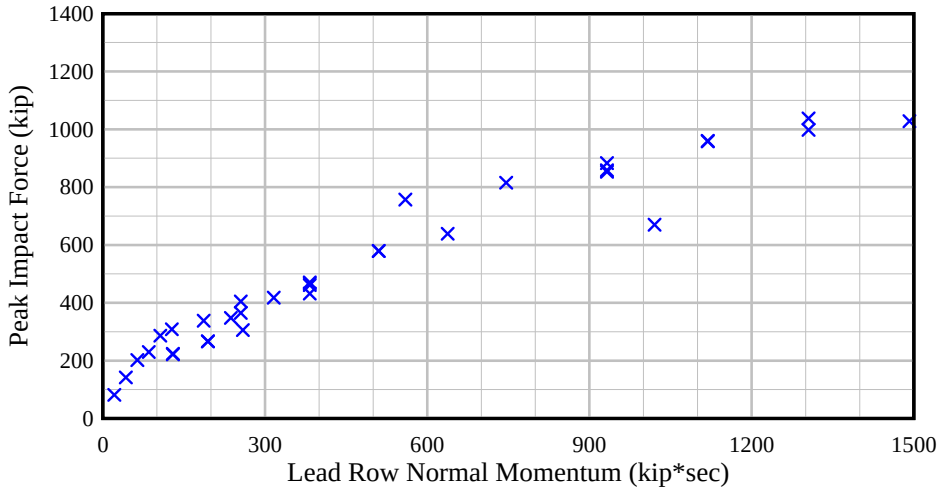

Figure 5.2. Peak force results from semi-flexible wall (Winfield) study (34 cases)

5.2.1.3 Pile-founded guide wall – Mississippi River Lock and Dam No. 2

Results from fifty-seven (57) impact simulations against a pile-founded guide wall (MRLD2) model (Table 5.3) for use in developing a unified load prediction model for oblique impacts are presented. Results from additional simulations performed for multiple investigations to quantify peak force sensitivity to a variety of modeling parameters (see Appendix D) are not included in the interest of conservatism.

As with the preceding rigid and semi-flexible wall studies, analysis of results from this pile founded guide wall study revealed the highest correlation with peak impact force is lead-row barge momentum normal to the guide wall. Thus, the tabulated results (Table 5.3) are plotted against lead-row momentum normal to the pile-founded (MRLD2) guide wall (Figure 5.3).

5.2.1.4 Flexible timber guide wall

Results from thirty (30) impact simulations against a flexible timber guide wall (Catfish Point) model (Table 5.4) are used for development of a unified load prediction model for oblique impacts. Two soil profiles are included in the results from the flexible timber guide wall study. The baseline soil condition developed using soil data provided by USACE from the Northwest of Larose (LGM) site is denoted by SSx1. An amplified soil condition, is a scaled version of SSx1 by a factor of two, i.e. a 100% increase in stiffness, and is denoted by SSx2. Twelve (12) of the thirty (30) simulations in the flexible timber guide wall data set (Table 5.4) incorporate an SSx2 soil profile. These soil sensitivity (SSx2) simulations are included in the interest of conservatism as higher peak impact forces result from the stiffer soil profile. Results from simulations performed for additional sensitivity studies are not included in the interest of conservatism.

Table 5.3. Peak force results from pile-founded guide wall (MRLD2) study

Flotilla	Speed (FPS)	Angle (deg)	Normal Lead-Row Momentum (kip-in)	Peak Normal Force (kip)
1 x 3	1.0	5	11	29
1 x 3	2.0	5	22	70
1 x 3	4.0	5	43	130
1 x 3	1.0	10	22	84
1 x 3	2.0	10	43	145
1 x 3	6.0	10	130	343
1 x 3	1.0	15	32	114
1 x 3	2.0	15	64	225
1 x 3	4.0	15	129	357
1 x 3	1.0	20	43	163
1 x 3	2.0	20	85	290
1 x 3	4.0	20	170	424
1 x 3	1.0	25	53	169
1 x 3	2.0	25	105	300
1 x 3	4.0	25	210	439
1 x 3	6.0	25	315	523
2 x 3	1.0	5	22	39
2 x 3	2.0	5	43	73
2 x 3	4.0	5	87	149
2 x 3	1.0	10	43	105
2 x 3	2.0	10	86	190
2 x 3	6.0	10	259	388
2 x 3	1.0	15	64	154
2 x 3	2.0	15	129	281
2 x 3	4.0	15	257	417
2 x 3	1.0	20	85	212
2 x 3	2.0	20	170	360
2 x 3	4.0	20	340	496
2 x 3	1.0	25	105	155

Flotilla	Speed (FPS)	Angle (deg)	Normal Lead-Row Momentum (kip-in)	Peak Normal Force (kip)
2 x 3	2.0	25	210	216
2 x 3	4.0	25	420	314
3 x 3	1.0	5	33	61
3 x 3	2.0	5	65	126
3 x 3	4.0	5	130	222
3 x 3	1.0	10	65	146
3 x 3	2.0	10	130	256
3 x 3	4.0	10	259	379
3 x 3	6.0	10	389	443
3 x 3	1.0	15	97	228
3 x 3	4.0	15	386	494
3 x 3	6.0	15	579	596
3 x 5	1.0	5	33	62
3 x 5	2.0	5	65	128
3 x 5	4.0	5	130	227
3 x 5	1.0	10	65	147
3 x 5	2.0	10	130	259
3 x 5	4.0	10	259	382
3 x 5	6.0	10	389	446
3 x 5	1.0	15	97	229
3 x 5	4.0	15	386	496
3 x 5	6.0	15	579	596
3 x 3	4.0	20	510	621
3 x 3	6.0	20	765	786
3 x 3	8.0	20	1021	814
3 x 3	4.0	25	630	751
3 x 3	6.0	25	946	886
3 x 3	8.0	25	1261	902

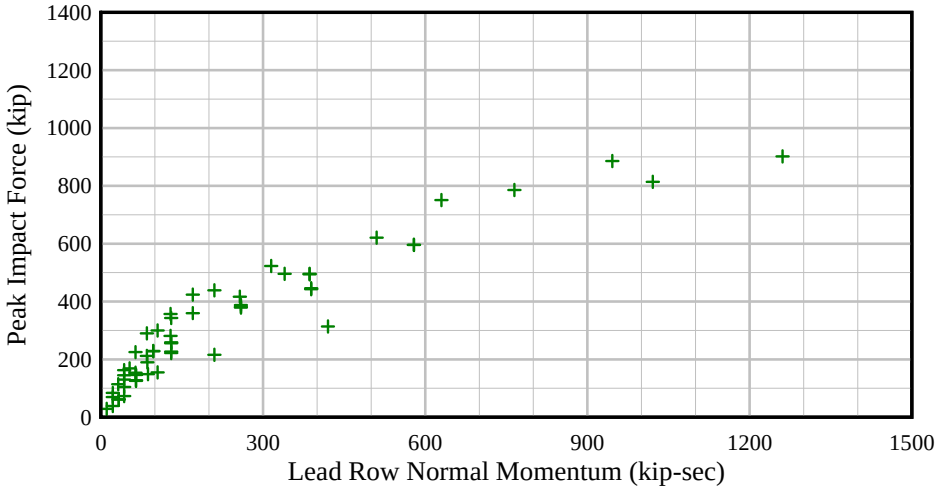

Figure 5.3. Peak force results from pile-founded guide wall (MRLD2) study (57 cases)

Table 5.4. Peak force results from flexible timber guide wall study

Flotilla	Speed (FPS)	Angle (deg)	Normal Lead-Row Momentum (kip-in)	Peak Normal Force (kip)
1 x 1	2.0	25	105	76
1 x 1	4.0	15	129	124
1 x 1	4.0	15	129	133
1 x 2	2.0	15	64	68
1 x 2	4.0	25	210	214
1 x 2	4.0	15	129	148
1 x 3	2.0	15	64	71
1 x 3	2.0	25	105	135
1 x 3	2.0	15	64	85
1 x 3	4.0	15	129	146
1 x 3	4.0	25	210	191
1 x 3	4.0	15	129	132
2 x 1	2.0	15	129	83
2 x 1	2.0	25	210	147
2 x 1	2.0	25	210	172

Flotilla	Speed (FPS)	Angle (deg)	Normal Lead-Row Momentum (kip-in)	Peak Normal Force (kip)
2 x 1	4.0	15	257	192
2 x 1	4.0	25	420	255
2 x 1	4.0	15	257	167
2 x 2	2.0	15	129	100
2 x 2	2.0	25	210	163
2 x 2	2.0	25	210	187
2 x 2	4.0	15	257	211
2 x 2	4.0	25	420	312
2 x 2	4.0	25	420	333
2 x 2	4.0	15	257	176
2 x 2	6.0	15	386	248
2 x 2	6.0	15	386	267
2 x 2	6.0	15	386	250
2 x 3	2.0	15	129	119
2 x 3	6.0	15	386	247

As with the preceding oblique impact studies, analysis of results from the flexible-timber guide wall study revealed the highest correlation with peak impact force is lead-row barge momentum normal to the guide wall. Further discussion regarding this correlation is provided in Consolazio and Wilkes (2013). Thus, the tabulated results (Table 5.4) are plotted against lead-row momentum normal to the flexible-timber guide wall (Figure 5.4).

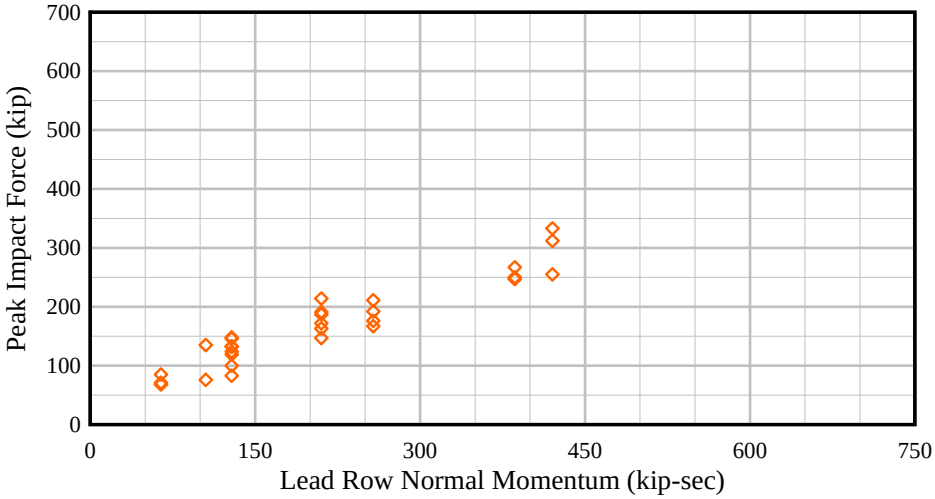

Figure 5.4. Peak force results from flexible timber guide wall study (30 cases)
(Note: horizontal and vertical plot-ranges differ from concrete wall data presented earlier)

5.2.2 Unified load prediction models for oblique flotilla impacts

Two fundamentally different approaches to the development of unified load prediction models for oblique flotilla impacts on wall structures are presented here. The first involves empirically relating—through an error-minimization curve fitting process—maximum impact forces to flotilla momentum (specifically, the component of lead row momentum oriented

normal to the impacted wall). The empirical curve-fitting approach is applied in a unified sense—described in greater detail below—to data obtained from large-mass concrete guide wall impact simulations (rigid wall, semi-flexible wall, and pile-founded guide wall). In contrast, because the flexible timber guide wall has far less stiffness and mass than the concrete walls, its dynamic response differs significantly thus necessitating the development of a separate (case-specific) empirical curve fit. Consequently, two empirical load prediction models are developed: a unified model for concrete walls, and a case-specific model for flexible timber guide walls.

In order to develop a *single* unified load prediction model that is applicable to *all* walls (concrete walls, flexible timber guide walls, etc.), a more sophisticated approach—one that accounts for both the stiffness and mass characteristics of the wall—is also developed and presented here. In this latter approach, a two-dimensional low-order (low degree-of-freedom; low-DOF) dynamic model is used to represent, in a simplified sense, the interaction between the barge flotilla and the specific wall under consideration (characterized by stiffness and mass). In this approach, impact forces are quantified by conducting a simplified dynamic analysis of the low-order model for the impact conditions (mass, speed, angle) of interest.

Key objectives in formulating both types unified load prediction model (empirical and low-order dynamic) are to provide methods that are both simple to use and conservative (relative to peak force data obtained from high-resolution oblique flotilla impact simulations). Hence, with regard to simplicity of use, only the structural (wall) and flotilla parameters that most strongly influence peak impact forces are included in the prediction models.

5.2.2.1 Empirical curve fiting

To facilitate development of a unified empirical load prediction model for large-mass concrete guide walls, the data described previously for the rigid wall (Figure 5.1), semi-flexible wall (Figure 5.2), and pile-founded (MRLD2) guide wall (Figure 5.3) are merged together and plotted in Figure 5.5. Evident from the figure, the data exhibit a linear relationship at low momentum levels, followed by an approximately linear relationship—with reduced slope—at moderate to high momentum levels. Such trends suggest that a bilinear curve-fit is appropriate for representing the relationship between impact force and momentum: one linear segment to represent low-momentum impacts, and a second to represent moderate to high momentum impacts.

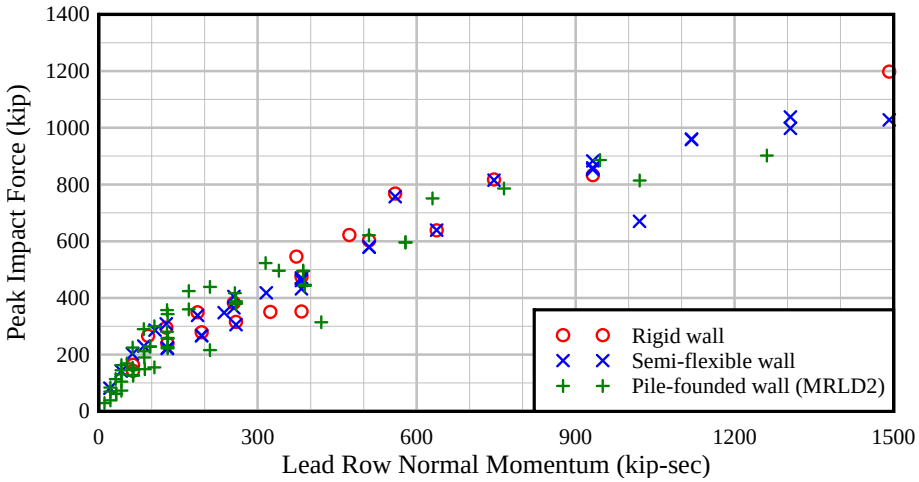

Figure 5.5. Peak force data for all concrete guide walls (111 cases)

However, it is also important to recognize that prior studies have demonstrated a correlation between impact force and the stiffness of the impacted structure. Particularly in moderate to high momentum impacts, where contact between the barge and the wall is of a sustained nature, it has been found that increasing the structural stiffness (e.g., lateral wall stiffness) generally increases the magnitude of impact force generated. Consequently, the unified empirical load prediction model developed in this study for concrete walls uses a bilinear representation (Figure 5.6) in which the slope (S_1) of the first segment is constant, but the slope (S_2) of the second linear segment (representing moderate to high momentum levels) is itself a linear function of wall stiffness. Functionally, the bilinear curve has the form:

$$F = \begin{cases} S_1\, m_{LR} v \sin\theta & \text{if } m_{LR} v \sin\theta \le (F_{12}/S_1) \\ F_{12} + \underbrace{\left(S_{2A} + (S_{2B})(k)\right)}_{S_2} \left(m_{LR} v \sin(\theta) - (F_{12}/S_1)\right) & \text{otherwise} \end{cases} \tag{5.1}$$

where F is the impact force normal to the wall, F_{12}, S_1, S_{2A}, and S_{2B} are bilinear curve fitting parameters, k is the lateral stiffness of the wall at the impact point, m_{LR} is the mass of all barges in the lead row of the flotilla, v is the impact velocity, and θ is the angle between the direction of flotilla travel and the longitudinal axis of the wall.

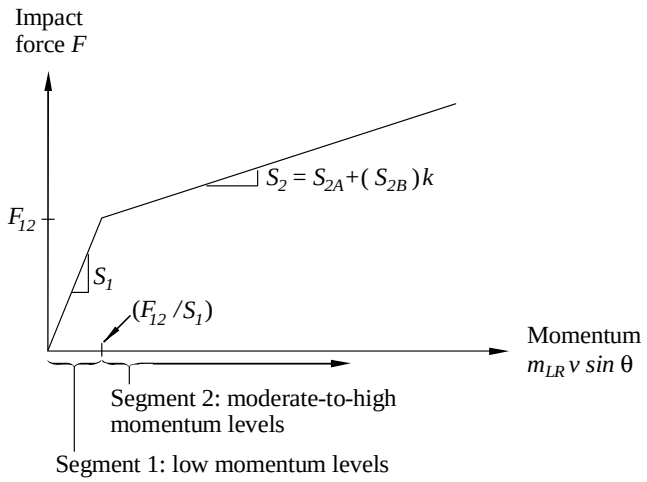

Figure 5.6. General form of unified bilinear curve fit used for concrete walls

In order to compute values of the best fit parameters F_{12}, S_1, S_{2A}, and S_{2B} that unify all three concrete wall data sets (rigid, semi-flexible, MRLD2) in an optimal manner, an error function minimization process is used. The error function used here is defined as the sum of the squares of the load prediction errors—differences between impact simulation force data and predictions from Eqn. (5.1)—accumulated across all three concrete wall data sets (i.e., 111 data points in total). Since the bilinear load prediction model is a function of lateral wall stiffness (k), determination of prediction errors requires that a stiffness value be assigned to each point in the data set. For each pile founded guide wall (MRLD2) data point shown in Figure 5.5, a lateral stiffness of 592 kip/in. is assigned, based on results from a quasi-static lateral load analysis of the MRLD2 wall that was described earlier in this report. For each semi-flexible wall data point in

Figure 5.5, a lateral stiffness of 767 kip/in. is assigned—i.e., the lateral stiffness at the mid-length (assumed impact point) of the waterway wall at Winfield Lock and Dam. For rigid walls, lateral stiffness is hypothetically infinity, however beyond a certain threshold level of stiffness, maximum forces for oblique impacts tend to be controlled by the barge flotilla stiffness rather than the wall stiffness. Through separate cases-by-case (i.e., wall-by-wall) bilinear curve-fitting and correlation processes (not presented here), it was empirically determined that assigning a lateral stiffness of approximately 1000 kip/in. to each rigid wall data point in Figure 5.5 results in a nearly optimal linear correlation between wall stiffness k and slope S_2, as defined in Eqn. (5.1) and illustrated in Figure 5.6. Consequently, in using the load prediction model developed herein, any wall with a stiffnesses exceeding 1000 kip/in. should be considered 'rigid', and subsequently assigned the limiting value of 1000 kip/in for load calculation purposes.

Upon assigning the respective stiffnesses of 1000 kip/in., 767 kip/in., and 592 kip/in. to the appropriate rigid, semi-flexible, and pile-founded data points in Figure 5.5, and then subsequently minimizing the cumulative square error function with respect to the fitting parameters F_{12}, S_1, S_{2A}, and S_{2B}, the following unified load prediction model is established for concrete walls:

$$F = \begin{cases} 2.266\, m_{LR} v \sin\theta & \text{if } m_{LR} v \sin\theta \le 143 \text{ kip-sec} \\ 325 + (0.491 + 0.000173\, k)(m_{LR} v \sin\theta - 143) & \text{otherwise} \end{cases} \tag{5.2}$$

where $m_{LR} v \sin\theta$ is the lead row momentum normal to the wall in units of kip-sec., k is the lateral wall stiffness in units of kip/in. (and limited to no larger than 1000 kip/in), and F is the impact force normal to the wall in units of kips.

In Figure 5.7, the unified load prediction model, Eqn. (5.2), is evaluated for all three concrete wall lateral stiffnesses, and compared to the overall impact force data set. Comparisons between the unified load prediction model and *individual* data sets are presented for the rigid wall in Figure 5.8, semi-flexible wall in Figure 5.9, and pile founded guide wall in Figure 5.10.

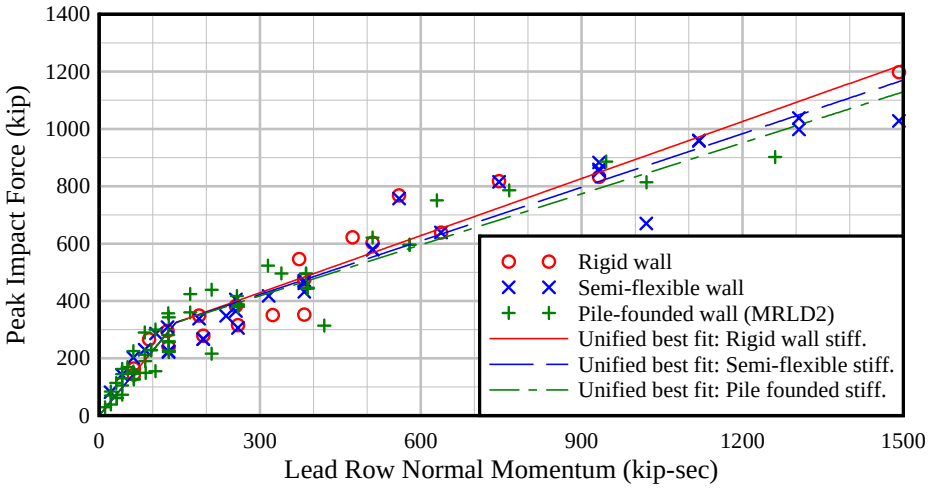

Figure 5.7. Comparison of all concrete wall data and unified bilinear curve fit (the latter evaluated using the appropriate stiffnesses, *k*, of the associated walls)

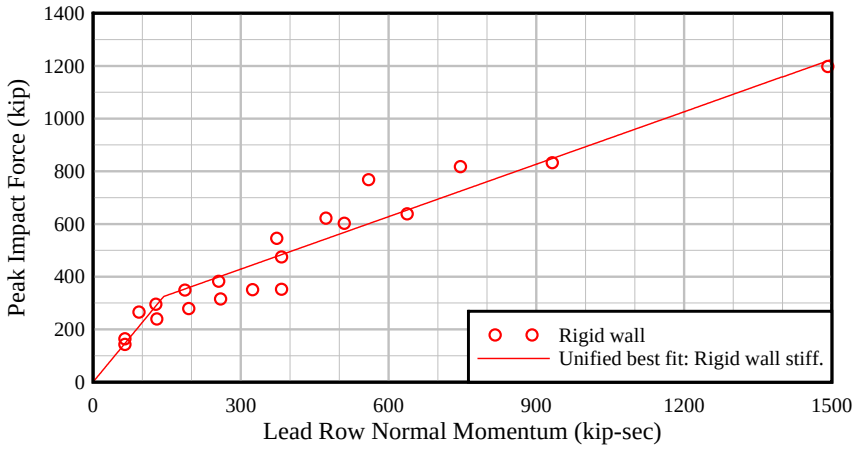

Figure 5.8. Comparison of rigid wall data and unified load prediction model (the latter evaluated using a wall stiffness k = 1000 kip/in)

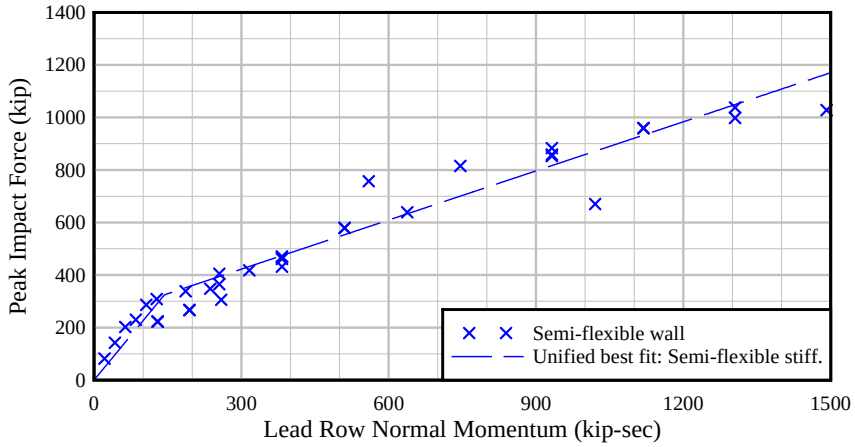

Figure 5.9. Comparison of semi-flexible wall data and unified load prediction model (the latter evaluated using a wall stiffness k = 767 kip/in)

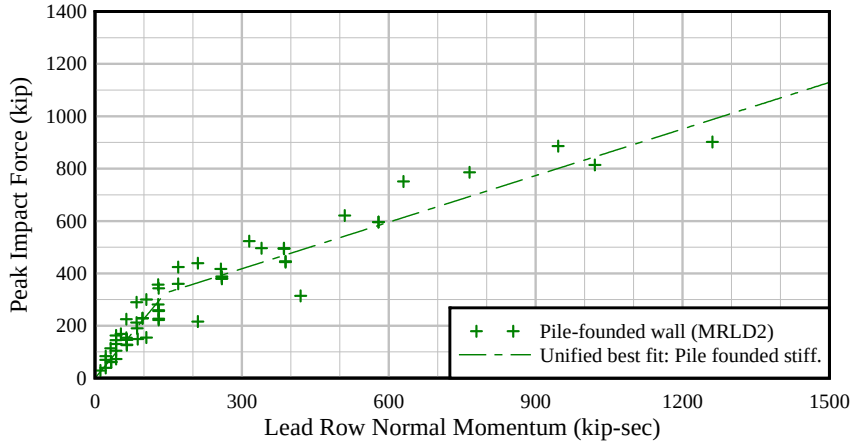

Figure 5.10. Comparison of pile founded guide wall (MRLD2) data and unified load prediction model (the latter evaluated using a wall stiffness k = 592 kip/in)

As noted earlier, due to significant differences of mass and stiffness between the concrete guide walls considered above and the flexible timber guide wall, the dynamic response of the latter differs significantly. As a result, it is not feasible to incorporate, or 'unify', data from the flexible timber guide wall into the load prediction model presented above in Eqn. (5.2). Instead, a separate, case-specific empirical load prediction model is developed from the flexible timber guide wall data summarized earlier in Figure 5.4. For the sake of consistency with Eqn. (5.2), the flexible timber guide wall load prediction model is also formulated as a bilinear curve-fit. However, impact force data are only available for a single configuration of flexible timber guide wall with a single lateral stiffness (specifically, 120 kip/in. which corresponds to a single transverse line of piles and assumes load sharing to adjacent pile lines; see Consolazio and Wilkes, 2013 for additional details). Consequently, the slope S_2 of the bilinear curve fit (recall Figure 5.6), which was linearly dependent on stiffness k in Eqn. (5.1), is instead formulated—for the flexible timber guide wall—as a constant (non-stiffness-dependent) value. This leads to the following bilinear functional form:

$$F = \begin{cases} S_1 \, m_{LR} v \sin\theta & \text{if } m_{LR} v \sin\theta \le \left(F_{12}/S_1\right) \\ F_{12} + S_2 \left(m_{LR} v \sin\theta - \left(F_{12}/S_1\right)\right) & \text{otherwise} \end{cases} \tag{5.3}$$

Upon solving for the parameters F_{12}, S_1, S_2 that best fit the data shown in Figure 5.4—using the same type of error minimization process that was described above for concrete walls—the following load prediction model is established for flexible timber guide walls:

$$F = \begin{cases} 1.156 \, m_{LR} v \sin\theta & \text{if } m_{LR} v \sin\theta \le 87 \text{ kip-sec} \\ 101 + 0.553 \left(m_{LR} v \sin\theta - 87\right) & \text{otherwise} \end{cases} \tag{5.4}$$

where $m_{LR} v \sin\theta$ is lead row momentum normal to the wall in units of kip-sec. and F is the impact force normal to the wall in units of kips. In Figure 5.11, the load prediction model, Eqn. (5.4), is compared to force data used in the fitting process.

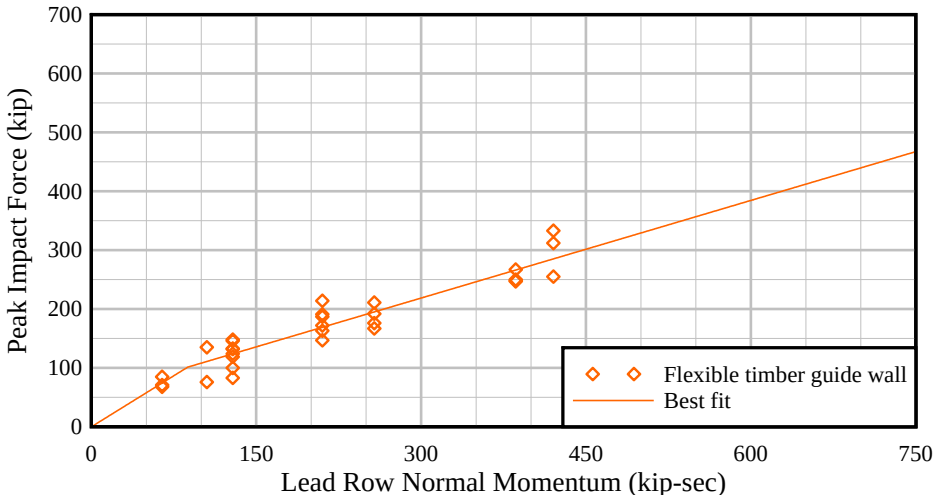

Figure 5.11. Comparison of flexible timber guide wall data and load prediction model (Note: horizontal and vertical plot-ranges differ from concrete wall data presented earlier)

5.2.2.2 Low-order dynamic model

The unified empirical load prediction model for concrete walls, described in the previous section, accounts—in a limited manner—for variations in structural configuration by incorporating lateral wall stiffness (k) into the formulation. However, dynamic structural (wall) response, and therefore impact force, is also a function of mass. Moreover, as was noted above, significant differences between large mass concrete walls and small mass flexible timber guide walls makes it impractical to unify both types of structures into a single *empirical* load prediction model.

Hence, to account for both stiffness *and* mass characteristics of the wall structure (as well as the stiffness and mass characteristics of the impacting barge flotilla), and to develop a model that *unifies all walls* (concrete, timber, etc.), an alternative load prediction method consisting of a simplified two-dimensional low-order (low degree-of-freedom; low-DOF) dynamic model (Figure 5.12) is developed. This dynamic model represents key wall and flotilla behaviors during oblique flotilla impact events within a two-dimensional space, i.e. all model constituents are defined in a single horizontal plane.

The low-order model consists of a small number of concentrated masses (lead barge row, trailing barge rows, lateral wall mass), a small number of rotational springs (flotilla flexural stiffness between each row of barges), and two translational springs (barge corner crushing-stiffness and lateral wall stiffness at the point of impact). Stiffness of the impacting bow-corner is represented by a non-linear translational spring oriented normal to the impacted surface. The nonlinear compression-only force-deformation curve (or crush curve) for the bow-corner is developed using impact results from the highest-energy oblique impact simulation conducted in all previous studies: 3x5 – 30° – 8 FPS, rigid wall study (Consolazio et al. 2012). The 'ground' (Figure 5.12), wall, and bow corner nodes are constrained to translate an equivalent distance in the X-direction, i.e. parallel to the surface of the wall.

Both the translational mass and the rotational (rotary) mass moment of inertia of each row of barges are represented in the low-order model. Each row is modeled using a single node located at the center-of-mass of the respective row of barges (Figure 5.12). The rotational stiffnesses between each adjacent row of barges—related primarily to lashing stiffness and geometric configuration—are represented by nonlinear rotational springs.

Representative comparisons of force-time histories obtained from finite element analyses (impact simulations) are compared to corresponding results obtained from the low-order model for: rigid wall (Figures 5.13 and 5.14), semi-flexible wall (Figures 5.15 and 5.16), pile founded guide wall (MRLD2) (Figures 5.17 and 5.18), and flexible timber guide wall (Figures 5.19 and 5.20). Summaries of peak impact forces obtained for wider ranges impact conditions are also presented for the rigid wall (Figure 5.21), semi-flexible wall (Figure 5.22), pile founded guide wall (MRLD2) (Figure 5.23), and flexible timber guide wall (Figure 5.24). These summaries indicate that across a very wide range of structural stiffnesses and masses—spanning from the rigid wall to the flexible timber guide wall—impact forces obtained from the low-order dynamic model are generally in favorable agreement with corresponding high-resolution FEA results. Hence, the low-order model clearly constitutes a 'unified' approach to impact load prediction. Moreover, in the vast majority of cases, the low-order model tends to err on the side of predicting *conservative* estimates of impact force—clearly, a desirable characteristic of any simplified load prediction methodology.

It recommended that, before this method is provided to structural engineers as a practical tool for load determination, additional testing be conducted, and that the method be implemented into a dedicated software package.

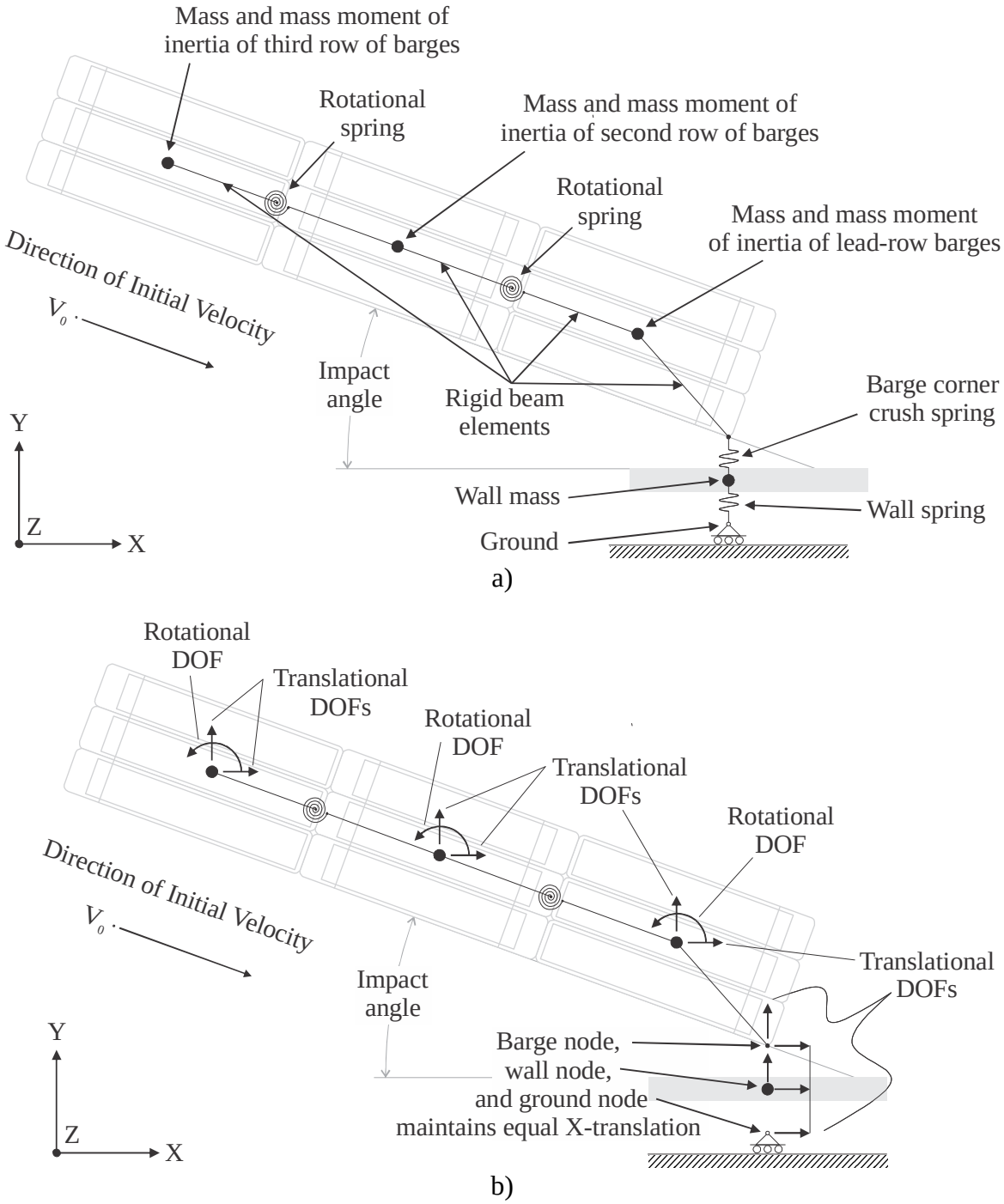

Figure 5.12. Low order (low degree-of-freedom; low-DOF) dynamic model:
a) Constituents representing FEA model; b) Degree-of-freedoms
(Note: 3x3 flotilla shown for illustrative purposes only)

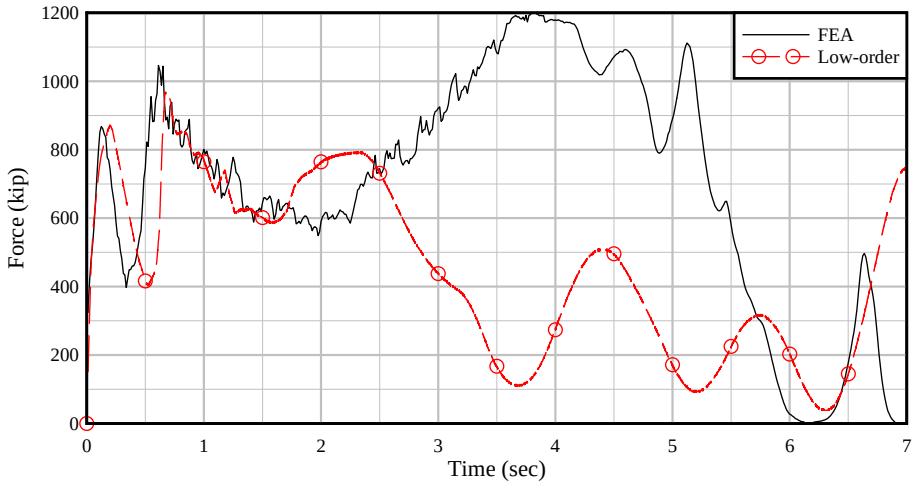

Figure 5.13. Comparison of forces for rigid wall: 3x5 – 30° – 8 FPS

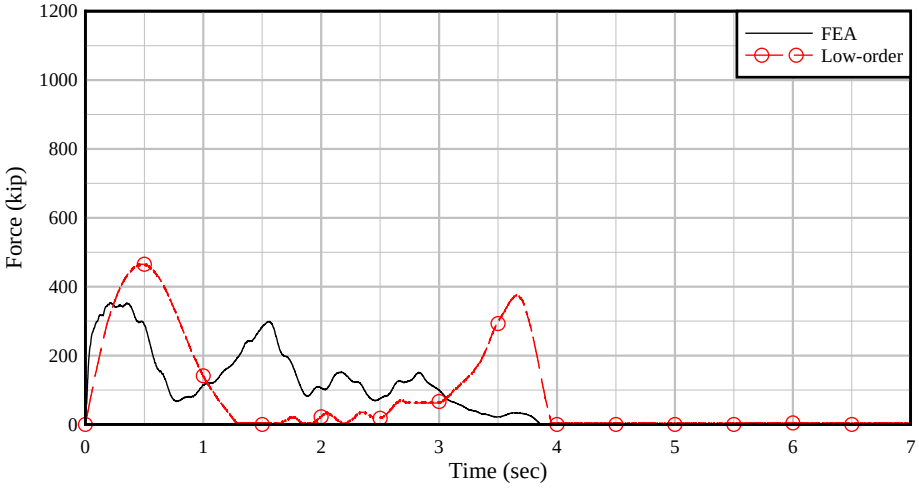

Figure 5.14. Comparison of forces for rigid wall: 3x5 – 30° – 1 FPS

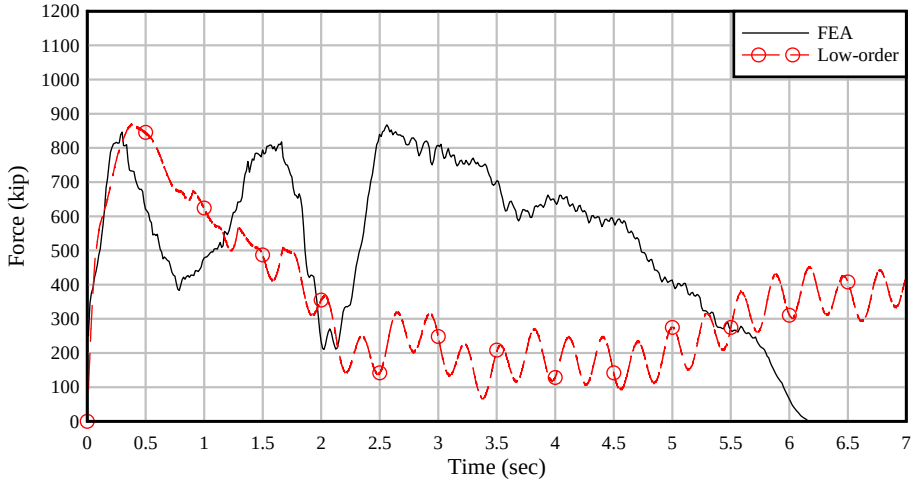

Figure 5.15. Comparison of forces for semi-flexible wall: 3x5 – 30° – 5 FPS

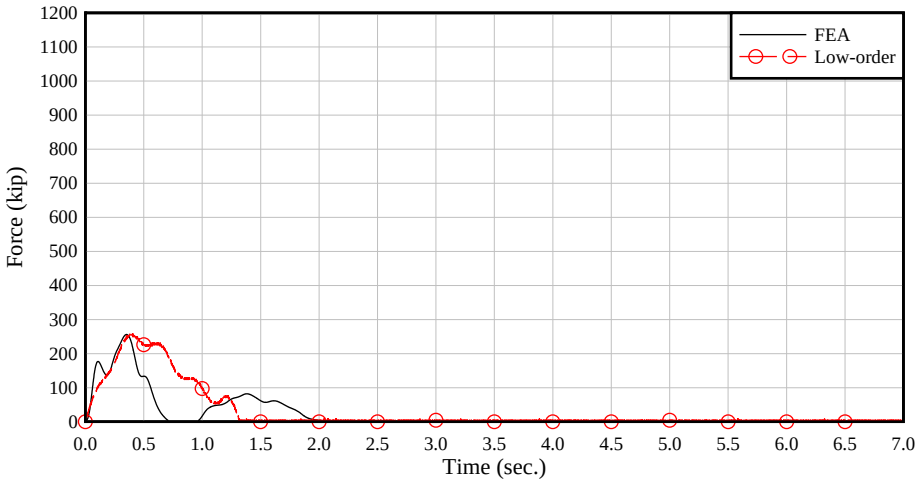

Figure 5.16. Comparison of forces for semi-flexible wall: 3x3 – 10° – 2 FPS

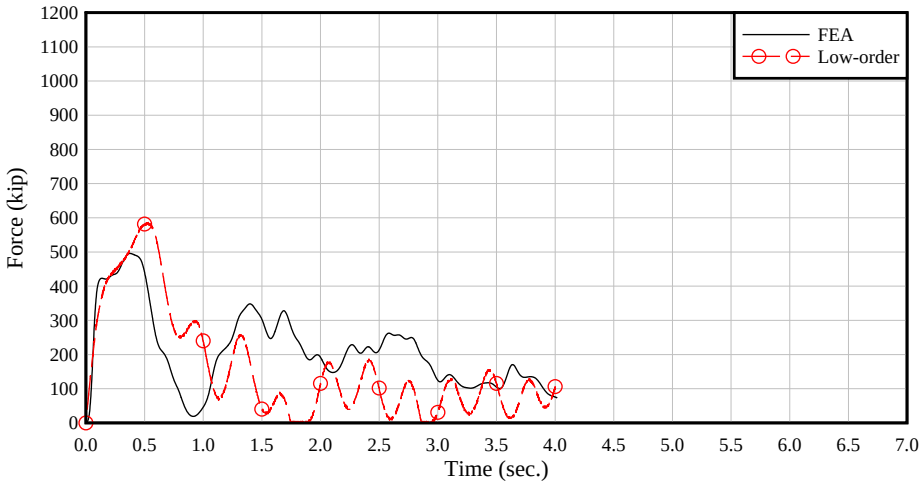

Figure 5.17. Comparison of forces for pile founded guide wall (MRLD2): 3x5 – 15° – 4 FPS

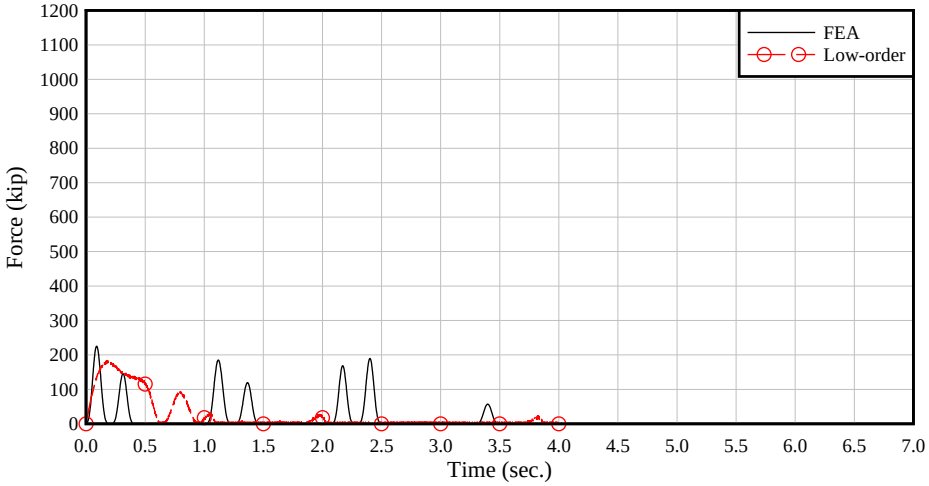

Figure 5.18. Comparison of forces for pile founded guide wall (MRLD2): 1x3 – 15° – 2 FPS

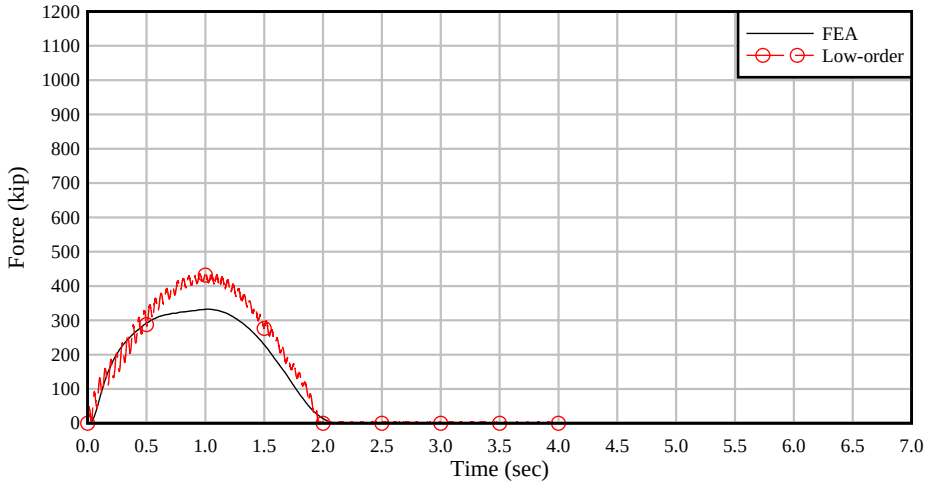

Figure 5.19. Comparison of forces for flexible timber guide wall: 2x2 – 25° – 4 FPS – SSx2

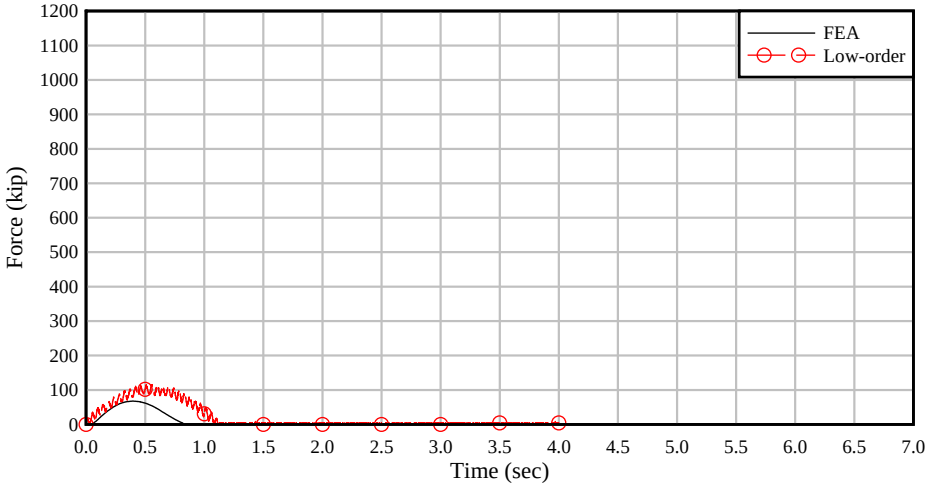

Figure 5.20. Comparison of forces for flexible timber guide wall: 1x2 – 15° – 2 FPS – SSx1

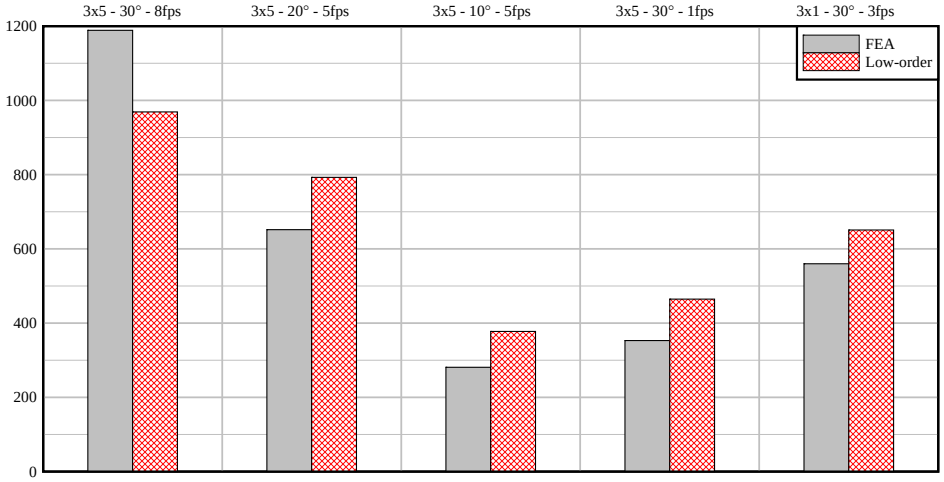

Figure 5.21. Summary of peak forces for rigid wall impacts

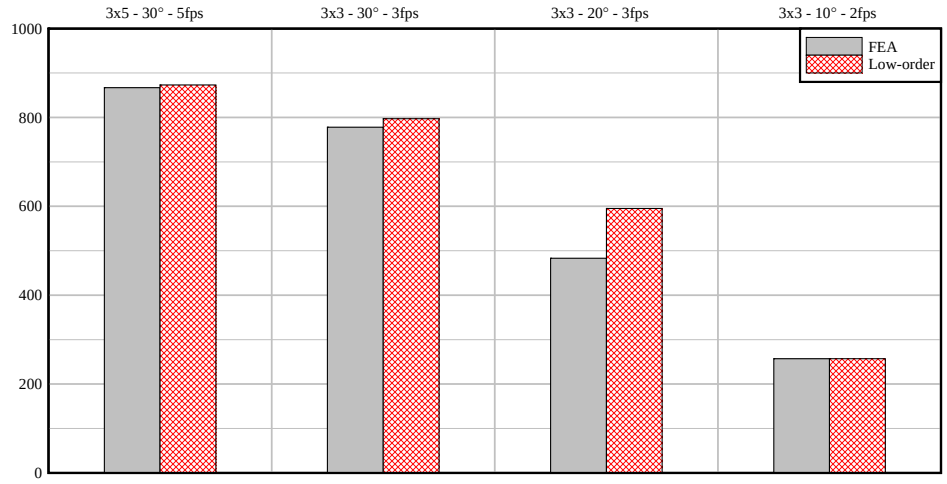

Figure 5.22. Summary of peak forces for semi-flexible guide wall impacts

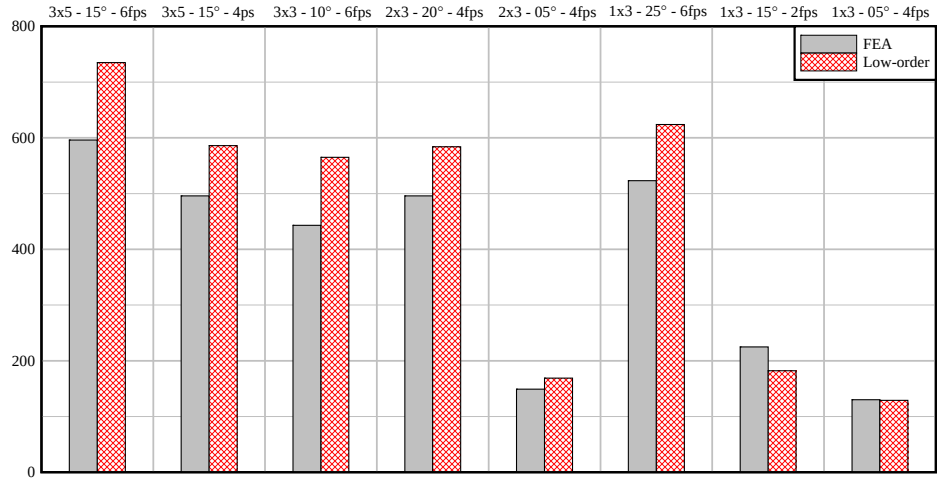

Figure 5.23. Summary of peak forces for pile founded guide wall (MRLD2) impacts

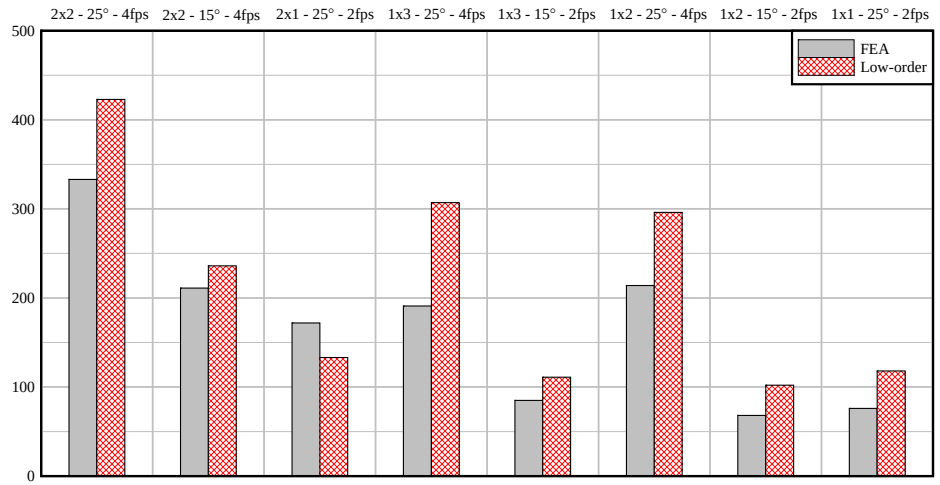

Figure 5.24. Summary of peak forces for flexible timber guide wall impacts

5.3 Head-on impacts on bullnoses

Head-on flotilla impacts against bullnose structures were investigated in a preceding study described in Consolazio and Wilkes (2013). Finite element models used in that study included a 35 ft diameter vertical-face semi-circular bullnose, a 10 ft diameter vertical-face semi-circular bullnose, and a 2:1 sloped-V bullnose (MRLD7). Results from impact simulations for these three structures are used in the present study to develop load prediction models for head-on flotilla impacts on bullnose structures. As with the empirical load prediction models described in the previous section for oblique wall impacts, a key objective in formulating the head-on bullnose load prediction models is simplicity of use (e.g., for design purposes). Consequently, only the bullnose and flotilla parameters that most strongly influence impact loads are included in the developed models.

5.3.1 Summary of data used in developing unified load prediction model

Impact force results quantified in the previous bullnose study (Consolazio and Wilkes, 2013) are summarized for the 35 ft diameter semi-circular bullnose in Table 5.5; for the 10 ft diameter semi-circular bullnose in Table 5.6; and for the 2:1 sloped-V bullnose in Table 5.7. The same study revealed that the impact parameter yielding the highest correlation to peak impact forces on the bullnose structures was the *total flotilla momentum* (as opposed to lead row momentum). Consequently, peak impact force data are plotted as functions of total flotilla momentum for the 35 ft diameter semi-circular bullnose in Figure 5.25, the 10 ft diameter semi-circular bullnose in Figure 5.26, and the 2:1 sloped-V bullnose in Figure 5.27.

5.3.2 Unified empirical load prediction models for head-on flotilla impacts

As discussed in detail in Consolazio and Wilkes (2013), the impact-interaction between a barge flotilla and a vertical face semi-circular bullnose differs significantly from that which occurs when a barge flotilla impacts a sloped-V bullnose. In the latter case, the bow of the impacting barge tends to ride partially up the sloped face of the bullnose. As a result, the relationship between impact force and impact momentum for vertical face bullnoses differs significantly from that which is applicable to the sloped-V bullnose. Since maintaining maximum simplicity in the bullnose impact load prediction model is deemed desirable, it is necessary to separate vertical face semi-circular bullnose impact conditions from sloped-V impact conditions. As such, the approach taken here is to develop a *unified* load prediction model for semi-circular vertical face bullnose structures of varying diameters, and a separate, case-specific load prediction model for the sloped-V bullnose.

In Consolazio and Wilkes (2013), impact forces for semi-circular bullnoses were quantified for two distinct diameters: 35 ft and 10 ft. As is evident in Figure 5.28, which compares the 35 ft and 10 ft data sets, at moderate to high levels of impact momentum, increasing the bullnose diameter tends to produce an increase in impact force. This finding is consistent with numerous prior analytical studies (e.g., Consolazio et al. 2009, Getter and Consolazio 2011) in which the magnitudes of barge impact forces for *circular bridge piers* have been found to be linearly dependent on pier diameter. Consequently, in the semi-circular bullnose load prediction model developed here, impact forces for moderate to high momentum impacts conditions are assumed to be linearly dependent on bullnose diameter, denoted $\varnothing$.

Table 5.5. Peak force results from 35 ft diameter semi-circular bullnose study

Flotilla	Speed (FPS)	Total Flotilla Momentum (kip-in)	Peak Normal Force (kip)
3 x 5	6.0	11189	1983
3 x 5	6.0	11189	1996
3 x 5	2.0	3730	1586
3 x 5	2.0	3730	1604
3 x 3	2.0	2238	1341
3 x 3	6.0	6713	1836
3 x 3	2.0	2238	1601
2 x 5	2.0	2486	1326
2 x 3	2.0	1492	1323

Flotilla	Speed (FPS)	Total Flotilla Momentum (kip-in)	Peak Normal Force (kip)
1 x 5	6.0	3730	1642
2 x 5	6.0	7459	1816
2 x 3	6.0	4476	1669
1 x 5	2.0	1243	1317
1 x 3	2.0	746	1260
1 x 3	6.0	2238	1637
1 x 1	2.0	249	1022
1 x 1	6.0	746	1610

Table 5.6. Peak force results from 10 ft diameter semi-circular bullnose study

Flotilla	Speed (FPS)	Total Flotilla Momentum (kip-in	Peak Normal Force (kip)
3 x 5	6.0	11189	1653
3 x 5	2.0	3730	1249
3 x 5	6.0	11189	1477
3 x 5	2.0	3730	1480
3 x 3	4.0	4476	1413
3 x 3	2.0	2238	1304

Flotilla	Speed (FPS)	Total Flotilla Momentum (kip-in)	Peak Normal Force (kip)
2 x 5	4.0	4973	1427
2 x 3	4.0	2984	1429
1 x 5	4.0	2486	1335
1 x 3	4.0	1492	1313
1 x 1	4.0	497	1119

Table 5.7. Peak force results from 2:1 sloped-V bullnose study

Flotilla	Speed (FPS)	Total Flotilla Momentum (kip-in)	Peak Normal Force (kip)
3 x 5	2.0	3730	991
3 x 5	6.0	11189	1935
3 x 5	2.0	3730	994
3 x 5	6.0	11189	1351
3 x 4	5.0	7459	1210
3 x 3	6.0	6713	1336
2 x 5	6.0	7459	1362
2 x 3	6.0	4476	1221
3 x 3	2.0	2238	900

Flotilla	Speed (FPS)	Total Flotilla Momentum (kip-in)	Peak Normal Force (kip)
3 x 3	2.0	2238	902
2 x 5	2.0	2486	910
1 x 5	2.0	1243	789
1 x 5	6.0	3730	1192
2 x 3	2.0	1492	890
1 x 3	2.0	746	629
1 x 3	6.0	2238	1204
1 x 1	2.0	249	488
1 x 1	6.0	746	937

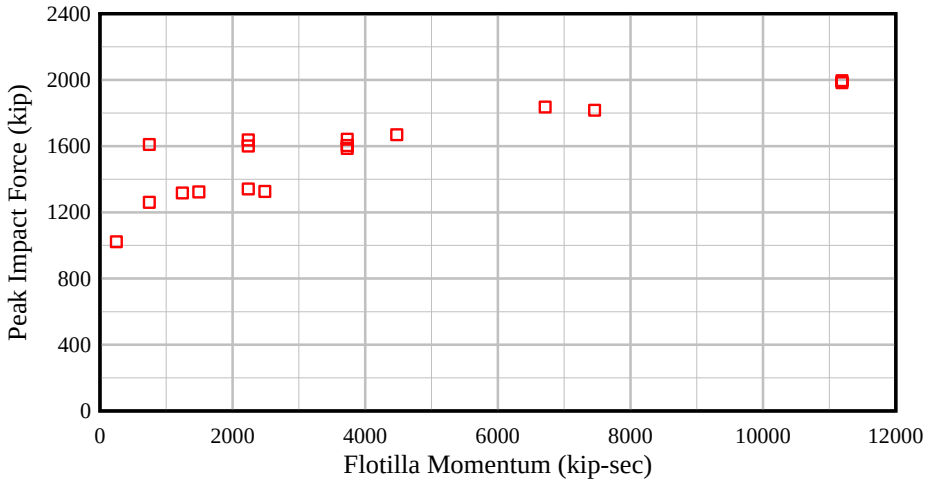

Figure 5.25. Peak force results from 35 ft diameter bullnose impacts (17 cases)

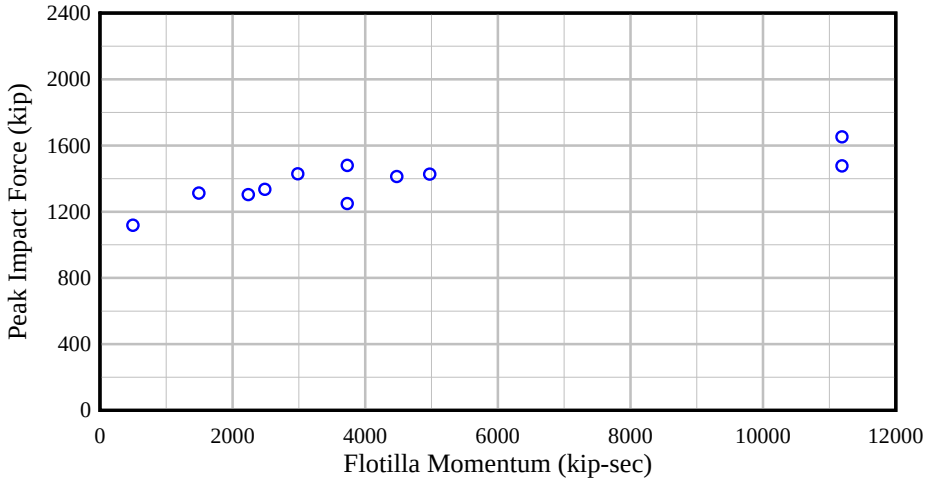

Figure 5.26. Peak force results from 10 ft diameter bullnose impacts (11 cases)

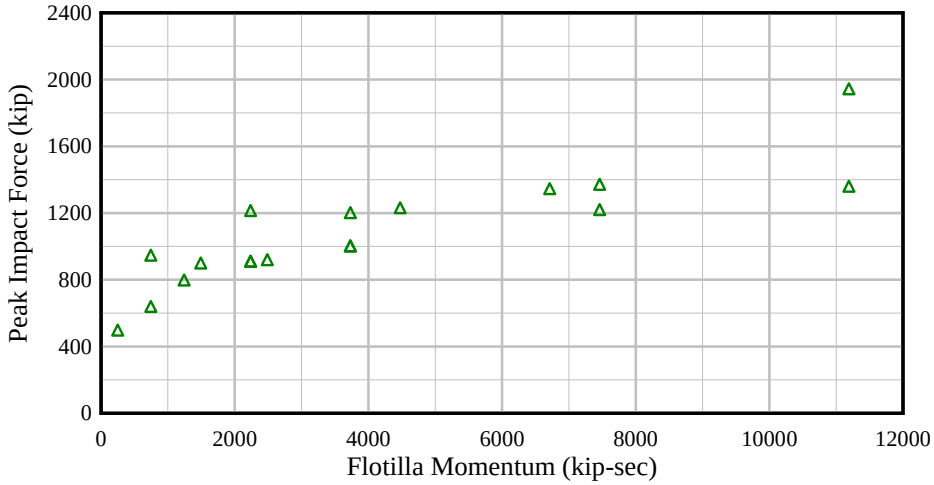

Figure 5.27. Peak force results from sloped-V bullnose impacts (18 cases)

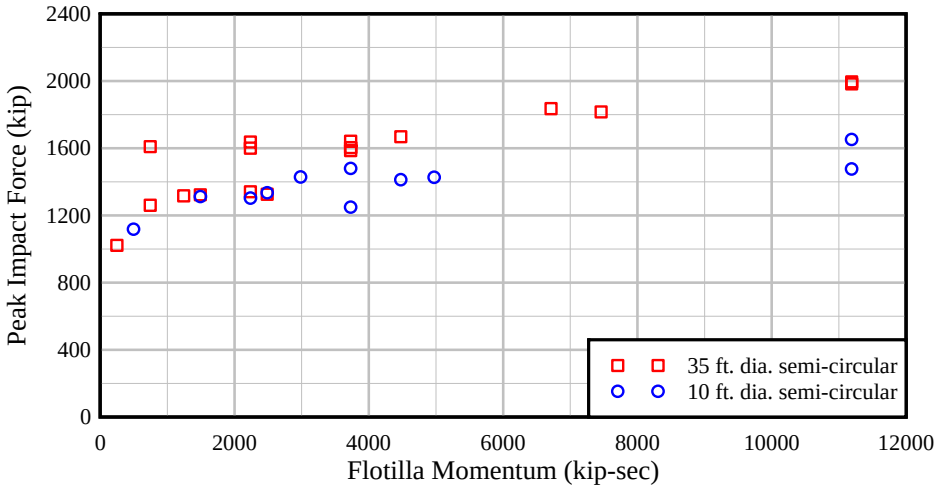

Figure 5.28. Peak force results from 35ft and 10 ft diameter bullnose impacts (28 cases)

Moreover, for the sake of consistency with the previously described oblique wall impact load prediction models, the semi-circular bullnose load prediction model is formulated as bilinear (Figure 5.29):

$$F = \begin{cases} S_1\, mv & \text{if } mv \le \left(F_{12}/S_1\right) \\ F_{12} + \underbrace{\left(S_{2A} + \left(S_{2B}\right)\left(\varnothing\right)\right)}_{S_2}\left(mv - \left(F_{12}/S_1\right)\right) & \text{otherwise} \end{cases} \tag{5.5}$$

where F is the impact force normal to the wall, F_{12}, S_1, S_{2A}, and S_{2B} are bilinear curve fitting parameters, $\varnothing$ is the bullnose diameter, m is the total mass of all barges in the flotilla, and v is the impact velocity.

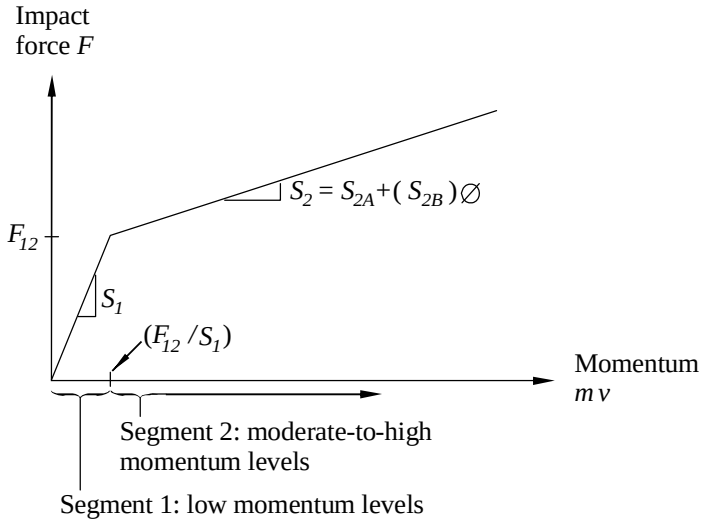

Figure 5.29. General form of unified bilinear curve fit used for semi-circular bullnoses

Upon assigning diameters of 35 ft and 10 ft to the appropriate data points in Figure 5.28, and subsequently minimizing—with respect to the fitting parameters F_{12}, S_1, S_{2A}, and S_{2B}—a cumulative square error function analogous to that described previously for oblique wall impact conditions, the following unified (in a least-square error sense) load prediction model is established for semi-circular bullnoses:

$$F = \begin{cases} 4.128\, mv & \text{if } mv \le 320 \text{ kip-sec} \\ 1321 + \left(0.003 + 0.001863\, \varnothing\right)\left(mv - 320\right) & \text{otherwise} \end{cases} \tag{5.6}$$

where mv is the total momentum of all barges in the flotilla in units of kip-sec., $\varnothing$ is the bullnose diameter in units of ft., and F is the impact force in units of kips.

In Figure 5.30, the unified (i.e., diameter-dependent) load prediction model, Eqn. (5.6), is evaluated for diameters of 35 ft and 10 ft, and compared to the impact force data shown in Figure 5.28. It is worth noting that the 35 ft and 10 ft curves presented in Figure 5.30 are similar to the simpler linear fits previously reported (for these same data sets) in Consolazio and Wilkes (2013). As such, the general observations and discussion presented in Consolazio and Wilkes (2013) for these cases remain valid. However, the unified model, Eqn. (5.6), offers two additional features relative to the previously developed (2013) linear models: 1) the introduction of an initial linear transition ('ramp up') segment for low-momentum impact conditions, and 2) a rationally derived functional dependence on bullnose diameter.

Additional comparisons of the unified load prediction model to *individual* data sets are presented for the 35 ft diameter bullnose in Figure 5.31, and for the 10 ft diameter bullnose in Figure 5.32.

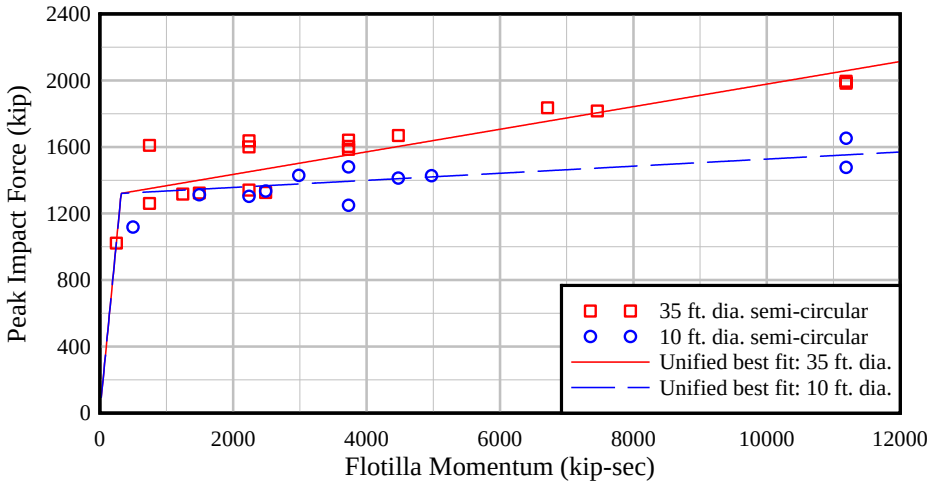

Figure 5.30. Comparison of semi-circular bullnose data and unified bilinear curve fit (the latter evaluated using diameters $\varnothing$=35 ft. and $\varnothing$=10 ft.)

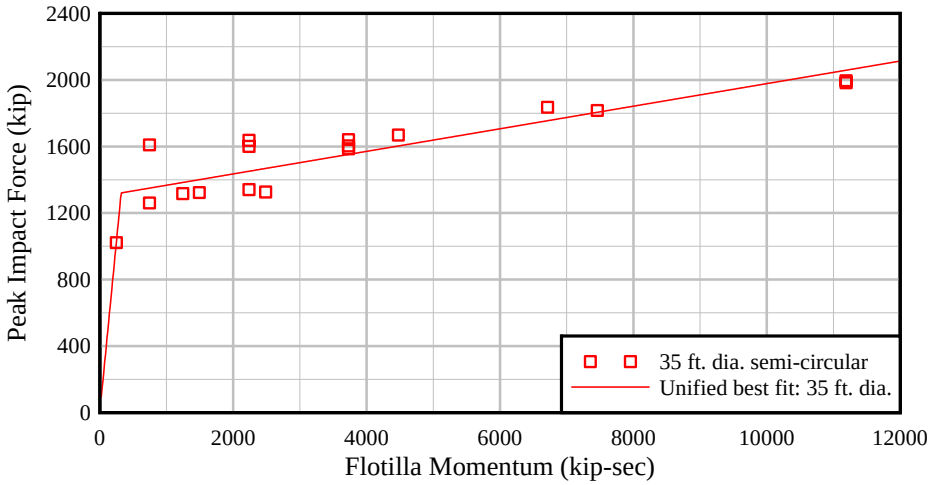

Figure 5.31. Comparison of 35 ft semi-circular bullnose data and unified bilinear curve fit (the latter evaluated with diameter ∅=35 ft.)

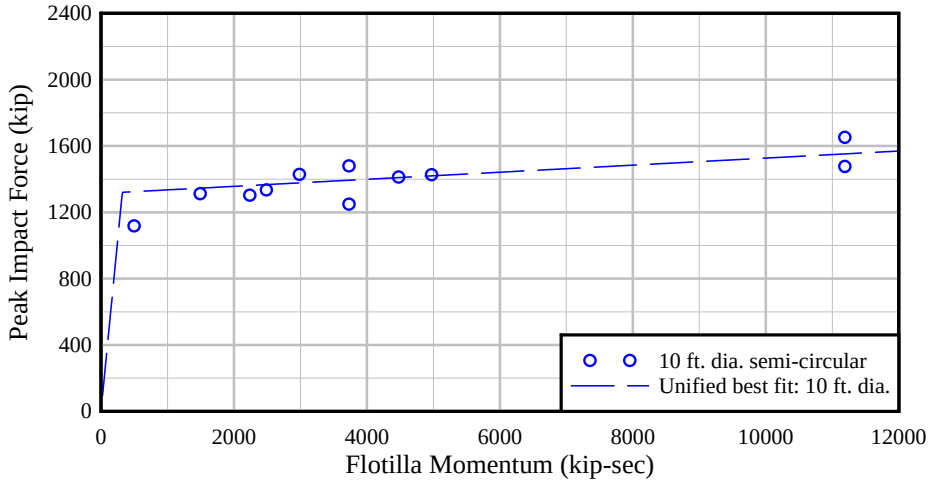

Figure 5.32. Comparison of 10 ft semi-circular bullnose data and unified bilinear curve fit (the latter evaluated with diameter ∅=10 ft.)

As noted earlier, the mechanics of barge impacts with vertical face semi-circular bullnoses differ significantly from impacts against the 2:1 sloped-V bullnose. In the latter case, the vertically sloped face of the bullnose allows the impacting barge bow to partially ride up the structure, thereby dissipating energy and reducing impact loads. In addition, the plan-view wedge shape (V-shape) of the sloped-V bullnose produces a deformation zone in the barge bow that differs significantly from that produced by a semi-circular bullnose. Consequently, the relationships between momentum, bow deformation, and impact force for the sloped-V differ from those associated with semi-circular bullnoses.

For these reasons, it is not practical to incorporate, or to 'unify', the impact force data for the sloped-V bullnose into the semi-circular load prediction model presented above in Eqn. (5.6). Instead, a separate, case-specific empirical load prediction model is developed for the sloped-V bullnose from the data summarized in Figure 5.27. As before, for the sake of consistency, the

sloped-V impact load prediction model is formulated as a bilinear function. Furthermore, since impact force data are only available for a single configuration of sloped-V bullnose, the slope S_2 of the general bilinear curve fit (recall Figure 5.29), which was linearly dependent on diameter $\varnothing$ in Eqn. (5.5), is instead formulated—for the specific case of the sloped-V bullnose—as a constant (non-diameter-dependent) value. This leads to the following bilinear functional form:

$$F = \begin{cases} S_1\, mv & \text{if } mv \le \left(F_{12}/S_1\right) \\ F_{12} + S_2\left(mv - \left(F_{12}/S_1\right)\right) & \text{otherwise} \end{cases} \tag{5.7}$$

Upon solving for the parameters F_{12}, S_1, S_2 that best fit the data shown in Figure 5.27, the following impact load prediction model is established for the sloped-V bullnose:

$$F = \begin{cases} 1.963\, mv & \text{if } mv \le 407 \text{ kip-sec} \\ 799 + 0.078\left(mv - 407\right) & \text{otherwise} \end{cases} \tag{5.8}$$

where mv is the total momentum of all barges in the flotilla in units of kip-sec., and F is the impact force in units of kips. In Figure 5.33, the load prediction model, Eqn. (5.8), is compared to the force data used in the fitting process.

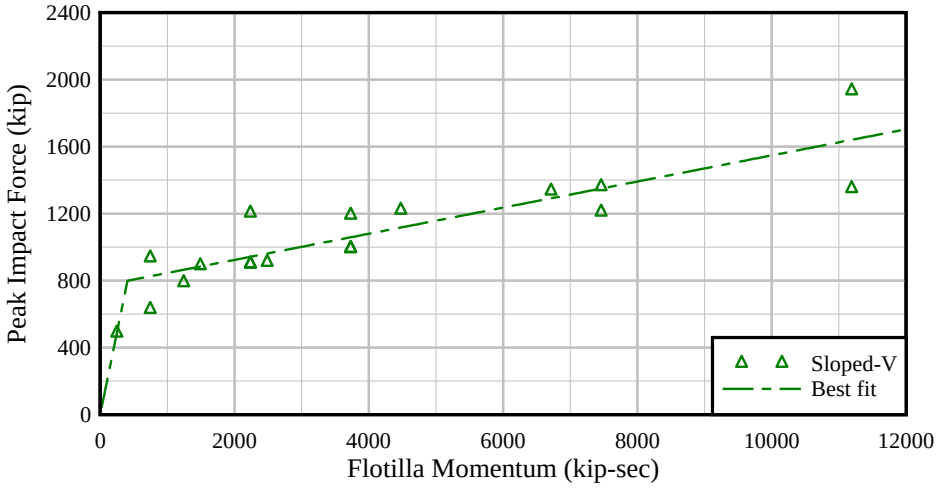

Figure 5.33. Comparison of 2:1 sloped-V bullnose data and load prediction model

CHAPTER 6
SUMMARY AND CONCLUSIONS

The first portion of this study makes use of nonlinear dynamic finite element simulations to quantify maximum impact forces on pile-founded guide wall structures subjected to oblique barge flotilla impacts. Finite element models of two types of pile-founded guide wall structures are developed. The first model is representative of the USACE's inventory of large-mass concrete guide walls supported on traditional foundations of timber piling and is developed from as-built plans of the upper pool interior monoliths at Mississippi River Lock and Dam No. 2 (MRLD2). The second model is representative of large-mass concrete guide walls that are supported on a unique combination of rock-filled timber cribbing and timber piling. This second model is based on as-built plans of the lower pool interior monoliths at Mississippi River Lock and Dam No. 3 (MRLD3).

Each pile-founded guide wall model is integrated with previously developed barge flotilla models to simulate dynamic barge-wall impact events, and quantify both time-varying impact forces and maximum (peak) impact forces. Simulations are conducted using 1x3, 2x3, 3x3, and 3x5 flotilla configurations; impact speeds ranging from 1 FPS to 6 FPS; and impact angles ranging from 5° to 25°. In total seventy-one (71) 'primary' parametric impact simulations are performed: fifty-seven (57) for the MRLD2 structure, and fourteen (14) for timber-cribbed MRLD3 structure. In addition to the 'primary' parametric impact simulations, a large number of 'supplementary' simulations are conducted to investigate impact force sensitivity to parameters such as guide wall-to-pile connection (fixed or pinned); presence of backfill soil; barge impact elevation; and presence of adjacent monoliths.

Results from the impact simulations indicate that maximum impact forces for the MRLD2 wall, which is laterally stiffer than the timber-cribbed MRLD3 structure, are generally larger than forces quantified for MRLD3 (with the exceptions being primarily related to low-energy impacts). In addition, simulation results also indicate that maximum impact forces for pile founded guide walls, similar in configuration to MRLD2 and MRLD3, are most strongly related *not* to the total momentum of the flotilla, but instead to the momentum of the *lead row* of barges in the flotilla. This finding is consistent with previous studies of oblique flotilla impacts on other types of wall structures (rigid, 'semi-flexible' concrete, and highly flexible timber guide walls).

The second portion of this study focuses on the development of load prediction models for waterway structures using data collected from the current study and preceding studies. Since oblique (glancing blow) flotilla impacts on wall structures differ significantly from head-on impacts against rigid structures (e.g. bullnoses), load prediction models are developed separately for each of these two broad categories of structural type.

For oblique impacts on walls, two distinctly different approaches are used to develop impact load prediction models: 1) empirical curve fitting, and 2) a simplified two-dimensional low-order (low degree-of-freedom; low-DOF) nonlinear dynamic model. To develop empirical oblique impact load prediction models based on curve fitting, available wall impact force data are separated into two categories: 1) data corresponding to large mass concrete walls, 2) and data corresponding to flexible timber guide walls (which have far less stiffness and mass than typical concrete walls). For each set of collected data, bilinear curve-fits are empirically formulated to relate impact force (normal to the wall) to the momentum of the lead row of barges (normal to the wall). For concrete walls, impact force data collected from rigid wall, semi-flexible guide

wall (Winfield), and pile founded guide wall (MRLD2) impact simulations are simultaneously incorporated into an error minimization curve fitting process to produce a 'unified' load prediction model that is a function of lateral wall stiffness at the impact location. The model is referred to as being 'unified' as it is applicable to a range of concrete wall structures, and incorporates dependency on wall stiffness in the load calculation process.

In contrast, because the flexible timber guide wall structure (also considered in this study) has far less stiffness and mass than typical concrete walls, its dynamic response differs significantly. As a result, it is not feasible to incorporate, or 'unify', data from the flexible timber guide wall into the load prediction model developed for concrete walls. Instead, a separate, case-specific bilinear empirical load prediction model is developed for the flexible timber guide wall.

With the goal of developing an oblique impact load prediction methodology capable of addressing both large mass concrete walls and flexible timber guide walls, within a single unified framework, an alternative approach involving dynamic analysis of a low-order (low degree-of-freedom; low-DOF) flotilla-wall model is developed. Demonstrations of the method indicate acceptable levels of accuracy are obtainable for widely varying structural types (ranging from rigid wall to flexible timber guide wall). It recommended that, before this method is provided to structural engineers as a practical tool for load determination, additional testing be conducted, and that the method be implemented into a dedicated software package.

For head-on barge flotilla impacts with bullnose structures, empirical load prediction models are developed for semi-circular bullnoses of varying diameters and for the 2:1 sloped-V bullnose. However, since the impact-interaction between a barge flotilla and a vertical face semi-circular bullnose differs significantly from that which occurs when a barge flotilla impacts a sloped-V bullnose, the relationships between impact force and impact momentum for vertical face bullnoses differ significantly from that which is applicable to the sloped-V bullnose. For this reason, separate empirical load prediction models are developed for the semi-circular bullnoses and the sloped-V bullnose. In both scenarios, however, empirical bilinear curve-fits are formed to relate head-on impact force to the *total* momentum of the flotilla (in contrast to the *lead-row* momentum term used in the oblique wall impact load prediction models).

For semi-circular bullnoses, force data collected from impact simulations of 35 ft diameter and 10 ft diameter bullnoses are simultaneously incorporated into an error minimization curve fitting process, the outcome of which is a 'unified' bilinear load prediction model that is linearly dependent on bullnose diameter. The model is considered to be 'unified' in that, by making the load calculation process dependent on diameter, it is applicable to a range of semi-circular bullnoses. (It is also worth noting that the assumption of a linear relationship between impact force and structure diameter is corroborated not only by the data used in this study, but also by prior analytical barge impact studies published in the literature.)

As noted, head-on flotilla impacts against sloped-V bullnoses involve different modes of barge deformation and response, and therefore different relationships between momentum, deformation, and load. As a result, it is not feasible to 'unify' data from the sloped-V bullnose into the load prediction model developed for semi-circular bullnoses. Instead, a separate, case-specific bilinear empirical load prediction model is developed specifically for the sloped-V bullnose.

REFERENCES

Consolazio, G. R., Davidson, M. T., and Cowan, D. R., "Barge bow force-deformation relationships for barge-bridge collision analysis." *Transportation Research Record 2131*, Transportation Research Board, Washington, DC, 3–14, 2009.

Consolazio, G.R., Davidson, M.T., and Getter, D.J., *Development and support of dynamic numerical modeling of aberrant rake barges impacting hurricane protection structures subjected to forces from a hurricane environment*, Final report to U.S. Army Corps of Engineers, Structures Research Report 2010/83710, University of Florida, Department of Civil and Coastal Engineering, 112 p., 2010.

Consolazio, G.R., Walters, R.A., Harper, Z.S., *Development of Finite Element Models for Studying Multi-Barge Flotilla Impacts*, Final report to U.S. Army Corps of Engineers, Structures Research Report 2012/87754, University of Florida, Department of Civil and Coastal Engineering, 61 p., 2012.

Consolazio, G.R., Walters, R.A., *Development Of Multi-Barge Flotilla Finite Element Models For Use In Probabilistic Barge Impact Analysis Of Flexible Walls*, Final report to U.S. Army Corps of Engineers, Structures Research Report 2012/94753, University of Florida, Department of Civil and Coastal Engineering, 79 p., 2012.

Consolazio, G.R. and Wilkes, J.R., *Determination of Multi-Barge Flotilla Impact Loads on Bullnose Structures and Flexible Timber Guide Walls*, Final report to U.S. Army Corps of Engineers, Structures Research Report 013/96918, University of Florida, Department of Civil and Coastal Engineering, 162 p., 2013.

FB-MultiPier, *FB-MultiPier User's Manual*. Florida Bridge Software Institute, University of Florida, Gainesville, Florida, 2013.

Getter, D. J., and Consolazio, G. R., "Relationships of barge bow force-deformation for bridge design: Probabilistic consideration of oblique impact scenarios." *Transportation Research Record 2251*, Transportation Research Board, Washington, DC, 3-15, 2011.

Kulhawy, F. H., Mayne, P. W., *Manual on Estimating Soil Properties for Foundation Design*, Electric Power Research Institute, EL-6800, 1990.

LSTC, *LS-DYNA Keyword User's Manual*, Livermore Software Technology Corporation, Livermore, CA, 2013.

Skempton, A. W., *Standard penetration test procedures and the effects in sands of overburden pressure, relative density, particle size, ageing and consolidation*, Geotechnique 36(3): 425-447, 1986.

U.S. Army Corps of Engineers, *2007 Flood Control and Navigation Maps: Mississippi River*, U.S. Army Corps of Engineers, Washington D.C., 2007.

U.S. Army Corps of Engineers, *Lock and Dam 3 General Re-Evaluation Report, Geotechnical and Geology*, 2013.

U.S. Army Corps of Engineers, *Upper Mississippi Rives Locks and Dams*, 2012.

APPENDIX A
BARGE FLOTILLA LASHING CONFIGURATIONS

A flotilla is a grouping of individual barges bound together using wire ropes (or lashings) that wrap around bitts (cylindrical posts) which protrude from the barge deck (Figure A.1). In this study, the lashings are pre-tensioned to 50% of ultimate capacity and anchored to cleats on the barge deck. Each wire rope within the finite element model is assigned an appropriate geometric configuration; a set of material properties that represent the nonlinear stiffness of the lashing; and a failure criterion based on ultimate capacity. An ultimate tensile strength of either 90 kips (for 1 in. diameter wire rope) or 120 kips (for 1.25 in. diameter wire rope) is assigned to each of the wire ropes. By including a wire rope (lashing) failure criterion, each flotilla model has the ability to experience break-up wherein individual barges are free to separate and move independently.

Figure A.1. Typical lashing configuration on barge flotilla

Each pair of adjacent barges within a flotilla are lashed together by wrapping the barge bitts in a specific pattern, referred to as a lashing configuration. Different configurations are used to lash different types of barge pairs (end-to-end, side-to-side, or diagonal) and to resist different loads imposed by common flotilla maneuvers. Lashings are layered on top of each other when more than one configuration is required at the same location. For a detailed description of the finite element (mathematical) modeling of the lashings, see Consolazio et al. (2012).

Seven different lashing configurations are used in this study. The lashing designations are numbered followed by a ‘p’ (for port) or ‘s’ (for starboard), designating the tensioning end being anchored to a cleat on either the port or starboard side of the respective barge. For example, L1p denotes the lashing has configuration L1 and is anchored to the port side of the respective barge. The seven lashing configurations are shown in Figures A.2 through A.6. Lashings with breaking strengths of 90 kip (Figure A.2) and 120 kip (Figures A.3 and A.4) are used for fore-aft wires connecting end-to-end barge pairs at both corners. Breast wires (Figure A.5), which join side-to-side barge pairs at both corners, are rated at 120 kip breaking strength. Scissor wires (Figure A.6), also rated at a 120 kip breaking strength, connect diagonal barge pairs at all four-corner interfaces.

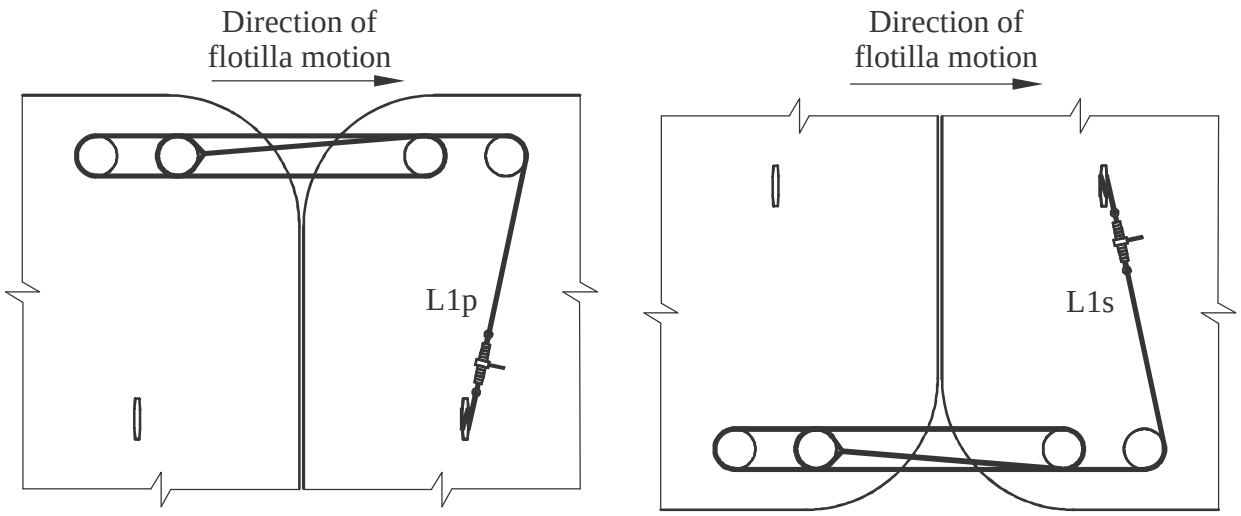

Figure A.2. Fore/aft wires rated for 90 kip break strength:
a) port anchored; b) starboard anchored

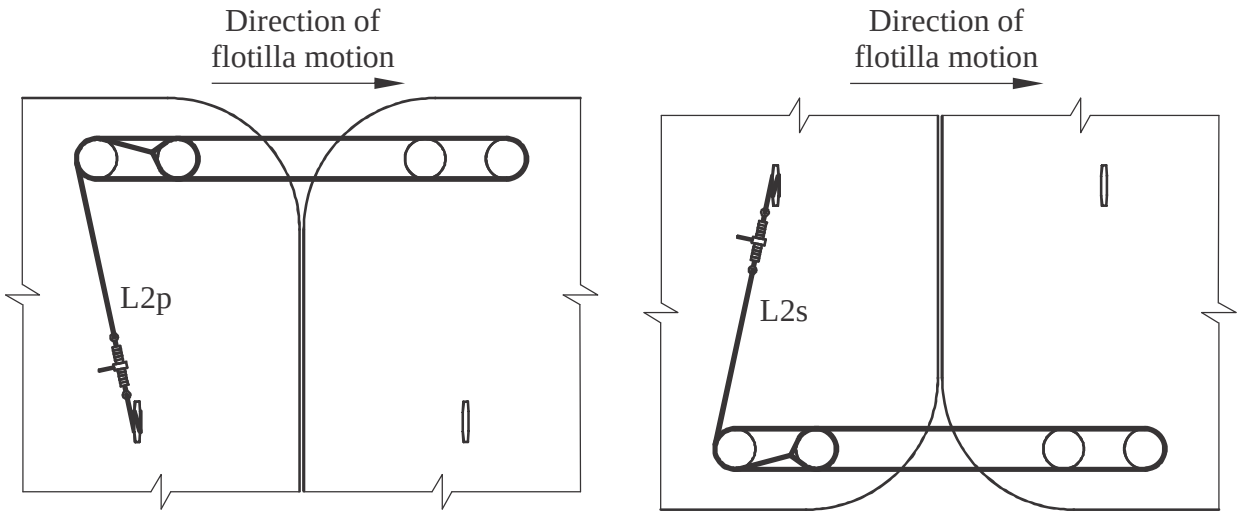

Figure A.3. Fore/aft wires rated for 120 kip break strength in 2x and 3x flotillas:
a) port anchored; b) starboard anchored

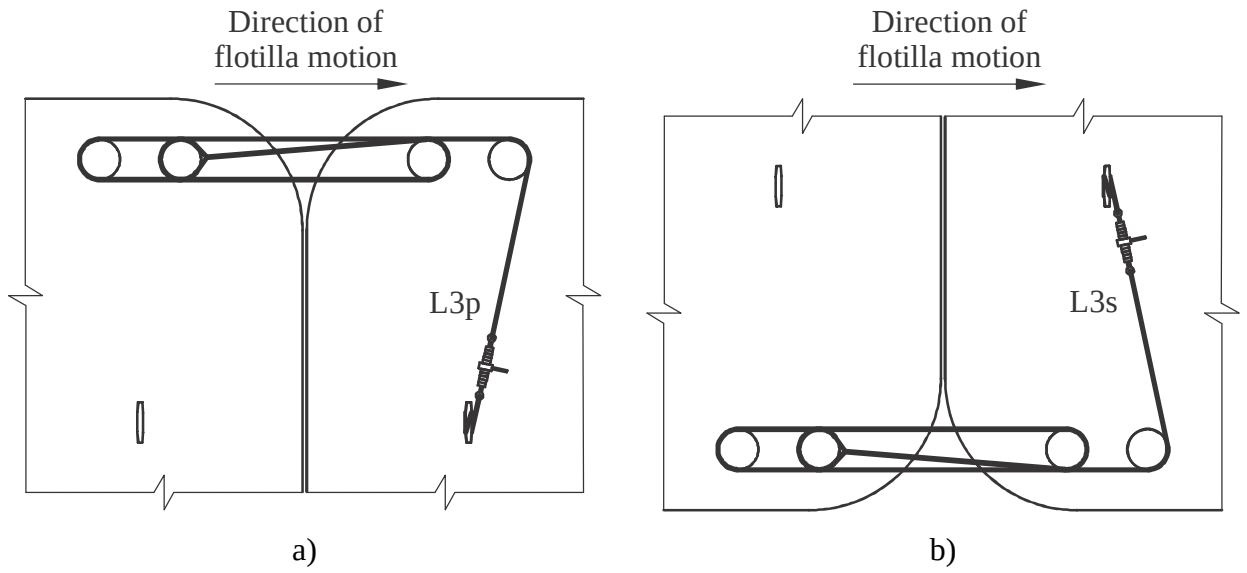

Figure A.4. Fore/aft wires rated for 120 kip break strength in 2x and 3x flotillas:
a) port anchored; b) starboard anchored

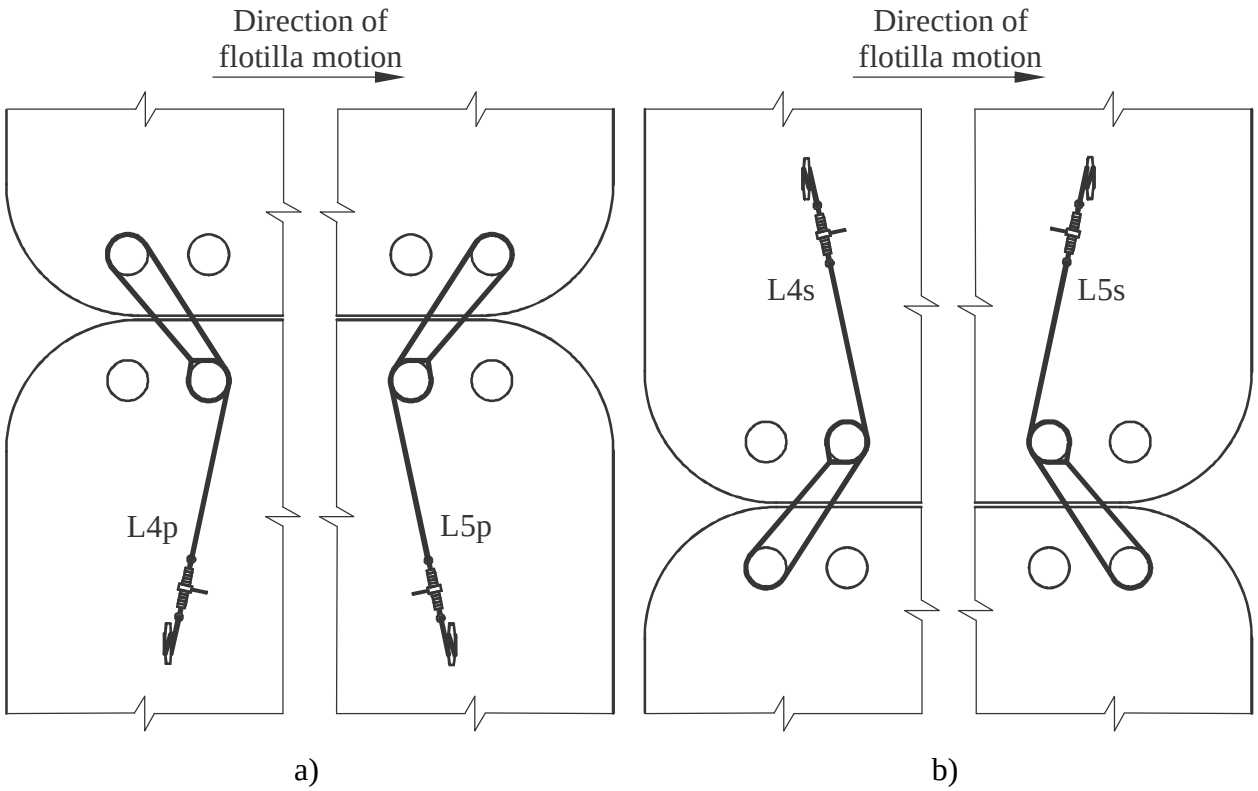

Figure A.5. Breast wires rated for 120 kip break strength:
a) port anchored; b) starboard anchored

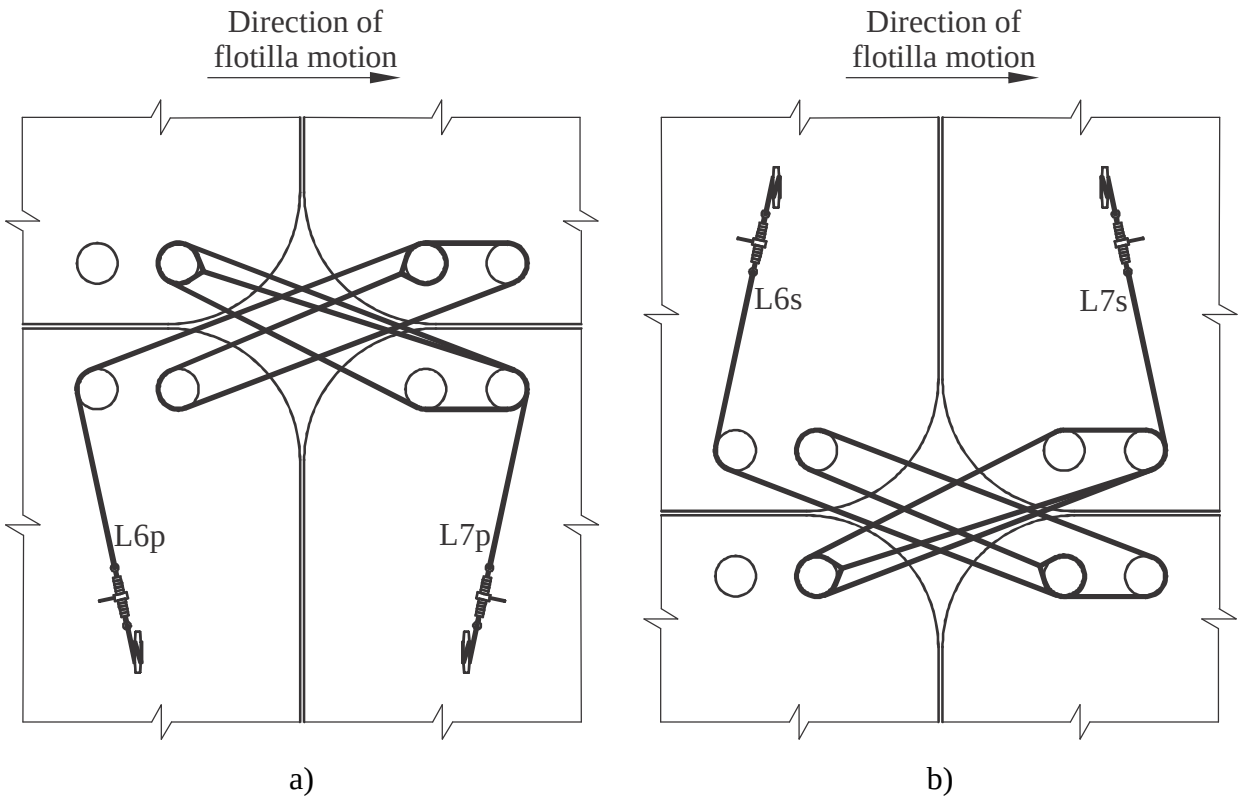

Figure A.6. Scissor wires rated for 120 kip break strength:
A) port anchored; b) starboard anchored

The smallest flotilla model used in this study, a 1x3, includes four lashings with two different configurations (Figure A.7). The 2x3 flotilla model used in this study includes eighteen lashings with seven different configurations (Figure A.8). The 3x3 flotilla model includes thirty-two lashings with seven different configurations (Figure A.9). The largest flotilla model used in this study, a 3x5, includes sixty lashings with seven different configurations (Figure A.10).

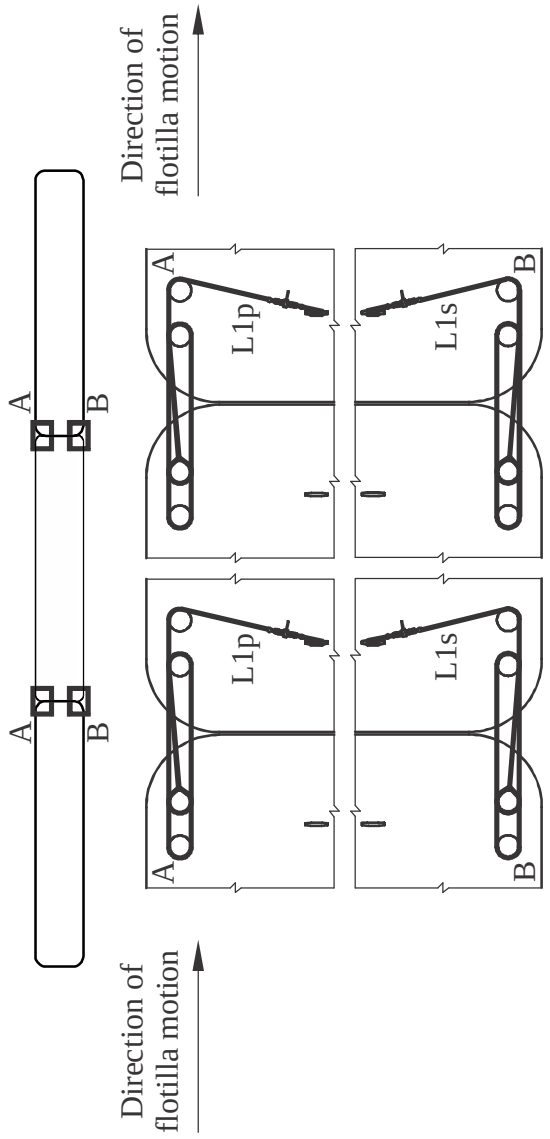

Figure A.7. Lashing configurations for 1x3 flotilla used in pfgw study

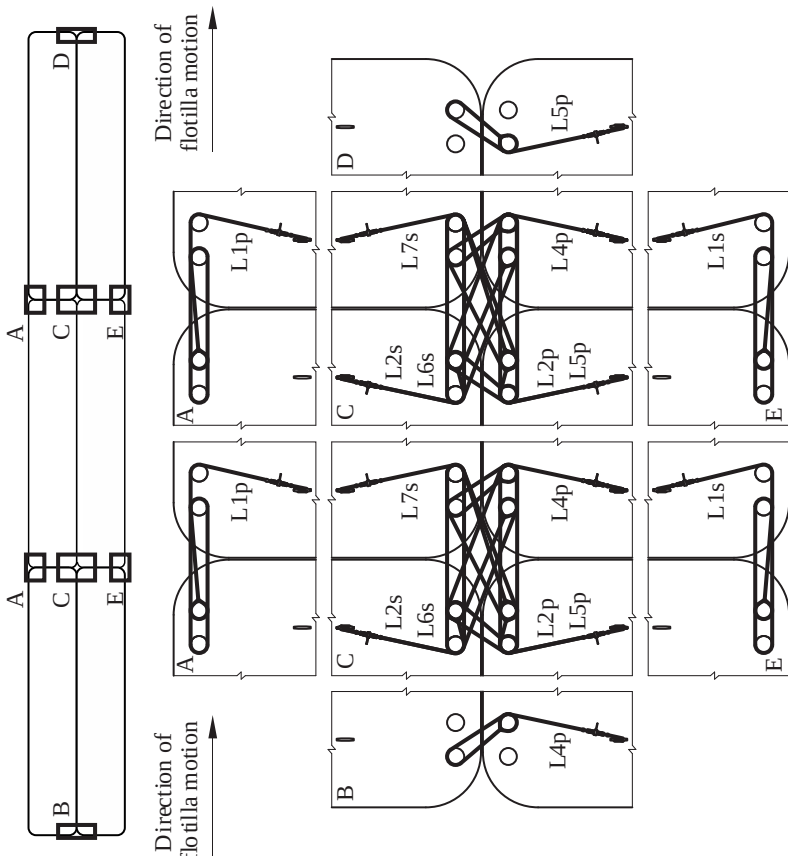

Figure A.8. Lashing configurations for 2x3 flotilla used in pile founded guide wall study

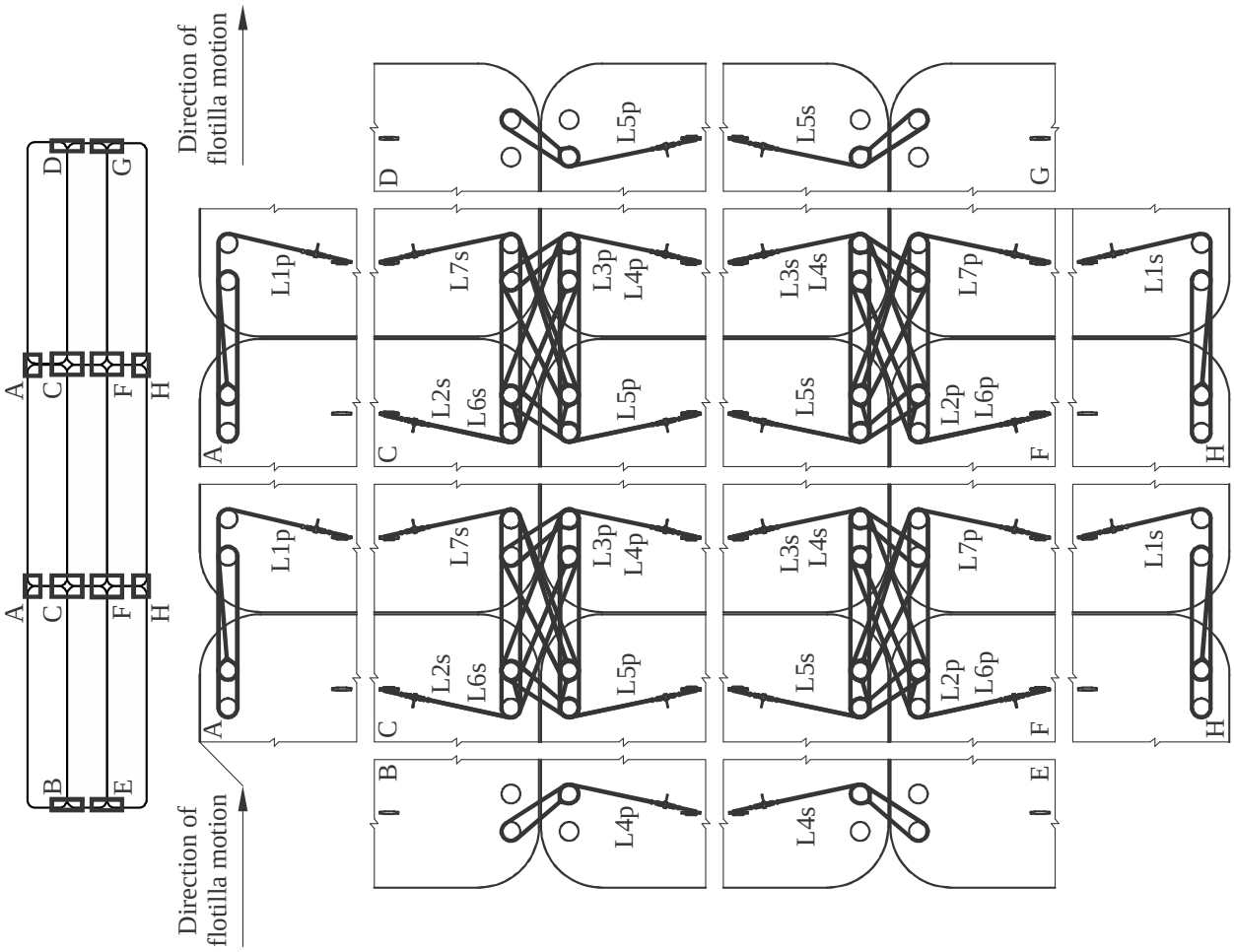

Figure A.9. Lashing configurations for 3x3 flotilla used in pile founded guide wall study

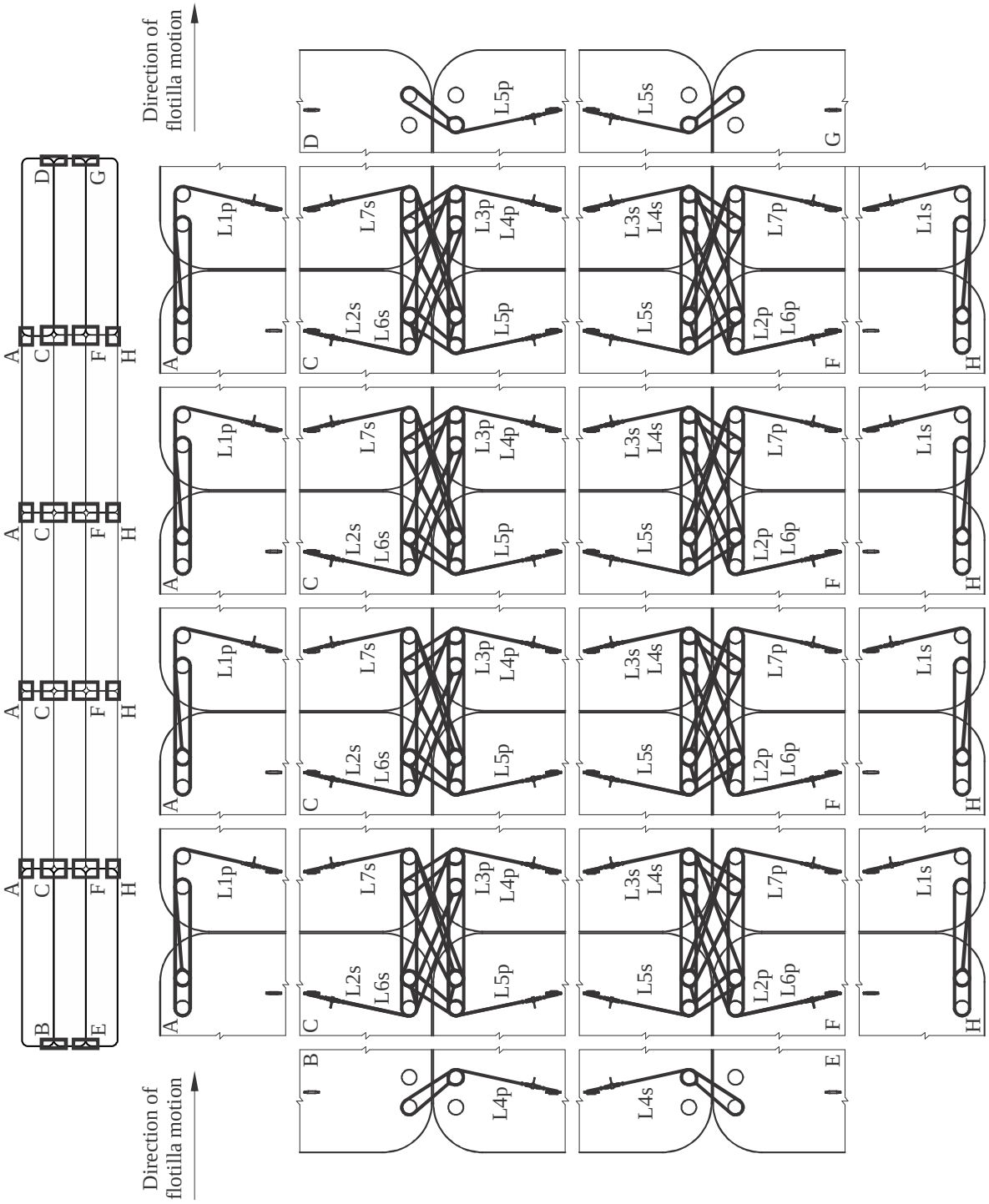

Figure A.10. Lashing configurations for 3x5 flotilla used in pile founded guide wall study

APPENDIX B
IMPACT FORCE-TIME HISTORIES FROM PILE-FOUNDED GUIDE WALL MRLD2 SIMULATIONS

Individual force-time histories for all MRLD2 impact simulations conducted in this study are plotted on the following pages. Each plot includes a trace of the *normal impact force in the horizontal plane*. All impact forces presented herein correspond to the contact force-time histories between the high-resolution impacting (deformable) barge model and the MRLD2 model. Also note that all forces presented in this appendix have been low-pass filtered using the procedure described earlier in this report.

The nomenclature used in each figure caption, to identify the impact condition that is plotted, is of the form:

NSxNR – SPEED – ANGLE – MRLD2

where:

NS	=	number of barge strings (barge columns) in the flotilla
NR	=	number of barge rows in the flotilla
SPEED	=	impact speed in ft/sec (FPS)
ANGLE	=	impact angle in degrees
MRLD2	=	Mississippi River Lock and Dam No. 2

For additional information regarding the MRLD2 impact conditions for which impact forces are plotted in this appendix, see Chapter 4.

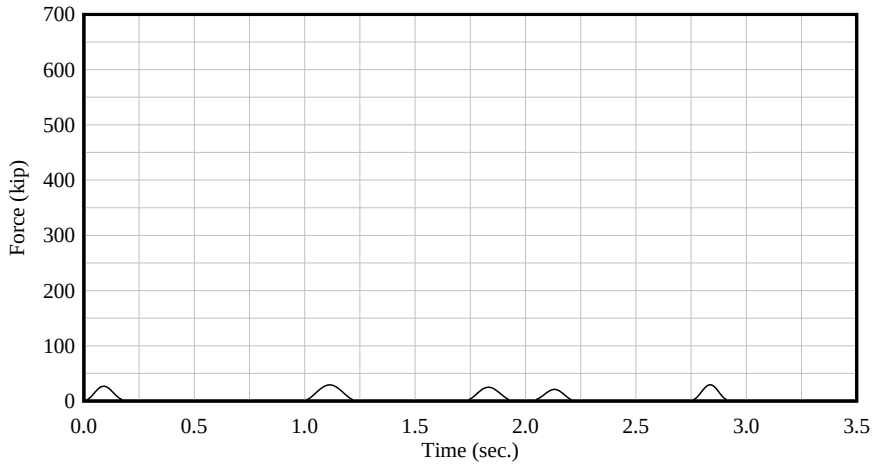

Figure B.1. 1x3 – 1 FPS – 5° – MRLD2

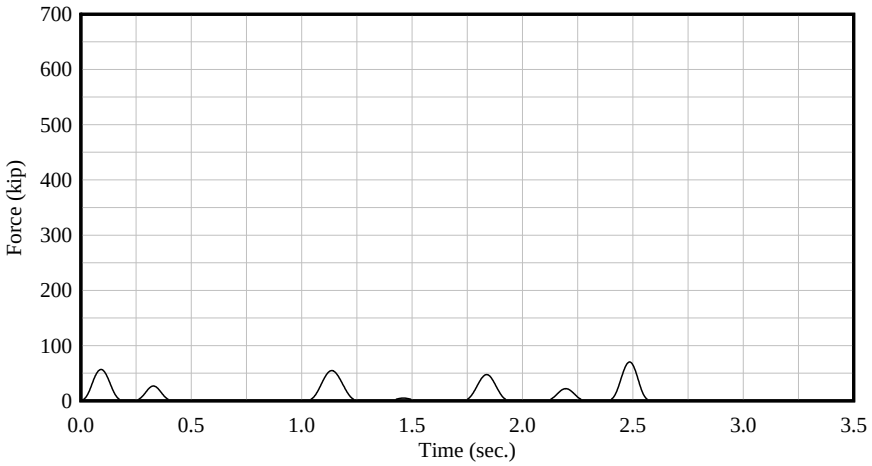

Figure B.2. 1x3 – 2 FPS – 5° – MRLD2

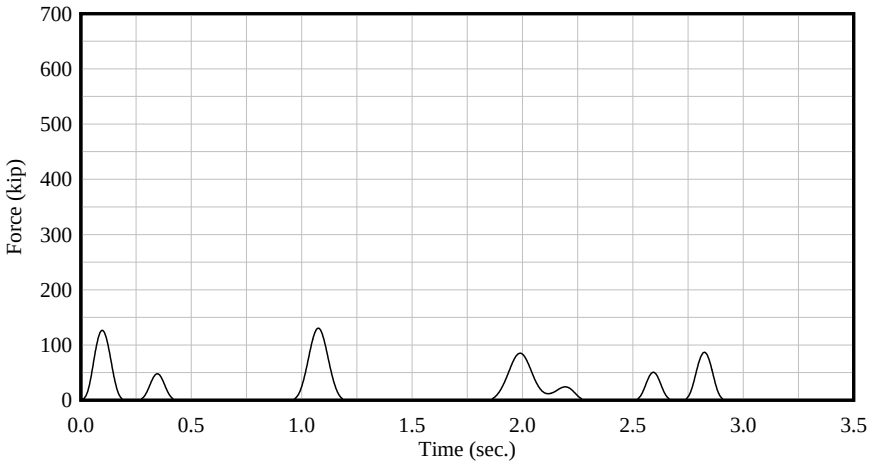

Figure B.3. 1x3 – 4 FPS – 5° – MRLD2

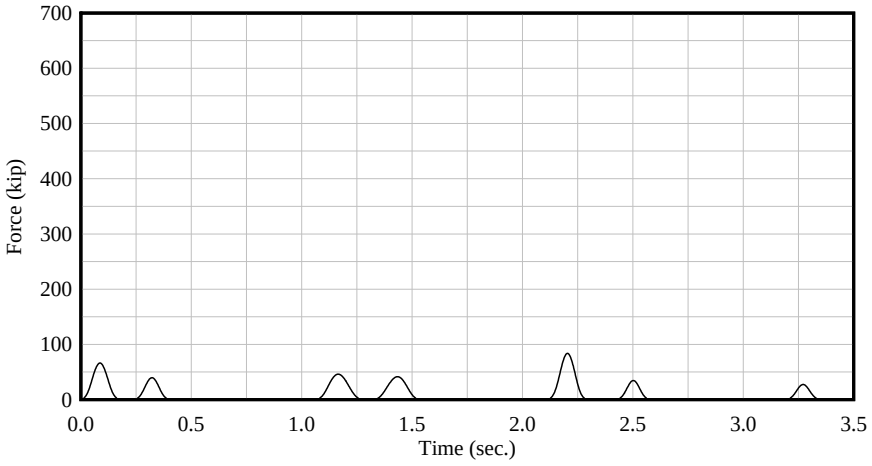

Figure B.4. 1x3 – 1 FPS – 10° – MRLD2

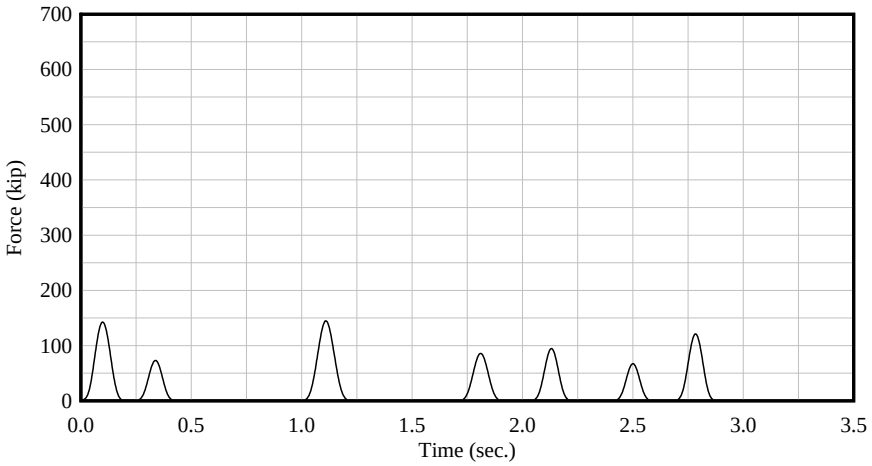

Figure B.5. 1x3 – 2 FPS – 10° – MRLD2

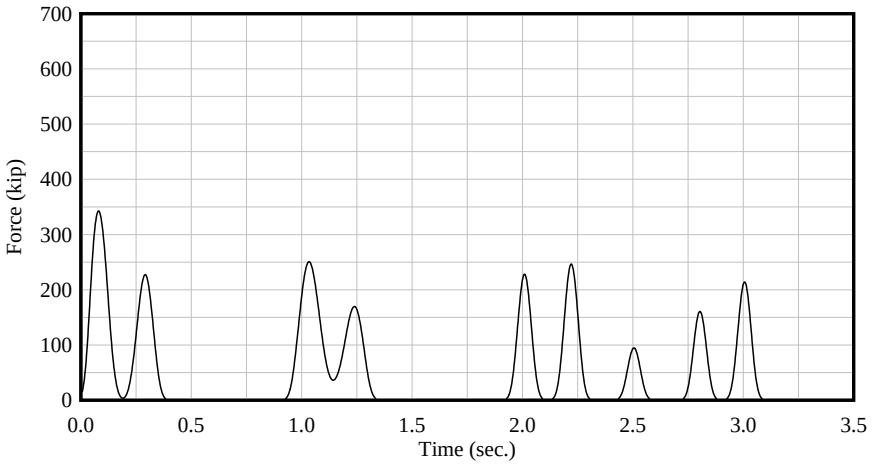

Figure B.6. 1x3 – 6 FPS – 10° – MRLD2

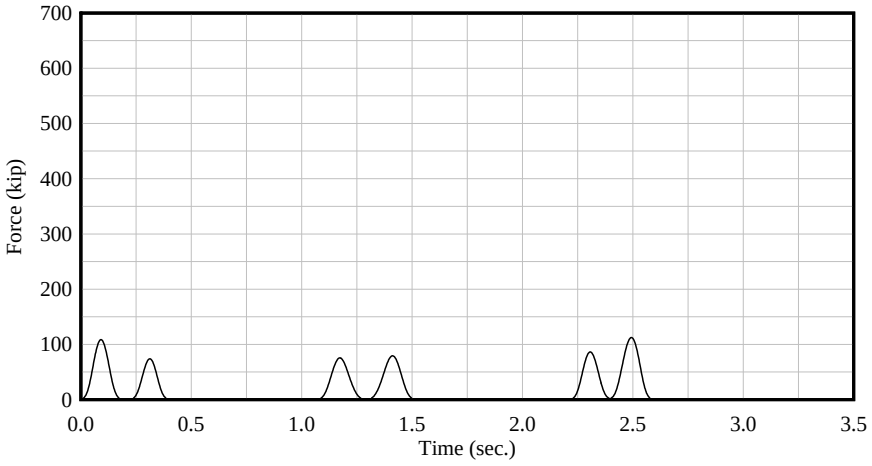

Figure B.7. 1x3 – 1 FPS – 15° – MRLD2

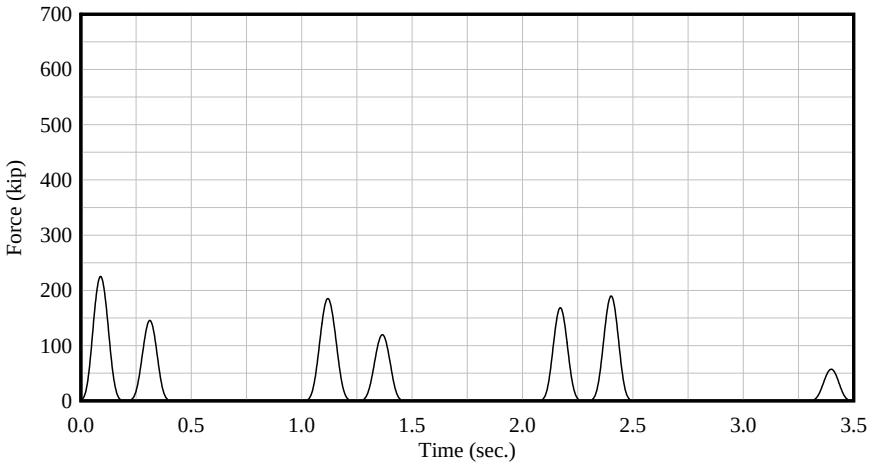

Figure B.8. 1x3 – 2 FPS – 15° – MRLD2

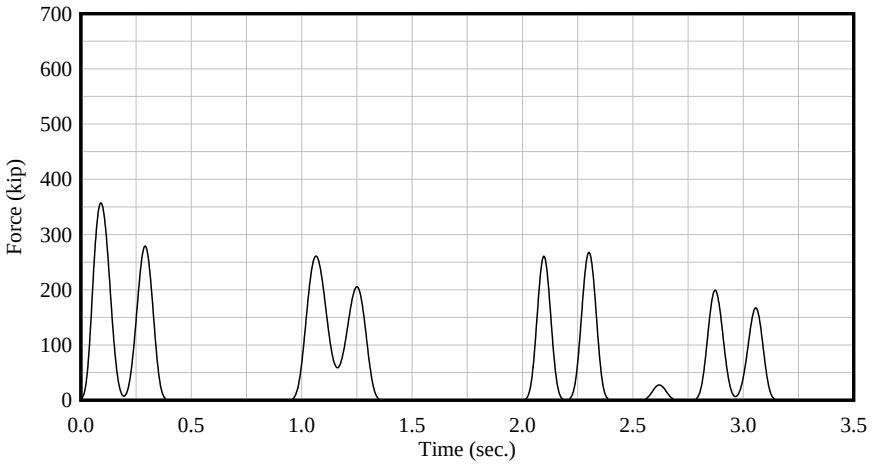

Figure B.9. 1x3 – 4 FPS – 15° – MRLD2

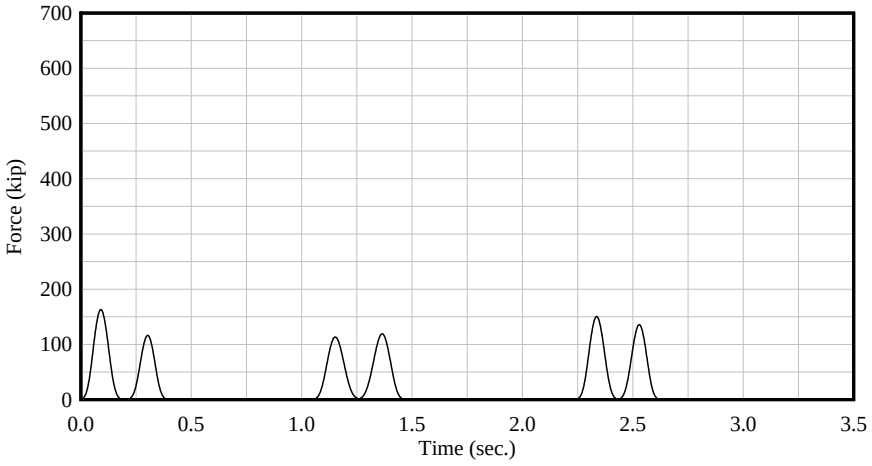

Figure B.10. 1x3 – 1 FPS – 20° – MRLD2

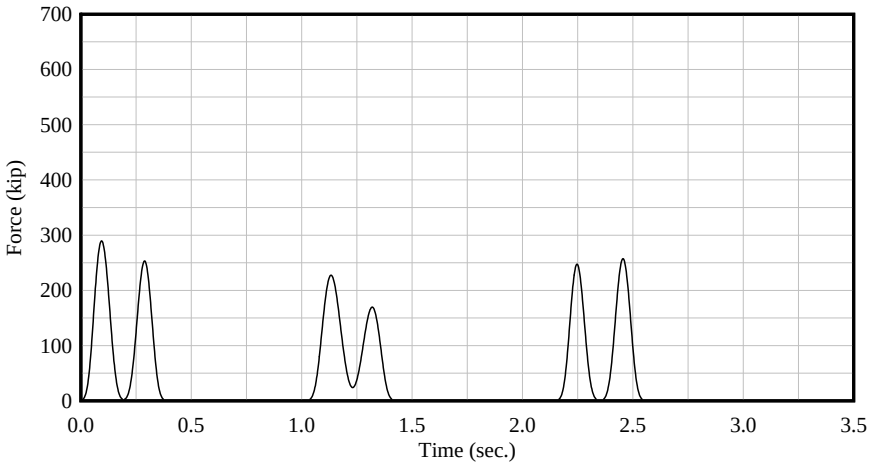

Figure B.11. 1x3 – 2 FPS – 20° – MRLD2

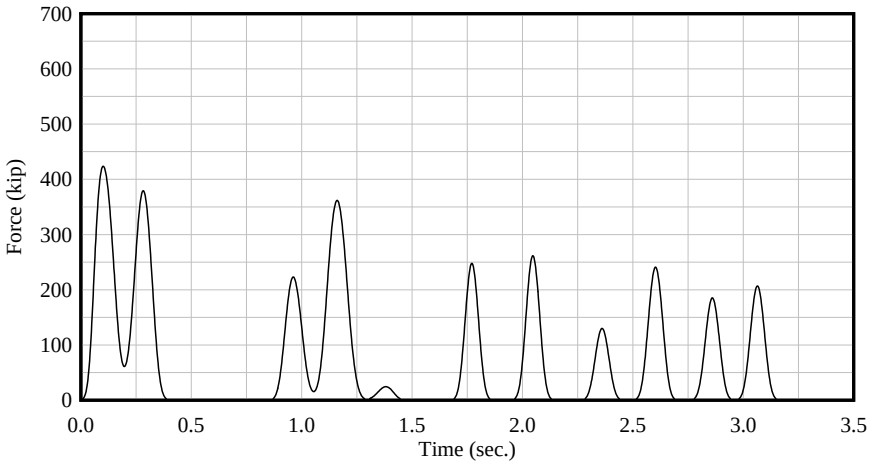

Figure B.12. 1x3 – 4 FPS – 20° – MRLD2

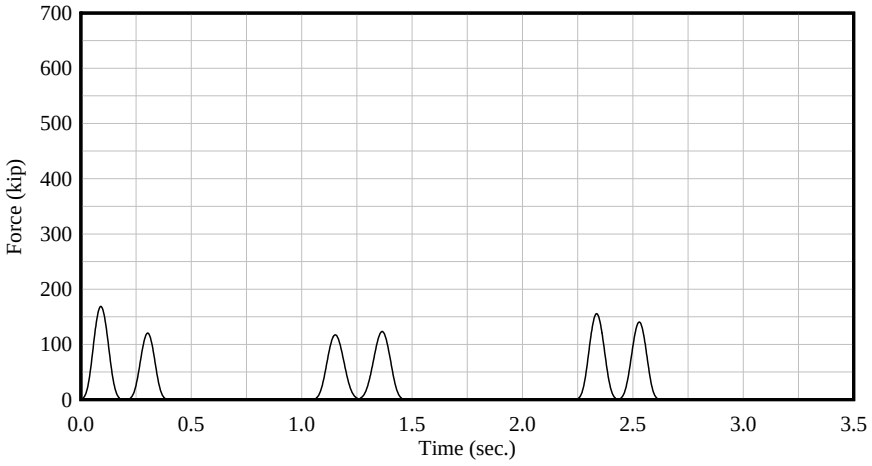

Figure B.13. 1x3 – 1 FPS – 25° – MRLD2

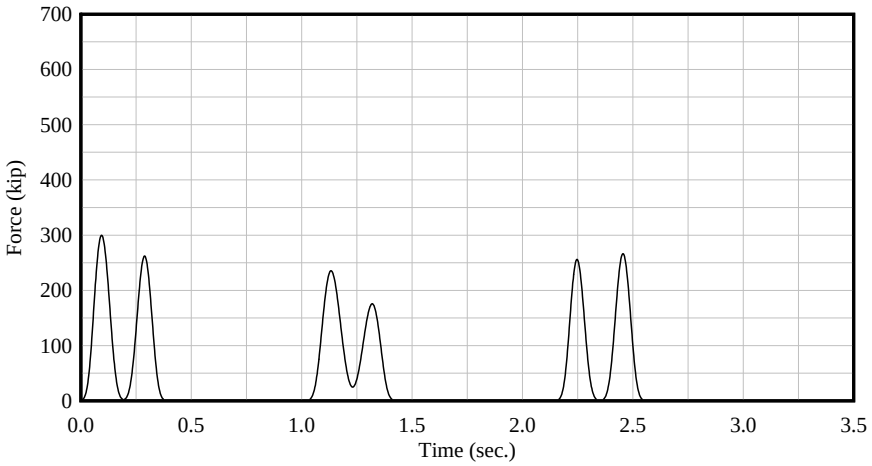

Figure B.14. 1x3 – 2 FPS – 25° – MRLD2

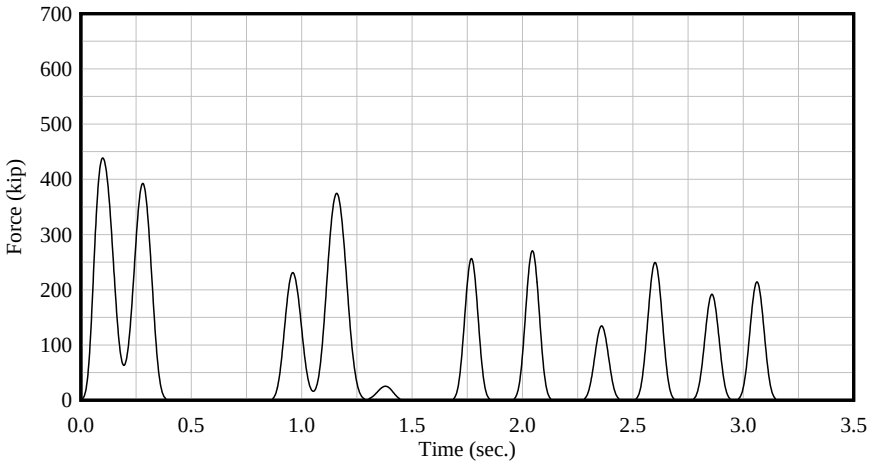

Figure B.15. 1x3 – 4 FPS – 25° – MRLD2

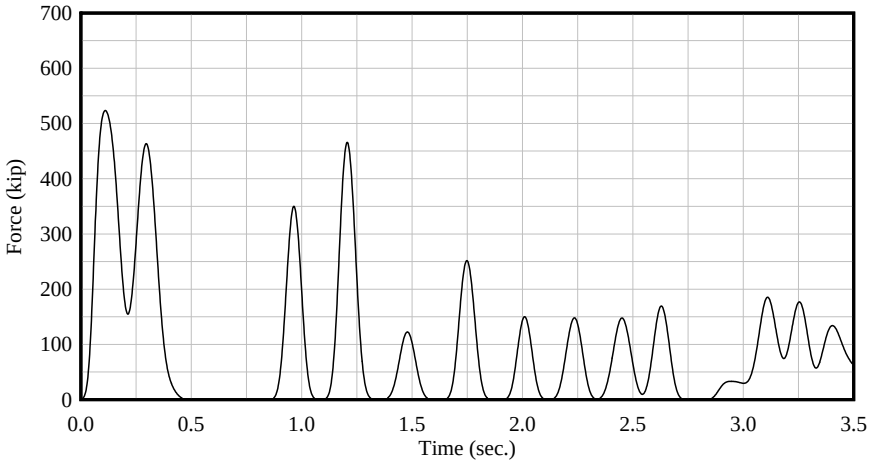

Figure B.16. 1x3 – 6 FPS – 25° – MRLD2

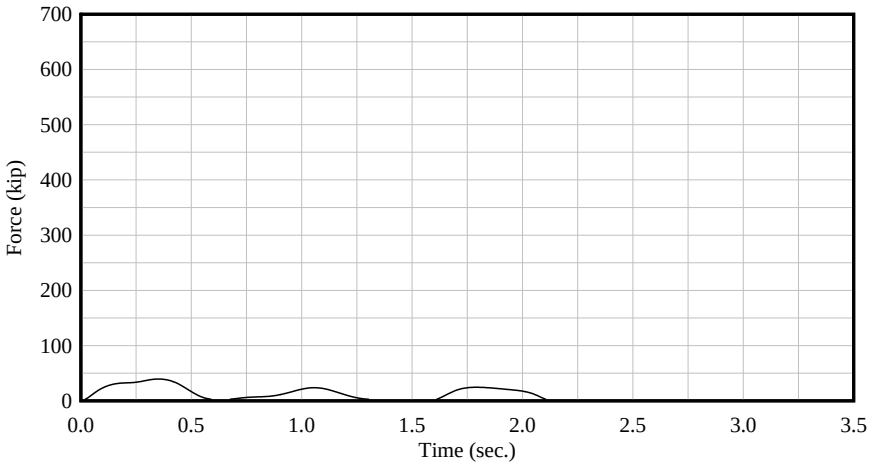

Figure B.17. 2x3 – 1 FPS – 5° – MRLD2

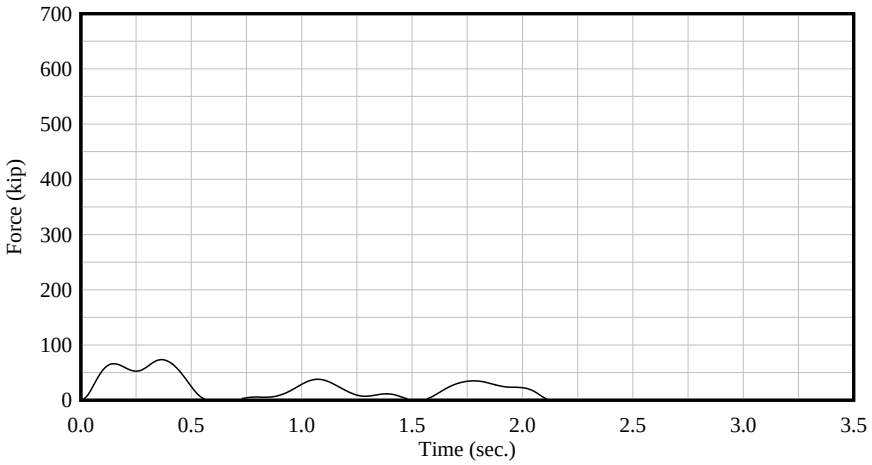

Figure B.18. 2x3 – 2 FPS – 5° – MRLD2

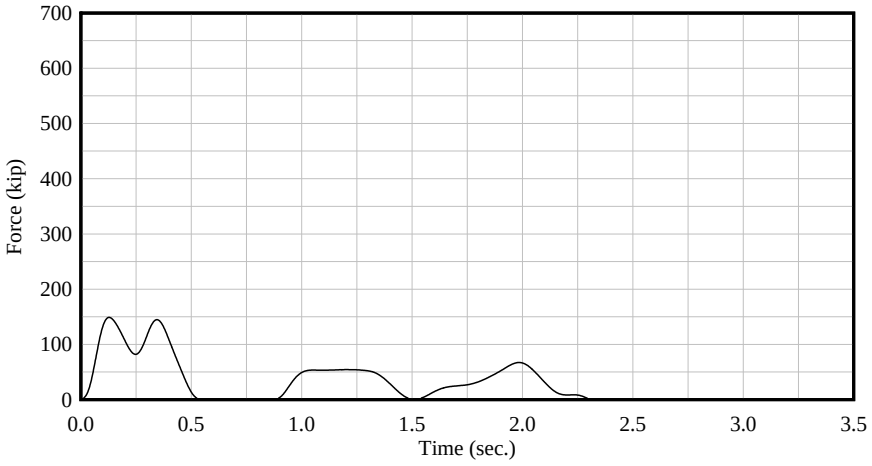

Figure B.19. 2x3 – 4 FPS – 5° – MRLD2

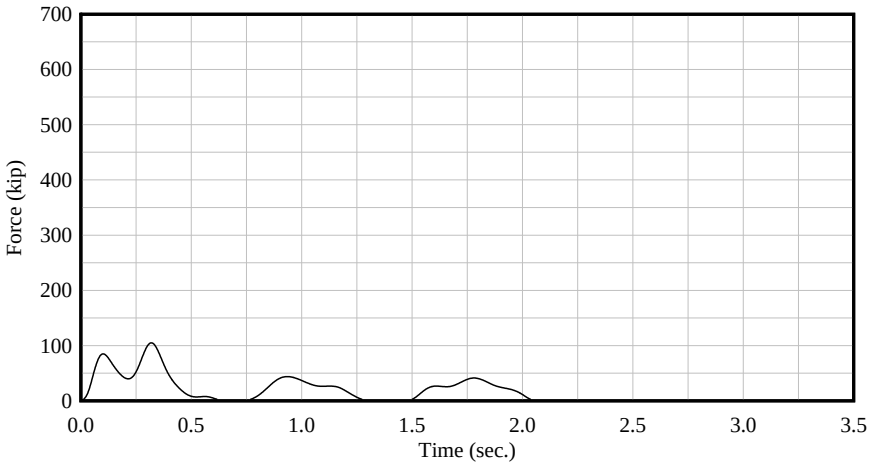

Figure B.20. 2x3 – 1 FPS – 10° – MRLD2

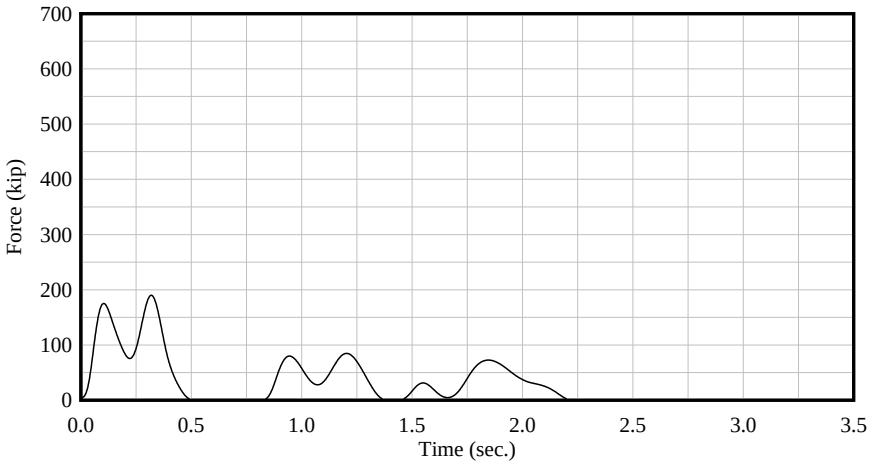

Figure B.21. 2x3 – 2 FPS – 10° – MRLD2

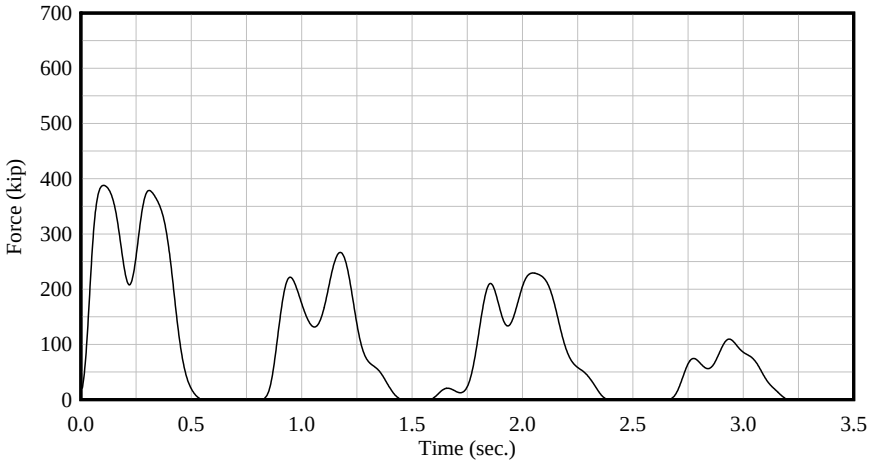

Figure B.22. 2x3 – 6 FPS – 10° – MRLD2

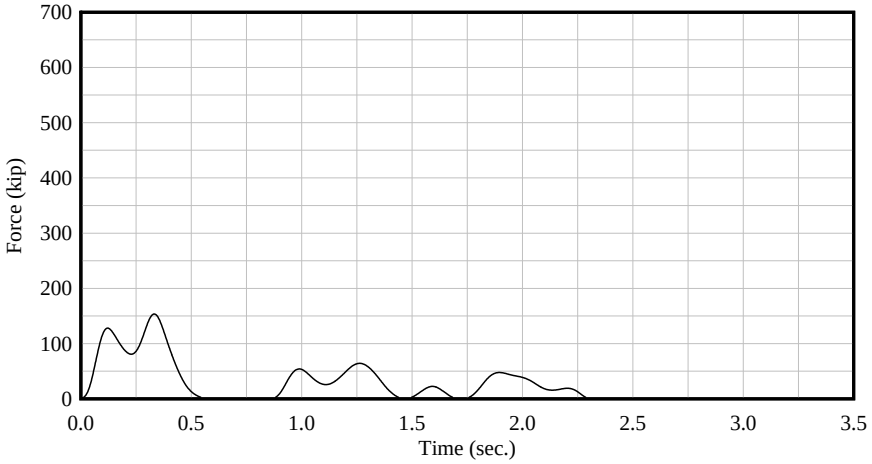

Figure B.23. 2x3 – 1 FPS – 15° – MRLD2

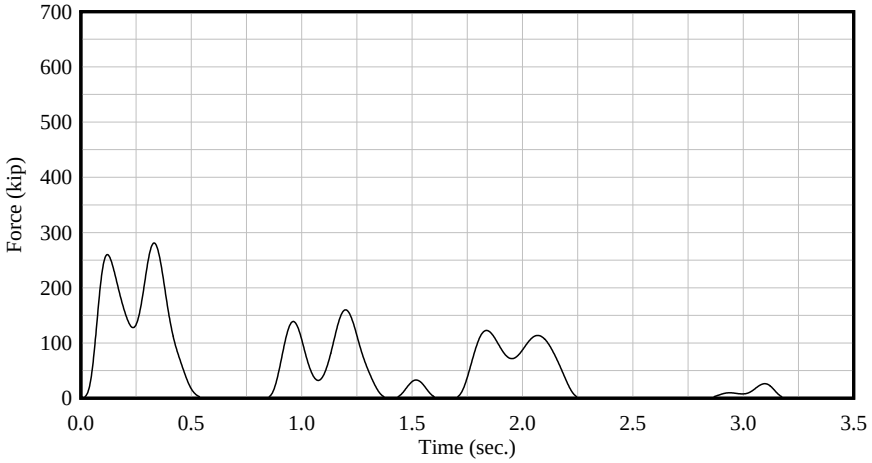

Figure B.24. 2x3 – 2 FPS – 15° – MRLD2

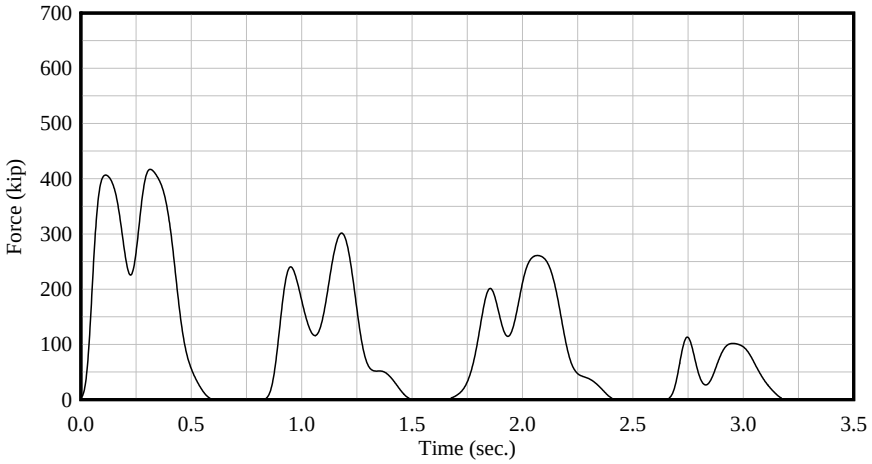

Figure B.25. 2x3 – 4 FPS – 15° – MRLD2

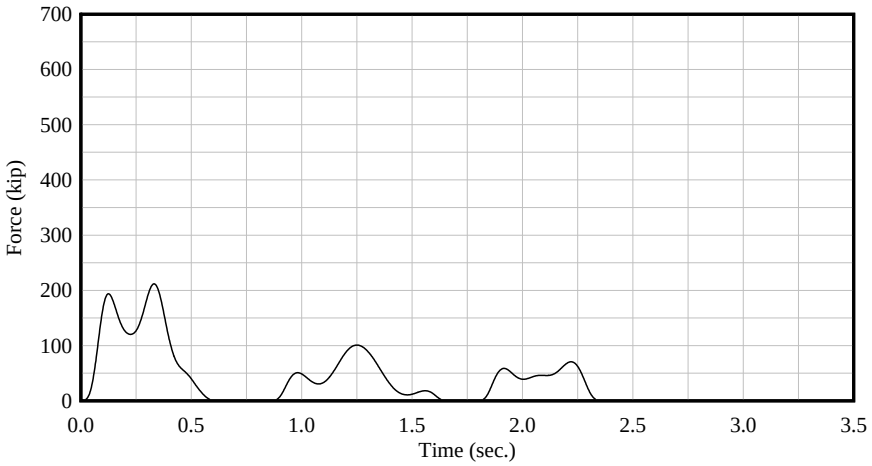

Figure B.26. 2x3 – 1 FPS – 20° – MRLD2

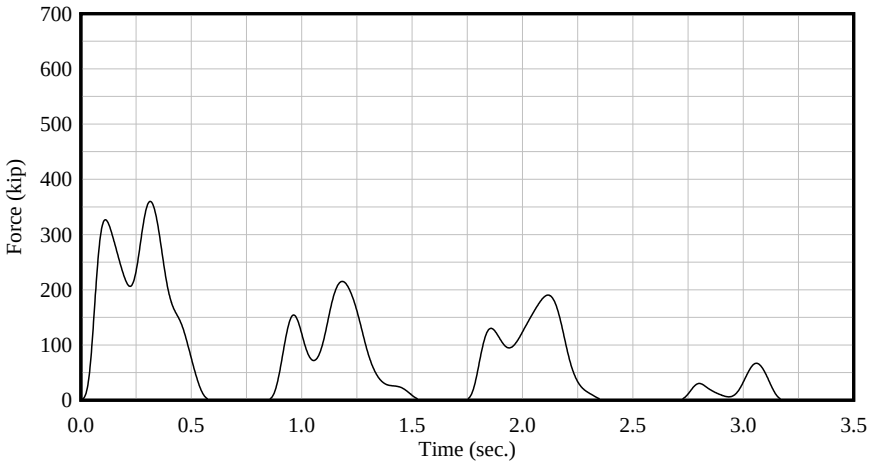

Figure B.27. 2x3 – 2 FPS – 20° – MRLD2

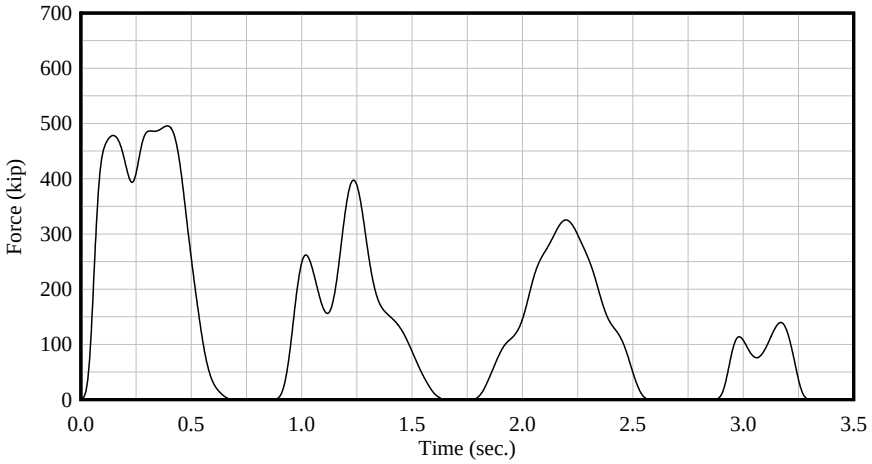

Figure B.28. 2x3 – 4 FPS – 20° – MRLD2

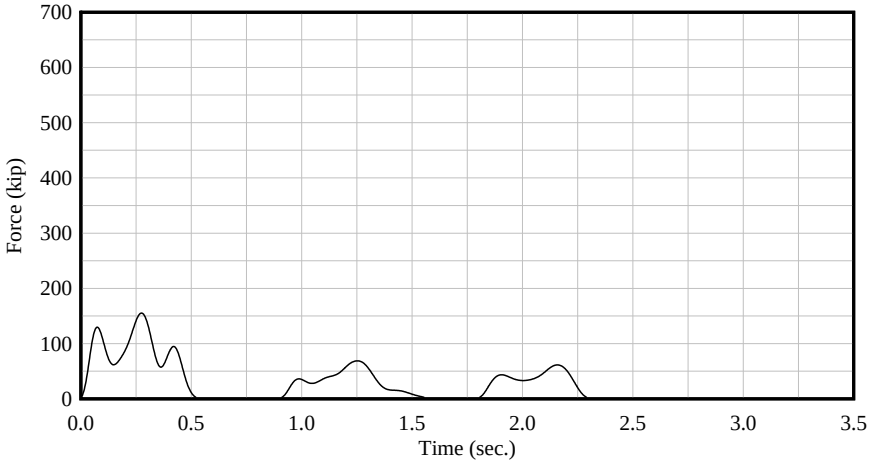

Figure B.29. 2x3 – 1 FPS – 25° – MRLD2

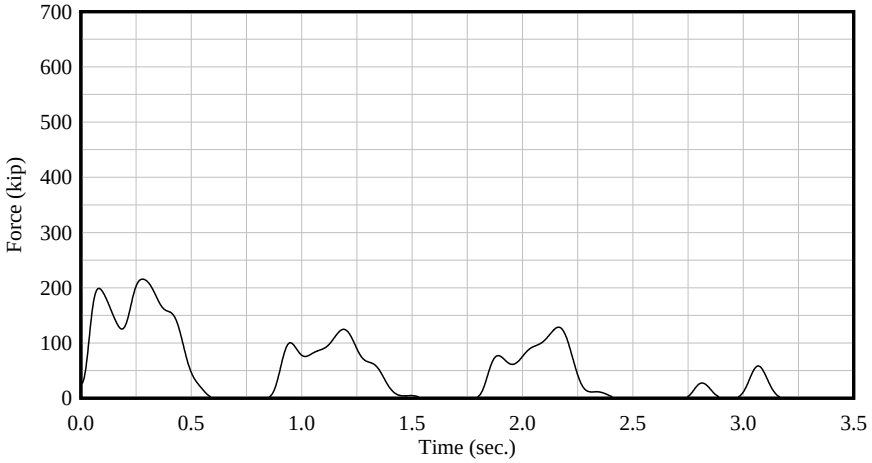

Figure B.30. 2x3 – 2 FPS – 25° – MRLD2

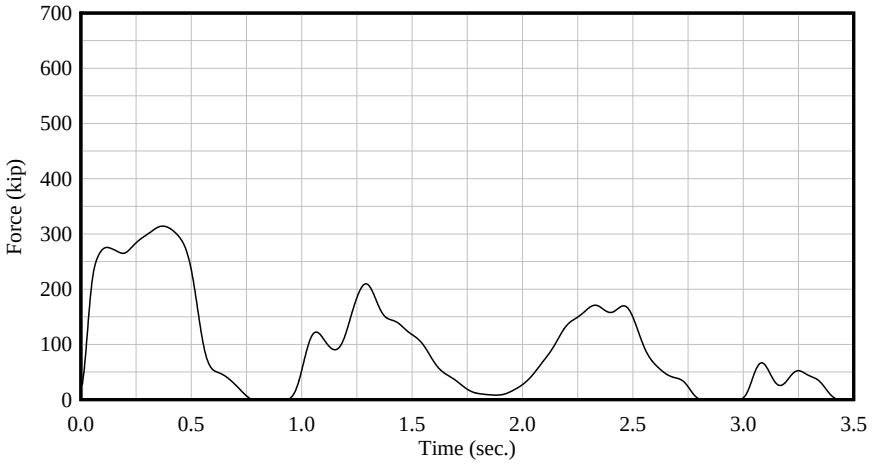

Figure B.31. 2x3 – 4 FPS – 25° – MRLD2

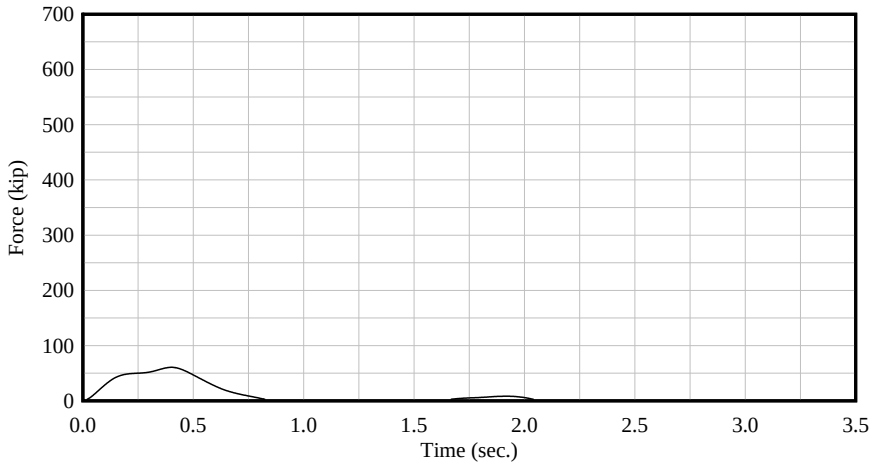

Figure B.32. 3x3 – 1 FPS – 5° – MRLD2

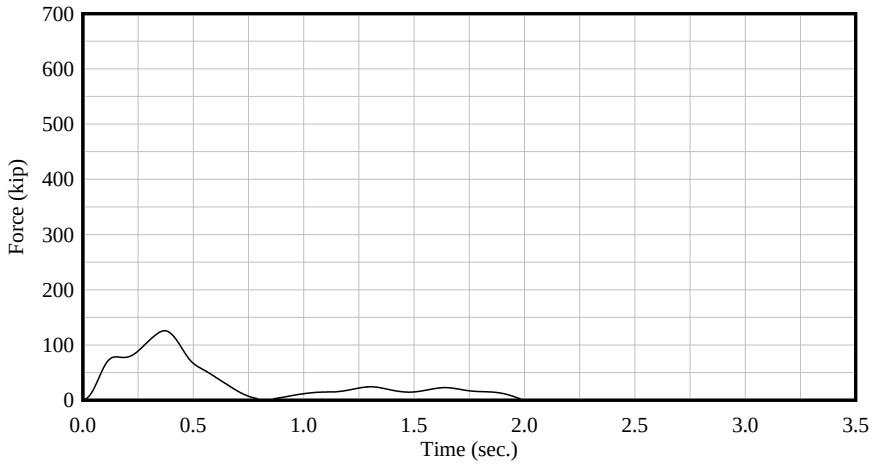

Figure B.33. 3x3 – 2 FPS – 5° – MRLD2

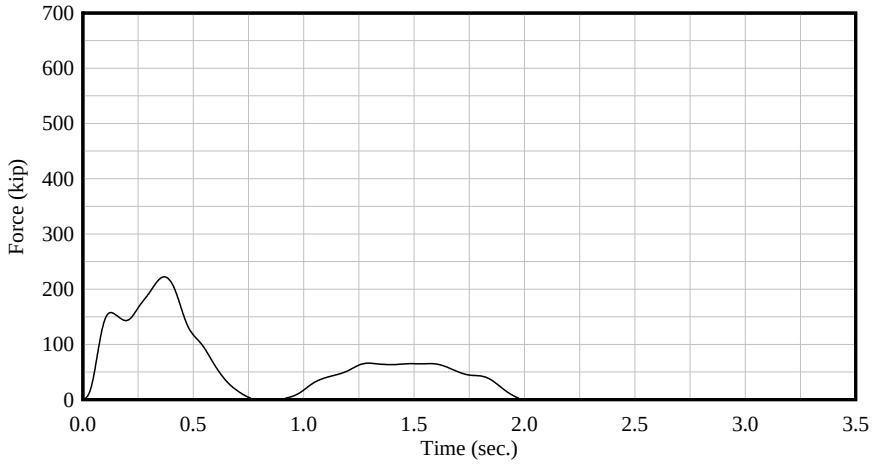

Figure B.34. 3x3 – 4 FPS – 5° – MRLD2

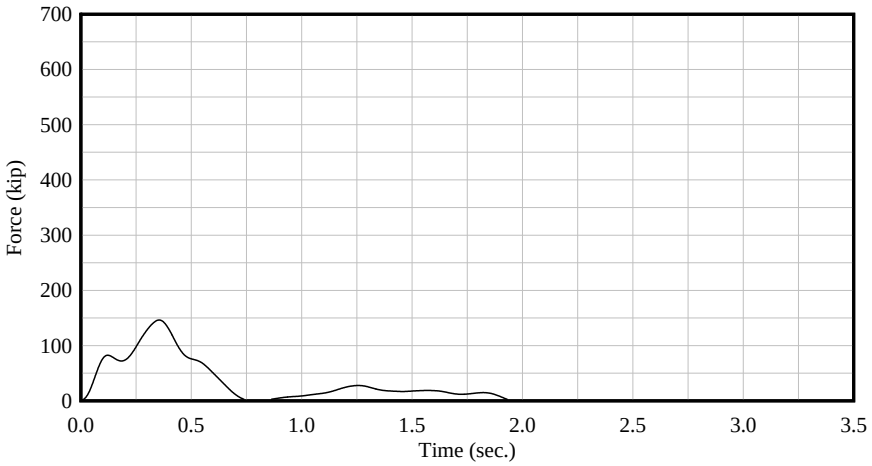

Figure B.35. 3x3 – 1 FPS – 10° – MRLD2

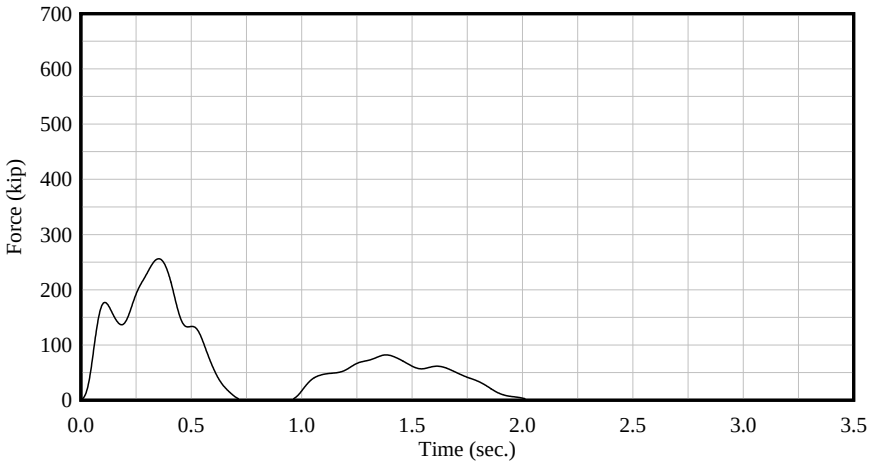

Figure B.36. 3x3 – 2 FPS – 10° – MRLD2

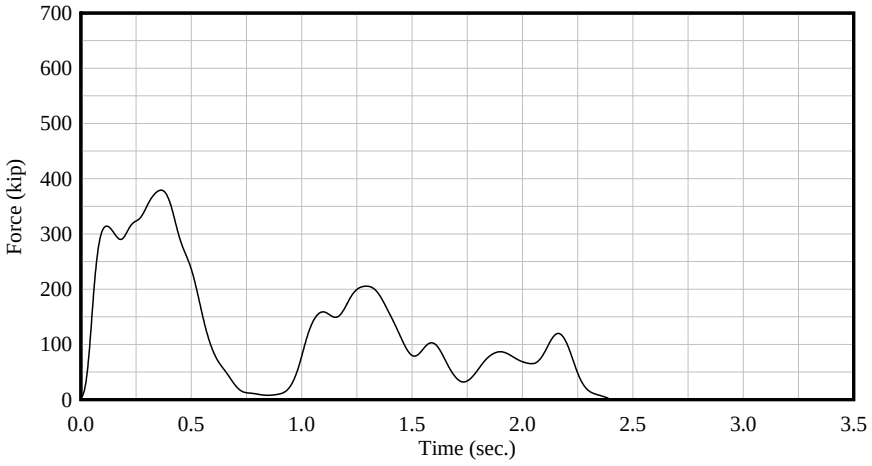

Figure B.37. 3x3 – 4 FPS – 10° – MRLD2

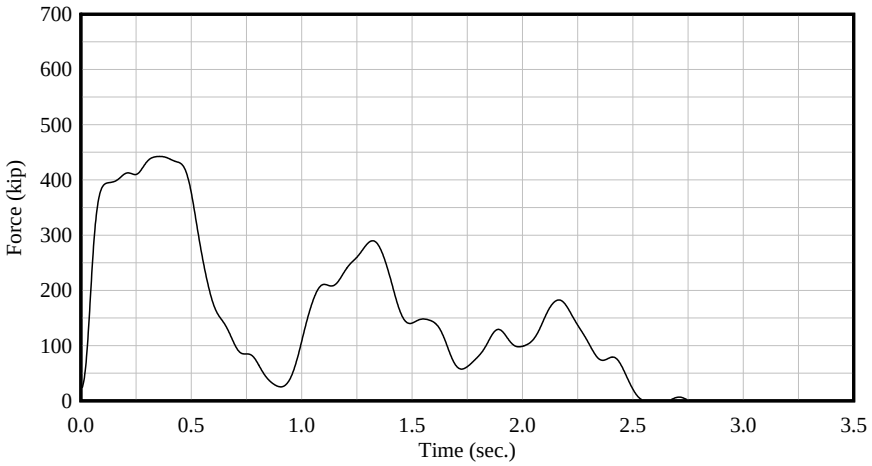

Figure B.38. 3x3 – 6 FPS – 10° – MRLD2

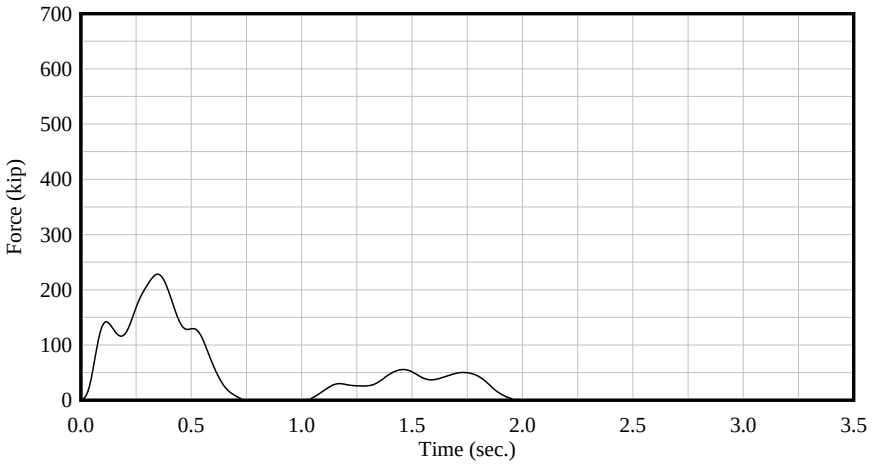

Figure B.39. 3x3 – 1 FPS – 15° – MRLD2

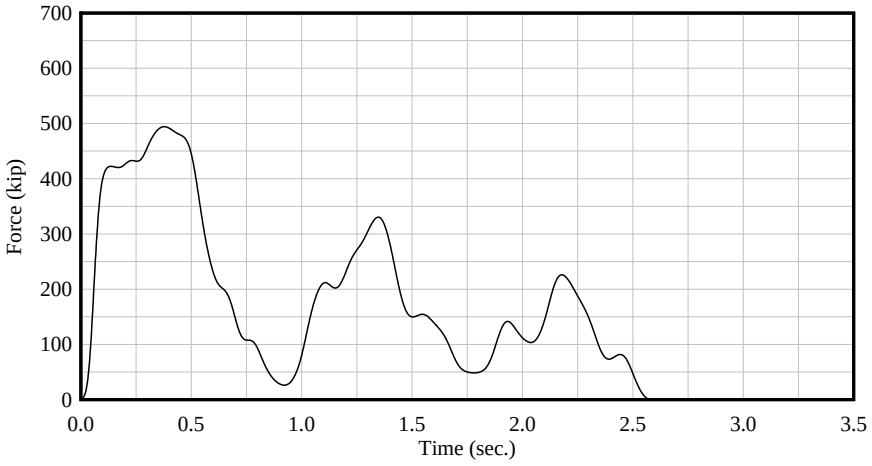

Figure B.40. 3x3 – 4 FPS – 15° – MRLD2

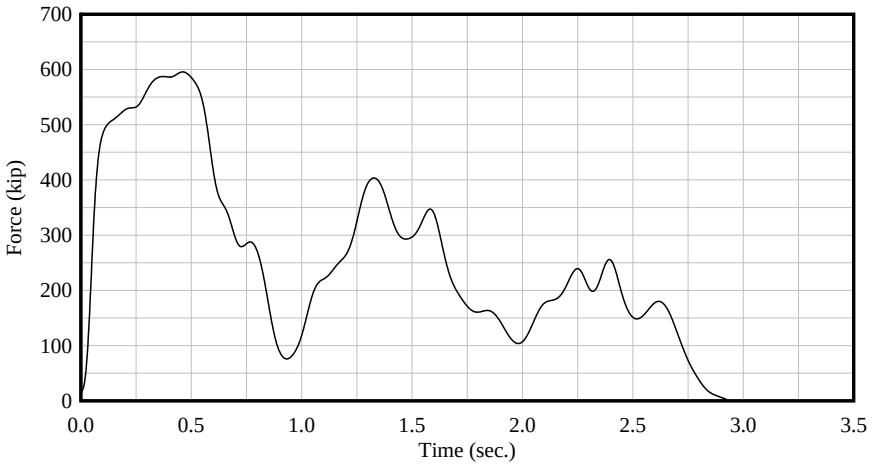

Figure B.41. 3x3 – 6 FPS – 15° – MRLD2

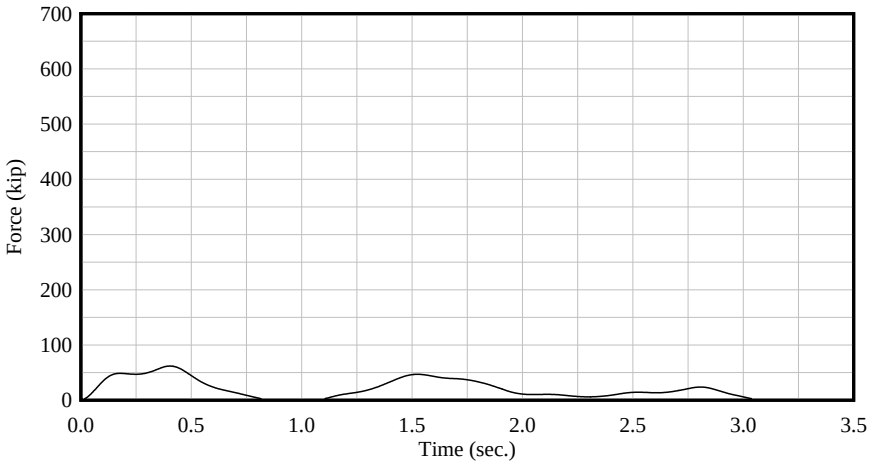

Figure B.42. 3x5 – 1 FPS – 5° – MRLD2

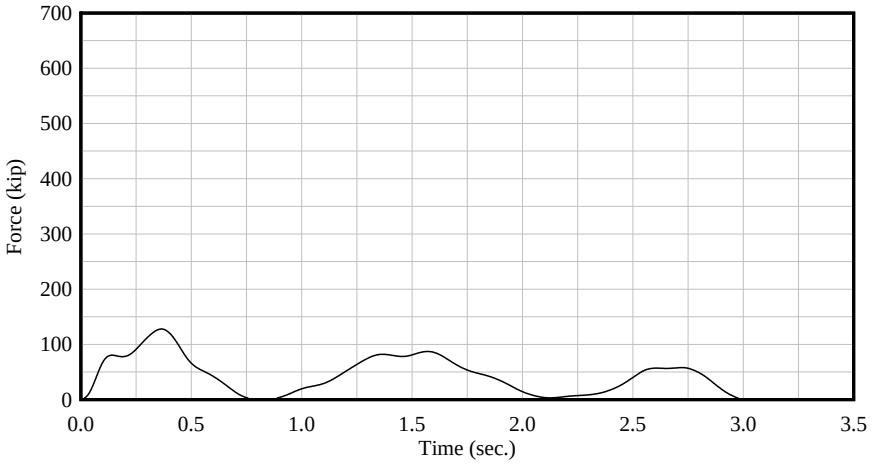

Figure B.43. 3x5 – 2 FPS – 5° – MRLD2

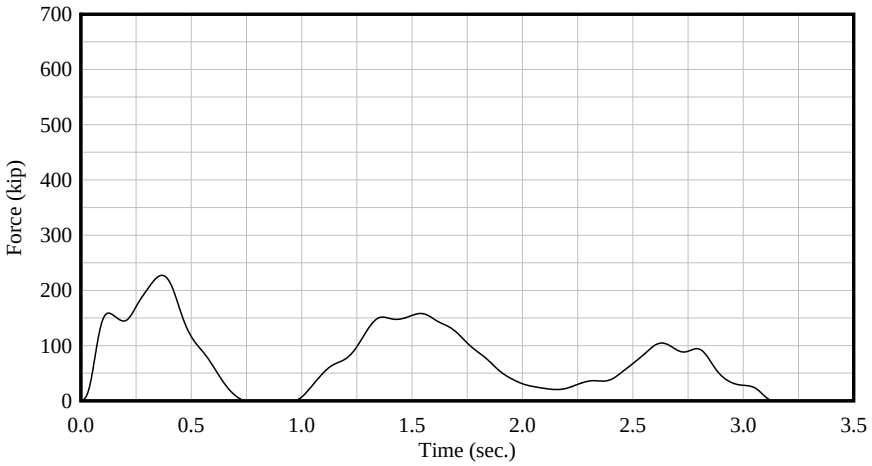

Figure B.44. 3x5 – 4 FPS – 5° – MRLD2

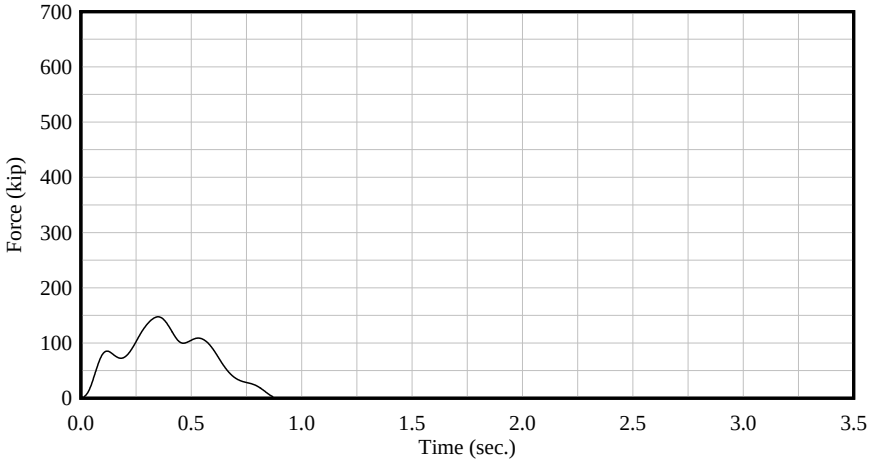

Figure B.45. 3x5 – 1 FPS – 10° – MRLD2

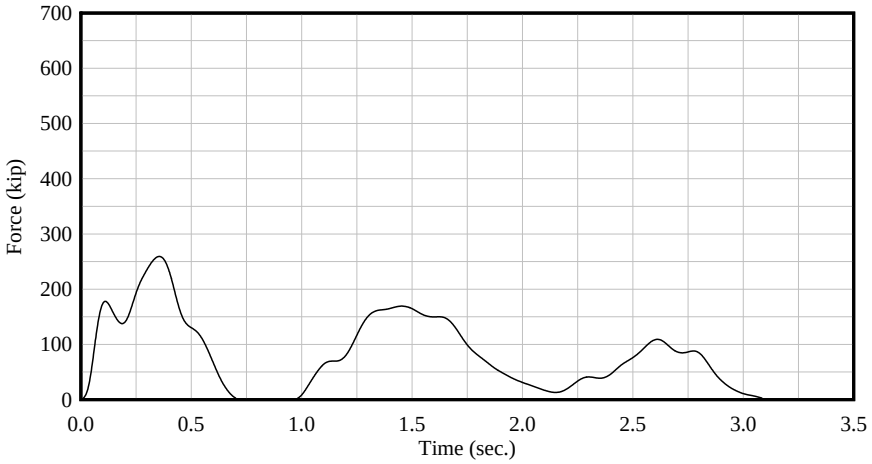

Figure B.46. 3x5 – 2 FPS – 10° – MRLD2

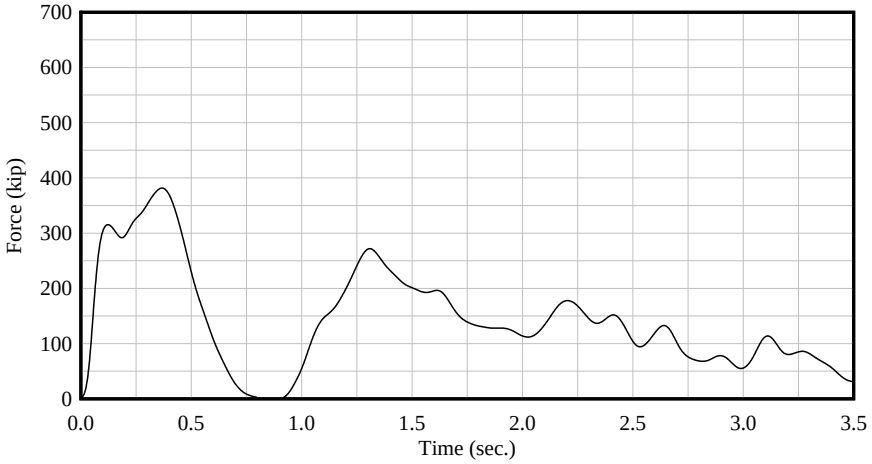

Figure B.47. 3x5 – 4 FPS – 10° – MRLD2

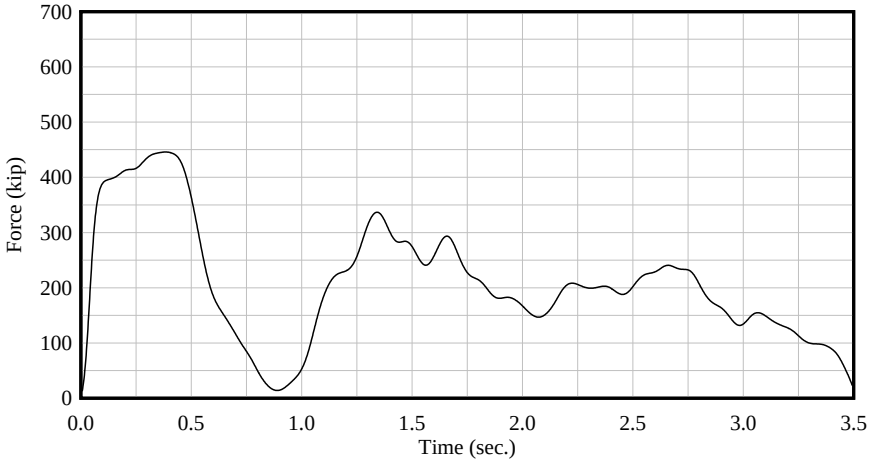

Figure B.48. 3x5 – 6 FPS – 10° – MRLD2

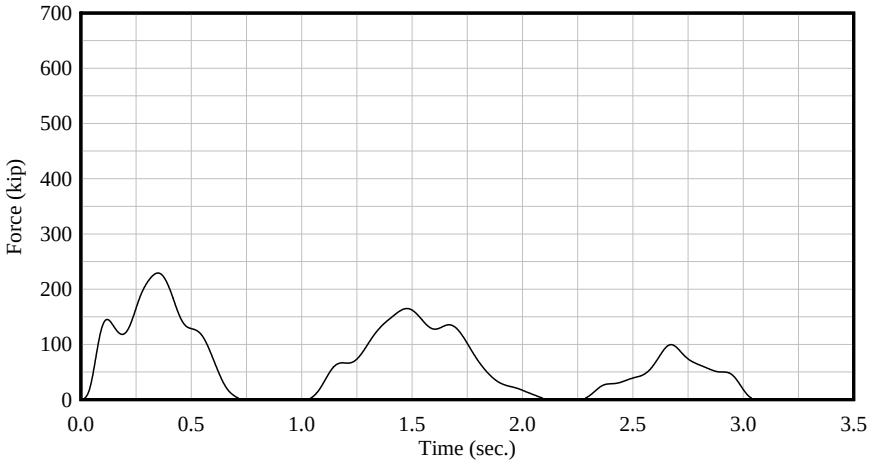

Figure B.49. 3x5 – 1 FPS – 15° – MRLD2

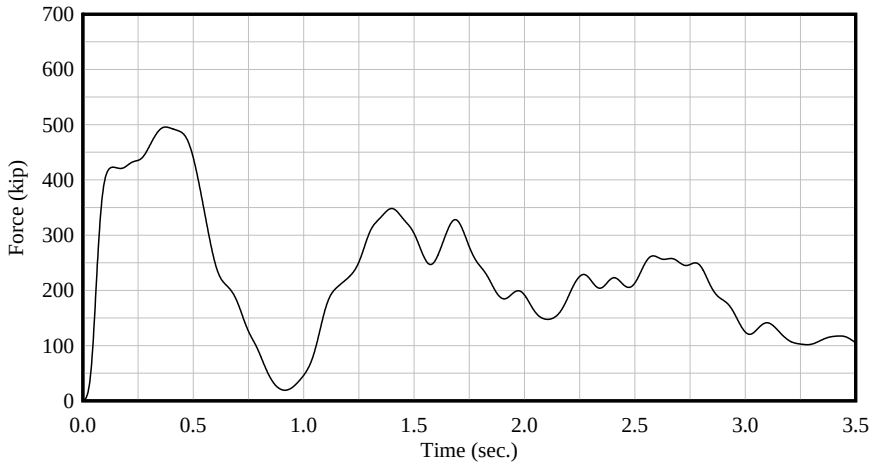

Figure B.50. 3x5 – 4 FPS – 15° – MRLD2

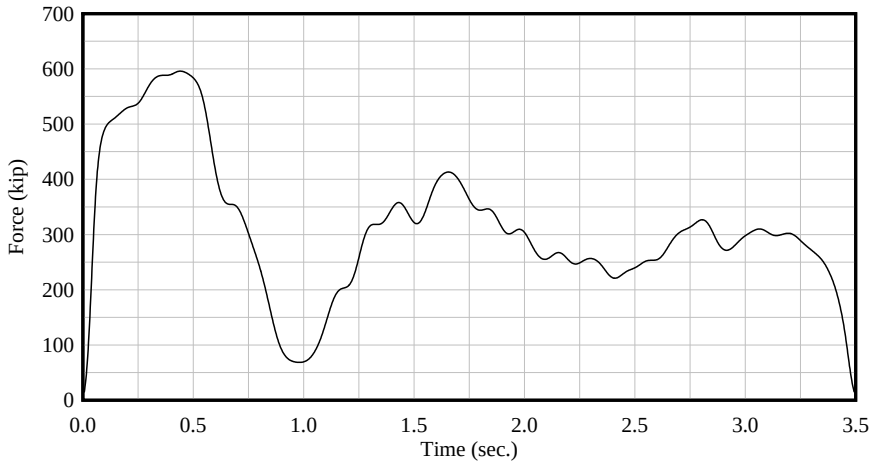

Figure B.51. 3x5 – 6 FPS – 15° – MRLD2

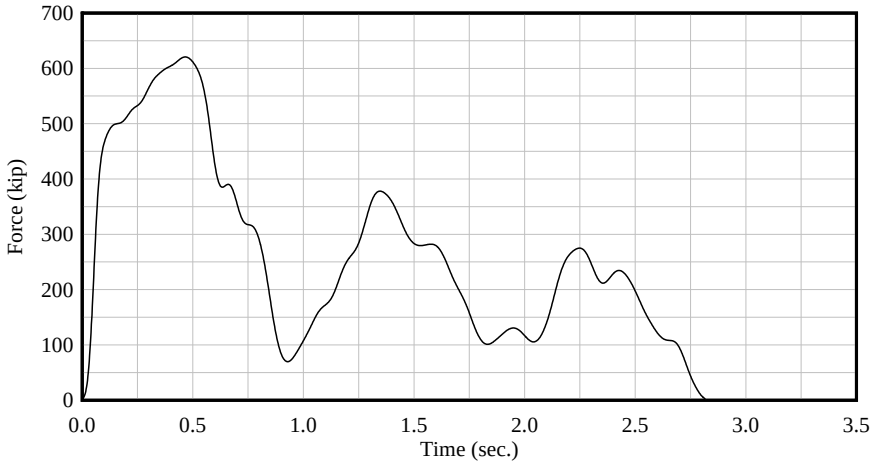

Figure B.52. 3x3 – 4 FPS – 20° – MRLD2

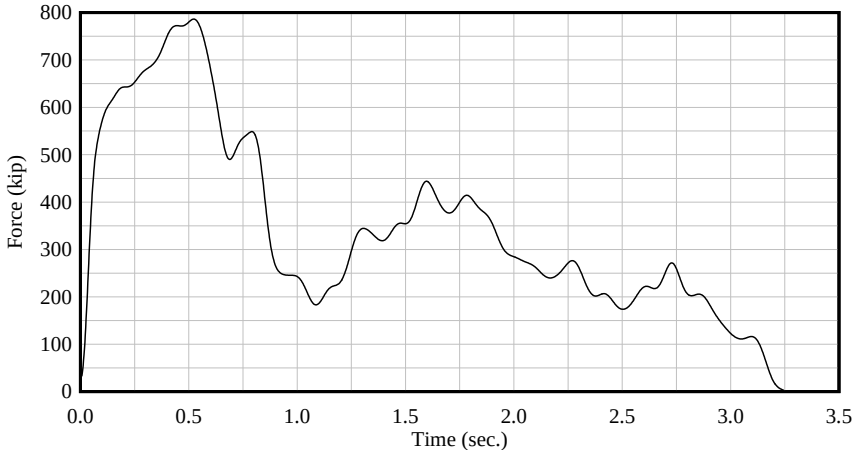

Figure B.53. 3x3 – 6 FPS – 20° – MRLD2
(range of force-scale differs from previous plots)

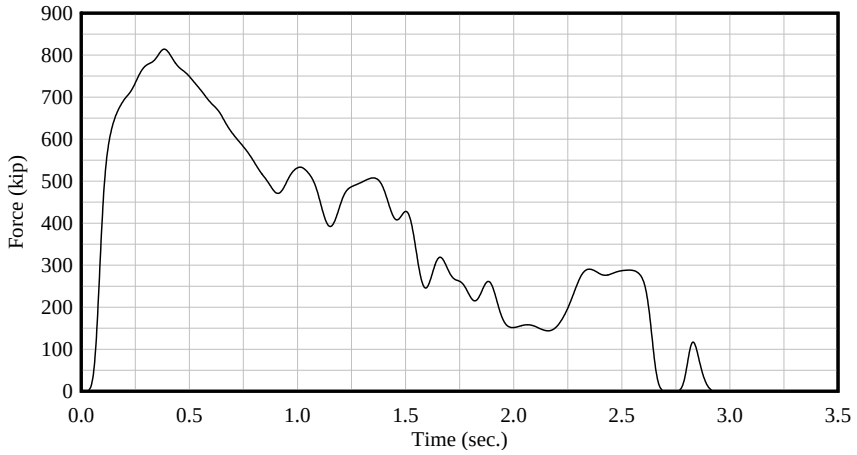

Figure B.54. 3x3 – 8 FPS – 20° – MRLD2
(range of force-scale differs from previous plots)

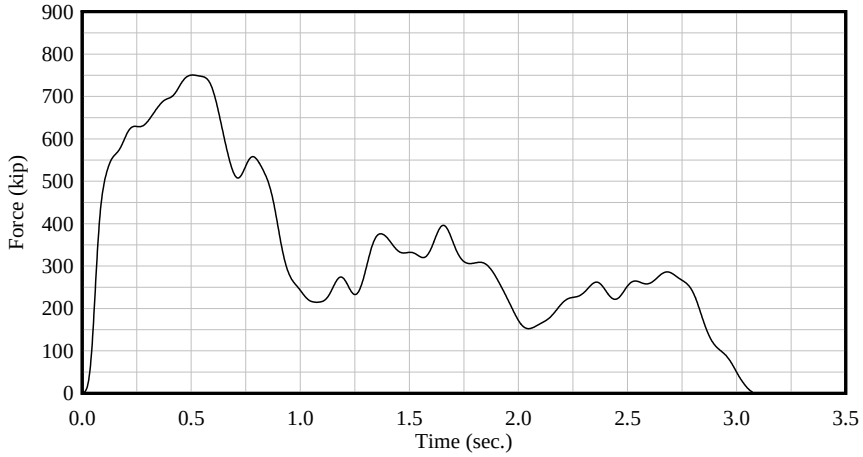

Figure B.55. 3x3 – 4 FPS – 25° – MRLD2
(range of force-scale differs from previous plots)

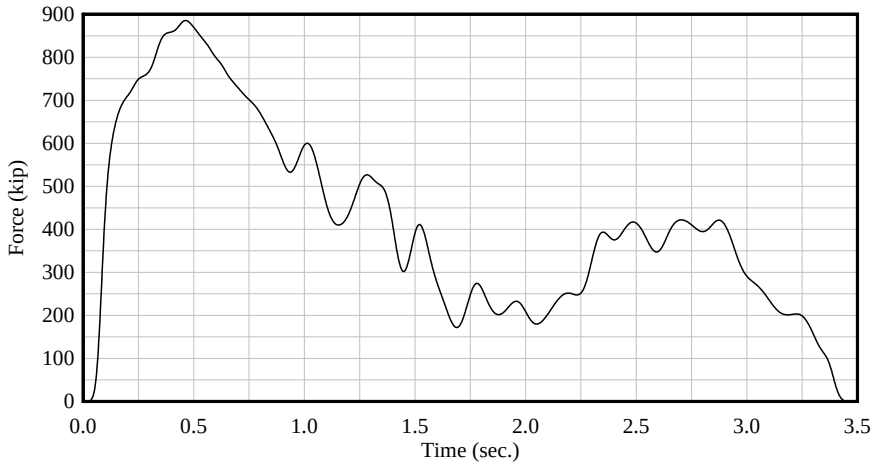

Figure B.56. 3x3 – 6 FPS – 25° – MRLD2
(range of force-scale differs from previous plots)

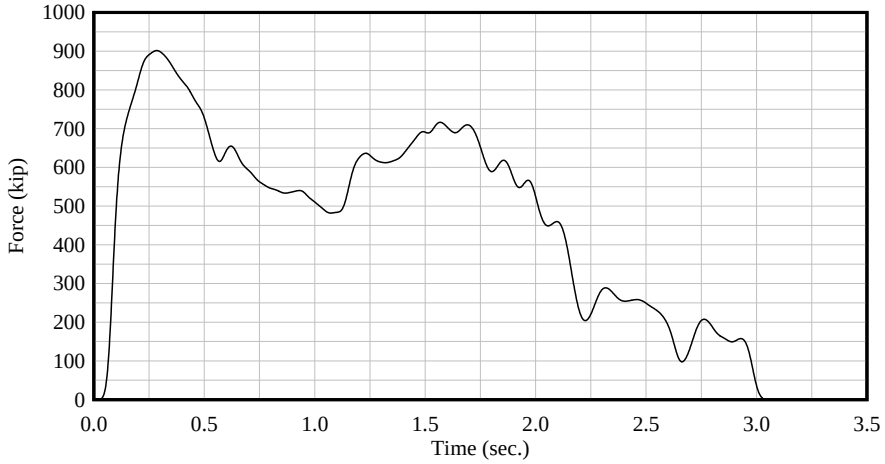

Figure B.57. 3x3 – 8 FPS – 25° – MRLD2
(range of force-scale differs from previous plots)

APPENDIX C
IMPACT FORCE-TIME HISTORIES FROM PILE-FOUNDED GUIDE WALL MRLD3 SIMULATIONS

Individual force-time histories for all MRLD3 impact simulations conducted in this study are plotted on the following pages. Each plot includes a trace of the *normal impact force in the horizontal plane*. All impact forces presented herein correspond to the contact force-time histories between the high-resolution impacting (deformable) barge model and the MRLD3 model. Also note that all forces presented in this appendix have been low-pass filtered using the procedure described earlier in this report.

The nomenclature used in each figure caption, to identify the impact condition that is plotted, is of the form:

NSxNR – SPEED – ANGLE – MRLD3

where:

NS	=	number of barge strings (barge columns) in the flotilla
NR	=	number of barge rows in the flotilla
SPEED	=	impact speed in ft/sec (FPS)
ANGLE	=	impact angle in degrees
MRLD3	=	Mississippi River Lock and Dam No. 3

For additional information regarding the MRLD3 impact conditions for which impact forces are plotted in this appendix, see Chapter 4.

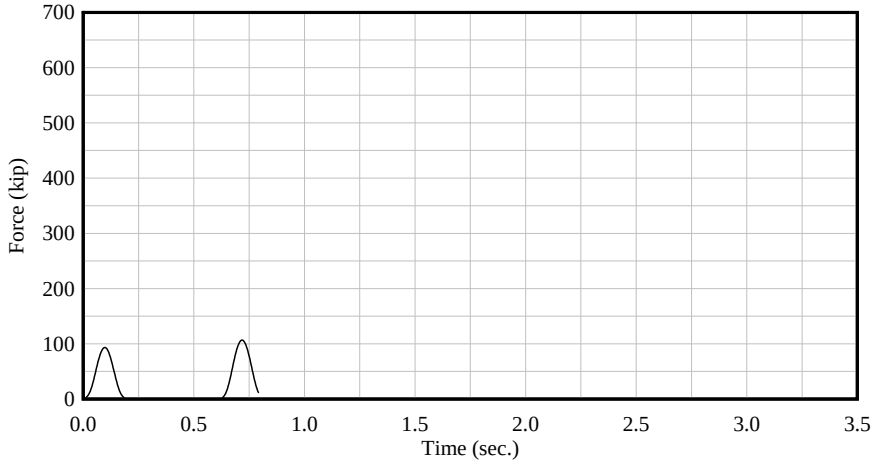

Figure C.1. 1x3 – 2 FPS – 5° – MRLD3

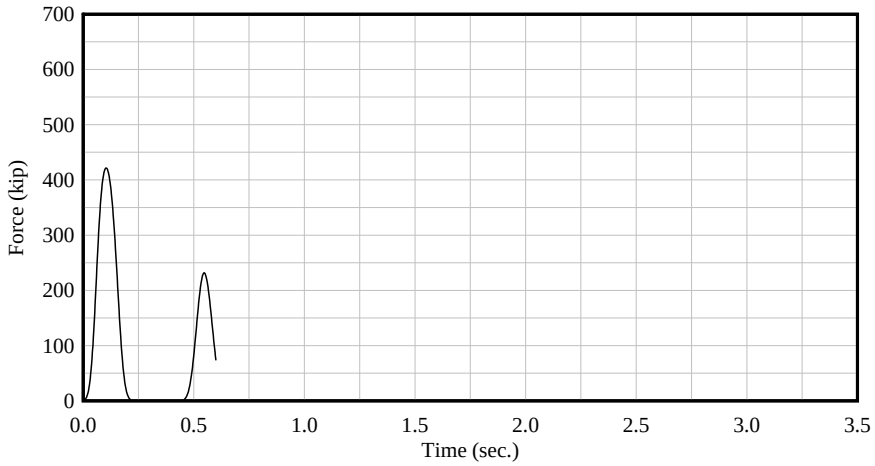

Figure C.2. 1x3 – 4 FPS – 20° – MRLD3

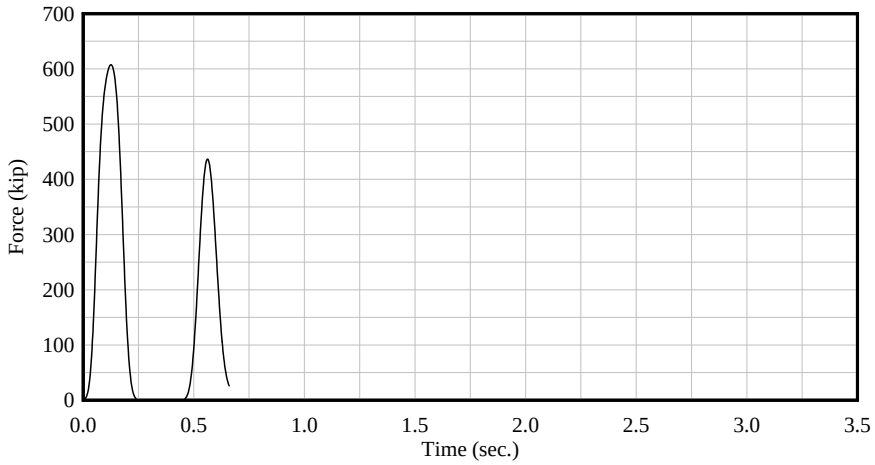

Figure C.3. 1x3 – 6 FPS – 25° – MRLD3

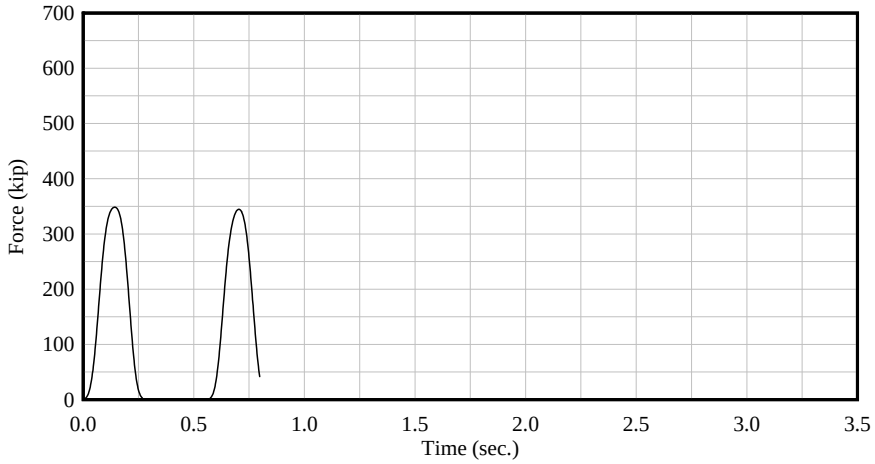

Figure C.4. 2x3 – 6 FPS – 10° – MRLD3

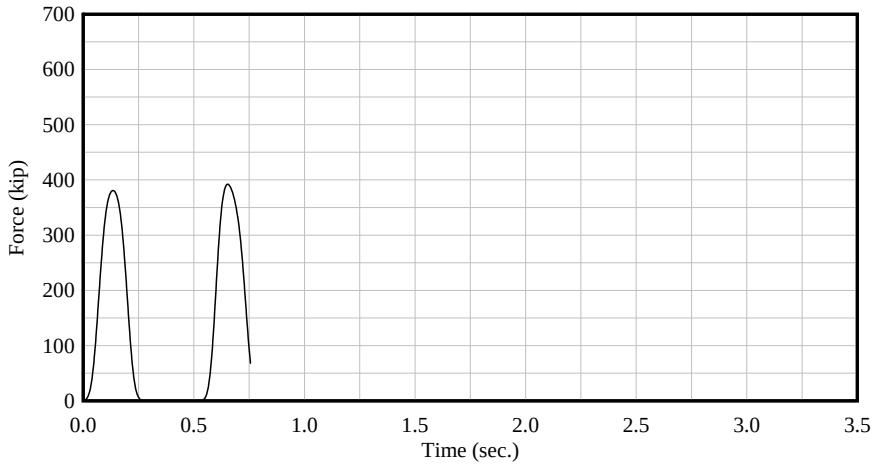

Figure C.5. 2x3 – 4 FPS – 15° – MRLD3

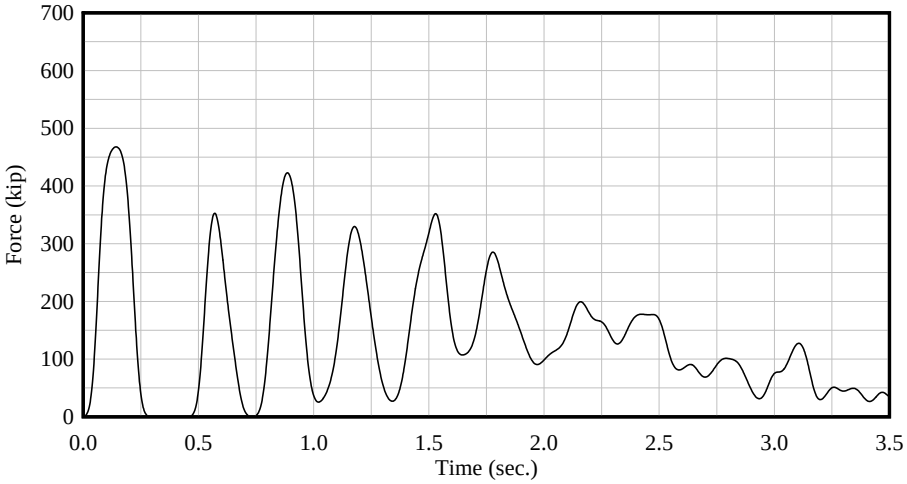

Figure C.6. 2x3 – 4 FPS – 20° – MRLD3

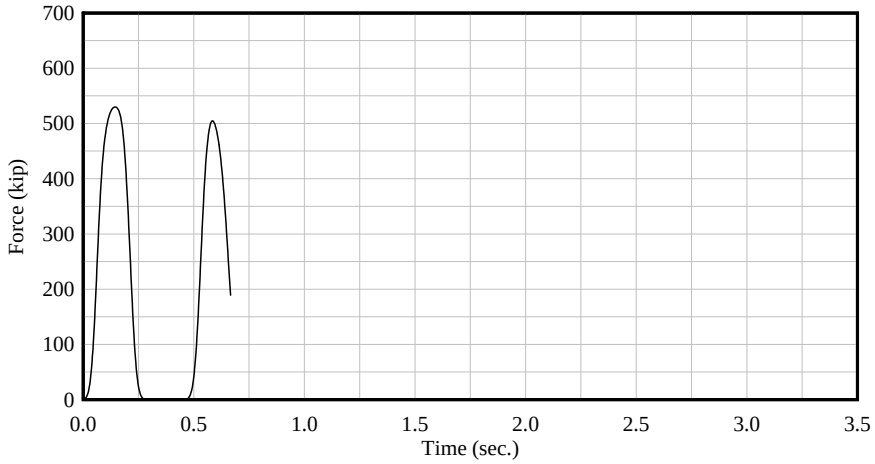

Figure C.7. 2x3 – 4 FPS – 25° – MRLD3

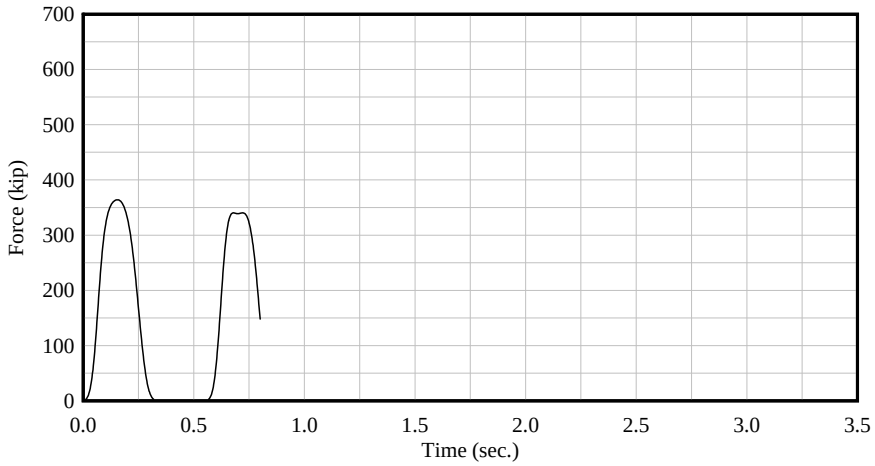

Figure C.8. 3x3 – 6 FPS – 10° – MRLD3

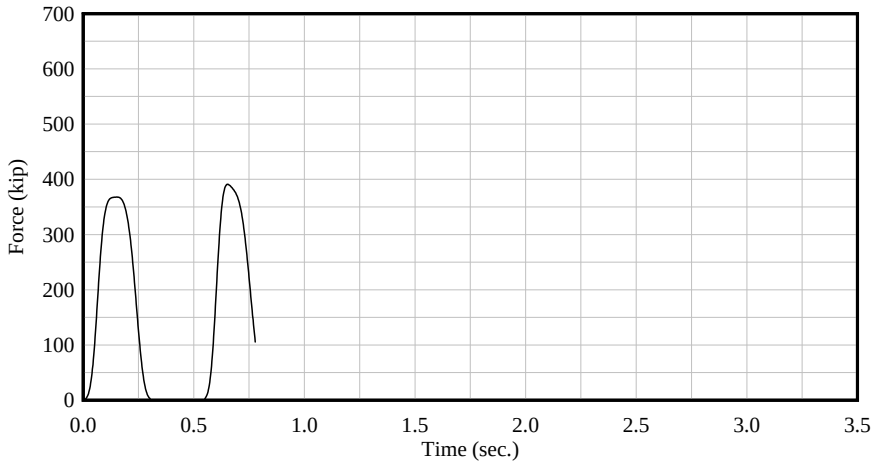

Figure C.9. 3x3 – 4 FPS – 15° – MRLD3

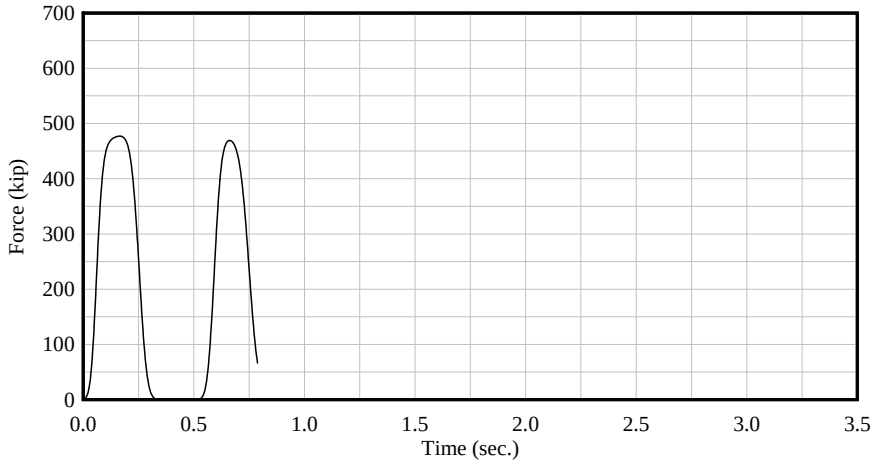

Figure C.10. 3x3 – 6 FPS – 15° – MRLD3

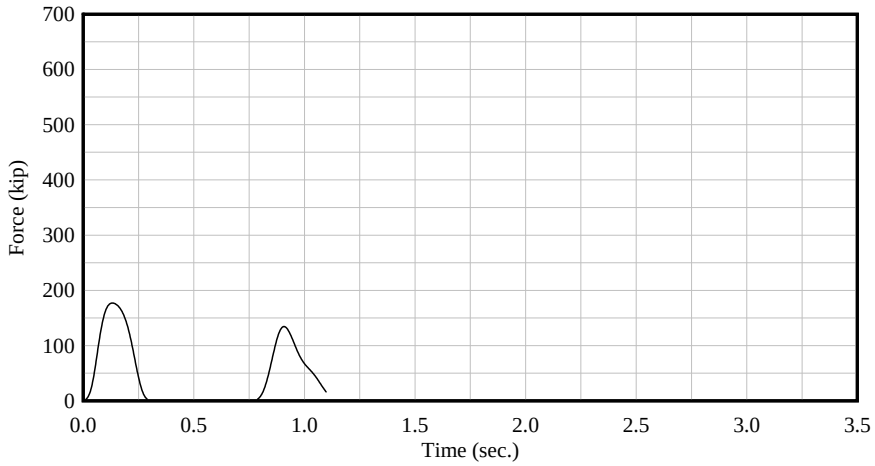

Figure C.11. 3x5 – 2 FPS – 5° – MRLD3

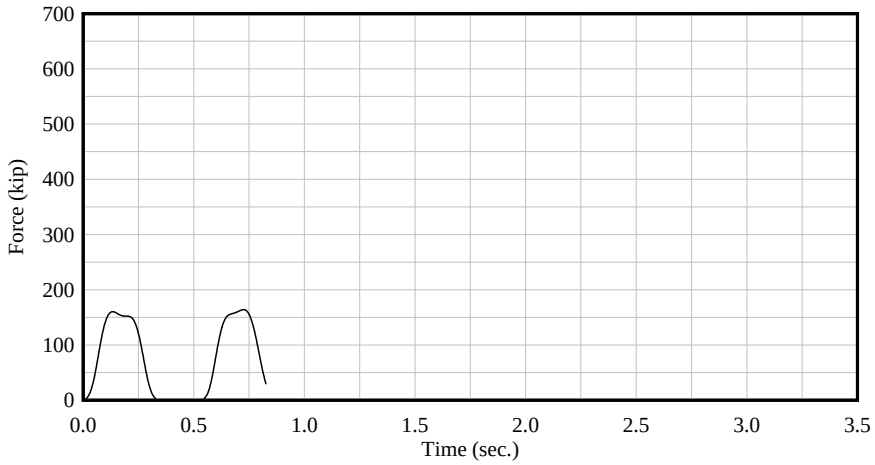

Figure C.12. 3x5 – 4 FPS – 5° – MRLD3

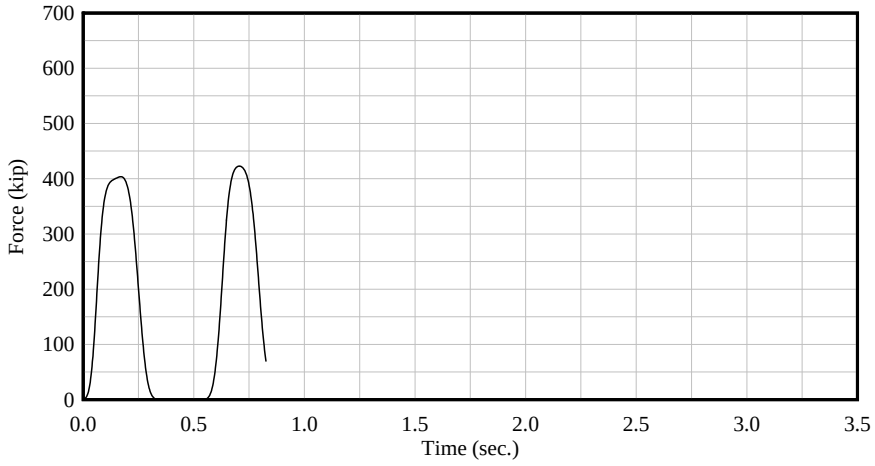

Figure C.13. 3x5 – 6 FPS – 10° – MRLD3

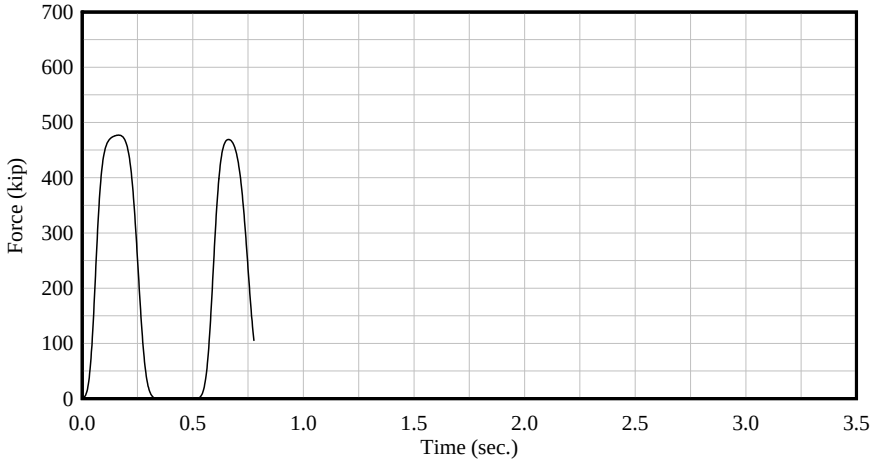

Figure C.14. 3x5 – 6 FPS – 15° – MRLD3

APPENDIX D
SUPPLEMENTARY SENSITIVITY STUDIES WITH PILE-FOUNDED GUIDE WALL MODELS

A multitude of sensitivity studies were performed to identify reasonably conservative impact conditions for use in the MRLD2 and MRLD3 parametric studies, as well as to gain a better understanding of the influence of select impact condition parameters on impact forces. Development of pile founded guide wall models with modified conditions; i.e. deviating from conditions present in the parametric study, and the associated results are discussed in further detail.

The nomenclature used in each figure caption, to identify the impact condition that is plotted, is of the form:

NSxNR – SPEED – ANGLE – PFGW – MISC

where:

NS	=	number of barge strings (barge columns) in the flotilla
NR	=	number of barge rows in the flotilla
SPEED	=	impact speed in ft/sec (FPS)
ANGLE	=	impact angled in degrees
PFGW	=	pile-founded guide wall structure impacted by barge flotilla: MRLD2: Mississippi River Lock and Dam No. 2 MRLD3: Mississippi River Lock and Dam No. 3
MISC	=	miscellaneous sensitivity study conditions: impact elevation; e.g. highest/lowest elevation impact (HEI, LEI) depth of backfill; e.g. zero depth (ZBF) or full depth (FBF) soil profile; e.g. original (SSx1), 50% soil stiffness reduction (SSx0.5), or 100% amplified soil stiffness (SSx2)

D.1 Fixed versus pinned guide wall-to-pile connection for MRLD2

As discussed in Chapter 3, the primary MRLD2 and MRLD3 parametric studies are performed with a fixed guide wall-to-pile connection using constrained nodal rigid bodies (CNRB). Prior to performing the main parametric studies however, multiple pinned (wall-to-pile) connection simulations were performed to verify the efficacy of the CNRB approach and to determine impact force sensitivity to rotational stiffness of the wall-to-pile connection.

To confirm efficacy of the CNRB, moments at the top of the pile are examined for simulations with fixed and pinned wall-to-pile connections, i.e. with and without the CNRB, respectively. As intended, pile moments are zero throughout the pinned connection simulations and non-zero for fixed connection simulations. To measure impact force sensitivity to the modeling methods employed at the wall-to-pile interface, comparative contact force-time histories between simulations with pinned and fixed connections were reviewed prior to development of the parametric study. After performing multiple sets of pinned connection simulations for this study, results confirm the moment-resisting behavior of the wall-to-pile connection does not affect the response of the MRLD2 model (during an oblique impact event)

to an extent sufficient for observing changes in the impact force-time history. To illustrate, a comparative force-time history plot for a high energy, high elevation impact condition without backfill soil is shown (Figure D.1). In short, impact forces are insensitive to the rotational stiffness of the wall-to-pile connection. This response of minimal moments at the top of the piles is expected given the pile spacing, depth of the guide wall, and stiffness of the wall relative to the timber piling (in bending). In addition, these results show impact loads are transferred between the guide wall and piling through essentially through axial and shear forces.

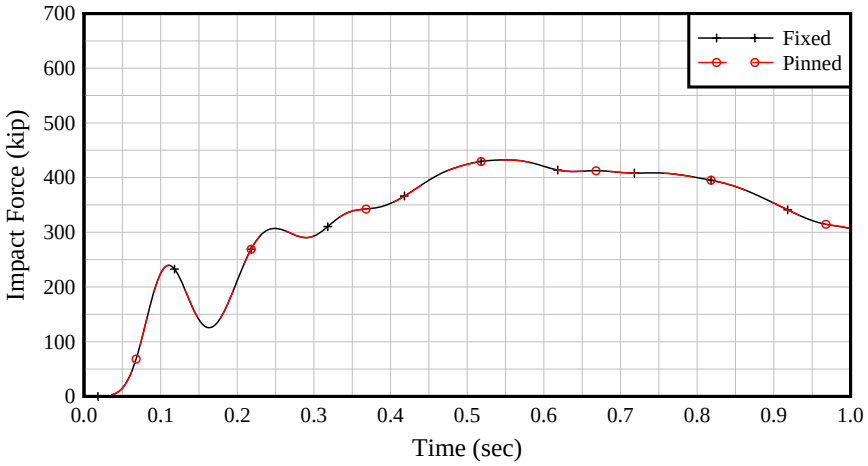

Figure D.1. Impact force-time histories for 3x5 – 4 FPS – 15°– MRLD2 – ZBF – HEI

Furthermore, it should be understood this insensitivity of impact force to rotational stiffness of the wall-to-pile connection is applicable to typical barge-pile founded guide wall impacts. To elaborate, a high-energy, high elevation, zero backfill impact event is most likely to elicit a different response from the guide wall, and hence a different force-time history, due to the impacting energy level and the decreased stiffness of the pile founded guide wall on account of the impact elevation and lack of lateral resistance from backfill soil. Thus, given the impact conditions of these high elevation, zero backfill simulations, the observed insensitivity of impact force to rotational stiffness of the wall-to-pile connection is anticipated for typical barge impact events. This insensitivity is also confirmed with additional low elevation, zero backfill simulations, where results revealed contact force-time histories from fixed and pinned connection simulations were also equivalent.

D.2 Backfill soils with MRLD2

In addition to modeling foundation soils and rock fill, backfill soils were considered. Prior to conducting the parametric studied discussed in Chapter 4, where simulations do not include the lateral resistance of backfill soils on the non-impact side of the guide wall, additional simulations with full-depth backfill soils were performed with the MRLD2 model to determine impact force sensitivity. To quantify the effect of full-depth backfill soils on impact forces, contact force-time histories from simulations with no (zero) and full-depth backfill are compared.

Backfill soils extend the full 29-0” height, or full-depth, of the MRLD2 guide wall and are modeled as loose granular, or cohesionless, soil with a density (γ) of 115 pounds per cubic foot (pcf) and an internal friction angle (ϕ) of 30 degrees (°). The two USACE provided soil parameters, γ and ϕ, are used in combination with the FB-MultiPier Soil Parameter Table (Bridge Software Institute, 2011) to select the remaining soil properties (Table D.1) needed for modeling soil with FB-MultiPier.

Table D.1 – Soil parameters for loose granular (cohesionless) backfill soil

Data source	USACE		FB-MultiPier Soil Parameter Table (Bridge Software Institute, 2011)					
Soil parameters	γ (pcf)	ϕ (°)	K	q_c (ksi)	G (ksi)	ν	f_s (psf)	E_s (pci)
Parameter value	115	30	0.50	0.50	0.41	0.40	200.0	40.0

γ: unit weight
ϕ: internal angle of friction
K: coefficient of lateral earth pressure
q_c: ultimate unit end bearing
G: shear modulus
ν: Poisson’s ratio
f_s : ultimate unit skin friction
E_s : subgrade modulus

An FB-MultiPier model (Figure D.2) is developed using these soil parameters to capture the lateral stiffness contribution of backfill to the non-impact side of the concrete wall. The FB-MultiPier model (Figure D.2) includes a 3’ x 3’ square concrete pile in 29’-0” of backfill soil, thereby matching the height of the MRLD2 wall and thus representing a full-depth backfill soil condition. A 3’ wide pile is chosen as it is corresponds to the 3’-0” wide section of guide wall with the repeating pile group as discussed in Chapter 3. The selected water elevation corresponds to the approximate mid-height of the guide wall, or 14’-0” below of the top of the wall, which is a typical water elevation given the upper and lower pool levels.

The concrete pile consists of 6” long beam elements, which corresponds to the 6” cubic solid elements representing the plain concrete wall in the LS-DYNA models. As was done for modeling the foundation soils, the nonlinear static force-displacement curves are extracted from each node in this concrete pile – backfill soil model for integration into the LS-DYNA models.

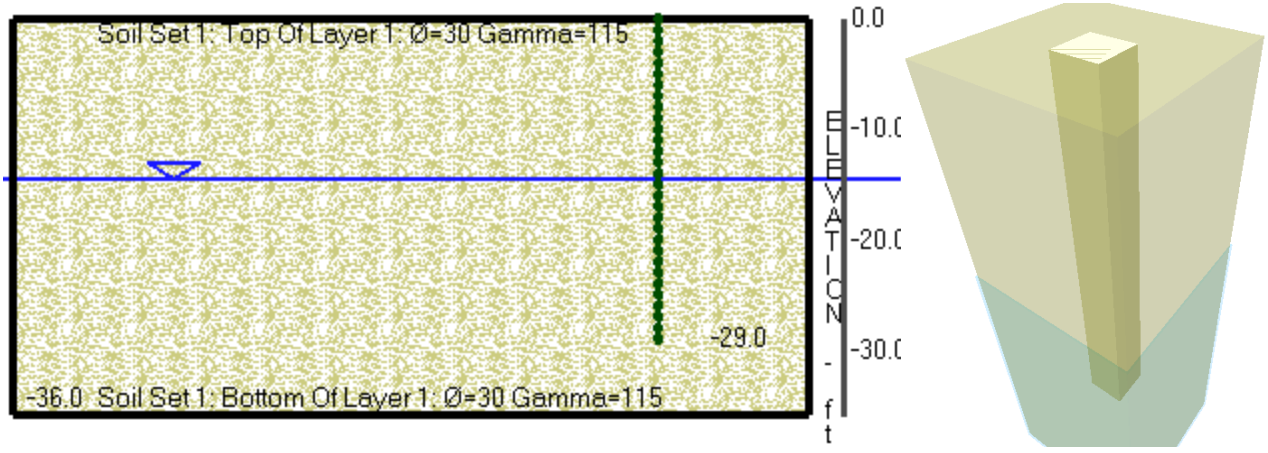

a) b)

Figure D.2. FB-MultiPier 3’ x 3’ square pile model using backfill soil properties per USACE: a) Soil profile with soil strength parameter shown per layer; b) 3-D rendering of model

In contrast to modeling the foundation soils with horizontal and vertical resistance, backfill soil is represented with horizontal resistance only. Vertical soil springs that would represent skin friction, t-z, and bearing resistance, q-z, are neglected. Lateral resisting soil springs (and associated restraints) similar to those used in the foundation soils are employed for backfill soils, with one significant modification. It is understood backfill soils apply compressive force only. As there are two soil springs at every pile node representing lateral stiffness of the foundation soils, these springs include both a tensile and compressive component (Figure D.3). As discussed in the previous section, the force-deformation curves from FB-MultiPier are mirrored prior to integration into the LS-DYNA models. As backfill soils are modeled to resist lateral forces in a compression-only manner, the mirroring operation performed for the foundation soils, which accounts for the tensile behavior, is not performed for these backfill soil springs. In addition, only the bearing component of the backfill soil is accounted for, i.e. the sliding frictional component is ignored. The static nonlinear curves from FB-MultiPier are integrated into the LS-DYNA models as compression only elements, as evidenced by the p-y curves (Figure D.3). As with the soil springs used for representing the foundation soils, translational restraints, which require element axes be oriented parallel to global axes, are employed (Consolazio et al. 2002).

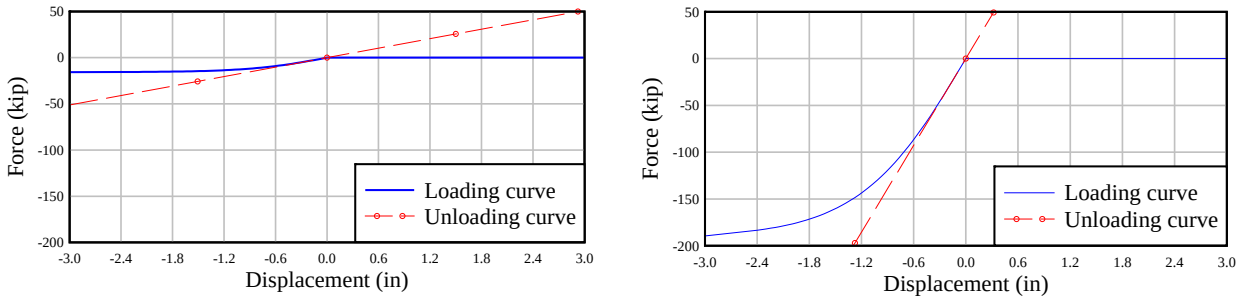

Figure D.3. Typical backfill soil force-displacement curves used in FE model:
a) P-y curve at 3’ below soil surface; b) P-y curve at 27’ below backfill soil surface

The resulting lateral soil curves (Figure D.3), at 6” vertical spacing, are integrated into the LS-DYNA FE model. These force-deformation curves are scaled by a factor of 1/6 for conversion from the FB-MultiPier concrete pile model, which represents a 3’ wide portion of the guide wall, to the LS-DYNA model, which consists of 6” cubic elements, i.e. a 6” x 6” grid spacing of nodes along the face of the guide wall. The force-deformation curves from the 3’ wide concrete pile model have a tributary width of 3’-0”, therefore requiring a reduction of 1/6 for application to springs representing a 6” wide section of the concrete wall. The guide wall shown in Figure D.4 illustrates the use of backfill soil springs along the non-impact side of the MRLD2 model.

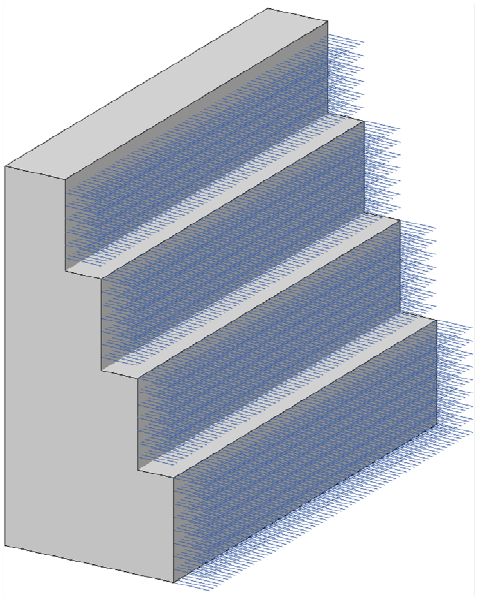

Figure D.4. Finite element model of MRLD2 wall with lateral, p-y, backfill soil springs
(Note: guide wall mesh, timber piling, and foundation soil springs not shown for clarity)

An additional FB-MultiPier retaining wall model is developed with both the foundation soil profile (recall Chapter 3, Table 3.3) as well as the backfill soil (Table D.1). This FB-MultiPier model represents a 3'-0" section for the MRLD2 guide wall, including five 12" diameter timber piles, of which four are plumb and one is battered (recall Chapter 3, Figure 3.10). As with all FB-MultiPier models, the timber piles and retaining wall, or guide wall, are represented with resultant beam elements. This timber pile model consists of 18" long beam elements, which correspond to all other FB-MultiPier models included in this study as well as the timber pile beam elements represented in the LS-DYNA models.

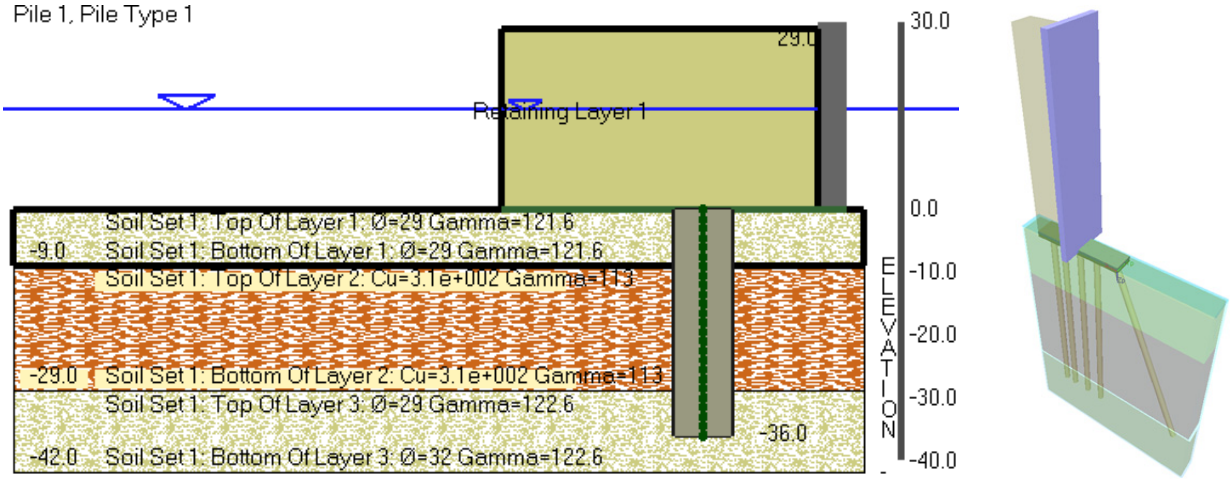

a) b)

Figure D.5. FB-MultiPier retaining wall model:
a) Soil profile with soil strength parameter shown per layer; b) 3-D rendering of model

Foundation soil curves from this retaining wall model (Figure D.5) match the soil curves (Figure D.6) from the previously discussed single timber pile model (Chapter 3, Figure 3.16), thereby verifying that the single timber pile model accurately accounts for the stiffening effect of overburden pressures from backfill soils. Again, the FB-MultiPier timber pile model used for development of the foundation soil springs accounts for the overburden pressure of full-depth backfill soils.

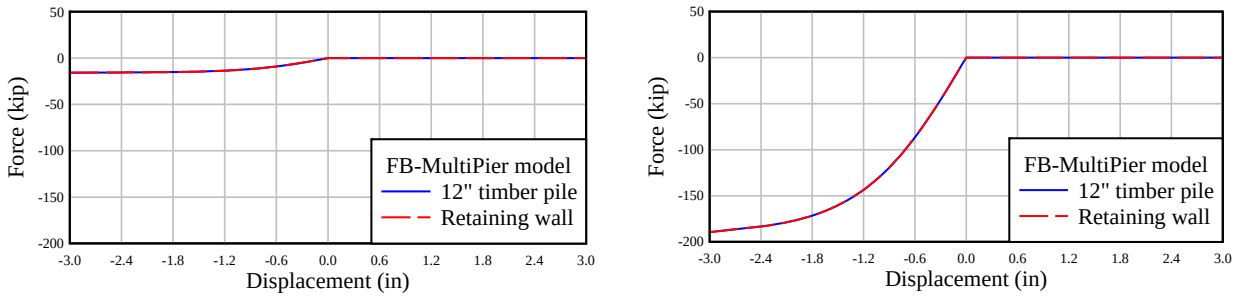

Figure D.6. Comparative force-deformation curves from two different FB-MultiPier FE models: a) P-x/p-y curve at 3’ below soil surface; b) P-x/p-y curve at 27’ below backfill soil surface

Several simulations are performed with full-depth backfill soil included in the MRLD2 model. The results from these additional simulations are reviewed to understand the sensitivity of impact forces to the presence of backfill. The following comparative force-time history plots illustrate that backfill soils cause moderately higher impact forces. This behavior is expected given the additional stiffness of the backfill soil springs on the non-impact side of the MRLD2 guide wall.

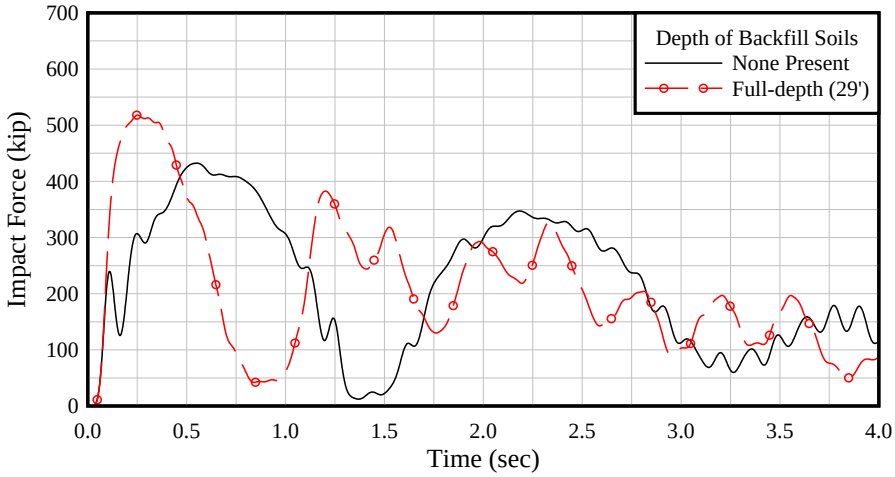

Figure D.7. 3x5 – 4 FPS – 15°– MRLD2 – HEI

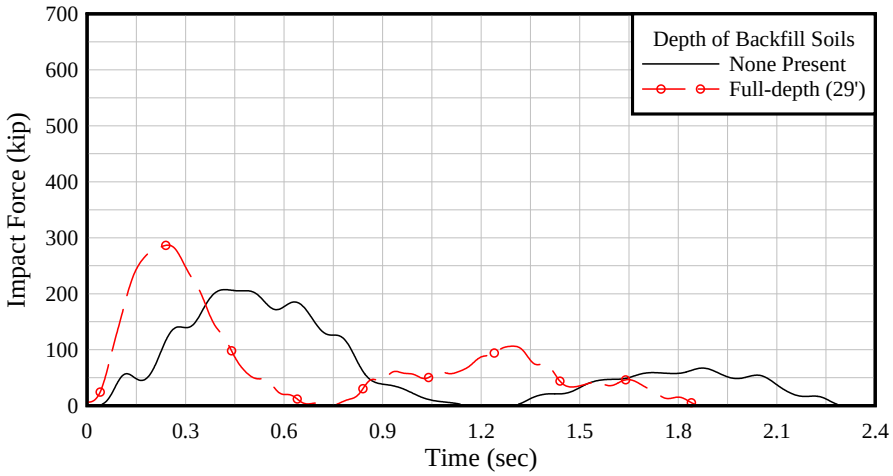

Figure D.8. 3x3 – 2 FPS – 10°– MRLD2 – HEI

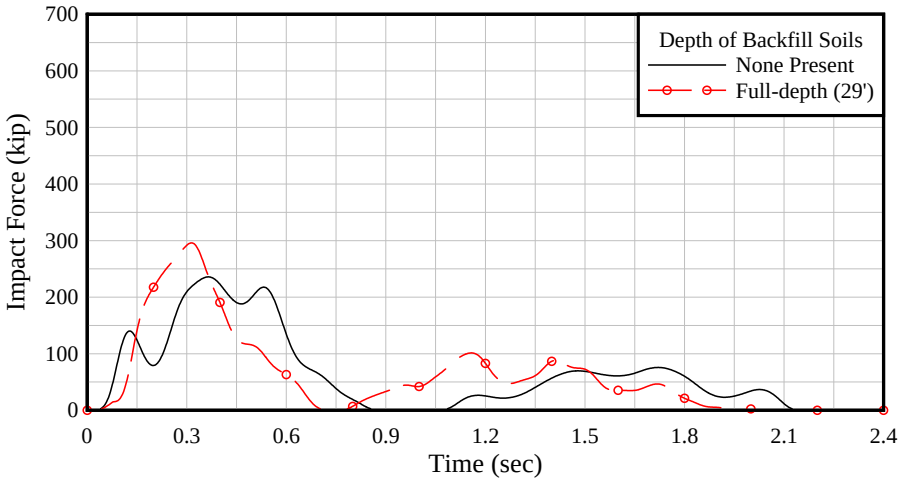

Figure D.9. 3x3 – 2 FPS – 10°– MRLD2 – LEI

Although the more conservative condition with respect to impact force corresponds to the presence of full-depth backfill soil, pile forces are dramatically reduced with the presence of backfill. Due to the added lateral stiffness and alternate load path from the backfill soil springs, loads transferred from the guide wall into the timber piles is dramatically reduced (Figure D.10). Thus, since impact forces differ only moderately, and in the interest of obtaining the most conservative maximum pile axial forces (and corresponding vertical soil response [skin friction]) backfill soils are *excluded* from the MRLD2 and MRLD3 parametric studies.

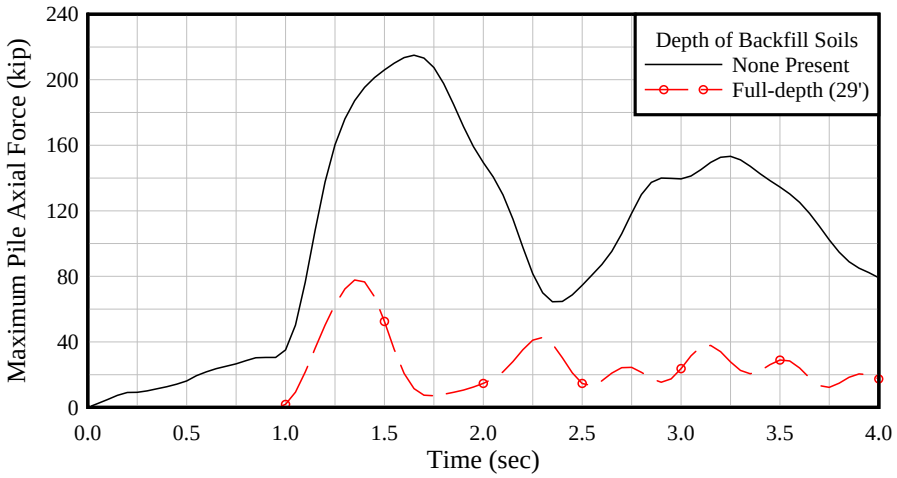

Figure D.10. Maximum pile axial time histories for 3x5 – 4 FPS – 15°– MRLD2 – HEI (Note: time history includes results from one-second initialization simulation)

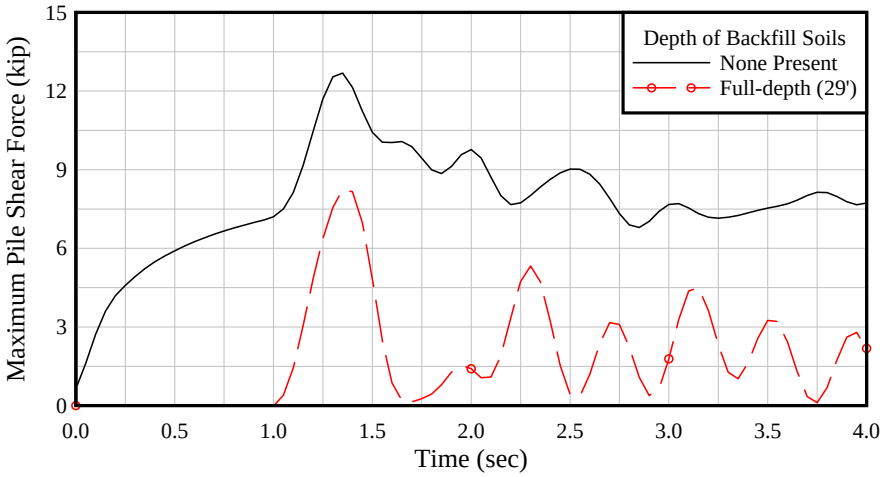

Figure D.11. Maximum pile shear force histories for 3x5 – 4 FPS – 15°– MRLD2 – HEI (Note: time history includes results from one-second initialization simulation)

It is also worth noting that the effect of backfill conditions on impact forces is minimal when lowest elevation impacts conditions are simulated (Figure D.12). (A more detailed discussion regarding the effects of impact elevation is provided in Section D.3.) As noted in Chapter 3, all primary parametric impact studies on MRLD2 and MRLD3 are conducted using the low elevation impact conditions.

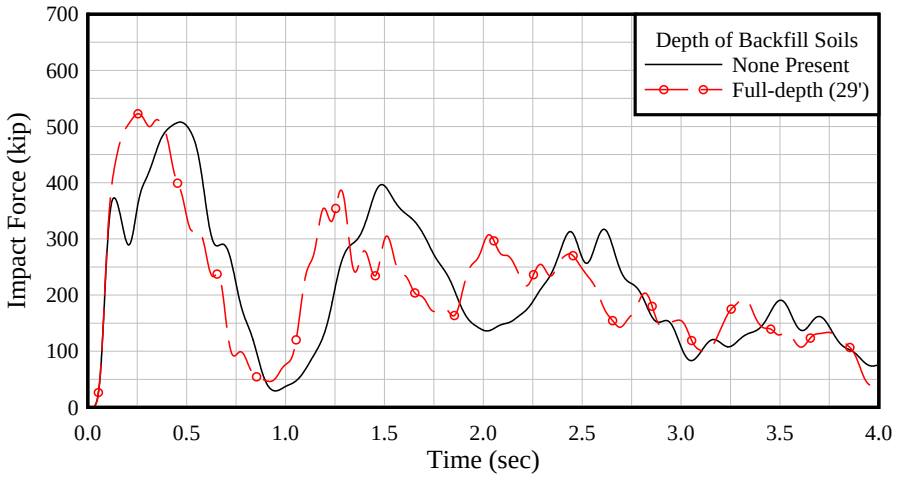

Figure D.12. 3x5 – 4 FPS – 15°– MRLD2 – LEI

D.3 Impact elevation

Multiple elevation impact simulations were conducted with the MRLD2 finite element model to determine impact force sensitivity to the impacting barge elevation with the primary motivation of identifying the most conservative impact elevation for use in the MRLD2 and MRLD3 parametric studies. Comparative impact force-time histories between simulations with barge elevations corresponding to the highest and lowest pool elevations were reviewed. In addition, this impact elevation study was performed in concert with the backfill soil study (Section D.2), thus all impact force-time histories are a function of both impact elevation and backfill soil.

The highest and lowest water elevation conditions, corresponding to the upper and lower pool levels, are considered for impacts against the MRLD2 model. The highest pool elevation corresponds to a water depth of 22’-4” above the base of the guide wall. Although the lowest pool elevation corresponds to a water depth of approximately 9’, a fully loaded hopper barge, weight = 2000 tons, drafts at an approximate depth of 10’-4”. Thus, the lowest elevation impact condition corresponds to a water depth of 10’-6”.

Additional simulations, with the impacting flotilla positioned at an elevation corresponding to the highest (water) pool elevation, are performed to determine the sensitivity of impact forces to impact elevation. The following comparative force-time history plots illustrate that the lowest elevation impacts cause larger impact forces. This behavior is expected given the proximity of the lateral load resisting soil springs to the impacting barge for lowest elevation impacts. Therefore, the most conservative impact condition corresponds to the lowest pool elevation, and thus lowest elevation impacts are used for the MRLD2 and MRLD3 parametric studies.

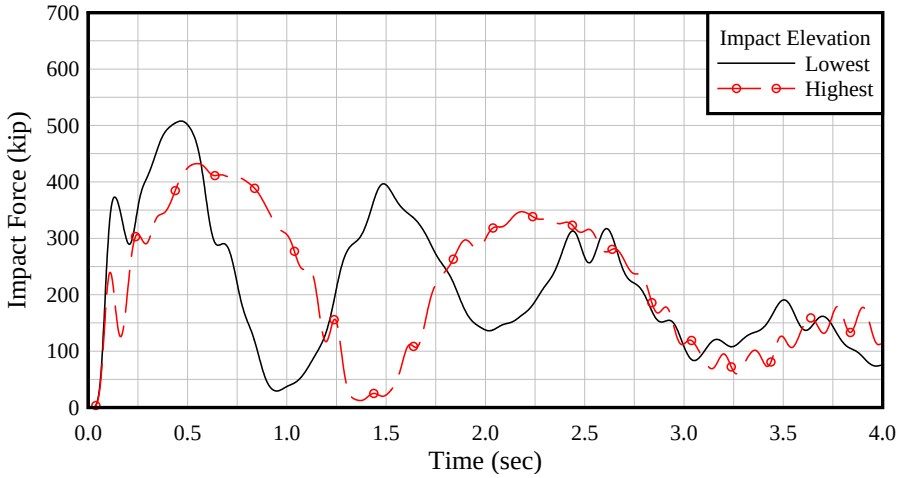

Figure D.13. Force-time histories for 3x5 – 4 FPS – 15°– MRLD2 – ZBF

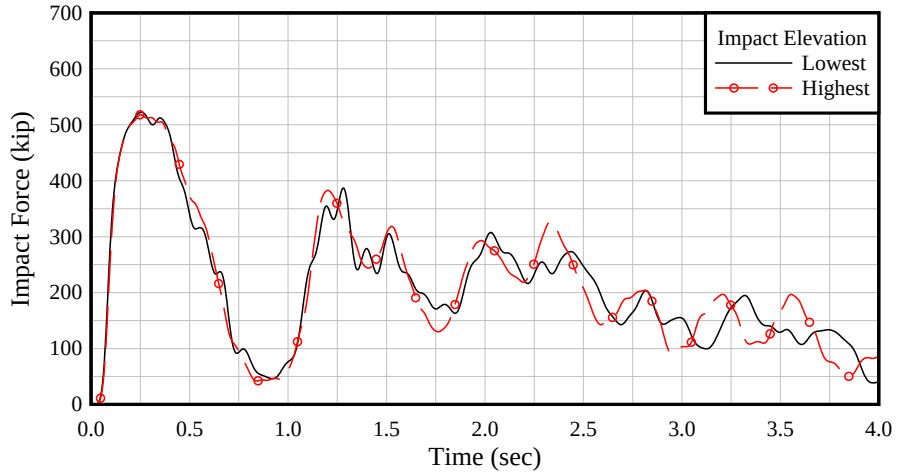

Figure D.14. Force-time histories for 3x5 – 4 FPS – 15°– MRLD2 – FBF

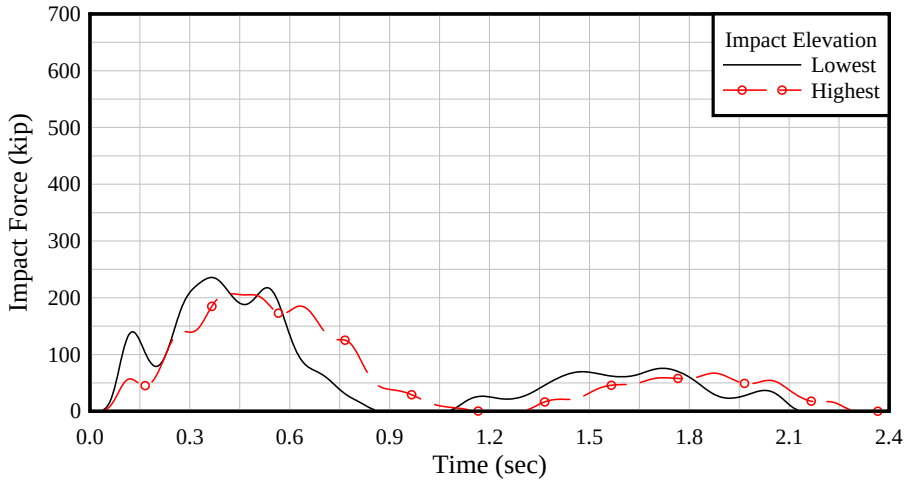

Figure D.15. Force-time histories for 3x3 – 2 FPS – 10°– MRLD2 – ZBF

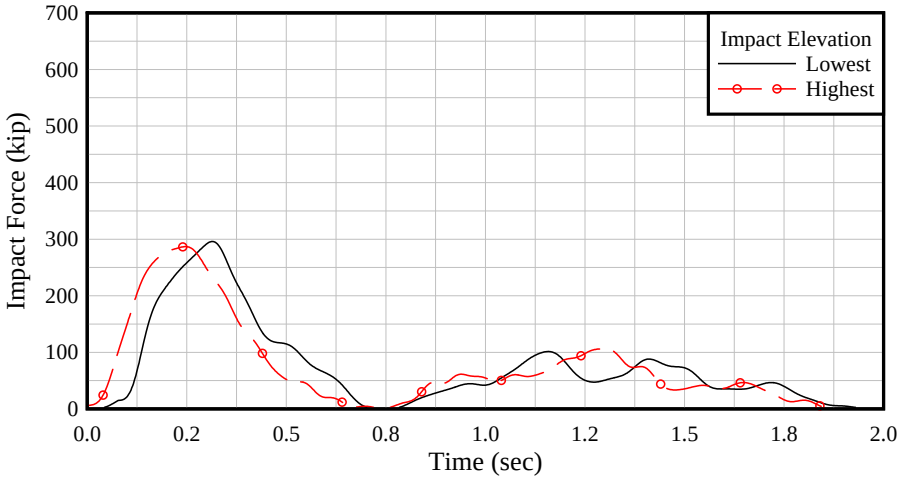

Figure D.16. Force-time histories for 3x3 – 2 FPS – 10°– MRLD2 – FBF

D.4 Adjacent monoliths for MRLD2

Prior to conducting the MRLD2 parametric study (Chapter 4), where simulations are limited to the presence of a single monolith, additional simulations with adjacent monoliths were performed to determine impact force sensitivity. To quantify the effect of adjacent monoliths on impact forces, contact force-time histories from one, two, and three monolith simulations are compared for the high energy impact condition: 3x5 – 4 FPS – 15°. The two-monolith model includes an additional monolith (adjacent the impacted monolith) in the downstream position. The three-monolith model includes two additional monoliths, one upstream, and one downstream. The additional monoliths, adjacent to the impacted monolith, are not contacted by the impacting barge and are therefore described as 'non-impacted' monoliths. The adjacent monoliths are positioned with a gap of 1/64" to account for construction tolerances. The inter-monolith contact definition uses a constant static and dynamic coefficient of friction value of 0.60 per ACI §11.6.4.3 (ACI 2011). All non-varying impact conditions are consistent among the three simulations. Except for impact elevation, all impact conditions are consistent with the primary MRLD2 parametric study. The comparative force-time history results (during the first force pulse) illustrate that adjacent, non-impacted, monoliths have a *minimal* effect on the MRLD2 impact forces (Figure D.17), pile axial forces (Figures D.18), and pile shear forces (Figure D.19). Hence, all impact simulations conducted for the MRLD2 parametric study include only a single monolith for computational efficiency.

D.5 Adjacent monoliths for MRLD3

Barge flotilla impact simulations were carried out on the MRLD3 model with a single monolith and three monoliths to quantify differences in peak impact forces due to presence of multiple monoliths. For simulations with multiple monoliths, both static and dynamic inter-monolith coefficients of friction are a constant 0.60 per ACI §11.6.4.3 (ACI 2011). The three-monolith model has monoliths placed on the upstream and downstream sides of the impacted monolith with a gap spacing of 1/64". Since the major concern of the sensitivity study was to understand the difference in peak impact forces, the simulation for one monolith was terminated after 1.5 sec of impact duration. Comparative impact force time histories and displacement

response of MRLD3 subjected to the same impact condition, 2x3 – 20° – 4 FPS, are presented (Figures D.20) for a 1.5 sec. impact duration. As is evident from Figure D.20, for a three-monolith model, the peak impact forces are approximately 10% larger. For the purposes of the MRLD3 study, all impact simulations are conducted using three (3) monoliths, with one monolith on either side (upstream and downstream) of the impacted monolith.

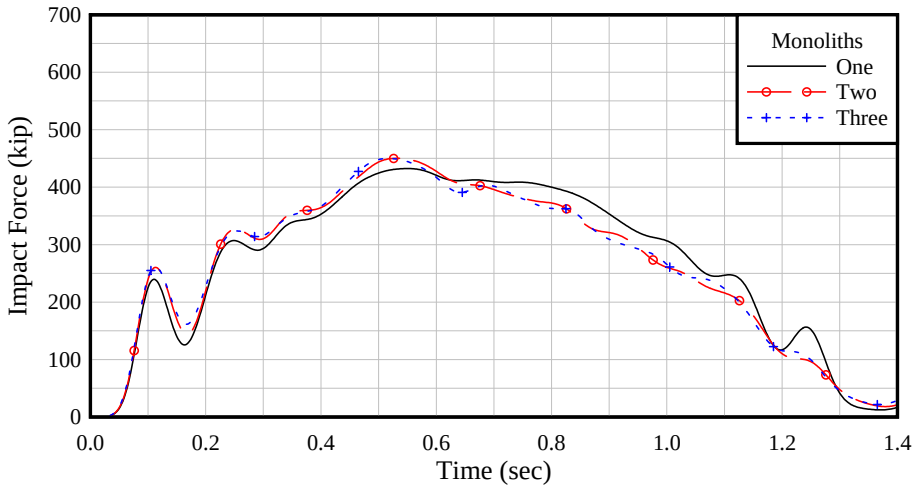

Figure D.17. Impact force-time histories for
3x5 – 4 FPS – 15°– MRLD2 – ZBF – HEI

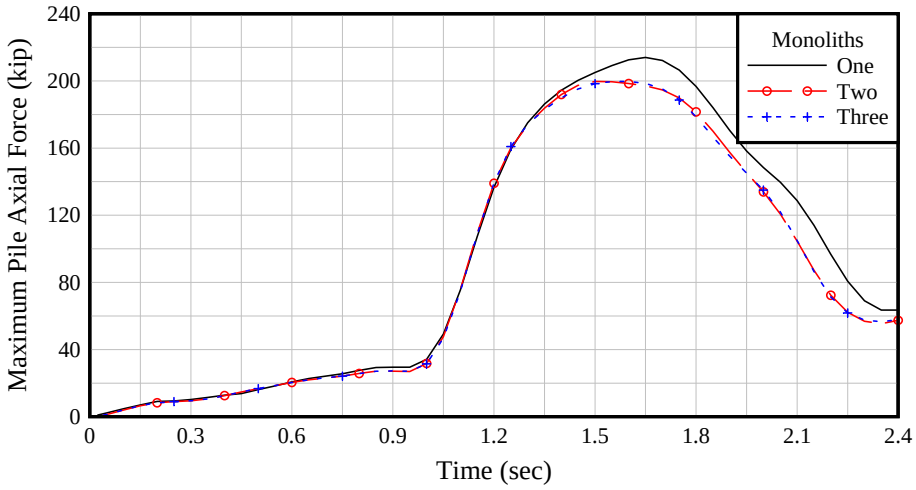

Figure D.18. Maximum pile axial force-time histories for
3x5 – 4 FPS – 15°– MRLD2 – ZBF – HEI
(Note: time history includes results from one-second initialization simulation)

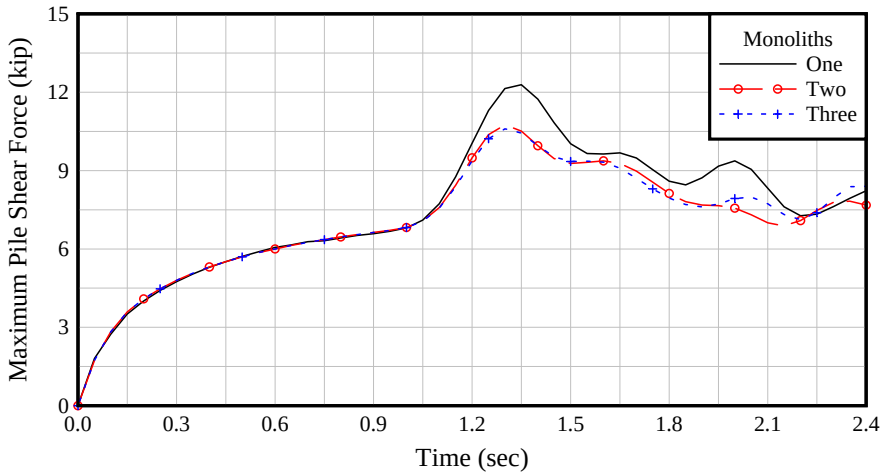

Figure D.19. Maximum pile shear force-time histories for
3x5 – 4 FPS – 15°– MRLD2 – ZBF – HEI
(Note: time history includes results from one-second initialization simulation)

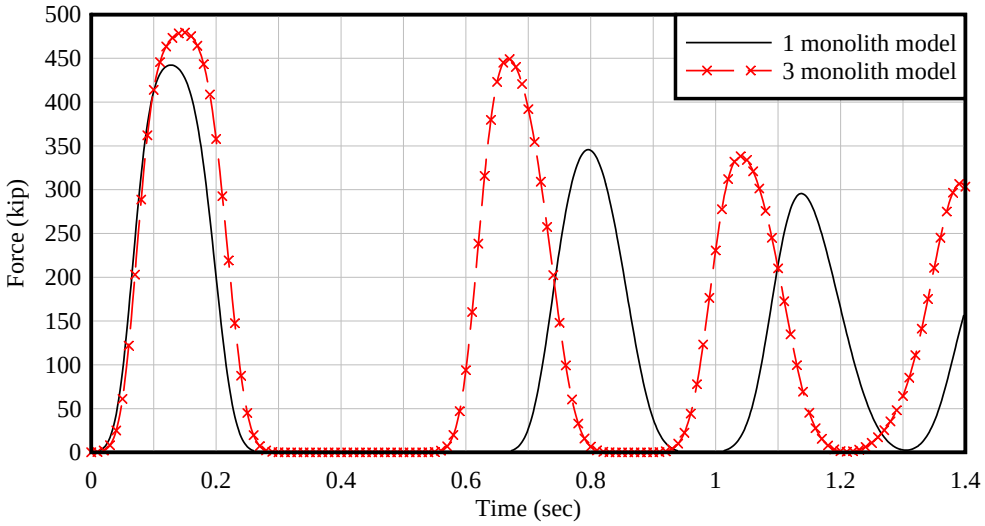

Figure D.20. Impact force-time histories for 2x3 – 4 FPS – 20°– MRLD3

D.6 Original versus modified soil stiffnesses for MRLD2

A series of impact simulations were performed to estimate impact force sensitivity to soil stiffness. Modified soil profiles were developed by scaling the forces in the soil force-deformation curves used in the primary MRLD2 parametric study by values of 2.0 and 0.5. These modifications were applied to all soil springs (horizontal, vertical, and tip) in the MRLD2 model. The 100% increase and 50% decrease in soil stiffness resulted in an 8% increase and < 1% decrease, respectively, in impact force for 2x3 flotilla impacts examined. For 3x3 flotilla impacts, the 100% increase and 50% decrease in soil stiffness resulted in a 10% increase and 7% decrease, respectively.

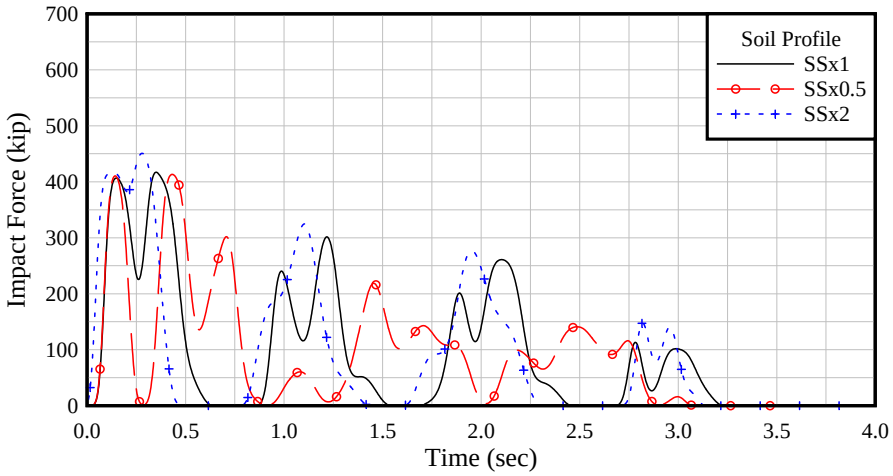

Figure D.21. Force-time histories for 2x3 – 4 FPS – 15°– MRLD2

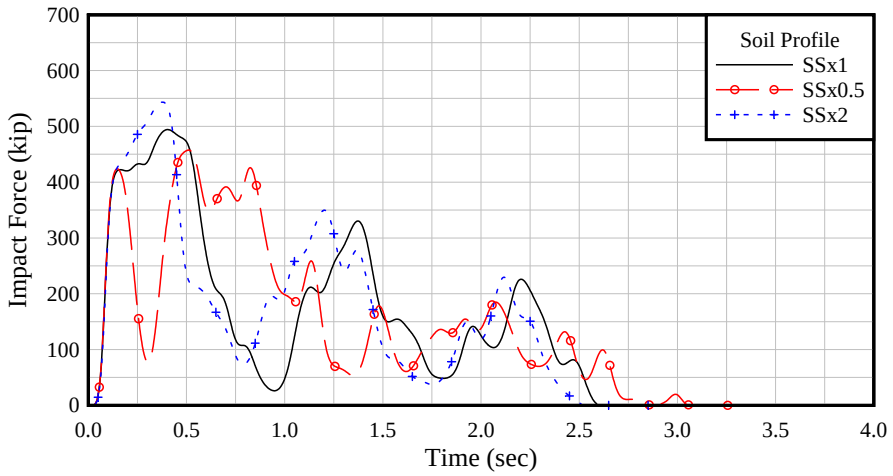

Figure D.22. Force-time histories for 3x3 – 4 FPS – 15°– MRLD2

D.7 Reduced diameter of timber piling for MRLD2

Additional simulations were conducted to assess the sensitivity of impact forces to the stiffness contribution from timber piling. Specifically, the twelve-inch diameter (12”) piling was reduced to six-inch diameter (6”) timber piling through modifications to the pile cross-sectional properties. Peak impact force was reduced ~10-15% as a result of the 75% reduction in cross-sectional area of the timber piling.

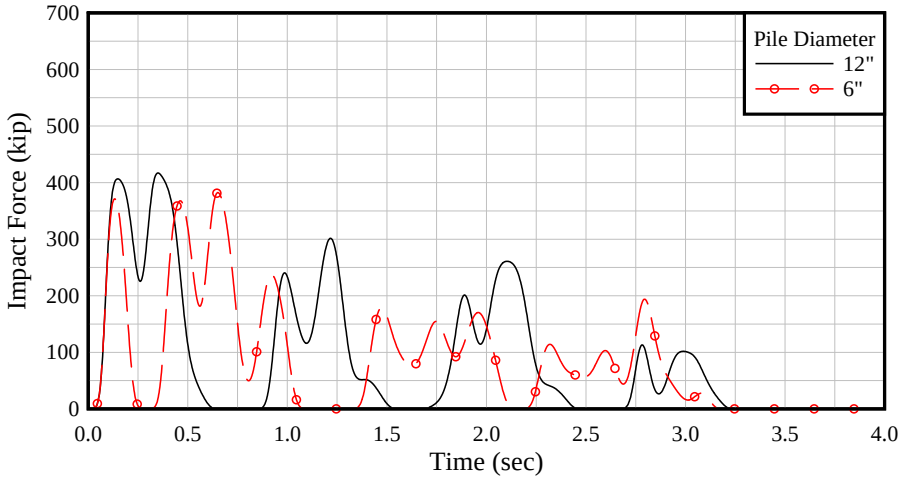

Figure D.23. Force-time histories for 2x3 – 4 FPS – 15°– MRLD2

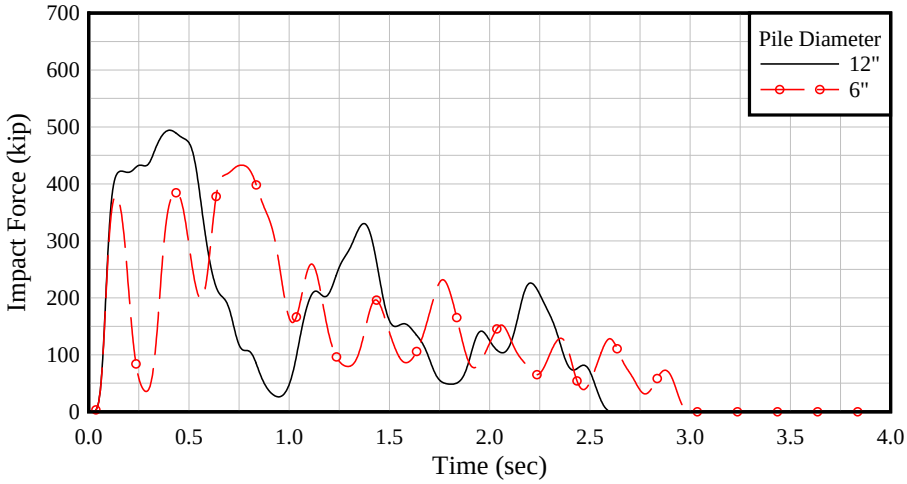

Figure D.24. Force-time histories for 3x3 – 4 FPS – 15°– MRLD2